MODELLING AND REDUCING GAS EMISSIONS FROM NATURALLY **VENTILATED LIVESTOCK BUILDINGS**

Biological and Chemical Engineering
Technical Report BCE-TR-2

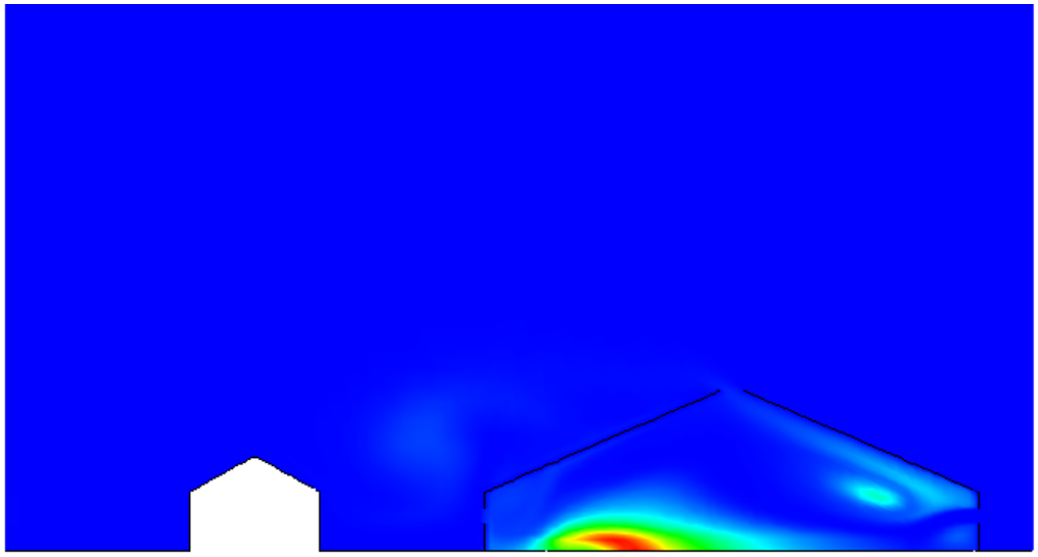

AARHUS
UNIVERSITY
DEPARTMENT OF ENGINEERING

DATA SHEET

Title: Modelling and reducing gas emissions from naturally ventilated livestock buildings

Subtitle: Biological and Chemical Engineering
Series title and no.: Technical report BCE-TR-2

Author: Wentao Wu
Department of Engineering – Biological and Chemical Engineering, Aarhus University

Internet version: The report is available in electronic format (pdf) at the Department of Engineering website http://www.eng.au.dk.

Publisher: Aarhus University©
URL: http://www.eng.au.dk

Year of publication: 2012 Pages: 151
Editing completed: September 2012

Abstract: Livestock buildings are identified to be a major source of ammonia emissions. About 30% of the total ammonia emission within livestock sectors is from naturally ventilated dairy cattle buildings. The main objectives of this study are to predict emissions from naturally ventilated dairy cattle buildings and to establish a systematic approach to curtail the emissions.
Gas concentrations were measured inside two dairy cattle buildings in mid-Jutland, Denmark. CO_2 balance method was thus applied to estimate ventilation and emission rates. Computational fluid dynamics (CFD) was used to find the optimum gas sampling positions for outlet CO_2 concentration. The gas sampling positions should be located adjacent to the openings or even in the openings. The NH_3 emission rates varied from 32 to77 g HPU^{-1} d^{-1} in building 1 and varied from 18 to30 g HPU^{-1} d^{-1} in building 2.
Scale model experiment showed that partial pit ventilation was able to remove a large portion of polluted gases under the slatted floor. In the full scale simulations, a pit exhaust with a capacity of 37.3 $m^3 h^{-1}$ HPU^{-1} may reduce ammonia emission only by 3.16% compared with the case without pit ventilation. When the external wind was decreased to 1.4 m s^{-1} and the sidewall opening area were reduced to half, such a pit ventilation capacity can reduce ammonia emission by 85.2%. The utilization of pit ventilation system must be integrated with the control of the natural ventilation rates of the building.

Keywords: Biotechnology; Computer fluid dynamics modeling; Emission; Environmental engineering; Housing systems; Ventilation and indoor climate

Supervisor: Guoqiang Zhang; Peter V. Nielsen; Peter Kai

Please cite as: Wentao Wu, 2012. Modelling and reducing gas emissions from naturally ventilated livestock buildings.
Department of Engineering, Aarhus University. Denmark. 151 pp. - Technical report BCE-TR-2

Cover image: Wentao Wu

ISSN: 2245-5817

MODELLING AND REDUCING GAS EMISSIONS FROM NATURALLY VENTILATED LIVESTOCK BUILDINGS

Wentao Wu

Aarhus University, Department of Engineering

Abstract

Livestock buildings are identified to be a major source of ammonia emissions. About 30% of the total ammonia emission within livestock sectors is from naturally ventilated dairy cattle buildings. The main objectives of this study are to predict emissions from naturally ventilated dairy cattle buildings and to establish a systematic approach to curtail the emissions. Gas concentrations were measured inside two dairy cattle buildings in mid-Jutland, Denmark. CO2 balance method was thus applied to estimate ventilation and emission rates. Computational fluid dynamics (CFD) was used to find the optimum gas sampling positions for outlet CO2 concentration. The gas sampling positions should be located adjacent to the openings or even in the openings. The NH3 emission rates varied from 32 to77 g HPU-1 d-1 in building 1 and varied from 18 to30 g HPU-1 d-1 in building 2.

Scale model experiment showed that partial pit ventilation was able to remove a large portion of polluted gases under the slatted floor. In the full scale simulations, a pit exhaust with a capacity of 37.3 m3 h-1 HPU-1 may reduce ammonia emission only by 3.16% compared with the case without pit ventilation. When the external wind was decreased to 1.4 m s-1 and the sidewall opening area were reduced to half, such a pit ventilation capacity can reduce ammonia emission by 85.2%. The utilization of pit ventilation system must be integrated with the control of the natural ventilation rates of the building.

Preface

This thesis is submitted as a partial fulfillment of the requirements for the Doctor of Philosophy (PhD) degree at Department of Engineering, Faculty of Science and Technology, Aarhus University, Denmark. The research was performed between June 2009 and June 2012 supervised by senior scientist Guoqiang Zhang. Scale model measurements were conducted in the wind tunnel at Air Physics Lab, Research Centre Bygholm, Horsens. Laboratory experiments using small wind tunnels were carried out at Air Physics Lab, Research Centre Foulum, Tjele. Full scale field measurements on gas emissions were completed in two naturally ventilated dairy cow buildings in Jutland. Part of the numerical simulations was done in the University of Colorado at Boulder, USA.

This thesis is based on the work presented in three published research papers and three manuscripts. They are:

1. **Wu, W.,** Zhang, G., Kai, P., 2012. Ammonia and Methane Emissions from Two Naturally Ventilated Dairy Cattle Buildings and the Influence of the Climatic Factors on Ammonia Emissions. Atmospheric Environment 61, 232-243.
2. **Wu, W.**, Zhang, G., 2012. Turbulent Air Characteristics in Two Naturally Ventilated Dairy Cattle Buildings. Submitted to a peer review journal.
3. **Wu, W.,** Zhai, J., Zhang, G., Nielsen, P.V., 2012. Evaluation of methods for determining air exchange rate in a naturally ventilated dairy cattle building with large openings using computational fluid dynamics (CFD). Submitted to a peer review journal.
4. **Wu, W.,** Kai, P., Zhang, 2012. An assessment of a partial pit ventilation system to reduce emission under slatted floor-Part 1: Scale Model Study. *Computers and Electronics in Agriculture* 83, 127-133.
5. **Wu, W.,** Zhang, G., Bjerg, B., Nielsen, P.V., 2012. An assessment of a partial pit ventilation system to reduce emission under slatted floor-Part 2: Feasibility of CFD prediction using RANS turbulence models. *Computers and Electronics in Agriculture* 83, 134-142.
6. **Wu, W.,** Zong, C., Zhang, G., 2012. Large eddy simulation of airflow and pollutant transport under slatted floor of a slurry pit model. Submitted to a peer review journal.

During this study, by collaborating with other scientists, the following publication was produced:

1. Saha, C.K., **Wu, W.**, Zhang, G., Bjerg, B., 2011. Assessing effect of wind tunnel sizes on air velocity and concentration boundary layers and on ammonia emission estimation using computational fluid dynamics (CFD). Computers and Electronics in Agriculture 78 (1), 49-60.

Acknowledgements

I wish to acknowledge the following persons who have contributed to my pursuing of PhD in diverse manners.

My first and foremost appreciation goes to my principal supervisor, Dr. **Guoqiang Zhang**, Senior scientist in Department of Engineering, Aarhus University. His broad knowledge and enthusiastic attitude on science always inspired me on my work. His great personality led me to shape myself in the very same fashion.

I would like to extend my appreciation to my co-supervisor - Professor **Peter V. Nielsen** from Aalborg University, project supervisor - Dr. **Peter Kai** from AgroTech, Denmark. Many thanks are given to Associate professor **Bjarne Bjerg** from Copenhagen University, Associate professor **John Zhai** from University of Colorado at Boulder, USA. When I stayed in these two universities, they advised me on Computational Fluid Dynamics (CFD) and my skills on CFD were quantitatively improved since then. I would like to express my gratitude to Dr. **Chayan Kumer Saha** from Leibniz-Institut für Agrartechnik Potsdam-Bornim e.V., Germany and PhD student **Raphael Kubeba** from Harper Adams University College, UK. They read through my thesis and helped me to improve it. I benefited from the cooperation with PhD student **Chao Zong** at Aarhus University.

I deliver my gratitude to the laboratory technicians **Jan Ove Johnsen** and **Jens Kristian Kristensen** at Aarhus University. The PhD project would not be possibly completed without their large contributions. I would like to thank **Anja Torup Hansen**, who helped me since I was on the way to Denmark. I am always feeling grateful to Dr. **Li Rong** at Aarhus University, Professor **Jing Liu**, Senior Engineer **Xiaoxin Man** from Harbin Institute of Technology, China. Their help or support enabled me to come to Denmark.

My special appreciation goes to the greatest and most beautiful country in this world – **Denmark**. In this ever loving land, I met several good friends – Dr. **Jana Boleckova** from Czech Republic, **Sebastiano Falconi** from Sardinia, **Emmanuel Arthur** from Ghana, **Miroslaw Marek Kasprzak** from Poland, **Grazina Kadziene** from Lithuania and **Kristin Barkve Andersen** from Norway. The friendship with **Jana** and **Sebastiano** was one of the most precious gifts for the three years in Denmark. **Pernille Bildsøe** and **Ole Jørgensen** never hesitated to translate Danish to English for me in diverse fashions. I can never stop writing this list. In brief, I gave my sincere thanks to **all the people** being helpful and kind to me.

Finally, I express my gratitude and love to my **grandma** and my **wife**. My **grandma** brought me up and provided me the opportunity to experience the wonderful trip in the life. The delicious dinner provided by my wife **Lei Wang** always erased the tiredness of the whole work day. This work is also dedicated to my grandma and my wife.

(Wentao Wu)

Summary

Emissions of ammonia to the atmosphere cause acidification of soil and increase eutrophication to sensitive ecosystems such as aquatic systems, while emissions of greenhouse gases such as nitrous oxide, carbon dioxide and methane influence global climate. Livestock buildings are identified to be a major source of those gas emissions. About 30% of the total ammonia emission within livestock sectors is from naturally ventilated dairy cattle buildings. Nearly no innovative low emission technology has been applied to cattle buildings. Besides mitigation techniques, methods to quantify gas emissions from naturally ventilated livestock buildings are still lacking. Therefore, the main objectives of this study are to predict emissions from naturally ventilated dairy cattle buildings and to establish a systematic approach to curtail the emissions.

Gas concentrations were measured inside two dairy cattle buildings in mid-Jutland, Denmark. CO_2 balance method was thus applied to estimate ventilation and emission rates. To evaluate the influence of climatic parameters on gas emissions, air velocity, turbulence and temperature were monitored inside and outside the buildings. Computational fluid dynamics (CFD) was used to find the optimum gas sampling positions for outlet CO_2 concentration. A concept of partial pit ventilation system was proposed to abate gas emissions. The hypothesis was verified first by a 1:2 scale model in wind tunnel measurements. Since a partial pit ventilation system cannot be found in practical cattle buildings, the investigation on the potential of such a system to reduce emission was carried out by CFD simulations.

The NH_3 emission rates varied from 32 to77 g HPU^{-1} d^{-1} in building 1 and varied from 18 to30 g HPU^{-1} d^{-1} in building 2. The average emission of CH_4 was 290 and 230 g HPU^{-1} d^{-1} from building 1 and 2, respectively. Diurnal pattern was found for NH_3 and CH_4 emission rates. From multiple linear regression models, there was a significant linear relationship between NH_3 emission rates and climatic factors including the external wind speed as well as the air temperature ($P<0.001$), but not with the external wind directions ($P>0.05$).

Air exchange rates (AER) predicted by integration of volume flow rate (VFR) and tracer gas decay (TGD) were in good agreement with each other within a large range of wind speeds. Large difference in AER estimation was found between VFR and constant tracer gas method (CTG) using the mean CO_2 concentration of the entire room as outlet concentration. It indicates that the mean CO_2 concentration of the entire room may not represent the outlet gas concentration. The gas sampling positions should be located adjacent to the openings or even in the openings. All the openings especially of different azimuths should possess sampling tubes. The maximum gas concentrations at different openings could be the optimum value to represent the concentration in the exit air.

Scale model experiment showed that partial pit ventilation was able to remove a large portion of polluted gases under the slatted floor. RANS turbulence models especially RSM can be used to

predict the removal capability of a partial pit ventilation system to reduce emission under slatted floor. In the full scale simulations, a pit exhaust with a capacity of 37.3 $m^3 h^{-1} HPU^{-1}$ may reduce ammonia emission only by 3.16% compared with the case without pit ventilation when the external wind was 4.2 m s^{-1}. When the external wind was decreased to 1.4 m s^{-1} and the sidewall opening area were reduced to half, such a pit ventilation capacity can reduce ammonia emission by 85.2%. The utilization of pit ventilation system must be integrated with the control of the natural ventilation rates of the building.

The study is helpful for emission inventory and also demonstrates that partial pit ventilation system may be a feasible approach to mitigate emission from naturally ventilated cattle buildings.

Resumé på Dansk

Ammoniak emission til atmosfæren, forsager forsuring af jord og forårsager eutrofiering af kvælstof-sensitive økosystemer såsom vandløb. Udledning af drivhusgasser såsom N_2O, kuldioxid og metan påvirker klimaet globalt. Landbrugets dyrehold bidrager væsentligt til drivhusgasser i det global klima regnskab. Omkring 30% af de samlede ammoniakemissioner fra dansk landbrug, stammer fra ventilation af kvægbygninger. Hidtil har anvendelsen af innovative teknologier til reduktion af emission været begrænset, dertil mangler der metoder til kvantificering af emissionsniveauer. Formålet med dette studie har derfor været at fastlægge emissioner fra bygninger med dyrehold, samt at finde en systematisk metode hvormed emissionerne kan begrænses.

I bestræbelserne på at fastlægge emissioner fra stalde med malkekvæg blev ventilationsluftmængden fastlagt indirekte ved hjælp af CO_2 balancemetoden. Computersimuleringer(CFD) blev brugt til at finde optimale placeringer af gas-sensorer for at anvende CO_2 massebalance metoden.

Et system med lokal luftudsugning i gyllekanalen, blev forslået med henblik på at begrænse gasemissionen. Tesen blev først afprøvet med en 1:2 skala model i vindtunnel forsøg. Da der ikke fandtes et eksisterende system til lokal ventilation af gyllekanalen, blev potentialet for emissions reduktion undersøgt med computer simuleringer.
Emissionen af NH_3 varierede fra 32-77 g HPU^{-1} d^{-1} i bygning 1 og 18-30 g HPU^{-1} d^{-1} i bygning 2. Det gennemsnitlige emissionsniveau for CH_4 for henholdsvis bygning 1 og 2 var 290 og 230 g HPU^{-1} d^{-1}. Emissionerne af NH_3 og CH_4 viste en tydelig døgnvariation. Fra et sæt af flere lineære regressioner, fandtes en signifikant linear sammenhæng mellem ammoniakemissionen og de klimatiske parametre, ekstern vindhastighed samt lufttemperaturen($P<0.001$), men ikke vindretningen ($P>0.05$).

Luftudskiftningshastigheden estimeret ved integration af den volumetriske flow rate (eng. AER), samt målinger på henfald af sporgasser (eng. TGD), viste god ovenstemmelse over et bredt interval af vindhastigheder. Store forskelle i luft-udskiftningshastigheden baseret på henholdsvis sporgas og integrationsmetoden, indikerer at den gennemsnitlige CO_2 koncentration i rummet, ikke svarer til koncentrationen målt i udluftnings- åbningen. Målepostionerne for gassensorer skal placeres tæt på udluftnings åbninger, eller helst i selve åbningen. Der skal monteres gas-samplinger i alle åbninger, især i vinklede rør. Den maximale gaskoncentration målt i de forskellige åbninger, fremgik som værende den optimale værdi til at repræsentere koncentrationen i ventilations luften.

Eksperimenter med skalamodeller af staldbygninger viste, at metoden med lokal udluftning af gyllekanaler er i stand til at fjerne en stor andel af de forurenende gasser, der produceres og frigives under spaltegulvet. RANS turnolens modeller og især RSM kan estimere potientialet for reduktion af gasniveauet ved lokal ventilation under spaltegulvet.

CFD simulationer af en fuldskala kvægstald viste, at luftudsugning under spaltegulvet med en

kapacitet på 37,3 $m^3h^{-1}HPU^{-1}$ kan give en reduktion i ammoniakemissionen på 3,16% sammenlignet med en traditionel gyllekanal ved ekstern vindhastighed på 4,2ms^{-1}. Hvis den eksterne vindhastighed reduceres til 1,4ms^{-1}, og ventilationsåbningsarealet i staldens facader reduceres til det halve, kan den luftudsugning reducere ammoniakemissionen med 85,2%. For at udnytte et gyllekanal luftudsugningssystem, er det nødvendigt at designet integreres med bygningens øvrige ventilation.

Studiet har demonstreret at lokal udluftning under spaltegulvet kan være en mulig løsning til begrænsning af emisionen af ammoniak fra naturligt ventilerede staldbygninger.

Table of Contents

Chapter 1

General Introduction

1.1. Ammonia emissions from naturally ventilated dairy cattle buildings

The recognition of the ammonia emissions as an environmental issue can be marked by the work of Van Breemen et al. (1982), which discovered the fact of soil acidification from atmospheric ammonium sulphate and identified the sources of the ammonia emissions – the livestock production units. Inventories have shown that animal housing, stored animal manure and exercise areas account for about 60-80% of the total emission of NH_3 in Europe (Hutchings et al., 2001). The estimated NH_3 emissions from various animal husbandry operations in some countries are shown in Table 1.1. Ammonia emissions from animal husbandry in Denmark during 1990 – 2005 are shown in Table 1.2.

Table 1.1 Ammonia emission estimates from different animal husbandry in three countries

Source	Ammonia emissions(Kg animal^{-1} year^{-1})		
	Denmark (Peterson, 2006)	Czech (Zapletal and Chroust, 2006)	USA (Battye et al., 2003)
Dairy cows	13.55	27.9	28
Other cattle	7.99	64.8	10.2
Sows	6.39	17.44	16.4
Pigs	6.24	14.8	6.4
Broilers	0.08	0.21	0.28
Hens	0.40	0.92	0.31

Table 1.2 Ammonia emission estimates from animal husbandry in Denmark during 1990 – 2005 (tones NH3-N) (Gyldenkærne and Mikkelsen, 2007)

Animal type	1990		2000		2005	
	Emissions	% of the total emissions	Emissions	% of the total emissions	Emissions	% of the total emissions
Cattle	33,598	41.8	22,201	36.6	16,140	30.0
Horses	1,246	1.55	1,211	1.99	1,174	2.18
Sheep	280	0.34	201	0.34	191	0.32
Pigs	36,139	44.9	28,179	46.4	27,452	51.1
Poultry	4,204	5.23	4,843	7.98	4,581	8.52
Fur animals	4,975	6.18	4,064	6.69	4,237	7.88
Total	80,441	100	60,699	100	53,774	100

The two tables show that the cattle buildings, which are usually naturally ventilated, constitute one of the largest NH_3 emission sources within agricultural production. More than 30% of the total ammonia emission originated from cattle buildings in Denmark before 2005 and this added weight to the concern of environmental pollution issues caused by naturally ventilated cattle buildings. The reliable measurement methods and protocols of ammonia concentrations and air volumes from

naturally ventilated houses were identified as key problems in European commission meeting in 1990. The first problem was the greatest uncertainty in the estimates of the natural ventilation rates. The second problem was the lack of the reliable measurement technologies to determine the outlet gas concentration to quantify the emission rates. To date, there has been little innovation for overcoming the two challenges. Meanwhile, limited application of emission abatement technologies can be found for ammonia reduction from cattle buildings. In order to find new low emission technologies to reduce emissions from naturally ventilated cattle buildings, quantification of ventilation rates and ammonia emission rates is the first key step.

1.2. Available methods to determine natural ventilation rates

For a mechanically ventilated livestock building, ventilation rate can be monitored by a pressure nozzle equipped to exhaust duct or by recording the speed of the exhaust fan. The method cannot be applied directly to naturally ventilated buildings which possess large openings. The openings may act as inlet at one condition and as outlet at another condition according to the external wind directions. The variability of the opening function requires special methods to determine natural ventilation rates. In 1978, Strøm developed equations for total and sensible heat productions. Afterwards, CIGR (1984 & 2002) working group derived further common balance equations for heat and moisture based on heat production. The three balance equations are:

Heat balance : $$S_b = AU\Delta T + V_r c\Delta T \quad (1.1)$$

Moisture balance : $$L = 680 V_r \Delta H \quad (1.2)$$

CO_2 balance : $$Q = V_r \Delta C \quad (1.3)$$

where, S_b is sensible heat production, W; A is the surface area of the livestock building, m^2; U is the heat transmission coefficient for building surfaces, W m^{-1} K^{-1}, ΔT is the temperature difference between indoors and outdoors, K; V_r is the ventilation rate, m^3 h^{-1}; c is the specific heat of air, J m^{-3} K^{-1}; L is latent heat production, W; ΔH is the difference in water content between indoor and outdoor air, kg m^{-3}; Q is the CO_2 production by animals, m^3 h^{-1}; ΔC is the difference in CO_2 content between indoor and outdoor air, ppm.

The establishment of the three balance equations enables natural ventilation rate to be calculated via heat or mass balance method. Pederson et al. (1998) compared three methods for calculation of the ventilation rate in Northern European livestock buildings on the basis of the balances of heat, moisture and CO_2 for dairy cattle; the result showed that a CO_2 production of 0.185 m^3 h^{-1} HPU^{-1} provided good agreement between ventilation rates calculated from CO_2 production and those from temperature and moisture; for naturally ventilated cattle buildings, CO_2 production method is superior to the other two methods due to the small difference of indoor and outdoor temperature and moisture in the air. The above methods are only validated for steady state conditions. Diurnal variation in the production of metabolic heat, water and CO_2 will limit the accuracy of those methods. The other uncertainties of this CO_2 balance method can be: (1) a

uniform distribution of CO_2 production is assumed, which is unlikely in practical buildings; (2) the ventilation based on equation (1.1 to 1.3) depends on the measurement location of the indoor temperature, water vapour and CO_2 content. Attempting to overcome uncertainty in estimation of ventilation rate brought by the heterogeneity of CO_2 distribution, Teye and Hautala (2007) developed theories for open stall dairy building without ideal mixing under strong wind. The mass balance within a short distance *dx* along the air flow at position *x* inside the building is:

$$C(x)V_r + LQdx / A' = C(x+dx)V_r \quad (1.4)$$

where, C denotes the gas concentration, ppm; L is the total length along the air flow, m; A' is the total area for CO_2 production, m^2; Integrating equation (1.4), they obtain:

$$Q = V_r \Delta C' \quad (1.5)$$

where, $\Delta C'$ is the gas concentration change within the building instead of the difference between indoor and outdoor gas concentrations. The equation (1.5) may guide to setup the measurements of gas concentrations. In other words, the equation can provide theoretical background for grid measurements with high space resolution to achieve accurate estimation of natural ventilation rates and gas emissions. However, equation (1.4) is questionable in several aspects. Firstly, the flow and gas distribution inside a cattle building are three dimensional. Hence, a one dimensional mass balance along *dx* cannot be correct. Instead, mass balance should be established based on a three-dimensional finite volume. Secondly, since the equation intends to consider ideal mixing, the heterogeneity of CO_2 production should also been considered. However, the distribution of CO_2 production expressed as Q/A' is still uniform. Additionally, the ventilation rate for mass balance at a micro position *dx* should be local ventilation rate, which changes according to positions. The assumption of constant local ventilation rate expressed as V_r in equation (1.4) is not acceptable. Therefore, grid measurement still cannot surely represent the position for sampling indoor temperature, water vapour and CO_2.

The deficiency of the CO_2 production method provokes scientist to develop other methods to calculate ventilation rates. Demmers et al. (2001) used the pressure difference across the ventilation openings to estimate the ventilation rate. A simple explanation of the method can be illustrated by the following equation.

$$\Delta p = \frac{1}{2A_o c_d^2} \rho V_r^{\ 2} \quad (1.6)$$

where, Δp is the pressure difference, Pa; A_o is the ventilation opening area, m^2; C_d is the discharge coefficient. But the method failed to balance the mass flow rates in and out through all openings of the building. This could be due to the inadequate information on obtaining C_d and the uncertain of measuring Δp. At low wind speeds (<2m s^{-1}), the pressure drop across openings was small and pressure difference cannot be measured reliably. The method is not practical until a more precise

understanding of the C_d for full scale building and more precise pressure sensor for low pressure difference measurement were available.

Tracer gas methods including tracer decay and constant tracer injection are widely used to measure natural ventilation rate. The constant tracer injection can be perceived as an equivalent method with mass balance method discussed in the above section. The method has the same deficiency with the mass balance method except that it can generate uniform release of the tracer. The principle of the tracer gas decay is to dose a quantity of tracer gas in the room and then to record the decay rate of the tracer concentration. Tracer gas decay was concluded as an appropriate technique to quantify ventilation rate from naturally ventilated buildings (Snell et al., 2003; Samer et al., 2011). However, the major shortcoming of the method is that it cannot discover the variation of the ventilation rate during this decay period. Meanwhile, it is difficult to use the meathod record ventilation rates continuously with respect to time.

Based on the discussion of the above methods, assessment of the different methods is necessary in order to find an optimum approach to quantify the natural ventilation rates from dairy cattle buildings.

1.3. The challenge to determine ventilation rates and gas emission rates

In order to quantify ammonia emission rates using CO_2 production model, two factors are prior: the ventilation rates and the average ammonia concentration in the air leaving the cattle building. The first barrier for estimating emission rates from naturally ventilated buildings is lacking of an efficient solution to estimate ventilate rate, which was discussed in section 1.2. The second barrier is lacking of sufficient knowledge on where to measure the gas concentrations to represent the outlet concentration, which was termed as representative gas concentration in this study. Much research has been attempted to develop approaches to find proper sampling positions to measure the representative gas concentration. Demmers et al. (1998) measured the representative gas concentration with two sampling systems: nine positions in openings around the perimeter of the building and a ring sampling line in the building; the ring line gave consistently higher ventilation rates than the perimeter discrete positions. However, the analysis of the influence of the two systems was not extended to emission rate while only perimeter samples were used for the calculation of the emission rate. Zhang et al. (2005), Ngwabie et al. (2009) and Samer et al. (2012) used the gas concentrations at multiple locations inside the building as the representative concentration; the uncertainty introduced by sampling locations was not discussed. Feidler and Müller (2011) recorded gas concentrations at 12 internal points and considered the variability of emissions by using gas concentration at different positions; they argued that more internal sampling positions were required to obtain a representative gas concentration. The conclusion seemed controversial to that drawn by Demmers et al. (1998), who addressed that the internal measuring positions could lead to high uncertainties.

1.4. Modelling naturally ventilated cattle building

Both the ventilation rate and the distribution of gas concentration depend on the external wind and internal airflow patterns including air velocities and turbulences. Due to the importance of the airflow features, devices are required to depict the flow characteristics in the building. Computational Fluid Dynamics (CFD) can offer effective solutions for flows in both spatial and temporal fields. Nielsen (1974) first applied CFD for room airflow prediction. The first CFD study on livestock buildings crudely approximated the representative geometry as a two dimensional rectangle (Choi et al., 1988). Afterwards, more scientists worked to develop CFD models to consider complicated geometrical details of livestock buildings (Sun et al., 2004; Bjerg et al., 2008a; Bjerg et al., 2010). Comprehensive simulations of naturally ventilated cattle buildings were performed by Norton et al. (2010a) and Norton et al. (2010b). All these work proved that CFD had the potential to model the naturally ventilated building and to provide concrete flow information for estimation of ventilation rate.

Issues concerning geometry simplification are always confronted to model naturally ventilated dairy cattle buildings. The detailed geometrical description including animals and partitions is difficult to model directly in a CFD simulation. The complexity of the geometry will require massive meshes and long time to iterate the calculations. The animal occupied zones (AOZ) and was tackled as porous media in the work of Sun et al. (2004), Bjerg et al. (2008a) and Norton et al. (2012a, b). The resistance coefficients of porous media need to be set up in the simulation but there is not enough data to derive the coefficients by measurement. Bjerg et al (2008b) assumed a uniform distribution of animals and extracted part of AOZ to calculate the pressure drop using CFD; the coefficients were obtained by a linear regression from the pressure drop and the associated inlet velocity.

For cattle buildings with slatted floor, two major airflow circulations exist: one is in the room space and one is in the pit headspace under the slatted floor. So far, some studies regarding airflow patterns and pollutant dispersion in dairy cow buildings have been limited to the space above the slatted floor (Norton et al., 2010a; Norton et al., 2010b). However, little attention has been given to the airflow characteristics under the slatted floor, which is important to understand ammonia emission from the slurry surface. Therefore, modelling of slatted floor becomes the main concern in order to illustrate the flow patterns in the pit headspace. The slot width in a real cattle building is about 0.02 m, while the shortest building dimension is generally longer than 5 m. The small ratio of slot width and building dimension prevents a direct modelling of the geometrical details. Therefore, slatted floor is usually tackled as porous media (Sun et al., 2004; Bjerg et al., 2008a; Bjerg et al., 2008b). However, up to date, the difference between a simulation of slatted floor with geometrical details and that using porous media cannot be found in literature. The uncertainty of using porous media should be documented before used in simulation.

1.5. Environmental technologies to curtail emissions

The aim of integration of knowledge on estimating ventilation rate and emission rate is to find solutions to curtail gas emissions from naturally ventilated dairy cow buildings. Measures to reduce the ammonia emission can be achieved by adjusting or regulating factors influencing ammonia emissions. These factors include:

- Diet including intake of crude protein content and feeding schedule (Philippe et al., 2011).
- Livestock type. If the animal is cow, milk yield also affects ammonia emission.
- Housing system such as slatted floor type, ventilation control, etc (Philippe et al., 2011).
- Manure removal system (Philippe et al., 2011).
- Meteorological and indoor climatic conditions: ambient temperature and relative humidity (Philippe et al., 2011), air velocity and turbulence intensities (Saha et al., 2010b).

Altering the diet is regarded as an effective and direct way of achieving reduction of nitrogen excretion in urine. Smits et al. (1995), Elzing and Monteny (1997) found approximately 40% ammonia emission can be abated by feeding cows with low-N diet instead of high-N diet. Possibilities for the reduction of the nitrogen content of the diet were presented by Valk et al. (1990) as well as Bussink and Oenema (1998). Indirect way of lowering nitrogen content in the urine can be achieved through flushing floors (Braam et al., 1997a), decreasing the PH value at the emitting surfaces by addition of acid (Monteny and Erisman, 1998).

Swiestra et al. (1995) reported a comparative study on ammonia emission from cubical houses for cattle with slatted and solid floors; the emission from the compartments with solid floors was about 50% of the emission of the compartment with the slatted floor. Braam et al. (1997b) compared two solid floor system (with and without slop) with the traditional slatted floor system; ammonia emission from the compartment with the non-sloped solid floor was almost equal to that from a compartment with slatted floor; the sloped solid floor reduced ammonia emission by 21% compared to the slatted floor. Studies showed that a reduction of ammonia emission can be expected from design of proper floor systems. But the efficiency was associated with manure removal systems (Braam et al., 1997a; Braam et al., 1997b). Fast removal of the urine on the floor may be superior to floor types in terms of ammonia emission reduction.

For a dairy cow building with slatted floors, the airflow pattern and the air speeds near the slatted floors and in the pit headspace are important factors on ammonia emission (Elzing and Monteny, 1997). Methodologies on regulating the airflow characteristics in that region can be a possibility for ammonia abatement. Saha et al. (2010b) applied an extra pit ventilation system to remove the highly concentrated gases from the pit headspace in a fatting pig room; by utilizing an air purification unit, reductions in the ammonia emission of 37-53% might be achieved. A similar research on partial pit ventilation system applied to a naturally ventilated cattle building in reality has not been found yet.

1.6. Research objectives

The above discussions have highlighted the importance of estimation of ventilation and ammonia emission rate from naturally ventilated dairy cow buildings. Although much research has been attempted to solve the issue (Demmers et al., 1998; Zhang et al., 2005; Ngwabie et al., 2009; Feidler and Müller, 2011; Samer et al., 2012), there is still a gap on techniques to calculate ventilation rate and determination of sampling positions for representative gas concentration. Moreover, low-emission technology should be proposed to dairy cattle buildings. A concept of partial pit ventilation system with air purification units may have the potential to reduce gas emissions and improve the air quality in cattle buildings. Thus, the main objective of the PhD thesis was to establish a validated CFD model to predict ventilation rate as well as determine the sampling positions for representative gas concentration, and to investigate the potential of a partial pit ventilation system to reduce gas emissions. The specific objectives of this study were to:

- measure and quantify ammonia emissions in the two cow buildings and study the effect of the climatic factors (external wind speed, wind direction, external air temperature) on ammonia emissions;
- evaluate velocity and turbulence characteristics of the airflow in two naturally ventilated dairy cattle buildings in terms of statistical descriptors, such as autocorrelation, kinetic energy, turbulence energy dissipation rate, integral time and length scale of turbulence, Kolmogorov microscale of length;
- develop a CFD model to calculate air exchange rate (AER) in one of the cow buildings and evaluate the performance of tracer gas decay and CO_2 balance method for quantifying the AER as well as determine optimum positions to sample representative CO_2 concentration in the exit air;
- investigate the ability of a partial pit ventilation system to reduce gas emissions by scale model measurements and CFD simulations;
- investigate the difference of airflow and pollutant transportation in the pit headspace between modelling slatted floor directly and modelling slatted floor as porous media using large eddy simulations;
- investigate the potential of a partial ventilation system applied to a full scale naturally ventilated dairy cattle building to reduce ammonia emissions by adopting CFD method.

1.7. Outline of this thesis

This thesis seeks to determine ventilation and emission rate from naturally ventilated dairy cattle buildings as well as to propose a systematic approach to curtail gas emissions. In chapter 2, ammonia and greenhouse gas concentrations were measured in the two buildings. Emissions of ammonia and methane were quantified using CO_2 balance method. The effect of climatic factors including the external wind speed, direction, the internal airflow velocity, the external and internal

air temperature on emissions of ammonia and methane were discussed. In chapter 3, three dimensional air velocities were measured outside and inside two naturally ventilated cattle buildings; the velocity and turbulence characteristics were presented to provide insight into the variables related to natural ventilation rate and distribution of gas concentrations, consequently related to gas emissions. Different techniques to estimate ventilation rate was assessed in chapter 4. The techniques included tracer gas decay, CO_2 balance and integration of the volume flow rates through outlet openings. The sampling locations were discussed to gain representative gas concentration in the exit air in order to predict gas emissions using CO_2 balance method. The subject of chapter 5 was to test the capability of partial pit ventilation system to reduce emission in a laboratory condition using a 1:2 scale model. In chapter 6, the similar investigation was also completed via CFD simulations using Reynolds-averaged Navior-Stokes turbulence models. So far, partial pit ventilation system was not applied to the existing cattle buildings. Thus the potential of the system to abate emission was studied by CFD models. The technical issue on dealing with slatted floors should be addressed before applying partial pit ventilation system to full scale buildings. The uncertainty of modelling slatted floor as porous media was described in Chapter 7. The potential of partial pit ventilation system to curtail emissions from full scale buildings was eventually tested by CFD methods and covered the chapter 8. The final chapter 9 summarized the main findings of the thesis.

References

Battye, W., Aneja, V., Roelle, P., 2003. Evaluation and Improvement of Ammonia Emissions Inventories. Atmospheric Environment 37, 3873-3883.

Bjerg, B., Zhang, G., Kai, P., 2008a. CFD investigations of a partly pit ventilation system as method to reduce ammonia emission from pig production units. The Eighth ASABE International Livestock Environment Symposium (ILES Ⅷ)

Bjerg B., Zhang, G., Kai, P., 2008b. Porous media as boundary condition for air inlet, slatted floor and animal occupied zone in numerical simulation of airflow in a pig unit. AgEng2008 International Conference on Agricultural Engineering, Hersonissos, Crete-Greece.

Bjerg, B., Andersen M., 2010. Numerical simulation of a pit exhausts system for reduction of ammonia emission from a naturally ventilated cattle building. XVIIth world congress of the international commission of agricultural and biosystems engineering (CIGR). Quebec City, Canada.

Braam, C. R., Ketelaars, J.J.M.H., Smits, M.C.J., 1997a. Effects of Floor Design and Floor Cleaning on Ammonia Emission from Cubicle Houses for Dairy Cows. *Netherlands Journal of Agricultural Science* 45, 49-64.

Braam, C. R., Smits, M.C.J., Gunnink, H., Swierstra, D., 1997b. Ammonia Emission from a Double-sloped Solid Floor in a Cubic House for Dairy Cows. *Journal of Agricultural Engineering Research* 68(4), 375-386.

Bussink, D.W., Oenema, O., 1998. Ammonia Volatilization from Dairy Farming Systems in Temperate Areas: A Review. *Nutrient Cycling in Agroecosystems* 51, 19-33.

Choi, K., Albright, L.D., Timmons, M.B., 1988. An application of the *k-ε* turbulence model to predict air distribution in a slot ventilated enclosure. Transactions of the ASAE 33, 274-278.

CIGR, 1984. Report of Working Group on Climatization of Animal Houses – Heat and Moisture Production at Animal and House Levels. *Scottish Farm Building Investigation Unit, Craibstone, Aberdeen, Scotland*.

CIGR, 2002. Report of Working Group on Climatization of Animal Houses – Heat and Moisture Production at Animal and House Levels. *CIGR Section II, Commission International Du Genie Rural (International Commission of Agricultural Engineering)*.

Demmers, T.G.M., Burgess, L.R., Short, J.L., Phillips, V.R., Clark, J.A., Wathes., C.M., 1998. First experiences with methods to measure ammonia emissions from naturally ventilated cattle buildings in the U.K. *Atmospheric Environment* 32,285-293.

Demmers, T.G.M., Burgess, L.R., Phillips, V.R., Clark, J.A., Wathes., C.M., 2000. Assessment of Techniques for Measuring the Ventilation Rate, using an Experimental Building Section. *Journal of Agricultural Engineering Research* 76,71-81.

Demmers, T.G.M., Phillips, V.R., Short, J.L., Burgess, L.R., Hoxey, R.P., Wathes., C.M., 2001.Validation of Ventilation Rate Measurement Methods and the Ammonia Emission from Naturally Ventilated Dairy and Beef Buildings in the United Kingdom. *Journal of Agricultural Engineering Research* 79 (1), 107-116.

Elzing, A., Monteny, G.J., 1997. Ammonia emission from a scale model of a dairy-cow house. *Transactions of the ASAE* 40: 713-720.

Feidler, A.M., Müller, H.J., 2011. Emissions of ammonia and methane from a livestock building natural cross ventilation. *Meteorologische Zeitschrift* 20 (1), 059-065.

Gyldenkærne, S., Mikkelsen, M.H., 2007. Projection of the Ammonia Emission from Denmark from 2005 until 2025. *Research notes from NERI No.239*, 2007.

Hutchings, N. J., Sommer, S. G., Andersen, J.M., W.A.H, 2001. A Detailed Ammonia Emission Inventory for Denmark. *Atmospheric Environment* 35, 1959-1968.

Monteny, G.J., Erisman, J.W., 1998. Ammonia Emission from Dairy Cow Buildings: a Review of Measurement Techniques, Influencing Factors and Possibilities for reduction. *Netherlands Journal of Agricultural Science* 46, 225-247.

Nielsen P.V. 1974. Flow in air-conditioned rooms. Ph.D. Thesis, Technical University of Denmark,23 Copenhagen, Denmark.

Ngwabie, N.M., Jeppsson, K.H., Nimmermark, S., Swensson, C., Gustafsson, G., 2009. Multi-location Measurements of Greenhouse Gases and Emission rates of Methane and Ammonia from a Naturally Ventilated Barn for Dairy Cows. *Biosystems Engineering* 103, 68-77.

Norton, T., Grant, J., Fallon, R., Sun, D.W., 2010a. Assessing the ventilation effectiveness of naturally ventilated livestock buildings under wind dominated conditions using computational fluid dynamics. Biosystems engineering 103 (1), 78-99.

Norton, T., Grant, J., Fallon, R., Sun, D.W., 2010b. A computational fluid dynamics study of air mixing in a naturally ventilated livestock building with different porous eave opening conditions. Biosystems engineering 106 (2), 125-137.

Pederson, S., Takai, H., Johnsen, J.O., Metz, J.H.M., Groot Koerkamp, P.W.G., Uenk, G.H., Phillips, V.R., Holden, M.R., Sneath, R.W., Short, J.L.L., White, R.P., Hartung, J., Seedorf, J., Schroder, M., Linkert, K.H., Wathes, C.M., 1998. A Comparison of Three Balance Methods for Calculating Ventilation Rates in Livestock Buildings. *Journal of Agricultural Engineering Research* 70,25-37.

Pederson, S., 2006. Agricultural Best Management Practices in Denmark. The workshop on Agricultrual Air Quality: State of Science, 2006. The Ecologial Society of America, 56-67.

Philippe, F.X., Cabaraux, J.F., Nicks, B., 2011. Ammonia Emissions from Pig Houses: Influencing Factors and Mitigation Techniques. *Agriculture, Ecosystems and Environment 141*, 245-260.

Samer, M., Fiedler, M., Muller, H.J., Glaser, M., Ammon, C., Berg, W., Sanftleben, P., Brunsch, R., 2011. Winter Measurements of Air Exchange Rates using Tracer Gas Technique and Quantification of Gaseous Emissions from a Naturally Ventilated Dairy Barn. *Applied Engineering in Agriculture* 27(6), 1015-1025.

Samer, M., Ammon, C., Loebsin, C., Fiedler, M., Berg, W., Sanftleben, P., Brunsch, R., 2012.Moisture Balance and Tracer Gas Technique for Ventilation Rates Measurement and Greenhouse Gases and Ammonia Emissions Quantification in Naturally Ventialted Buildings. *Building and environment* 50, 10-20.

Saha, C.K., Zhang, G., Ni, J., 2010a. Airflow and Concentration Characterisation and Ammonia Mass transfer Modelling in Wind Tunnel Studies. Biosystems Engineering 107 (4), 279-287.

Saha, C.K., Zhang, G., Kai, P., Bjerg, B., 2010b. Effects of a partial pit ventilation system on indoor air quality an ammonia emission from a fattening pig room. Biosystems Engineering 105 (3), 328-340.

Smits, M.C.J., Valk, H., Elzing, A., Keen, A., 1995. Effect of Protein Nutrition on Ammonia Emission from a Cubicle House for Dairy Cattle. *Livestock Production Science* 44: 147-156.

Snell, H.G.J., Seipelt, F., Van Den Weghe, H.F.A., 2003. Ventilation Rates and Gaseous Emissions from Naturally Ventilated Dairy Houses. Biosystems Engineering 86 (1), 67-73.

Strøm, J.S., 1978. Heat Loss from Cattle, Swine and Poultry as Basis for Design of Environmental Control Systems in Livestock Buildings. SBI-Landbrugsbyggeri 55, Danish Research Institute, Denmark (In Danish)

Sun, H.W., Keener, H.M., Deng, W., Michel, F., 2004. Development and Validation of 3-D Models to Simulate Airflow and Ammonia Distribution in a High-rise Hog Building during Summer and Winter Conditions. *Agricultural Engineering International CIGR Journal* 6, Manuscript BC 04 044.

Swiestra, D., Smits, M.C.J., Kroodsma, w., 1995. Ammonia Emission from Cubicle Houses for Cattle with Slatted and Solid Floors. *Journal of Agricultural Research* 62, 127-132.

Teye, F.K., Hautala, M., 2007. Measuring Ventilation Rates in Dairy Buildings. International Journal of Ventilation 6 (3), 247-256.

Valk, H., Klein Poelhuis H.W., Wentink, H.J., 1990. Effect of Fibrous and Starchy Carbohydrates Inconcentrates as Supplements in a Herbage-based Diet for High Yielding Dairy Cows. *Netherlands Journal of Agricultural Science* 38: 475-486.

Van Breemen, N., Burrough, P.A., Velthorst, E.J., Van Dobben, H.F., De Wit, T., Ridder, T.B., Reinders, H.F.R., 1982. Soil Acideification from Atmospheric Ammonium Sulphate in Forest Canopy Throughfall. Nature 299: 548-550.

Zapletal, M., Chroust, P., 2006. Spatial Distribution of Ammonia Emissions on the Territory of the Czech Republic. The workshop on Agricultrual Air Quality: State of Science, 4 June 2006. The Ecologial Society of America, 1258-1262.

Zhang, G., Strom, J. S., Li, B., Rom, H.B., Morsing, S., Dahl, P., Wang, C., 2005. Emission of Ammonia and other Contaminant Gases from Naturally Ventilated Dairy Cattle Buildings. *Biosystems Engineering* 92 (3), 355-364.

Chapter 2

Ammonia and methane emissions from two naturally ventilated dairy cattle buildings and the influence of the climatic factors on ammonia emissions

Paper I:

Wu, W., Zhang, G., Kai, P., 2012. **Ammonia and Methane Emissions from Two Naturally Ventilated Dairy Cattle Buildings and the Influence of the Climatic Factors on Ammonia Emissions**. *Atmospheric Environment* 61, 232-243.

Abstract

Based on the requirement of the international conventions, there is a pressing need for inventory of NH_3, CH_4, CO_2 and N_2O emissions from livestock buildings. The main aim of this study was to quantify the gas emissions and investigate the influence of the climatic factors on emissions. The measurements were carried out in two naturally ventilated dairy cattle buildings with different layouts, floor types and manure management systems during three periods covering winter and summer time. Air temperature and the three dimensional air velocities inside and outside the buildings were recorded over the course of summer period. Emission rates were determined by CO_2 production model. The results showed that the internal concentrations of NH_3, CH_4 and CO_2 were increased or decreased simultaneously. Low concentration of N_2O was measured outside and inside the buildings; the difference of the concentrations were also very low. The variation of CH_4 and CO_2 concentrations showed a strong correlation. The NH_3 emission rates varied from 32-77 g HPU^{-1} d^{-1} in building 1 and varied from 18-30 g HPU^{-1} d^{-1} in building 2. The average emission of CH_4 was 290 and 230 g HPU^{-1} d^{-1} from building 1 and 2, respectively. Diurnal pattern was found for NH_3 and CH_4 emission rates. From multiple linear regression models, there was a significant linear relationship between NH_3 emission rates and climatic factors including the external wind speed as well as the air temperature ($P<0.001$), but not with the external wind directions ($P>0.05$).

Key words: *Ammonia emission; air exchange rate; climatic factors; dairy housing; CO_2 production model*

2.1. Introduction

Emissions of ammonia (NH_3) to the atmosphere cause acidification of soil and increase eutrophication to aquatic systems, while emissions of greenhouse gases (nitrous oxide (N_2O), carbon dioxide (CO_2) and methane (CH_4)) to the atmosphere influence the global climate. Approximately 97% of the ammonia emission in Denmark is related to animal husbandry. About 16% of the total greenhouse gas emission originates from the agricultural sector. Denmark has approved the 1999 protocol to abate the ammonia emission to 56,800 tonnes NH_3-N per year by 2010. The Kyoto protocol requires Denmark to reduce the greenhouse gas emission by 22% compared with the level in 1990 till the first commitment period (2008-2012). Accurate inventories of NH_3 and greenhouse gas emissions from livestock buildings are quite essential to fulfil the obligations required in the international conventions.

Accurate quantification of gas emissions from livestock buildings to the atmosphere requires accurate determination of the ventilation rate and the representative gas concentration in the exhaust air. Natural ventilation rates of livestock buildings can be measured either directly by monitoring pressure differences over the ventilation openings (Demmers, 1997), or indirectly, using tracer gas methods (Demmers et al., 1998). Demmers et al. (2001) reported that the pressure difference method failed to balance the mass flow rates in and out through all openings. The large openings in naturally ventilated livestock buildings such as dairy cow houses also make the pressure difference method difficult to be applied. Tracer gas method can be used in two manners: decay and constant injection. The approach of tracer gas decay cannot be used to monitor ventilation rate continuously. The method of constant injection of tracer gas is equivalent to the CO_2 balance method, which assumes that CO_2 produced by animals can be calculated based on production models (CIGR, 2002). The method can be applied to gain continuous natural ventilation rates and gas emissions. Therefore, only the CO_2 production model is discussed in this paper.

For dairy cattle buildings, ammonia and other gas emission levels primarily depend on housing system, floor type and manure management system. Several researches have been carried out in order to reduce emissions by using different floor and manure management systems. Swierstra et al. (1995) performed measurements of ammonia emissions from an experimental dairy cattle house with either slatted or solid floors; and concluded that the emission from the compartments with solid floors and a central gutter was about 50% of the emission from the compartments with slatted floors. Braam et al. (1997a) investigated ammonia emissions from a double-sloped solid floor scraped 12 times per day in a mechanically ventilated dairy cow house; the solid floor with under-floor slurry storage can reduce ammonia by about 50% when compared with slatted floor. Braam et al. (1997b) compared the ammonia emissions from two different solid floor systems with emissions from the traditional slatted floor systems; the solid floor without a slope did not result in significant ammonia reduction while the solid floor with a 3% slope reduced ammonia emissions by 21% compared to a slatted floor. Zhang et al (2005) estimated emission rates

of NH_3, CH_4 and N_2O from naturally ventilated dairy cattle buildings with different floor types and manure-handling systems; the lowest ammonia emission was from buildings with solid, drained floors with smooth surface. However, they also found that urine puddles remained in many locations in a building with uneven surface of the concrete floor resulted in high ammonia emissions. Although there are previous studies on quantifying NH_3 emissions from different floor systems, these are limited in numbers and more case studies especially with respect to naturally ventilated buildings are still needed.

The interaction of the air in the naturally ventilated livestock house and the external atmosphere causes the dispersion of ammonia and greenhouse gases from livestock buildings to the surrounding atmospheric environment. The key climatic factors influencing the gas emissions include the external air temperature, the external wind speeds and directions. Pereira et al. (2010) reported direct measurements of NH_3 from 3 dairy cattle buildings in Portugal and observed positive relationships (P<0.05) between NH_3 emissions and inside mean air temperature by using multiple linear regression models. Fiedler and Müller (2011) measured the NH_3 concentration from two naturally ventilated cow sheds and found that the derived NH_3 emission rate strongly depended on the outside conditions such as wind direction and speed. Schrade et al. (2012) quantified NH_3 emissions from 6 naturally ventilated cubicle barns for dairy cows and employed a linear mixed-effects model to infer the significant influence of wind speed and outside temperature on NH_3 emissions. To map the NH_3 emissions with climatic parameters for national inventories of emissions, there is a strong need for reliable and detailed NH_3 emission data as well as climatic factors at high spatial and temporal resolution.

The objectives of this study were to:

(1) measure ammonia and greenhouse gas concentrations in two naturally ventilated dairy cow buildings;
(2) quantify the emissions of NH_3 and CH_4 using CO_2 production model;
(3) evaluate the effect of the climatic factors (external wind speed, wind direction, external air temperature) on NH_3 emissions.

2.2. Materials and Methods

The measurement periods in building 1: from Sep-16 to Oct-12, 2010; from Nov-12 to Nov-26, 2010 and from May-31 to Jun-11, 2011. The measurement periods in building 2 were: from Oct-18 to Nov-08, 2010; from Dec-02 to Dec-22, 2010 and from Jun-20 to Jul-14, 2011

2.2.1. Buildings

Two free-stall cubical dairy cattle buildings, which was naturally ventilated, in the Mid-west of Jutland with different housing and manure management systems were selected for the investigations. The measurement was not interfered by daily management.

Building 1 (see Fig. 2.1 a) was approximately 85 m long and 24 m wide. Measured from floor level, the height to the eave was 3.0 m, and the height to the ridge was 7.5 m and the height of the side wall was 1.2 m. The height of the side wall openings was 1.5 m. The width of the ridge opening was 0.6 m. Curtains for adjusting sidewall openings were mounted on the low edge of the opening and can be manually pulled up. The curtain height in the first two measurement periods was about 0.8 m and the curtains were fully open in the third period. One end of the building was entirely open with a dimension of 20.11×2.45 m, whereas the other end was closed except for a 5.7 x 2.75 m gate. The milking parlour was located in this end of the building. The feeding alley and resting area for cow to lie down had a raised platform. A narrow slatted floor in the centre of a lower walkway for cows was made of concrete. Underneath the slatted floors was manure channel equipped with scrapers. The manure in the gutters was scraped 12 times a day into manure storage tanks outside the buildings. Two floor scrapers run 4 times a day to remove the manure on the lower walkway. There were another two buildings (Fig. 2.1a) near the measured building, which had dimensions of 58.2 m×24 m×7.6 m and 48.6 m×24 m×8.4 m, respectively. They were 10 m and 49 m away from the measurement building. The closer one was also a dairy cattle house and the farther one was a storehouse. Behind the measurement building were a workshop, living houses and some trees in the right corner. Open field were anywhere else.

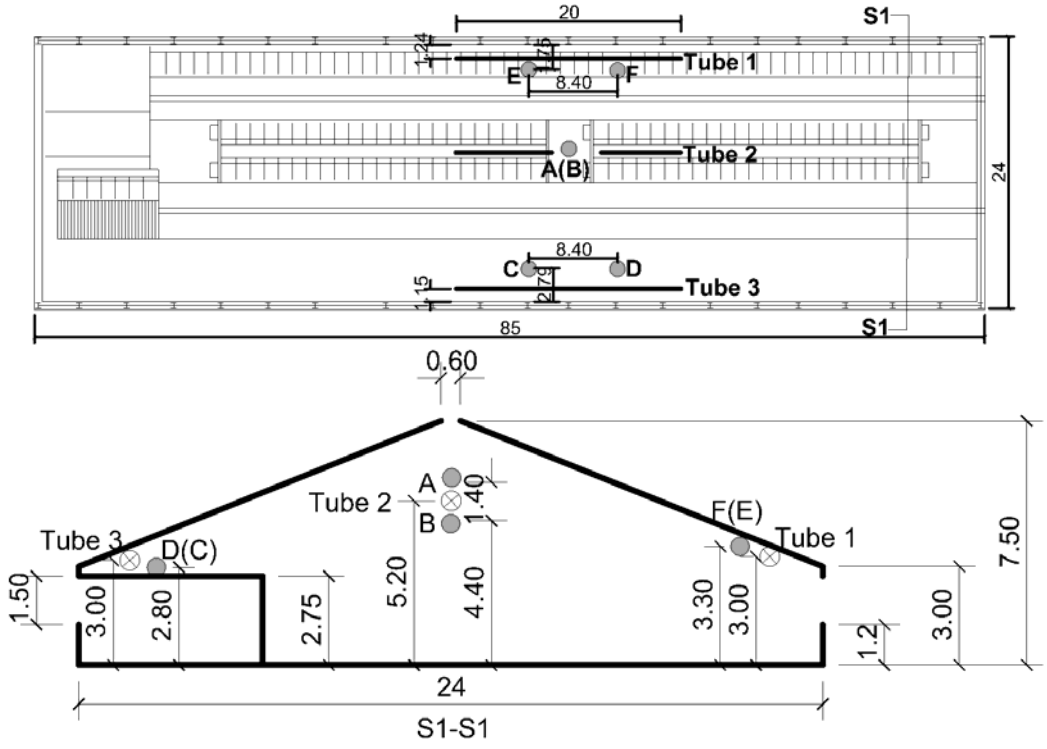

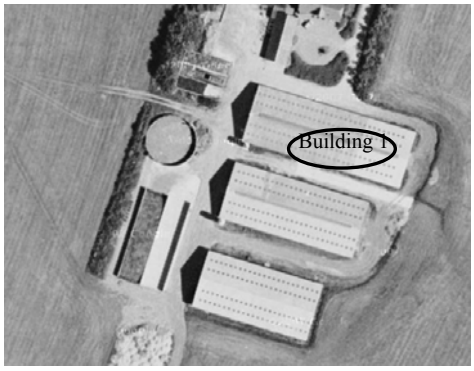

(a) Building 1

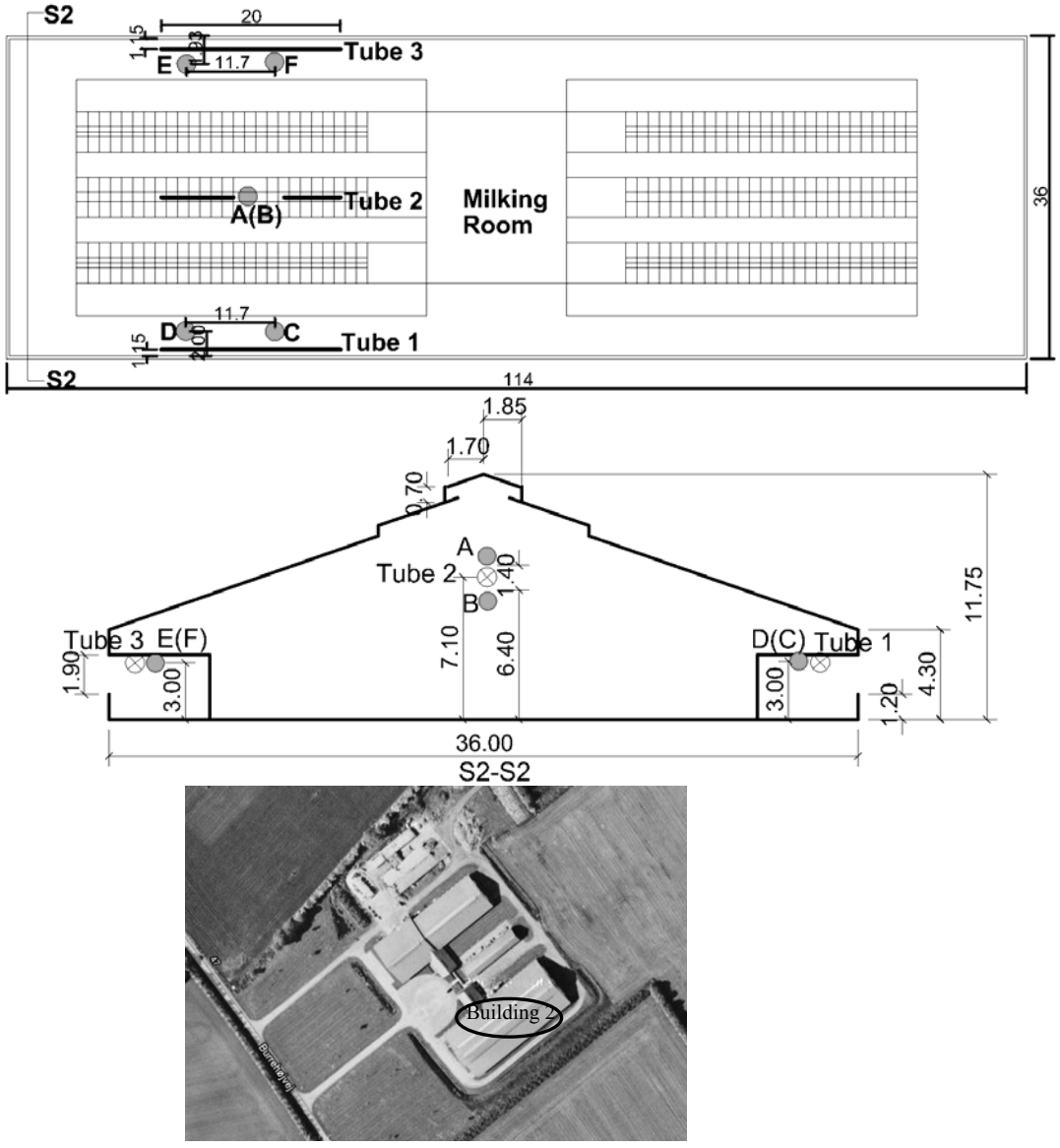

(b) Building 2

Fig. 2.1 Schematic of the measured section in the buildings and the sensor positions: Solid circles marked with A, B, C, D, E, F denote positions for velocity measurements; Thick lines and circles with cross denote the sampling locations for gas measurements.

Building 2 (see Fig. 2.1 b) was about 114 m long and 36 m wide. The building was divided into two sections, in the middle of which was a milking parlour. Measured from floor level, the height to the eave was 4.3 m, and the height to the ridge was 11.75 m, the height of the side wall was 1.2 m. The height of the sidewall openings was 1.9 m. There were two gates at one end of the barn and each of them had a dimension of 4.85×3.40 m. The width of the ridge opening was 2.5 m. The ridge opening was confined by a ridge space. The detailed roof configuration and the dimension of the building are shown in Fig.1b. The side wall openings were equipped with automatically controlled curtains. During winter, the curtains were adjusted according to wind speed. During summer, they were fully open. The aisle for feeding and the resting area for cow had a raised platform. The walking alley between the cubicles had slatted floor over a manure channel. A scraper robot scraped the entire slatted floor every second hour. The pit scrapers under slatted floor run 4 times a day and remove the manure to an outside slurry tank

2.2.2. Production and feed

In building 1, there were 165 cows with an average weight of 625 kg and an average milk yield of 31 kg per day. The percentage of the milk protein was 3.4%. The daily feed consumption per cow was: 8 kg grass, 4 kg maize and 8 kg concentrated food. The crude protein was 3.6 kg cow^{-1} day^{-1}. Building 2 held 125-128 (Holstein Frisian) dairy cows with an average weight of 625 kg on average and milk yield of 28-32 kg per day on average. The percentage of the milk protein was 3.7%. There were also 14-23 calves with a weight of 450-500 kg on average in this section. The feeding procedure was very complicated due to other experiments. The average feed consumption was about 47.5 kg cow^{-1} day^{-1} with crude protein intake of 3.7 kg cow^{-1} day^{-1}. The feeding time for the two buildings was around 11 am. Each cow got individually amount of concentrates in the milking parlour. The cows were milked twice per day (7 am and 4 pm) in building 1. The cows in building 2 were milked by automatic milking system.

2.2.3. Measurement setup

Gases inside the buildings were sampled by three 20 m long FEP (tetraflouroethylene-hexaflouropropylene) tubes. Each tube had 20 uniform distributed sampling openings. Each open was made to ensure the same airflow rate so that the air sampled at each tube represented the average of the 20 sampling openings. Demmers et al. (2001) reported large error in ventilation rate estimate using internal sampling points; they also indicated that no obvious zones or locations, which offered a representative concentration, could be identified within the building section. Another research carried out by Demmers et al. (1998) showed that the mean tracer gas concentration measured in the openings was better to represent the gas concentration in the exit air than that measured around a ring line in the building. Therefore, sampling tubes were placed near ventilation openings. Two of the tubes (Tube 1 and Tube 3) were at two sides of the building around 1.2 m away from the side wall openings and 3.0 m above the floor. Tube 2 was below the

ridge opening in the middle of the building and 7.1 m above the floor. Gases at two outside positions about 2 m from a side wall were also sampled as background reference. The transport tubes connecting the sampling tubes and the gas monitoring instruments were between 9 m and 50 m long with heating cables attached and were insulated in a plastic foam cover tube to avoid condensation of water vapor. All the sampling tubes and transport tubes were of FEP (tetraflouroethylene-hexaflouropropylene) with 6 mm inside diameter and 1 mm of tube thickness.

The gas concentrations were measured applying Innova Photoacoustic Field Gas monitor 1312 coupled with a multipoint sampler 1303 (INNOVA air Tech Instruments A/S, Denmark). The monitor equipped with filters at the inlet was placed inside a van parked outside the building. Five channels of the multiplexer 1303 were used to connect to the three indoor sampling lines and two outdoor measurement positions. Each channel had a suction pump with Teflon membrane (Model Eg 7130-4AY-RLT, 19w, GEFEG Motoren) with a flow rate of about 30 l s^{-1} to deliver the sampled air to the multiplexer. The sampling period for each measurement was 20 s, followed by 20 s cleaning time to replace the air in the measuring chamber of INNOVA before a new measurement started. Each channel was repeated six times. The measurement period for each channel was 5 min before switching to the next channel. To reduce measurement uncertainties caused by delay effects (Rom and Zhang, 2010), the NH_3 concentration at each location was determined by the average of the last three repeated values in the measurement, while other gas concentrations were calculated as the mean of all the six repeated values.

Air velocities were measured by three dimensional ultrasonic anemometers – WindMaster (Gill instruments Ltd, Hampshire, UK). The detailed information of the WindMaster can be found in Wu et al. (2012). The air velocities inside the buildings were recorded at 6 positions (Fig. 2.1a-b). Four velocity sensors (C, D, E and F) were located near the sidewall openings. Two velocity sensors (A and B) were placed in the centre of the buildings near the ridge openings. The positions for velocity measurement in building 1 and 2 are shown in Fig.1 a-b. The external wind speeds and directions were also monitored at 10 m above the ground. All the anemometers were connected to a multi-port adapter supplying electricity power to the anemometers and collecting three-dimensional velocities. The output frequency was 20 Hz.

The air temperature was recorded at one position inside the building and at one position outside the building. The temperature sensor was a standard type K thermocouple with an operating range of -40 to 85 °C and an accuracy of ±1 °C. Temperature readings were taken every 10 min through the entire measurement period.

2.2.4. Calculations of ventilation and emission rate

The CO_2 production model for dairy cows (CIGR, 2002) was used to calculate CO_2 produced in house and used to determine the air exchange rate. Following mass balance, ventilation rate can be calculated as

$$VR = \frac{10^6 E_{CO_2}}{C_{CO_2,in} - C_{CO_2,out}} \quad (2.1)$$

where, VR was ventilation rate, $m^3 h^{-1}$; E_{CO_2} was total CO_2 production from the measured building, kg s^{-1}; $C_{CO_2,in}$ was the CO_2 concentration inside buildings, mg m^{-3}; $C_{CO_2,out}$ was the minimum CO_2 concentration of the two outside sampling positions, mg m^{-3}.

The emission rate was expressed as emission per heat production unit (HPU), which was defined as 1000 W total heat produced by the animals at an ambient temperature 20 °C (Zhang et al, 2005). The emission rate per HPU was thus stated as

$$E_i = VR(C_{i,in} - C_{i,out}) / H_{total} \quad (2.2)$$

where, E_i was the emission rate per HPU of gas i, mg h^{-1} HPU^{-1}; i, symbolized the measured gases, NH_3, CH_4 and N_2O; $C_{i,in}$ was the average concentration of gas i at all the inside sampling positions, mg m^{-3}; $C_{i,out}$ was the minimum CO_2 concentration of gas i at the two outside sampling positions, mg m^{-3}; H_{total} was the total HPU produced by cows in the measured building. HPU per cow was derived based on body weight and milk production without considering pregnancy. The detailed description of HPU can be found elsewhere (Zhang et al, 2005; CIGR, 2002).

2.2.5. Statistical analysis

A multiple linear regression model was used to describe the relationships between NH_3 emission (E_{NH3}) and the influencing factors such as wind directions (WD), wind speeds (WS), outside air temperature (T_O), inside air temperature (T_i) and inside air velocity (V_i).

Data of E_{NH3} was preprocessed by a natural logarithmic transformation before the statistical analysis was carried out. The co-linearity of the influencing factors was also considered to take account into the effect of the interactions among different variables. This led to the following formula (Verzani, 2004):

$$\log_e(E_{NH_3}) = \sum \beta_i x_i + \sum \beta_{ij}(x_i \times x_j) + \varepsilon \quad (2.3)$$

where, β was the coefficient of the associated influencing factors; x was the influencing factors, which had significant effect on E_{NH3}; i and j represented different factors (WD, WS, T_O, T_i or V_i); $x_i \times x_j$ denoted the interaction between two influencing factors; ε was the error. The aim of the multiple linear regression was to comprehensively test the significance (P<0.05) of the influencing factors on the NH_3 emissions.

2.3. Results

2.3.1. Gas concentrations

Daily average concentration of NH_3, CH_4, CO_2 and N_2O over the three measurement periods is given in Fig. 2.2. The internal concentrations of NH_3, CH_4 and CO_2 was increased or decreased simultaneously.

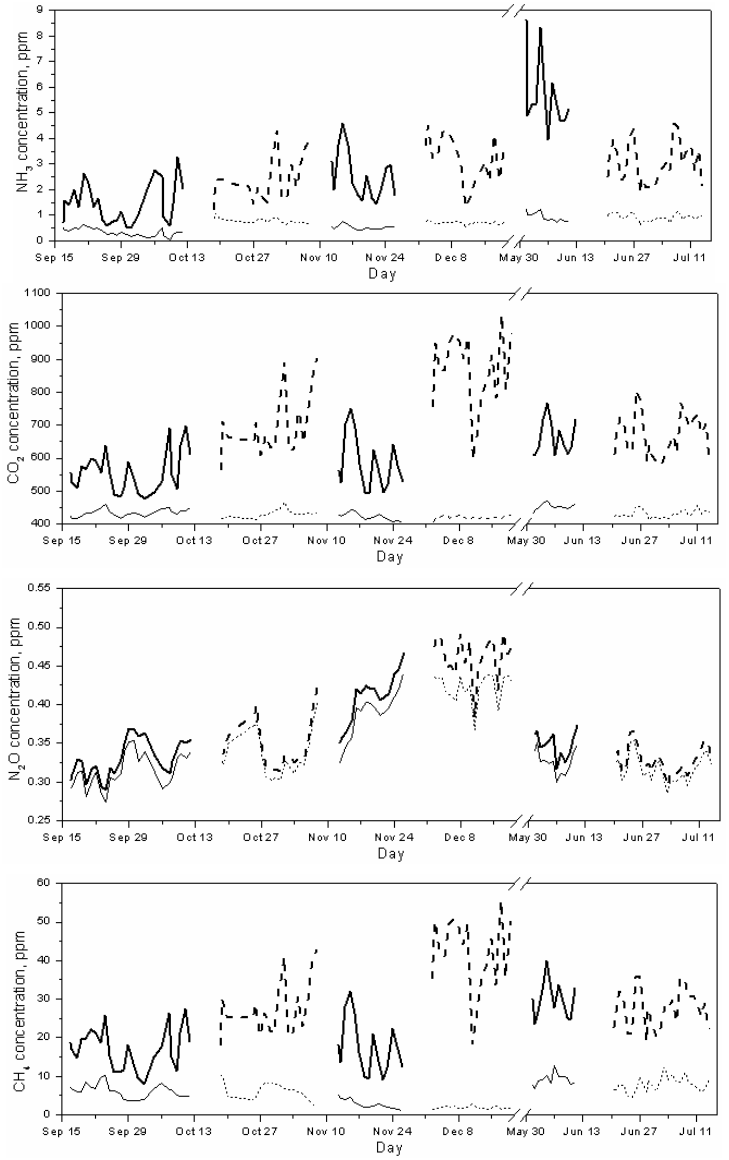

Fig. 2.2 Daily average concentration of NH_3, CO_2, N_2O and CH_4 over the three measurement periods (solid line-building 1, dashed line-building 2; thick line-inside building, thin -outside building). The measurement before and after the breakpoint was finished in 2010 and 2011, respectively.

Table 2.1 shows the mean value, standard deviation, maximum value and minimum value of indoor and outdoor gas concentrations of building 1 and 2 during the three measurement periods.

Table 2.1 Indoor and outdoor gas concentrations (Mean, standard deviation, maximum and minimum) of building 1 and 2 during the three measurement periods.

Gas	Period (MM/DD/YYYY)	Building	Concentration, ppm							
			Indoor				Outdoor			
			Mean	SD*	Max	Min	Mean	SD*	Max	Min
NH_3	09/17/2010-10/12/2010	1	1.46	0.79	3.29	0.50	0.34	0.15	0.64	0.04
	10/18/2010-11/08/2010	2	2.43	0.91	4.31	1.25	0.78	0.11	1.08	0.63
	11/12/2010-11/26/2010	1	2.54	0.94	4.57	1.46	0.53	0.09	0.76	0.41
	12/02/2010-12/22/2010	2	3.30	0.89	4.50	1.32	0.73	0.06	0.82	0.57
	05/31/2011-06/11/2011	1	5.73	1.42	8.62	3.96	0.94	0.18	1.25	0.73
	06/20/2011-07/14/2011	2	3.03	0.81	4.59	1.90	0.92	0.15	1.15	0.62
CO_2	09/17/2010-10/12/2010	1	559	62	697	477	433	11	458	417
	10/18/2010-11/08/2010	2	701	98	903	564	430	12	466	414
	11/12/2010-11/26/2010	1	583	82	749	492	422	11	442	405
	12/02/2010-12/22/2010	2	892	120	1066	598	422	8	439	408
	05/31/2011-06/11/2011	1	660	54	766	607	452	10	470	432
	06/20/2011-07/14/2011	2	668	65	805	576	430	12	456	413
CH_4	09/17/2010-10/12/2010	1	17.16	5.22	27.48	7.93	6.10	1.76	10.24	3.65
	10/18/2010-11/08/2010	2	27.65	7.36	42.79	18.13	6.27	2.27	10.21	2.54
	11/12/2010-11/26/2010	1	17.56	7.15	32.14	9.18	2.73	1.24	5.22	1.22
	12/02/2010-12/22/2010	2	43.55	10.00	57.33	18.39	1.83	0.35	2.84	1.48
	05/31/2011-06/11/2011	1	29.88	4.71	39.94	23.44	9.06	1.59	12.83	6.69
	06/20/2011-07/14/2011	2	27.37	5.18	35.98	19.14	7.85	1.88	12.26	4.50
N_2O	09/17/2010-10/12/2010	1	0.33	0.02	0.37	0.29	0.31	0.02	0.35	0.27
	10/18/2010-11/08/2010	2	0.35	0.03	0.43	0.31	0.34	0.03	0.40	0.30
	11/12/2010-11/26/2010	1	0.41	0.03	0.47	0.35	0.39	0.03	0.44	0.33
	12/02/2010-12/22/2010	2	0.47	0.03	0.54	0.38	0.43	0.02	0.45	0.37
	05/31/2011-06/11/2011	1	0.35	0.02	0.37	0.32	0.33	0.02	0.35	0.30
	06/20/2011-07/14/2011	2	0.33	0.02	0.36	0.30	0.32	0.02	0.35	0.29

*SD – Standard Deviation

The average concentration of NH_3 in building 1 was 1.46, 2.54 and 5.73 ppm for the three measurement periods, respectively. Average NH_3 concentrations of the three periods in building 2 were 2.43, 3.30 and 3.03 ppm. The average CO_2 concentrations of three measurement periods were 558, 583, 660 ppm for building 1 and 701, 891, 668 ppm for building 2. The average CH_4 concentrations of three measurement periods were 17.16, 17.56, 29.88 ppm for building 1 and 27.65, 43.55, 27.36 ppm for building 2. Inside and outside concentrations of N_2O were in the same level and they were very low. The N_2O concentration level was in the range of 0.29-0.47 ppm for building 1 and 0.30-0.54 ppm for building 2.

A strong correlation (R^2 is 0.94 for building 1, 0.97 for building 2) was found between the concentrations of CH_4 and CO_2 (Fig. 2.3 a-b). The ratio of CH_4 and CO_2 concentration was 0.05 for building 1 and 0.04 for building 2.

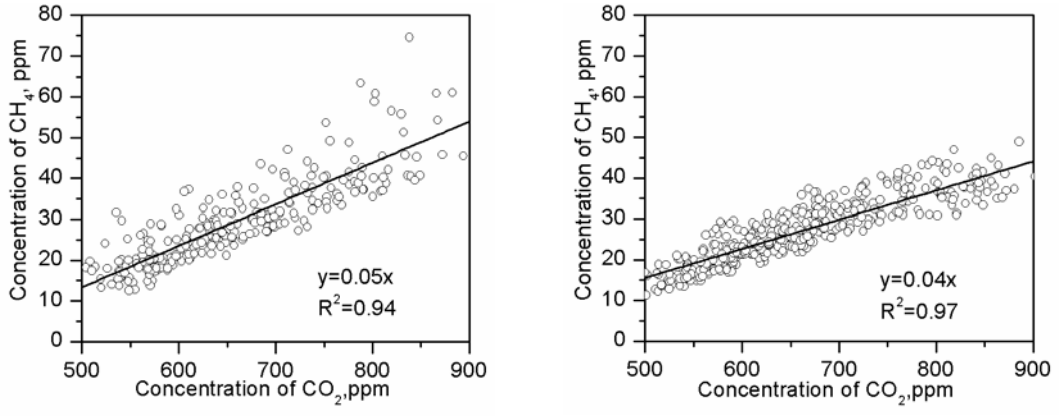

(a) Building 1 (b) Building 2

Fig. 2.3 The correlations between the concentration of CO_2 and CH_4 inside the two buildings

2.3.2. Daily average emission rates of NH_3 and CH_4 and diurnal variations

The daily averages on NH_3 and CH_4 emission are shown in Fig. 2.4. The NH_3 emission rates varied

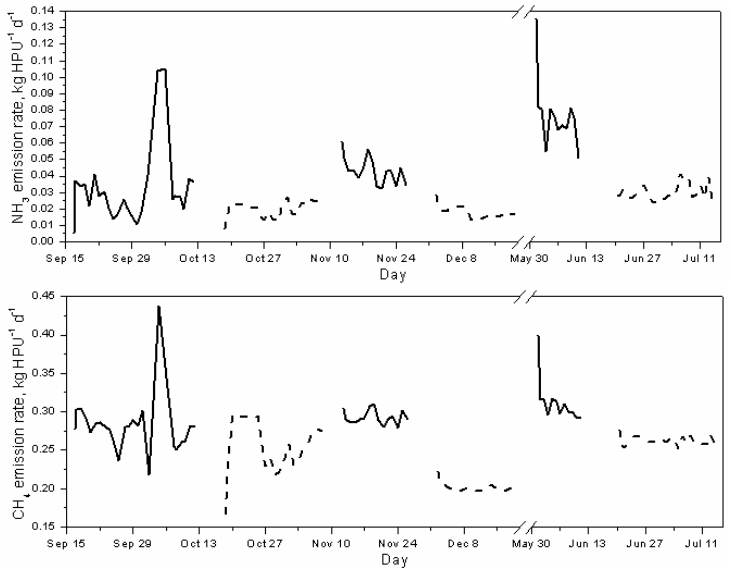

Fig. 2.4 Daily average emission rates of NH_3 and CH_4 over the three measurement periods (Solid line-building 1 and dashed line- building 2). The measurement before and after the breakpoint was finished in 2010 and 2011, respectively.

from 32-77 g HPU^{-1} d^{-1} in building 1 and varied from 18-30 g HPU^{-1} d^{-1} in building 2. NH_3 emission was at a relatively high level during both cold and warm periods in building 1, compared with that in building 2. Another difference of the NH_3 emissions from the two buildings was the extreme high peaks (around 120 g HPU^{-1} d^{-1}) observed in building 1 but not in building 2. The

variation of NH_3 in building 2 was quite smooth. The average emission of CH_4 was 290 and 230 g HPU^{-1} d^{-1} from building 1 and 2, respectively.

Examples of the diurnal variations on NH_3 and CH_4 emission rates are given in Fig. 2.5. Emission levels in building 1 varied more considerably than in building 2. An apparent diurnal pattern was found for NH_3 and CH_4 emission rates in building 1. The highest emissions took place around noon. The small changes on NH_3 (15-45 g HPU^{-1} d^{-1}) and CH_4 (220-300 g HPU^{-1} d^{-1}) emission rates in building 2 made the diurnal pattern not that obvious like in building 1. The emission rates were not significantly different between day and night.

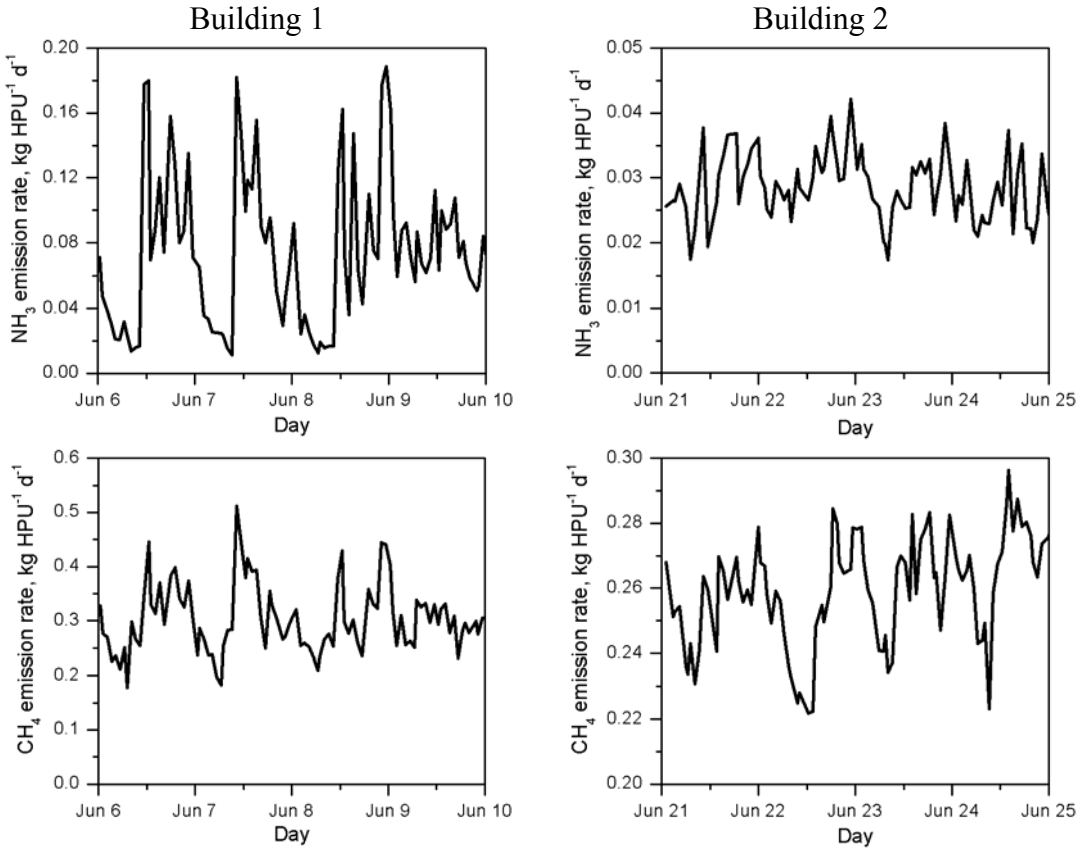

Fig. 2.5 Examples of diurnal variation of NH_3 and CH_4 emission rates

2.3.3. The effect of the climatic factors on the air exchange rate

Fig. 2.6 shows the effect of the climatic factors on the *ACR*. There were no consistent relationships between *ACR* and *WD* for both buildings. According to an analysis using multiple linear regressions, no significant influence of the wind direction on ACR can be found for both buildings ($P > 0.05$). Strong correlations (R^2=0.80 for building 1, 0.83 for building 2) between *ACR* and *WS* implied that more than 80% of the variance of *ACR* can be interpreted by the variance of *WS*.

Building 1 Building 2

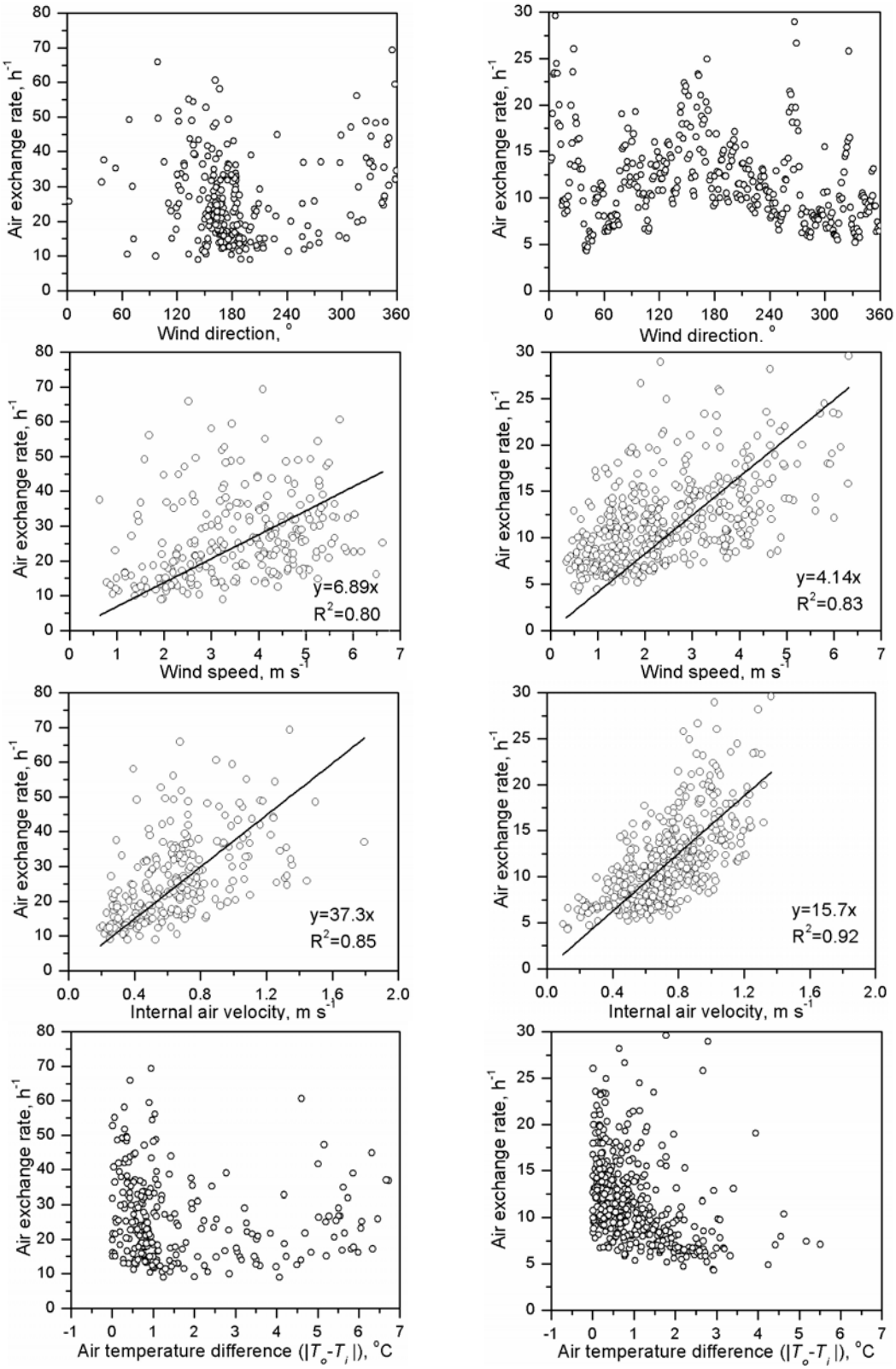

Fig. 2.6 The effect of the climatic factors on the air exchange rates of the two buildings.

The coefficients were 6.89 for building 1and 4.14 for building 2. The average of air velocities at the six measurement positions was used to represent the internal air velocity. The internal air velocity also showed positive correlations (R^2=0.85 for building 1, 0.92 for building 2) with ACR. The

coefficients 37.3 for building 1 and 15.7 for building 2 were 5.4-3.8 times of those for the external wind speeds. The absolute values of temperature difference between the internal and external air ($|T_o-T_i|$) were mainly below 3 °C. No significant influence of the air temperature difference on ACR was found for both buildings (P >0.05) in this study.

2.3.4. The effect of climatic factors on NH_3 emission rates

The variation of external temperature and NH_3 emission rates with respect to time is shown in Fig. 2.7 as an example to illustrate the dependency of NH_3 emission rates on the individual climatic factors. The mean temperature was 17 °C in this period for both buildings. The variations in air temperature happened more within a day than between days. The temperature variation ranged on average from 10 to 21 °C for building 1 and 14 to 25 °C for building 2 from the night to the day. The ammonia emission rate accordingly varied on average in between 36.2 and 152.9 g d^{-1} HPU^{-1} for building 1; and in between 20.5 and 48.6 g d^{-1} HPU^{-1} for building 2. The occurrence of peaks on ammonia emission followed the variations in air temperature.

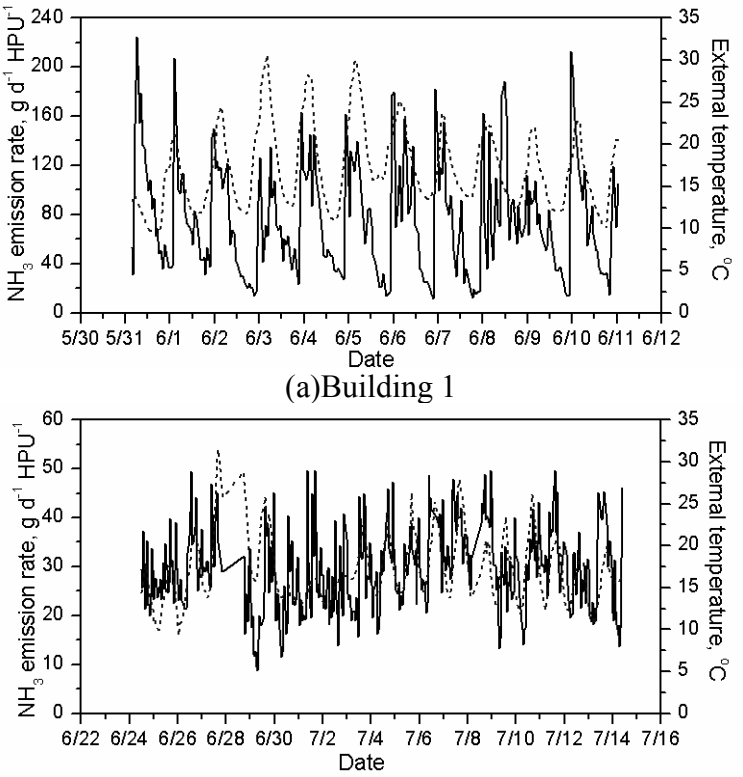

(a)Building 1

(b)Building 2

Fig. 2.7 Variations of external temperature and ammonia emission rates during warmer period for two buildings. Solid line - NH_3 emission rate; dashed line – external air temperature.

According to a multiple linear regression, no significant relationship was established between NH_3 emission rate and wind direction (P>0.05) for two buildings. There was a significant effect of wind speeds on NH_3 emission from building 1 (R^2=0.72, P<0.001) and from building 2 (R^2=0.67, P<0.001). Outside air temperature was shown to have a significant influence on emission from

building 1 (R^2=0.77, P<0.001) and building 2 (R^2=0.88, P<0.001). Moreover, the internal air velocities highly depended on the external wind speeds (R^2=0.84 for building 1, 0.85 for building 2). Meanwhile, the internal air temperature perfectly depended on the external air temperature (R^2=0.98 for building 1, 0.99 for building 2).According to the dependence of factor T_i and T_O, factor V_i and WS, only the influence from the independent variables (WD, WS and T_O) were considered in equation 3. The coefficients of equation 3 for NH_3 emission rate and the significance of each variable are given in Table 2.2. The NH_3 emission rate predicted by climatic variables was described as follow.

Building 1: $$\log_e(E_{NH_3}) = 0.828WS + 0.211T_O - 0.040(WS \times T_O) \quad (R^2=0.98) \qquad (4)$$

Building 2: $$\log_e(E_{NH_3}) = 0.996WS + 0.190T_O - 0.058(WS \times T_O) \quad (R^2=0.99) \qquad (5)$$

Table 2.2 NH_3 emission rates (E_{NH3}) as a function of wind speed (WS), external air temperature (T_O), the interaction of WS and T_O (WS: T_O)

Building 1				Building 2			
Factors	Coefficient	SD*	P value	Factors	Coefficient	SD*	P value
WS	0.828	0.039	<0.001	WS	0.996	0.041	<0.001
T_O	0.211	0.006	<0.001	T_O	0.190	0.003	<0.001
$WS \times T_O$	-0.040	0.003	<0.001	WS: T_O	-0.058	0.003	<0.001

*SD-standard deviation

The predicted NH_3 emission rate is given in Fig. 2.8. It explained 98% of the total variance of calculated ammonia emission rate by applying the three independent climatic variables. The multiple linear regression models also showed that WS (P<0.001) and T_O (P<0.001) influenced the ammonia emission significantly. Moreover, the interaction of WS and T_O ($WS \times T_O$) had a significant but negative effect on ammonia emission for both buildings (P<0.001).

2.4. Discussion

2.4.1. Gas concentrations

The transportation and distribution of gas concentrations inside naturally ventilated livestock buildings depended on air temperature and air velocity (Saha et al., 2010). The results showed that the difference of NH_3, CH_4 and CO_2 concentrations within both buildings varied following the temperature and air velocity during different measurement time. The similar results were also found in several published reports, e.g., Zhang et al. (2005). The low N_2O concentrations and low concentration difference between indoor and outdoor were consistent with the previous study (Jungbluth, 2001; Ngwabie et al, 2009). Similar N_2O indoor concentrations of 0.32-0.40 ppm were also measured in a dairy cattle building like building 2 with slatted floor (Berges and Crutzen, 1996). Monteny et al. (2006) argued that livestock buildings with liquid manure systems and external manure tanks were not a major source of N_2O and consequently, low emissions of N_2O were found in this kind of buildings.

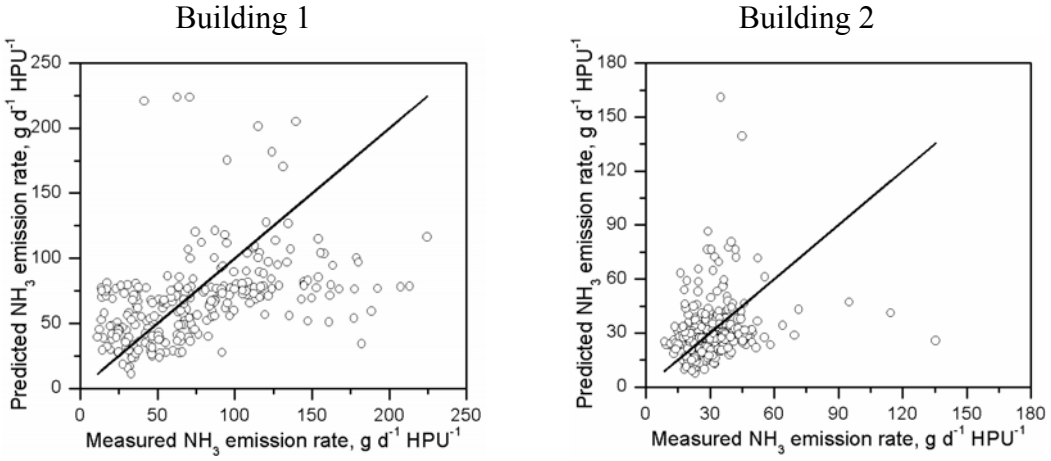

Fig. 2.8 Predicted NH_3 emission rates by the multiple linear equation versus the measured NH_3 emission rates

The linear correlation between the concentration of CH_4 and CO_2 was consistent with former research (Ngwabie et al., 2009; Madsen et al., 2010; Bjerg et al., 2011).The ratio of CH_4 and CO_2 concentration can be used to predict the emission rate of CH_4 based on the CO_2 production model (Madsen et al., 2010). The value of the CH_4 to CO_2 ratio found in this investigation was 0.05 for building 1 and 0.04 for building 2, while it was 0.08 in the work of Ngwabie et al. (2009). The data was fitted using a linear regression equation with a negative intercept by Ngwabie et al. (2009). However, the intercept was set to zero in Fig. 2.3 a-b. This was the reason for the difference of the ratio in this paper and in the work of Ngwabie et al. (2009). If the data in Fig. 2.3 a-b was fitted with a negative intercept, the ratio was 0.10 for building 1 and 0.07 for building 2; but the R^2 became smaller (0.76 for building 1 and 0.83 for building 2). The ratio was either 0.06 or 0.10 measured by using respiration chamber (Madsen et al., 2010). The ratio in this paper was at the same level with 0.06

2.4.2. NH_3 and CH_4 emission rates

The NH_3 and CH_4 emission rates were determined by CO_2 production model (CIGR, 2002). Several uncertainties related with CO_2 balance method may be involved in the calculation of emissions. CO_2 production was based on steady-state body weight and milk yield. This may increase the errors of emission estimation (Zhang et al., 2005). The accuracy of emission estimation was also influenced by the gas sampling positions (Demmers et al., 1998; Feidler and Müller, 2011). However, CO_2 production model was the best method for a continuous estimation of gas emissions. Moreover, CO_2 production model used animals as emission sources. Compared with tracer gas decay method, the randomly distributed animals provided better mix of CO_2 and room air.

The NH_3 emission rates calculated in this paper were in line with those in literature (Zhang et al., 2005). Zhang et al. (2005) investigated NH_3 emissions in 9 buildings with different floor

systems in Denmark and reported emission rates in the range of 8-76 g HPU^{-1} d^{-1}; the highest emission was observed in a building with solid floor and a scraper. The NH_3 emission rates in building 1 with solid floor and scrapers were higher than those in building 2 with slatted floor and robotic scrapers. One more reason responsible for low emission rates in building 2 could be the ventilation regulation by automatically adjusted opening curtains. The curtains may reduce both wind speed and ventilation rates, consequently the emission rate. Low NH_3 emission rates of 19-24 g HPU^{-1} d^{-1} was also reported in a dairy cattle building with automatically regulated ventilation flaps mounted on the side walls below the eaves and also at the ridge (Ngwabie et al., 2009).

The average CH_4 emission rates of 290 g HPU^{-1} d^{-1} for building 1and 230 g HPU^{-1} d^{-1} for building 2 fell in the range of 220-490 g HPU^{-1} d^{-1} found in the 9 buildings investigated by Zhang et al. (2005). In the study of Ngwabie et al. (2009), CH_4 emission rates calculated based on HPU were around 240 g HPU^{-1} d^{-1}. The CH_4 emission rates in this study were near to the enteric CH_4 emissions (234-263 g HPU^{-1} d^{-1}) measured in a respiratory chamber (Jungbluth et al., 2001). This was reasonable due to the fact that CH_4 in a cow barn was mainly produced from enteric fermentation (Monteny et al, 2006). The strong correlation between CO_2 and CH_4 concentrations also indicates CH_4 emission rate may be quickly estimated from the multiplication of CO_2 production rate from cow and a constant coefficient (about 0.06).

The diurnal variations in NH_3 and CH_4 emissions were also reported by other studies (Zhang et al., 2005; Ngwabie et al., 2009; Ngwabie et al., 2011). Peaks of gas emissions occurred around or after noon – one hour after the feeding time. Ngwabie et al. (2011) found that diurnal variations were related to the feeding schedule, which may change the animal activities. NH_3 emissions in building 2 were less fluctuated than building 1. This could be due to the difference of the floor and manure removal systems. The robotic scraper in building 2 can move the fresh manure into the pit in time compared to the scraper operation in building 1. The observed clear floor may keep the NH_3 emissions at lower level in building 2.

2.4.3. The effect of the climatic factors

Snell et al. (2003) reported that the wind speed but not direction was shown as a dominant factor of influencing *ACR*. During the measurement period, the mean outdoor wind speed was 3.50 m $s^{-1}$for building 1 and 2.45 m s^{-1} for building 2. The airflow inside the two buildings was mainly wind-driven. Meanwhile, the temperature differences were mainly below 3 °C. In this case, the wind effect was superior to the stack effect. Therefore, the temperature difference did not show significant influence on ACR.

Wind speed was previously identified as an important controlling variable for NH_3 emission from the surface of slurry (Sommer et al., 1991) and from the livestock buildings (Snell et al., 2003; Zhang et al., 2008; Schrade et al., 2012). It was clearly shown that the ventilation rates in the

buildings rose with increasing wind speed (Fig.6), consequently, leading to the increase of NH_3 emissions determined by ventilation rates.

The significant and positive linear relationship between emission rate and ambient temperature in this study was consistent with literature (Misselbrook et al., 2006; Pereira et al., 2010; von Bobrutzki et al., 2011; Schrade et al., 2012). NH_3 formation and release process was closely associated with temperature. The comparison of the variations of NH_3 emission and temperature in Fig.7 confirmed that higher temperature generally resulted in a considerable emission increase. The occurrence of peaks on ammonia emission followed the variations in air temperature. But there was a difference in the trend of variations on temperature and ammonia emission since temperature was not the only factor that affected the emission. The temperature gradually increased from night to day, while the overall ammonia emission also increased but with large fluctuations. The fluctuation could be caused by the rapid fluctuations of wind speeds in the day or in the night.

In addition to the direct effect of temperature on the NH_3 volatilization process, the effect from the interaction of temperature and wind speed was also significant. The negative coefficient seemed to imply that the interaction decreased the coherency of each individual factor (either wind speed or temperature) and the NH_3 emission.

Applying F-test to the coefficients in equation (4) and (5), the difference of coefficients for the associated variables was not significant (P>0.05). For example, the difference of coefficients for wind speed 0.828 (0.039) in equation (4) and 0.996 (0.041) in equation (5) was statistically insignificant (P>0.05). This may indicate that gas emission rates from the two naturally ventilated livestock buildings could be described by the same equation including the associated climatic factors such as wind speed and ambient temperature. Besides climatic factors, NH_3 emission rates were influenced by many other factors such urea content of tank milk (Schrade et al., 2012) and animal activity (Ngwabie et al., 2011). To derive NH_3 emission rates based on influencing factors, more inventories on naturally ventilated cattle buildings are still needed and more factors should be considered

2.5. Conclusions

Ammonia and methane emissions were measured from two naturally ventilated dairy cattle buildings in Denmark. The following conclusions were drawn.

The internal concentrations of NH_3, CH_4 and CO_2 were increased or decreased simultaneously due to …. Low concentration of N_2O was measured outside and inside the buildings; the difference of the concentrations were also very low. The variation of CH_4 and CO_2 concentrations showed a strong correlation.

The NH_3 emission rates varied from 32-77 g HPU^{-1} d^{-1} in building 1 and varied from 18-30 g HPU^{-1} d^{-1} in building 2. The average emission of CH_4 was 290 and 230 g HPU^{-1} d^{-1} from building 1 and 2, respectively. Diurnal pattern was found for NH_3 and CH_4 emission rates.

From multiple linear regression models, there was a significant linear relationship between NH_3 emission rates and climatic factors including the external wind speed as well as the air temperature (P<0.001), but not with the external wind directions (P>0.05).

It should be mentioned that the scraper operation frequency in Building1 was considerable lower than others with similar floor systems. Anyhow it provided some valuable emission information under such an operation. Future measurements on emissions under different scraper operation frequencies may benefit to identify the true effects of the scraper frequency.

Estimation of ammonia and other contaminant gas emissions from naturally ventilated building is still a challenge due to its large uncertainty. Therefore, more field measurements with well documented information of both airflow characteristics and gas concentration are needed for accurately quantifying the emission rate and modelling of the emission process. Research on optimizing gas sampling positions to find more representative gas concentration in the exit air will be helpful to reduce the uncertainty of estimating gas emissions. Researches may also be focused on development of simple measurement method to evaluate the effects of different floor and manure systems on emissions.

References

Berges, M.G.M., Crutzen, P.J., 1996. Estimates of Global N_2O Emissions from Cattle, Pig and Chicken Manure, including a Discussion of CH_4 Emissions. *Journal of Atmospheric Chemistry* 24(3), 241-269.

Bjerg, B., Zhang, G., Madsen, J., Rom, H.B., 2011. Methane emission from naturally ventilated livestock buildings can be determined from gas concentration measurements. *Environmental Monitoring and Assessment,* DOI 10.1007/s10661-011-2397-8.

von Bobrutzki, K., Müller, H.J., Scherer, D., 2011. Factors Affecting the Ammonia Content in the Air Surrounding a Broiler Farm. *Biosystems Engineering* 108, 322-333.

Braam, C. R., Smits, M.C.J., Gunnink, H., Swierstra, D., 1997a. Ammonia Emission from a Double-sloped Solid Floor in a Cubic House for Dairy Cows. *Journal of Agricultural Engineering Research* 68(4), 375-386.

Braam, C. R., Ketelaars, J.J.M.H., Smits, M.C.J., 1997b. Effects of Floor Design and Floor Cleaning on Ammonia Emission from Cubicle Houses for Dairy Cows. *Netherlands Journal of Agricultural Science* 45, 49-64.

CIGR, 2002. Report of Working Group on Climatization of Animal Houses – Heat and Moisture Production at Animal and House Levels. *CIGR Section II, Commission International Du Genie Rural (International Commission of Agricultural Engineering)*.

Demmers, T.G.M., 1997. Ventilation of livestock buildings and ammonia emissions. *Ph.D. Thesis, University of Nottingham.*

Demmers, T.G.M., Burgess, L.R., Short, J.L., Phillips, V.R., Clark, J.A., Wathes., C.M., 1998. First experiences with methods to measure ammonia emissions from naturally ventilated cattle buildings in the U.K. *Atmospheric Environment* 32,285-293.

Demmers, T.G.M., Phillips, V.R., Short, J.L., Burgess, L.R., Hoxey, R.P., Wathes., C.M., 2001.Validation of Ventilation Rate Measurement Methods and the Ammonia Emission from Naturally Ventilated Dairy and Beef Buildings in the United Kingdom. *Journal of Agricultural Engineering Research* 79 (1), 107-116.

Feidler, A.M., Müller, H.J., 2011. Emissions of ammonia and methane from a livestock building natural cross ventilation. *Meteorologische Zeitschrift* 20 (1), 059-065.

Jungbluth, T., Hartung, E., Brose, G., 2001. Greenhouse Gas Emissions from Animal Houses and Manure Stores. *Nutrient Cycling in Agroecosystems* 60(1-3), 133-145.

Madsen, J., Bjerg, B., Hvelplund., T., Weisbjerg, M.R., Lund, P., 2010. Methane and Carbon Dioxide Ratio in Excreted Air for Quantification of the Methane Production from Ruminants. *Livestock science* 129, 223-227.

Misselbrook, T.H., Webb, J., Gilhespy, S.L., 2006. Ammonia Emissions from Outdoor Concrete Yards Used by Livestock – Quantification and Mitigation. *Atmospheric Environment* 40, 6752-6763.

Monteny, G., Bannik, A., Chadwick, D., 2006. Greenhouse Gas Abatement Strategies for Animal Husbandry. *Agriculture, Ecosystems & Environment* 112 (2-3), 163-170.

Ngwabie, N.M., Jeppsson, K.H., Nimmermark, S., Swensson, C., Gustafsson, G., 2009. Multi-location Measurements of Greenhouse Gases and Emission rates of Methane and Ammonia from a Naturally Ventilated Barn for Dairy Cows. *Biosystems Engineering* 103, 68-77.

Ngwabie, N.M., Jeppsson K.H., Gustafsson, G., Nimmermark, S., 2011. Effects of Animal Activity and Air Temperature on Methane and Ammonia Emissions from a Naturally Ventilated Building for Dairy Cows. *Atmospheric Environment* 45, 6760-6768.

Pereira, J., Misselbrook, T., Chadwick, D.R., Coutinho, J., Trindade, H., 2010. Ammonia Emissions from Naturally Ventilated Dairy Cattle Buildings and Outdoor Concrete Yards in Portugal. *Atmospheric Environment* 44, 3413-3421.

Rom H B; Zhang G. (2010). Time Delay for Aerial Ammonia Concentration Measurements in Livestock Buildings. *Sensors*, 10(5), 4634-4642.

Saha, C.K., Zhang, G., Ni, J., 2010. Airflow and concentration characterisation and ammonia mass transfer modelling in wind tunnel studies. *Biosystems Engineering* 107 (4), 328-340.

Schrade, S., Zeyer, K., Gygax, L., Emmenegger, L., Hartung, E., Keck, M., 2012. Ammonia Emissions and Emission Factors of Naturally Ventilated Dairy Housing with Solid Floors and an Outdoor Exercise Area in Switzerland. *Atmospheric Environment* 47, 183-194.

Snell, H.G.J., Seipelt, F., Van Den Weghe, H.F.A., 2003. Ventilation Rates and Gaseous Emissions from Naturally Ventilated Dairy Houses. *Biosystems Engineering* 86 (1), 67-73.

Sommer, S.G., Olesen, J.E., Christensen, B.T., 1991. Effects of Temperature, Wind speed and Air Humidity on Ammonia Volatilization from Surface Applied Cattle Slurry. *Journal of Agricultural Science* 117, 91-100.

Swiestra, D., Smits, M.C.J., Kroodsma, w., 1995. Ammonia Emission from Cubicle Houses for Cattle with Slatted and Solid Floors. *Journal of Agricultural Research* 62, 127-132.

Verzani, J., 2004. Using R for Introductory Statistics. *Chapman and Hall/CRC, 1st edition*: 432pp.

Wu, W., Kai, P., Zhang, 2012. An assessment of a partial pit ventilation system to reduce emission under slatted floor-Part 1: Scale Model Study. *Computers and Electronics in Agriculture* 83, 127-133.

Zhang, G., Strom, J. S., Li, B., Rom, H.B., Morsing, S., Dahl, P., Wang, C., 2005. Emission of Ammonia and other Contaminant Gases from Naturally Ventilated Dairy Cattle Buildings. *Biosystems Engineering* 92 (3), 355-364.

Zhang G; Bjerg B; Strøm JS; Morsing S; Kai P; Tong G; Ravn P, 2008. Emission Effects of Three different Ventilation Control Strategies - A Scale Model Study. Biosystems Engineering 100(1), 96-104.

Chapter 3

Turbulent air characteristics in two naturally ventilated dairy cattle buildings

Paper II:

Wu, W., Zhang, G., 2012. **Turbulent Air Characteristics in Two Naturally Ventilated Dairy Cattle Buildings**. (Submitted to a peer review journal).

Abstract

Natural ventilation has been applied to dairy cattle buildings due to its advantages of energy conservation and low investment. An insight into air velocities and turbulences will be helpful to improve the microclimate quality in livestock buildings. Air velocity and turbulence were measured in two naturally ventilated dairy cattle buildings with three dimensional ultrasonic anemometers. The turbulence was described by autocorrelation, length scales, kinetic energy and microscales. The results showed autocorrelation coefficients decayed to zero then started to behave erratically. The distribution of time integral scale was very irregular. The integral length scale inside the buildings ranged from 1.08 m to 77.57 m. The length scales did not keep the same level when the external wind conditions were very similar and did not show positive correlations with the varied external wind speeds. The internal kinetic energy at different positions had positive correlations with the external wind speed. Larger turbulence energy dissipation rate (0.49 $m^2 s^{-3}$) was found near side openings, where the integral length scale was smaller. Kolmogorov microscales were quite isotropy in this study. Air velocities near downwind side openings possessed higher power spectra, compared with those in the middle section or near upwind side openings.

Key words: *autocorrelation; cross-correlation; spectral analysis; length scales; energy spectrum*

3.1. Introduction

Natural ventilation has been applied to dairy cattle buildings due to its advantages of energy conservation and low investment. However, the microclimate conditions are more complex in naturally ventilated buildings than mechanically ventilated buildings due to that natural ventilation highly depends on the external weather. The microclimate conditions in livestock buildings are of very importance for sustainable livestock production (Ecim-Djuric and Topisirovic, 2010). One of the microclimate issues is emissions including odour, gas and particle from naturally ventilated livestock buildings. Intensive research has been done to investigate gas emissions (Braam et al, 1997; Zhang et al, 2005; Gustafsson et al, 2005; Ngwabie et al, 2009; Samer et al., 2011). The challenge is the determination of natural ventilation rate and a representative gas concentration for the exit air. Both the ventilation rate and the gas concentration distribution depend on the external wind and internal airflow patterns including air velocities and turbulences. Therefore, knowledge on those specific parameters is necessary in order to improve the microclimate quality.

Analysis of air turbulence can be achieved by different methods such as calculation of kinetic energy, dissipation rate, length scale and energy spectrum. Zhang et al (1992) conducted detailed measurements of air distribution inside a mechanically ventilated room. They found out a difference among different locations in terms of turbulent kinetic energy and power spectrums. Heber and Boon (1993) evaluated turbulence characteristics and airflow patterns generated by a horizontal non-isothermal ventilation air jet in the special case of a full-scale livestock building for swine production. They reported that the dominant frequency of air turbulence varied according to locations and turbulence length scales increased with jet travel distance. These experiments are valuable for understanding the turbulent characteristics of indoor ventilation flows. However, the experiments were carried out in mechanically ventilated room spaces. Boulard et al (2000) studied the mean and turbulence characteristics of air velocity components in an empty greenhouse tunnel by spectral analysis; analysis of the energy spectra showed that all the locations had similar spectral levels in the dissipation region. Although the greenhouse tunnel was naturally ventilated, the correlation between the external wind and the internal air velocities were not reported.

The objectives of this study are to: (1) evaluate velocity and turbulence characteristics of the airflow in naturally ventilated dairy cattle buildings in terms of statistical descriptors, such as autocorrelation, kinetic energy, turbulence energy dissipation rate; (2) analyze the different scales of turbulence eddies, including integral time and length scale, Kolmogorov microscale of length; (3) investigate the coherency of the external and internal velocities by spectral analysis.

3.2. Methods and materials

3.2.1. Experimental details

The air velocity data recorded by Wu et al. (2012a) was used to analyze the characteristics of the turbulent flow outside and inside the buildings. The measurements were carried out in two naturally ventilated dairy cattle buildings, denoted as building 1 and building 2 to be convenient for further description and discussion. Air velocities were measured by ultrasonic anemometers – WindMaster (Gill instruments Ltd, Hampshire, UK). All the anemometers were connected to a multi-port adapter with interfaces supplying power to the anemometers and transferring data to a computer. The frequency of ultrasonic anemometer is crucial. Too high frequency requires unnecessary instrument speed and it may give the same result with a comparatively lower but reasonable frequency. However, too low sampling frequency will result in losing the information of turbulences in small eddies. Larsen (2006) compared the difference between measurements with 100 Hz and a series of test frequencies; 10 Hz was found good enough to capture the necessary information on turbulence in naturally ventilated room. 20 Hz was used in this measurement. More information on the ultrasonic can be found in the work of Wu et al. (2012b). The measurement periods were May 31th 14:00 to June 16th 10:00 and June 24th 10:39 to July 14th 09:54 in 2011 for building 1 and 2, respectively. An ultrasonic anemometer was placed 10 m above the ground to monitor the external wind velocities. Air velocities were measured at 6 positions (Fig.2.1) inside the buildings. Two positions A, B were in the middle section of the building and near the ridge opening. Two positions C, D were near one sidewall opening and two positions E, F were near another sidewall opening. More detailed description of the measurements can be found in the work of Wu et al. (2012a).

3.2.2. Data analysis

The measurement was conducted for weeks and a large number of data on velocities was produced. However, it was not possible to analyze all the experimental data. Hence only 16 periods were picked out for data analysis. Table 3.1 gives the measurement time, mean velocities and standard deviation of the 16 periods categorized as 16 cases. The first 8 cases had the same external wind direction and air velocity magnitudes at the same level. The last 8 cases had the same wind direction but varied wind speeds.

3.2.3. Background of statistical methods

The appearance of turbulence manifested itself as random fluctuations of the velocity component about a mean value. In other words, velocity exhibits a time dependent behaviour. The velocity time series u_t can be decomposed into a steady mean component $\overline{u_t}$ and a time fluctuating component $u_t^{'}$. The decomposition process is known as Reynolds decomposition. $\overline{u_t}$ over a time period Δt is defined as,

Table 3.1 Mean and standard deviations (SD) of the external wind and internal air velocities at different positions (m s^{-1})

Cases	Building	Measured time(y-m-d h)	External wind				A		B		C		D		E		F	
			Direction(°)	SD(°)	Speed	SD	Speed	SD	Speed	SD	Speed	SD	Speed	SD	Speed	SD	Speed	SD
1		2011-06-01 02			4.97	1.43	0.40	0.17	0.41	0.17	0.72	0.34	0.59	0.30	0.82	0.42	0.71	0.30
2	1	2011-06-04 15	182.8	1.41	4.94	1.16	0.44	0.18	0.39	0.18	1.04	0.49	0.88	0.38	0.78	0.53	0.64	0.35
3		2011-06-09 03			4.70	1.23	0.39	0.18	0.40	0.16	0.57	0.29	0.57	0.28	0.69	0.31	0.68	0.27
4		2011-06-10 05			5.30	1.42	0.37	0.19	0.39	0.18	0.70	0.37	0.58	0.32	0.82	0.45	0.73	0.38
5		2011-06-30 11			3.47	1.13	0.68	0.25	0.69	0.30	1.47	0.94	1.31	0.86	0.53	0.39	0.69	0.45
6	2	2011-07-01 22	43.44	0.93	3.42	1.04	0.25	0.19	0.26	0.20	0.88	0.68	1.04	0.72	0.52	0.21	0.50	0.29
7		2011-07-11 16			2.98	1.01	0.65	0.26	0.69	0.27	1.18	0.72	1.09	0.66	0.50	0.37	0.64	0.44
8		2011-07-12 20			2.93	0.87	0.60	0.23	0.63	0.26	1.47	0.74	1.27	0.72	0.36	0.16	0.42	0.21
9		2011-06-07 16			2.90	0.65	0.25	0.12	0.25	0.13	0.78	0.38	0.60	0.29	0.48	0.38	0.36	0.23
10	1	2011-06-02 15	167	3.1	4.88	1.19	0.41	0.16	0.38	0.16	1.15	0.57	1.03	0.47	0.92	0.63	0.69	0.41
11		2011-06-15 00			5.10	1.28	0.43	0.19	0.39	0.20	1.05	0.52	0.92	0.43	0.73	0.55	0.73	0.35
12		2011-06-14 16			6.60	1.71	0.43	0.20	0.48	0.21	1.19	0.58	1.04	0.52	1.06	0.67	0.99	0.47
13		2011-06-30 10			3.11	1.01	0.57	0.25	0.61	0.28	1.41	0.82	1.32	0.73	0.41	0.18	0.47	0.21
14	2	2011-06-30 19	41.5	1.3	4.22	1.33	0.29	0.15	0.36	0.19	1.36	0.83	1.35	0.86	0.53	0.20	0.53	0.22
15		2011-07-01 15			4.73	1.42	0.57	0.26	0.61	0.31	1.91	1.09	1.78	1.06	0.76	0.23	0.68	0.26
16		2011-06-24 13			6.21	1.91	0.62	0.36	0.71	0.45	2.08	1.47	2.03	1.39	0.96	0.60	1.26	0.90

Table 3.2 Mean air velocities and their standard deviations (SD) at different positions during the whole measured period (m s^{-1})

Building	External wind		Air velocities inside the buildings, at position											
			A		B		C		D		E		F	
	Mean	SD	Mean	SD	Mean	SD	Mean	SD	Mean	SD	Mean	SD	Mean	SD
1	3.61	1.32	0.43	0.19	0.48	0.27	0.78	0.36	0.79	0.40	0.82	0.54	0.75	0.54
2	2.50	1.31	0.46	0.18	0.50	0.19	0.95	0.56	0.85	0.51	0.78	0.51	0.83	0.46

$$\overline{u_t} = \frac{1}{\Delta t}\int_0^{\Delta t} u_t dt \tag{3.1}$$

The time dependent behaviour of the fluctuating component can be described by some statistical terms, such as variance, correlation and so on.

3.2.3.1. Variance and kinetic energy

The descriptor used to indicate the spread of the fluctuations $u_t^{'}$ about the mean value $\overline{u_t}$ is the variance $\overline{(u_t^{'})^2}$, denoted σ^2. The root mean square of the variance expresses the average magnitude of velocity fluctuations. The variance is of particular importance since it is proportional to the momentum fluxes induced by turbulence eddies, which cause normal stresses. Variance has a further interpretation as the half of the mean kinetic energy contained in the velocity fluctuations of each component. The total kinetic energy of the turbulence at a given location can be defined as

$$k = \frac{\sigma_u^2 + \sigma_v^2 + \sigma_w^2}{2} \tag{3.2}$$

where, *u*, *v* and *w* represent three components of the velocity.

3.2.3.2. Autocorrelation and cross-correlation functions

The structure of the turbulence can be obtained by studying the relationship between the fluctuations at different times. The autocorrelation function based on time series x_t is defined as

$$R_{x_t^{'}x_t^{'}}(\tau) = \frac{\overline{x_t^{'}x_{t+\tau}^{'}}}{\sqrt{\overline{(x_t^{'})^2}\,\overline{(x_{t+\tau}^{'})^2}}} \tag{3.3}$$

where, τ is the time difference; the autocorrelation function measures the linear dependence between two points on the same series observed at different time.

Cross-correlation function is based on two velocity time series x_t and y_t and is defined as

$$R_{x_t^{'}y_t^{'}}(\tau) = \frac{\overline{x_t^{'}y_{t+\tau}^{'}}}{\sqrt{\overline{(x_t^{'})^2}\,\overline{(y_{t+\tau}^{'})^2}}} \tag{3.4}$$

The two velocity series may be shifted by a certain distance, for example, the relationship of the turbulence of the air velocities measured at different positions inside the livestock building can be analyzed by cross-correlation.

The large eddy causes a certain degree of local structure in the flow. Therefore, there will be correlation between the values of $x_t^{'}$ and a short time later (τ) or at a given location ($x_t^{'}$) and a small distance away ($y_t^{'}$). The correlation will decrease gradually over the time scale and the space scale of an eddy. In other words, the autocorrelation and cross-correlation functions measure the time and size scale of a turbulent eddy.

3.2.3.3. The integral time and length scale of turbulence

The integral time and length scale, which represent concrete measures of the average period or size of a turbulent eddy, can be computed from integrals of the autocorrelation function with respect to time shift or distance in the direction of the velocity component. The integral time scale is defined as the integral of autocorrelation over time from zero to the first zero crossing (Pasquill and Smith, 1983),

$$t_{\int} = \sum_{\tau=0}^{n} R_{x_t^{'}x_t^{'}}(\tau)\Delta t \tag{3.5}$$

where, $R_{x_t^{'}x_t^{'}}(n)$=0; Δt can be perceived as sampling frequency.

The length scale should be calculated following the motion of the air,

$$L_{\int} = t_{\int}\left|\overline{x_t}\right| \tag{3.6}$$

3.2.3.4. Turbulence energy dissipation and small scales

Viscous shear stresses perform deformation work which increases the internal energy of the fluid at the expense of kinetic energy of turbulence. Therefore, turbulence is always dissipative. The turbulence energy dissipation rate is (Tennekes and Lumley, 1972)

$$\varepsilon \approx \frac{\overline{u_t^{'3}}}{L_{\int}} \tag{3.7}$$

The dissipation of turbulence energy mostly takes place at the smallest turbulence scales-Kolmogorov microscales. The Kolmogorov microscale of length can be formed as (Tennekes and Lumley, 1972)

$$\eta = (\upsilon^3/\varepsilon)^{1/4} \tag{3.8}$$

where, υ is kinetic viscosity, $m^2\ s^{-1}$.

3.2.4. Theory of spectral analysis

Velocity time series can also be analysed in the frequency domain by calculating the power spectrum. This might be useful in identifying where energy is transferred and in quantifying its dissipation. The spectral density function between two velocity time series is defined as

the Fourier transform of the correlation function, and distributes the variance of wind time series over frequency. The application of power spectrum is to identify the frequency of the major energy containing large eddies responsible for dispersion of ventilated air and gaseous contaminants in a space. The similarity of power spectrum of inside and outside velocities will help to build the correlation between inside velocity and outside wind. The difference of them will help to find the mechanism of the effect that building superimposes on inside velocities. The spectral density is defined as,

$$f(w) = \sum_{h=-\infty}^{\infty} R_{x_t' x_t'}(\tau) e^{-2\pi i w \tau} \tag{3.9}$$

where, w is angular frequency (2π times normal frequency).

3.3. Results and discussion

3.3.1. Hourly averaged air velocities outside and inside the buildings

Records of the external wind speeds and the internal air velocities during the entire measurement period are given in Fig. 3.2 and Fig. 3.3. Outside wind speed and direction varied significantly over time for both buildings. No sign showed that variations of internal air velocities followed the change of the external wind speeds. But the internal air velocities at the positions in the same side showed the same trend of fluctuation. The air velocities measured at different heights in the middle of the building also showed the same variation with respect to time. The mean wind speed was 3.61±1.32 m s^{-1} for building 1 and 2.50±1.31 m s^{-1} for building 2. The mean velocities at different positions inside the two buildings during the whole measured period are shown in Table 3.2.

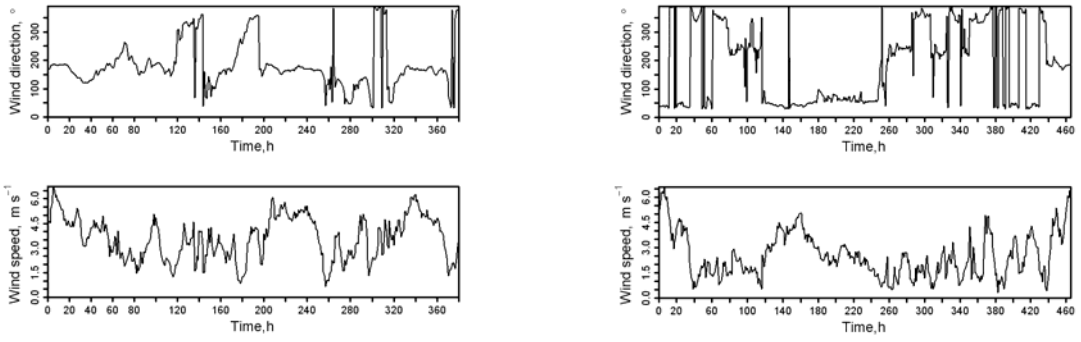

(a) (b)

Fig. 3.2 Measurements of wind direction and speed outside two naturally ventilated buildings (a) Building 1, and (b) Building 2

3.3.2. Sampling period for statistical and spectral analysis

A one-hour period of outside wind speed measurements was chosen outside building 1 and is shown in Fig. 3.4 a. The sampling frequency was 20 Hz. The mean value of the entire period was 4.03 m s^{-1}. During this one-hour period, the mean value and standard deviation were

investigated as a function of the time interval over which they were averaged. The mean and standard deviation reached a nearly constant after 20 minutes (Fig. 3.4 b). A 20-min measured velocity time series was then used for spectral analysis for each case.

3.3.3. Autocorrelation and integral turbulence length scales

Autocorrelation functions describe the correlation between consecutive values of the time series. Utilizing the Taylor's frozen turbulence hypothesis, the autocorrelation of the velocity fluctuations becomes useful tool for finding repeating patterns such as the presence of a periodic circulating structure. In this study, autocorrelation analysis was applied to detect eddies and to calculate integral turbulence time scale.

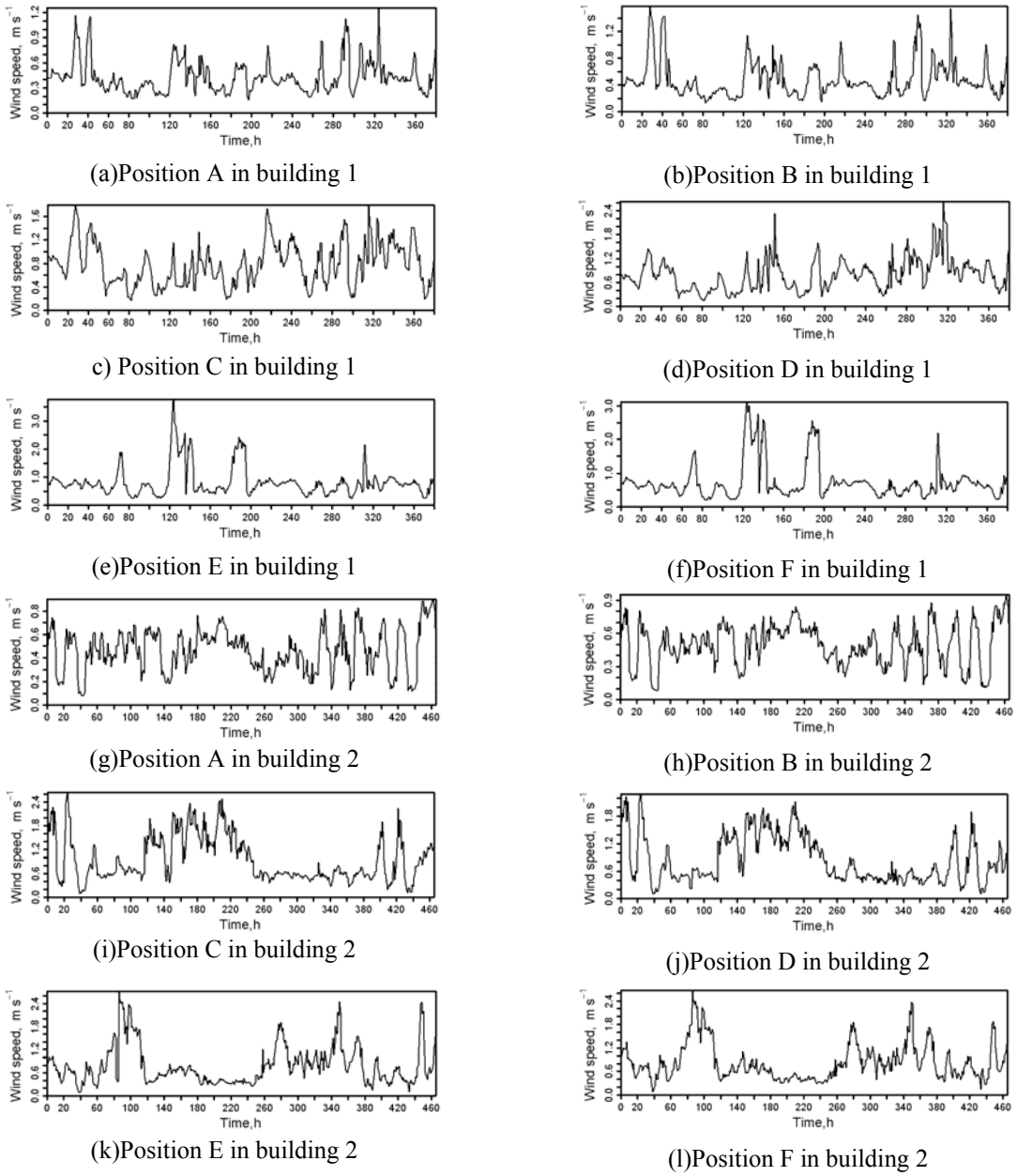

(a)Position A in building 1 (b)Position B in building 1

c) Position C in building 1 (d)Position D in building 1

(e)Position E in building 1 (f)Position F in building 1

(g)Position A in building 2 (h)Position B in building 2

(i)Position C in building 2 (j)Position D in building 2

(k)Position E in building 2 (l)Position F in building 2

Fig. 3.3 Measurements of air velocities inside two naturally ventilated buildings at different positions

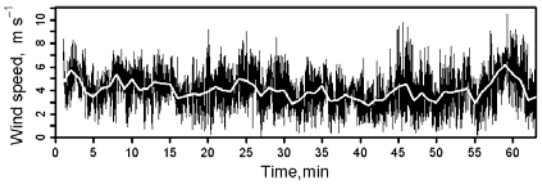

(a)

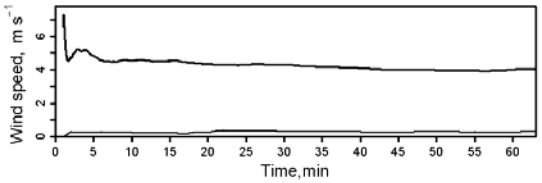

(b)

Fig 3.4. Investigation of sampling period: (a) Wind speed over one-hour period; the white line shows one minute average; (b) Mean and standard deviation of the wind speed as a function of the time period over which the values were averaged.

As an example, autocorrelation functions for outside wind speed and inside velocity magnitudes at positions A, C, E for case 1 and case 5 are shown in Fig. 3.5. Autocorrelation coefficients decayed to zero and started to behave periodically, which was consistent with the work of Brett and Tuller (1991). The decay rate for that at the downwind position E was faster than other positions in building 1. Whereas, the decay rate at the middle position A was faster than other positions in Building 2. A determined trend of autocorrelation coefficients could not be achieved for velocities at different positions. The discrepancy between two buildings could be caused by the different building dimensions, the different configurations of the roof opening and the surrounding buildings. According to the study on mechanically ventilated airflow (Heber and Boon, 1993), autocorrelation coefficients should decay slower and slower when air travelled from upwind to downwind side in the room. But this was not the case in the two naturally ventilated buildings. It indicates the airflow patterns inside a naturally ventilated building were rather complicated due to the numerous openings.

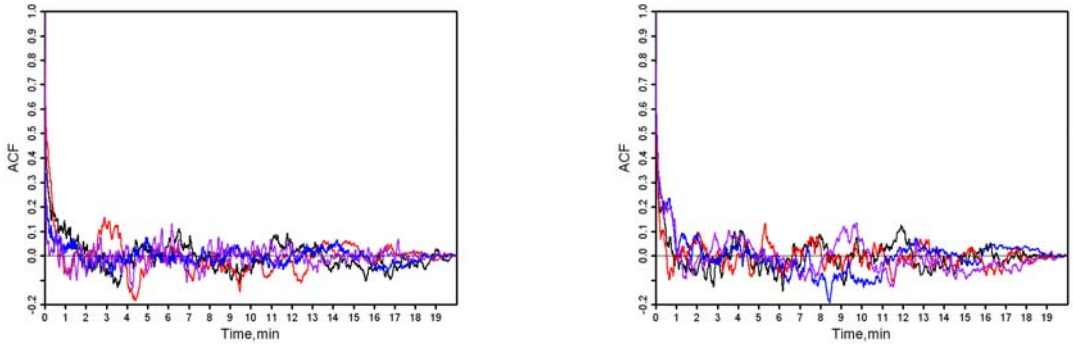

(a) (b)

Fig. 3.5 Auto correlation function for wind velocities at different positions (black line-outside; blue line-C, at upwind side; red line-A, in the middle section of the room; purple line-E, at downwind side) for case 1 and case 5. (a) building 1 (b) building 2

Table 3.3 shows the integral time scales for the air velocity magnitudes and their three velocity components. Direction u and v are shown in Fig. 2.1. Direction w was vertical with respect to ground. The integral time scale determined from summarizing autocorrelation functions could be used to describe the time required for an eddy to pass the measured position. The distribution of time integral scale was very irregular.

Table 3.4 shows the integral length scales for the air velocity magnitudes and their three velocity components. It should be noted that most of the integral length scales for w direction are of the magnitude level with the dimension of the measurement volume of ultrasonic. Larger uncertainties were introduced to determine the length scales for w direction. This kind of uncertainty was also detected by Heber and Boon (1993). The turbulence length scale of the outside velocity magnitudes ranged from 15.39 m to 120.56 m for all the cases. The integral length scale inside the buildings ranged from 1.08 m to 77.57 m. The length scales in building 2 were generally higher compared with those in building 1. For the first 8 cases, although the external wind condition were very similar, the length scales did not keep the same level. For case 9-12 and case 13-16, the external wind speed was increased respectively for building 1 and 2. However, the length scales did not show positive correlations with the varied external wind speeds. The reason is not clear but could be due to the large difference of autocorrelations among different time series. The integral time scale and length scale may be not only influenced by velocity magnitude, building dimensions but also the inherent structure of turbulence itself.

3.3.4. Turbulence kinetic energy, dissipation rate and small scales

Table 3.5 shows the turbulence kinetic energy for different cases. The average value of the turbulence kinetic energy for external wind was 1.63 $m^2 s^{-2}$ and was 5 times larger than that inside the buildings. It became weakest in the middle of the building – 15 to 20 times lower than that of external wind. Boulard et al (2000) also found a weak kinetic energy in the centre of a greenhouse tunnel; the kinetic energy was also 10 times lower than that of the external wind. Kinetic energy increased near the sidewall openings, when compared to the values measured in the middle of the building. When the external wind was kept at the same level, the internal kinetic energy at different positions was also at the same level (see in case 1-4 and case 4-8). Table 5 also shows that the kinetic energy has a positive correlation with the external wind speed (see in case 9-12 and case 13-16). When the external wind speed was increased, the internal kinetic energy at all the measured internal positions was increased accordingly.

Table 3.6 shows the turbulence dissipation rates for the air velocity magnitudes and their three velocity components. The large dissipation rates were mostly found near side openings, the largest of which was 0.49 $m^2 s^{-3}$ for air velocity magnitude near downwind opening in building 1. Turbulence energy dissipation rate is the rate of energy supplied from

Table 3.3 Integral time scale of the air velocity magnitudes and associated three components for different cases (s)

Cases	External wind				A				B				C				D				E				F			
	τ	τu	τv	τw	τ	τu	τv	τw	τ	τu	τv	τw	τ	τu	τv	τw	τ	τu	τv	τw	τ	τu	τv	τw	τ	τu	τv	τw
1	7.61	4.89	6.28	1.01	5.69	3.54	8.50	3.87	6.32	4.90	7.19	6.08	4.25	1.22	4.18	1.06	4.92	1.53	4.96	1.96	1.60	5.16	7.05	1.18	1.78	5.41	6.92	1.05
2	10.94	5.66	10.06	1.28	13.78	6.31	21.72	3.56	12.13	7.21	26.43	8.61	9.49	1.62	9.08	1.48	3.67	2.49	3.21	2.87	1.95	7.01	20.02	1.18	1.68	5.59	14.74	1.39
3	8.38	2.35	8.12	0.77	9.11	12.09	10.30	4.24	9.67	6.42	7.48	6.24	4.50	1.36	5.98	1.10	4.30	2.63	5.05	1.47	2.53	7.28	8.51	2.40	8.94	6.62	25.00	2.89
4	9.43	7.71	14.85	2.05	4.35	20.80	15.38	8.86	6.74	8.32	6.57	2.94	5.03	1.10	4.46	0.96	4.94	1.85	8.23	1.16	1.64	3.97	5.30	0.88	1.76	3.45	4.44	1.06
5	8.99	29.79	15.47	0.95	5.16	48.70	5.11	8.32	2.80	47.10	3.16	10.51	52.63	65.65	16.06	2.86	32.82	32.80	2.48	1.00	63.74	3.42	106.45	7.71	57.30	14.47	98.87	5.46
6	7.31	5.03	6.86	1.11	25.37	20.75	58.35	12.04	25.04	20.55	66.12	8.08	15.90	15.87	1.61	2.70	7.79	7.10	1.40	1.03	21.90	17.79	19.71	8.46	10.63	4.88	27.60	6.70
7	29.62	9.03	34.18	2.71	12.61	7.79	12.22	4.87	10.06	7.33	9.04	7.14	25.03	29.83	11.93	7.33	11.52	12.05	3.37	1.02	20.68	8.33	26.88	12.59	24.93	10.37	31.89	7.55
8	8.67	5.01	7.99	1.35	5.55	5.40	5.60	3.63	5.05	4.15	6.32	2.75	18.36	16.92	1.29	1.59	3.38	2.73	0.87	0.66	7.87	5.66	17.58	13.37	8.58	10.00	17.37	4.65
9	18.97	29.46	18.45	1.67	12.18	14.93	12.94	5.07	10.65	6.52	31.60	5.96	7.37	1.73	4.18	0.93	12.11	2.94	8.95	1.47	11.84	14.49	19.15	1.66	5.14	15.25	17.02	2.61
10	24.73	18.03	17.11	2.08	11.52	4.80	16.35	3.46	16.81	4.26	39.60	5.38	6.22	1.68	5.31	1.62	12.81	1.48	8.39	1.68	2.80	4.37	9.48	0.82	3.27	8.51	20.23	1.15
11	9.98	5.96	8.30	1.11	10.36	7.62	14.64	3.94	7.20	8.19	17.08	5.02	6.48	1.66	5.54	1.32	4.81	1.72	3.76	1.50	2.30	4.78	7.36	1.61	1.91	4.00	9.19	1.60
12	4.19	3.44	4.05	0.82	3.69	7.50	12.07	3.76	5.00	11.74	11.23	4.76	4.18	1.02	3.74	0.94	3.59	1.19	2.85	1.40	1.70	4.71	7.89	0.65	2.13	3.92	6.12	0.61
13	15.84	3.01	17.04	1.00	27.89	6.92	13.14	3.93	18.88	10.14	4.90	4.52	12.51	11.26	1.87	2.24	7.70	10.64	0.88	0.68	4.73	5.87	48.36	12.42	14.99	13.51	12.98	12.61
14	14.88	3.55	12.53	0.68	23.20	11.00	7.40	4.86	16.82	9.55	9.53	4.84	6.38	5.56	1.75	1.27	5.19	3.18	1.19	0.72	5.76	4.50	12.52	3.76	5.75	4.98	11.76	2.72
15	3.25	2.08	3.39	0.72	4.41	9.18	3.17	3.61	3.45	5.27	2.67	2.88	5.09	5.59	1.36	1.61	1.96	2.23	0.91	0.52	6.37	4.30	9.37	2.84	6.77	4.63	10.23	2.88
16	10.51	19.71	10.08	0.95	40.76	51.65	8.73	6.55	46.56	56.20	8.77	6.26	32.52	33.75	1.16	4.69	17.96	18.24	1.25	0.53	13.66	4.74	74.34	2.75	18.65	4.30	75.07	6.29

τ - turbulence time scale; u, v, w – air velocity direction; A, B, C, D, E, F – measuring positions.

Table 3.4 Integral length scale of the air velocity magnitudes and associated three components for different cases (m)

Cases	Extemal wind				A				B				C				D				E				F			
	L	Lu	Lv	Lw	L	Lu	Lv	Lw	L	Lu	Lv	Lw	L	Lu	Lv	Lw	L	Lu	Lv	Lw	L	Lu	Lv	Lw	L	Lu	Lv	Lw
1	37.78	10.46	27.22	0.11	2.29	0.51	1.57	0.06	2.61	1.23	0.77	0.09	3.08	0.11	2.41	0.03	2.92	0.09	1.96	0.04	1.31	1.07	2.18	0.05	1.26	2.16	1.96	0.06
2	54.08	14.23	41.37	0.23	6.09	1.11	6.92	0.15	4.78	1.10	4.42	0.11	9.88	0.01	8.13	0.10	3.24	0.08	2.28	0.15	1.52	1.02	1.92	0.06	1.08	1.20	2.65	0.06
3	39.41	4.74	33.21	0.08	3.59	2.19	2.18	0.11	3.89	1.54	1.51	0.11	2.55	0.10	2.55	0.03	2.44	0.09	1.93	0.04	1.75	2.31	2.68	0.02	6.12	2.94	8.00	0.13
4	49.98	16.60	69.11	0.48	1.61	3.44	0.37	0.08	2.65	1.91	0.07	0.08	3.53	0.10	2.42	0.00	2.87	0.10	3.11	0.00	1.34	0.93	1.76	0.02	1.28	1.27	1.05	0.03
5	31.19	20.75	48.49	0.05	3.51	1.30	2.64	0.05	1.93	8.20	1.33	0.11	77.57	72.76	0.50	0.46	43.10	32.01	0.03	0.07	33.82	0.62	6.82	0.23	39.42	5.26	17.06	0.39
6	24.98	3.18	21.72	0.03	6.33	1.10	5.57	0.48	6.42	0.28	8.16	0.34	13.94	8.70	0.00	0.04	8.09	5.07	0.06	0.02	11.47	5.40	5.89	0.65	5.31	1.05	3.31	0.31
7	88.41	4.34	93.22	0.16	8.18	0.78	6.68	0.26	6.94	0.52	4.77	0.40	29.62	25.63	1.40	1.07	12.58	9.51	0.42	0.07	10.40	0.65	4.57	0.04	16.06	2.34	10.60	0.36
8	25.42	3.67	21.10	0.10	3.35	0.05	2.67	0.06	3.19	0.81	2.55	0.02	26.92	20.61	0.07	0.37	4.28	2.67	0.01	0.04	2.79	0.66	2.14	0.73	3.58	2.53	0.52	0.19
9	54.92	62.08	33.33	0.23	3.09	0.26	2.13	0.04	2.69	0.29	0.54	0.01	5.75	0.07	2.62	0.00	7.22	0.41	3.81	0.01	5.64	2.21	1.51	0.06	1.87	0.96	1.29	0.08
10	120.56	57.28	60.62	0.49	4.68	0.42	5.10	0.01	6.33	0.43	7.84	0.01	7.16	0.19	5.20	0.00	13.14	0.24	6.83	0.02	2.57	2.31	1.40	0.05	2.24	0.23	2.18	0.05
11	50.95	20.95	29.05	0.22	4.41	0.23	4.58	0.18	2.79	0.64	1.89	0.11	6.79	0.24	4.78	0.00	4.45	0.42	2.55	0.06	1.68	0.97	0.27	0.04	1.39	1.12	2.92	0.05
12	27.68	13.19	20.79	0.20	1.57	1.02	1.03	0.03	2.41	2.34	0.87	0.09	4.97	0.18	3.65	0.00	3.72	0.22	2.21	0.02	1.81	0.24	2.50	0.03	2.12	1.60	2.64	0.05
13	49.30	1.95	48.53	0.05	15.82	0.66	5.81	0.09	11.57	0.81	2.00	0.14	17.61	12.81	0.02	0.32	10.15	11.08	0.02	0.06	1.95	0.88	7.08	0.35	7.09	4.41	0.54	1.02
14	62.80	2.86	49.12	0.00	6.83	0.84	1.15	0.32	6.04	0.44	2.16	0.33	8.65	5.73	0.15	0.21	6.99	3.00	0.08	0.02	3.05	1.52	2.46	0.33	3.03	1.92	0.45	0.28
15	15.39	2.23	14.61	0.03	2.53	1.65	1.06	0.23	2.09	1.46	0.66	0.08	9.72	8.30	0.15	0.44	3.50	2.96	0.10	0.05	4.83	1.21	5.46	0.41	4.63	1.85	3.16	0.33
16	65.32	17.04	58.35	0.11	25.30	5.26	3.55	0.26	33.18	11.82	3.83	0.15	67.58	49.89	0.04	1.13	36.50	26.58	0.02	0.03	13.09	1.30	15.65	0.12	23.41	1.36	32.69	0.31

L – turbulence length scale; u, v, w – air velocity direction; A, B, C, D, E, F – measuring positions.

large eddies to small eddies. Therefore, it should be related with the length scale of the large eddies. Since the length scales (Table 4) near side openings were generally small, the large eddies at this region might dissipate into small eddies more quickly. Heber et al (1996) also reported a trend of larger turbulence dissipation rate where integral length scale was shorter, although a different formula was used to estimate the dissipation rate. Like turbulence integral time and length scale, the correlation between dissipation rate and the external wind speed was not apparent.

Table 3.5 Turbulence kinetic energy of the air velocities for different cases (m^2 s^{-2})

Cases	External wind	A	B	C	D	E	F
1	1.66	0.07	0.06	0.15	0.14	0.35	0.18
2	1.25	0.05	0.07	0.26	0.21	0.43	0.23
3	1.39	0.05	0.04	0.11	0.13	0.19	0.12
4	1.88	0.07	0.07	0.16	0.15	0.35	0.24
5	1.50	0.13	0.18	0.90	0.75	0.20	0.25
6	1.17	0.04	0.04	0.46	0.54	0.07	0.14
7	1.13	0.09	0.13	0.57	0.49	0.18	0.22
8	0.92	0.09	0.13	0.58	0.58	0.06	0.08
9	0.54	0.03	0.04	0.18	0.12	0.17	0.09
10	1.24	0.04	0.06	0.34	0.29	0.47	0.31
11	1.53	0.06	0.09	0.30	0.26	0.40	0.24
12	2.69	0.10	0.12	0.38	0.35	0.74	0.42
13	1.08	0.09	0.14	0.66	0.59	0.08	0.08
14	1.78	0.04	0.05	0.71	0.83	0.08	0.08
15	2.33	0.12	0.16	1.27	1.27	0.09	0.13
16	4.00	0.17	0.24	2.12	1.97	0.58	1.05

Table 3.7 shows the Kolmogorov mircoscales for the air velocity magnitudes and their three velocity components. The micro-scale of turbulence ranged between 3×10^{-5} m near the sidewall openings to 6×10^{-4} m for all the positions. The distribution of Kolmogorov mircoscales were quite uniform at different positions, compared with the values of integral length scales. They were around 1 mm. The results of small scales in this study was consistent with the assumption that small eddies could be treated as isotropic eddies (Tennekes and Lumley, 1972).

3.3.5. Cross-correlation and power spectrum

Analysis of spatial correlation was intended to find the dependent and coherent link between two velocity time series. The spatial correlation (Table 3.8) between the internal air velocities and the external wind speeds were generally small. The velocities at upwind side (position C) showed a little higher correlation with outside wind; the average of the correlation

Table 3.6 Turbulence dissipation rate of the air velocity magnitudes and associated three components for different cases ($\times 10^{-3}$, m^2s^{-3})

Cases	External wind				A				B				C				D				E				F			
	ε	εu	εv	εw	ε	εu	εv	εw	ε	εu	εv	εw	ε	εu	εv	εw	ε	εu	εv	εw	ε	εu	εv	εw	ε	εu	εv	εw
1	26.51	21.72	36.56	12.19	1.776	10.45	8.693	88.64	0.551	0.401	9.993	6.353	11.36	219.9	8.285	78.61	9.082	87.63	5.006	14.56	142.1	684.3	39.42	100.4	58.83	137.5	19.58	81.01
2	1.101	4.916	1.086	246.7	0.138	0.211	1.283	0.735	0.284	0.001	2.77	10.53	13.39	3149	11.43	154.5	10.4	218.5	9.665	24.14	220.7	656.4	27.07	46.23	104.4	316.2	12.23	90.16
3	11.19	18.18	12.65	362.2	1.39	1.638	4.041	47.59	0.531	0.249	1.513	2.94	14.79	189.2	8.738	115.1	10.34	128.7	6.931	66.23	45.45	137.4	12.81	0.055	7.471	59.89	1.206	2.056
4	12.13	15.9	11.66	87.66	6.771	2.859	25.68	108.9	1.502	0.023	18.82	6.901	20.04	126.3	19.51	10192	13.02	121.8	7.218	1143	200.5	934.3	31.53	99.73	134	467.8	45.61	121.1
5	0.597	3.605	4.818	1074	1.702	14.5	3.159	143.4	9.168	4.517	6.771	78.26	7.61	8.106	262.8	174.1	16.26	21.51	7269	1179	5.439	209.5	27.34	70.8	6.598	22.55	21.34	37.9
6	11.61	49.38	2.93	1725	3.944	20.67	1.585	2.591	3.391	64.76	1	2.342	42.07	74.3	4346	1524	71.62	104.3	2975	2695	0.71	0.027	1.498	1.203	15.98	46.13	34.88	8.607
7	2.437	20.02	0.904	258.1	0.369	19.68	0.546	8.843	0.89	52.72	1.176	11.16	13	16.69	91.73	46.17	28.92	38.43	307.2	494.1	10.68	112.4	18.31	307	11.02	33.76	18.26	27.38
8	13.37	25.58	9.231	258	1.167	550.5	3.337	75.41	2.625	27.36	2.748	277.8	7.887	9.673	1381	66.02	87.76	126.1	24139	934.9	2.465	0.686	3.932	6.328	8.653	0.573	70.73	16.63
9	0.09	0.723	1.369	80.41	0.262	1.023	1.186	1.384	1.179	4.841	14.52	57.7	13.51	350.3	22.06	2359	4.168	11.81	5.956	488.4	21.81	82.92	7.508	10.8	17.28	70.7	2.194	11.66
10	2.347	3.005	1.983	126.2	0.461	0.569	1.629	20.24	0.32	2.061	1.178	12.39	22.53	328.6	25.33	8321	7.771	47.47	10.91	460.9	149.2	218.3	5.324	61.24	65.21	1521	20.03	33.47
11	4.687	6.362	12.41	153.8	0.727	27.68	0.998	0.633	3.153	10.35	6.163	2.721	27.23	232.7	30.62	99129	18.62	22.9	20.5	299	224	651.3	144.4	17.72	70.54	326	26.92	5.943
12	7.158	55.21	39.21	475.3	5.285	5.916	6.725	305.7	2.659	0.261	28.64	9.34	38.92	293.4	40.34	7229	38.51	164.4	45.97	1150	494.8	8162	73.86	13.07	124.5	655.1	55.82	70.94
13	8.145	0.704	7.727	304.8	0.358	30.59	0.093	55.72	1.407	60.41	1.295	59.91	26.72	37.97	5033	175.5	39.95	31.12	6987	691.9	5.36	10.5	3.491	11.16	1.758	0.044	31.14	1.503
14	8.722	177.9	4.814	14815	0.409	7.311	1.524	0.972	1.596	20.73	1.878	0.861	74.21	107.2	1105	377.5	116.2	245.8	3653	5271	3.038	24.45	7.719	7.369	5.65	13.53	75.43	8.614
15	40.52	275.4	21.73	2104	3.573	10.88	3.32	25.66	10.96	18.81	2.469	26.27	88.07	93.1	3158	318.2	365.9	380.6	5240	2935	0.464	22	6.524	6.032	6.668	16.53	38.26	12.08
16	12.96	18.76	8.114	2030	2.276	14.37	4.494	34.69	3.597	12.78	7.47	79.79	55.71	70.46	18510	431.7	105.9	134.4	57924	9570	41.65	486.3	27.88	419.9	77.73	818.1	57.63	345.9

ε - turbulence dissipation rate; u, v, w – air velocity direction; A, B, C, D, E, F – measuring positions.

Table 3.7 Kolmogorov microscale in turbulence of the air velocity magnitudes and associated three components for different cases ($\times 10^{-3}$, m)

Cases	External wind				A				B				C				D				E				F			
	η	ηu	ηv	ηw	η	ηu	ηv	ηw	η	ηu	ηv	ηw	η	ηu	ηv	ηw	η	ηu	ηv	ηw	η	ηu	ηv	ηw	η	ηu	ηv	ηw
1	0.52	0.55	0.48	0.64	1.03	0.66	0.69	0.39	1.38	1.49	0.67	0.75	0.65	0.31	0.70	0.40	0.68	0.39	0.79	0.61	0.34	0.23	0.47	0.38	0.43	0.35	0.56	0.40
2	1.16	0.80	1.16	0.30	1.95	1.75	1.12	1.28	1.63	6.43	0.92	0.66	0.62	0.16	0.65	0.34	0.66	0.31	0.67	0.54	0.31	0.23	0.52	0.46	0.37	0.28	0.64	0.39
3	0.65	0.58	0.63	0.27	1.09	1.05	0.84	0.45	1.39	1.68	1.07	0.91	0.61	0.32	0.69	0.36	0.66	0.35	0.73	0.42	0.46	0.35	0.63	2.45	0.72	0.43	1.13	0.99
4	0.64	0.59	0.64	0.39	0.74	0.91	0.53	0.37	1.07	3.04	0.57	0.73	0.56	0.35	0.57	0.12	0.63	0.36	0.72	0.20	0.32	0.21	0.50	0.38	0.35	0.26	0.46	0.36
5	1.35	0.86	0.80	0.21	1.04	0.61	0.89	0.34	0.68	0.81	0.74	0.40	0.72	0.70	0.30	0.33	0.59	0.55	0.13	0.20	0.78	0.31	0.52	0.41	0.74	0.55	0.55	0.48
6	0.64	0.45	0.91	0.18	0.84	0.56	1.06	0.94	0.88	0.42	1.19	0.96	0.47	0.40	0.03	0.19	0.41	0.37	0.16	0.16	1.29	2.92	1.07	1.13	0.59	0.46	0.49	0.69
7	0.95	0.56	1.22	0.30	1.52	0.56	1.38	0.69	1.22	0.44	1.14	0.65	0.63	0.59	0.38	0.46	0.51	0.48	0.28	0.25	0.66	0.36	0.57	0.28	0.65	0.49	0.57	0.52
8	0.62	0.53	0.68	0.30	1.14	0.25	0.88	0.40	0.93	0.52	0.92	0.29	0.71	0.67	0.19	0.42	0.39	0.35	0.10	0.21	0.95	1.31	0.84	0.75	0.69	1.37	0.41	0.59
9	2.17	1.29	1.10	0.40	1.66	1.18	1.14	1.10	1.14	0.80	0.61	0.43	0.62	0.27	0.55	0.17	0.83	0.64	0.76	0.25	0.55	0.39	0.72	0.66	0.58	0.41	0.98	0.64
10	0.96	0.90	1.00	0.35	1.44	1.37	1.05	0.56	1.58	0.99	1.14	0.63	0.55	0.28	0.53	0.12	0.71	0.45	0.65	0.26	0.34	0.31	0.78	0.42	0.42	0.19	0.56	0.49
11	0.81	0.75	0.63	0.34	1.29	0.52	1.19	1.33	0.89	0.66	0.75	0.92	0.52	0.30	0.50	0.07	0.57	0.54	0.56	0.29	0.31	0.24	0.34	0.58	0.41	0.28	0.52	0.76
12	0.73	0.44	0.47	0.25	0.78	0.76	0.74	0.28	0.93	1.66	0.51	0.68	0.48	0.29	0.47	0.13	0.48	0.33	0.46	0.20	0.25	0.12	0.41	0.62	0.36	0.23	0.43	0.41
13	0.70	1.30	0.71	0.28	1.54	0.51	2.15	0.43	1.09	0.43	1.11	0.43	0.52	0.48	0.14	0.33	0.47	0.50	0.13	0.23	0.78	0.66	0.87	0.65	1.03	2.59	0.50	1.07
14	0.69	0.33	0.80	0.11	1.48	0.72	1.07	1.20	1.06	0.56	1.01	1.23	0.40	0.37	0.21	0.27	0.36	0.30	0.15	0.14	0.90	0.53	0.71	0.72	0.77	0.62	0.40	0.69
15	0.47	0.29	0.55	0.18	0.86	0.65	0.88	0.53	0.65	0.57	0.95	0.52	0.39	0.38	0.16	0.28	0.27	0.27	0.14	0.16	1.44	0.55	0.74	0.76	0.74	0.59	0.48	0.64
16	0.63	0.57	0.70	0.18	0.97	0.61	0.82	0.49	0.86	0.63	0.72	0.40	0.43	0.41	0.10	0.26	0.37	0.35	0.08	0.12	0.47	0.25	0.52	0.26	0.40	0.22	0.43	0.28

η – Kolmogorov microscale; u, v, w – air velocity direction; A, B, C, D, E, F – measuring positions.

Table 3.8 Spatial correlations of internal air velocities and external wind at different positions for case 9-16

Cases	External wind	A	B	C	D	E	F
	Cross-correaltion between external wind and air velocities at different positions						
9	1.00	0.04	0.14	0.23	0.26	0.01	0.03
10	1.00	0.08	0.12	0.36	0.30	0.16	0.02
11	1.00	0.02	0.00	0.22	0.20	0.02	0.01
12	1.00	0.01	0.02	0.22	0.15	0.07	0.02
13	1.00	0.19	0.04	0.16	0.19	0.02	0.11
14	1.00	0.16	0.25	0.28	0.26	0.15	0.01
15	1.00	0.05	0.06	0.16	0.12	0.14	0.06
16	1.00	0.15	0.19	0.22	0.22	0.03	0.00
	Cross-correaltion between air velocities at location C and those at other positions						
9	0.23	0.01	0.09	1.00	0.22	0.11	0.07
10	0.36	0.08	0.09	1.00	0.32	0.25	0.01
11	0.22	0.03	0.02	1.00	0.26	0.10	0.01
12	0.22	0.02	0.01	1.00	0.31	0.13	0.05
13	0.16	0.05	0.12	1.00	0.32	0.11	0.02
14	0.28	0.06	0.13	1.00	0.27	0.18	0.06
15	0.16	0.11	0.04	1.00	0.25	0.17	0.03
16	0.22	0.41	0.43	1.00	0.45	0.18	0.25

coefficients was around 0.15 for two buildings under different wind conditions. Lay and Bragg (1988) studied the spatial correlations of jet velocity and air velocities at different separation distances with jet inlet. They reported that the correlation coefficient was below 0.50 after a minimum distance (0.7 m) from jet inlet. In this study, the spatial distance was more than 13 m among different positions. The correlations of two velocity series could be interfered by unexpected perturbations. The small spatial correlations indicate that the dependence between outside wind and inside velocity series cannot be simply described by cross-correlation.

The cross-correlation among internal air velocities was also investigated. As an example, the correlation coefficients between air velocities at position C and at A, B, D, E, F are also shown in Table 3.8. Very low correlation coefficients were also generally found. The air velocity at position D at the same side with C showed higher correlations (>0.2).

To detect the coherency of the external wind and the internal air velocity, a comparison of the power spectra of the external wind and the internal velocities at different positions are given in Fig 3.6 for case 9 to16. External wind contained more energy. The power spectra of downwind side E possessed more energy than those at upwind side and in the middle section of the room. For building 1 (case 9-12), the power spectra at high frequency at upwind side (C) was at the same level as those at E. In the high frequency range, the decay rate of the power spectra is close to $f^{-5/3}$, agreeing with that found in the isotropic turbulence (Hinze,

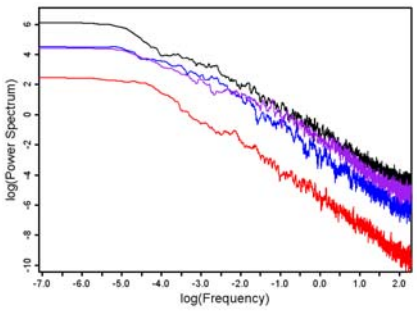

Case 9

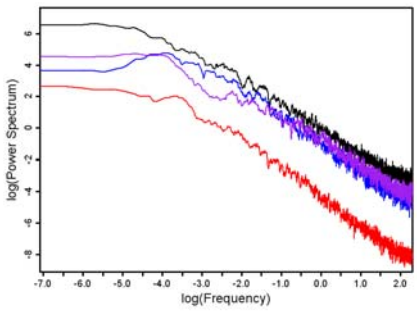

Case 10

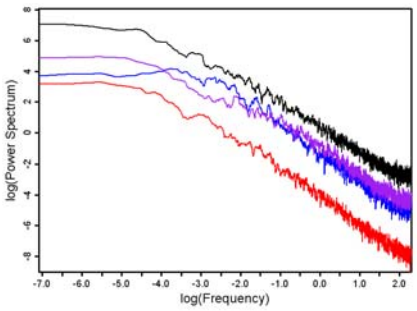

Case 11

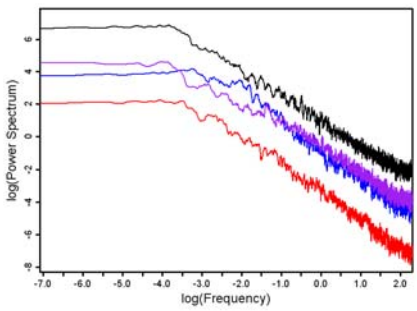

Case 12

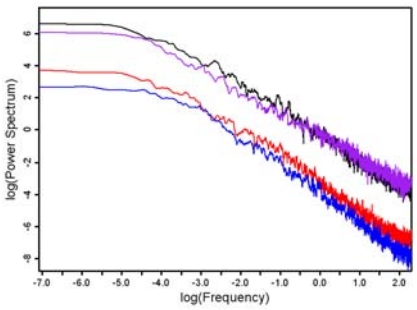

Case 13

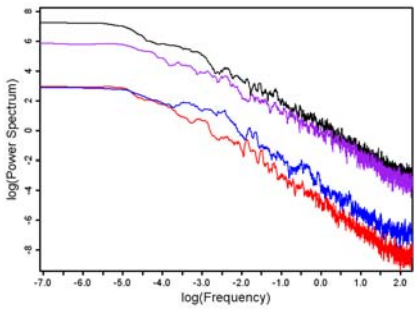

Case 14

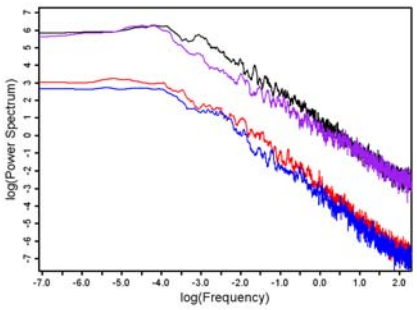

Case 15

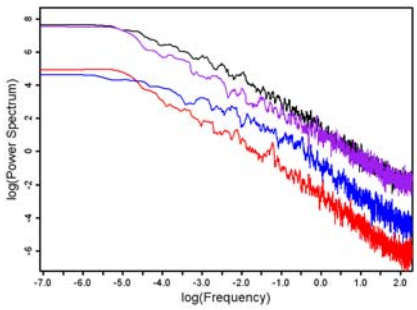

Case 16

Fig. 3.6 Spectral energy distribution of the external wind and internal airflow at position A, C, E (black line-outside; blue line-C, at upwind side; red line-A, in the middle of the room; purple line-E, at downwind side) for case 9-16Table 3.3 Integral time scale of the air velocity magnitudes and associated three components for different cases (s)

τ - turbulence time scale; u, v, w – air velocity direction; A, B, C, D, E, F – measuring positions.

1975). The sampling frequency 20 Hz is sufficient to establish the -5/3 slope of the power spectra at high frequencies.

3.4. Conclusions

Air velocity and turbulence were measured in two naturally ventilated dairy cattle buildings with three dimensional ultrasonic anemometers. Statistical methods and spectral analysis was applied to study the turbulence characteristics. Following conclusions can be drawn from this study:

(1) A sampling period of 20 min was enough to reach a constant value for mean and standard deviation of velocity time series measured in the two naturally ventilated buildings for a chosen steady state condition;

(2) Autocorrelation coefficients decayed to zero then started to behave erratically. The distribution of time integral scale was very irregular.

(3) The turbulence length scale of the outside velocity magnitudes ranged from 15.39 m to 120.56 m for all the cases. The integral length scale inside the buildings ranged from 1.08 m to 77.57 m. The length scales did not keep the same level when the external wind conditions were very similar. The length scales did not show positive correlations with the varied external wind speeds.

(4) When the external wind was kept at the same level, the internal kinetic energy at different positions was also at the same level. When the external wind speed was increased, the internal kinetic energy at all the measured internal positions was increased accordingly.

(5) Larger turbulence energy dissipation rate (0.49 m^2s^{-3}) was found near side openings, where the integral length scale was smaller. Microscale of turbulence ranged 3×10^{-5} m near side openings to 6×10^{-4} m in the middle section. Kolmogorov microscales were quite isotropy for the natural airflow in this study.

(6) External wind contained more energy. Air velocities near downwind side openings possessed higher power spectra at both low and high frequency, compared with those in the middle section or near upwind side openings.

References

Boulard, T., Wang, S., Haxaire, R., 2000. Mean and turbulent air flows and microclimatic patterns in an empty greenhouse tunnel. Agricultural and Forest Meteorology 100, 169-181.

Braam, C. R., Smits, M.C.J., Gunnink, H., Swierstra, D., 1997. Ammonia Emission from a Double-sloped Solid Floor in a Cubic House for Dairy Cows. *Journal of Agricultural Engineering Research* 68(4), 375-386.

Brett, A.C., Tuller, S.E., 1991. The autocorrelation of hourly wind speed observations. Journal of Applied Meteorology 30, 823-833.

Ecim-Djuric, O., Topisirovic, G., 2010. Energy efficiency optimization of combined ventilation systems in livestock buildings. Energy and buildings 42, 1165-1171.

Gustafsson, G., Jeppsson, K.H., Hultgren, J., Sanno, J.O., 2005. Techniques to Reduce the Ammonia Release from a Cowshed with Tied Dairy Cattle. *Agricultural Engineering International: the CIGR Journal, 7. Manuscript BC 04 010. Vol. VII. November*, 2005.

Heber, A.J., Boon, C.R., 1993. Air velocity characteristics in an experimental livestock building with non-isothermal jet ventilation. ASHRAE Transactions 99, 1139 – 1151.

Hinze, J.O., 1975. Turbulence. New York, McGraw-hill.

Larsen, T. S., 2006. Natural ventilation driven by wind and temperature difference. Ph.D. Thesis. Department of Civil Engineering, Aalborg University.

Lay, R. M., Bragg, G. M., 1988. Distribution of Ventilation air – Measurement and Spectral Analysis by Microcomputer. Building and Environment, 23 (3), 203-213.

Ngwabie, N.M., Jeppsson, K.H., Nimmermark, S., Swensson, C., Gustafsson, G., 2009. Multi-location Measurements of Greenhouse Gases and Emission rates of Methane and Ammonia from a Naturally Ventilated Barn for Dairy Cows. *Biosystems Engineering* 103, 68-77.

Samer., M., Loebsin, C., Feidler, M., Ammon, C., Berg, W., Sanftleben, P., Brunsch, R., 2011. Heat balance and tracer gas technique for airflow rates measurement and gaseous emissions quantification in naturally ventilated livestock buildings. Energy and buildings 43, 3718-3728.

Tennekes, H., Lumley, J.L., 1972.A first course in turbulence. *MIT press*.

Wu, W., Zhang, G., Kai, P., 2012a. Ammonia and methane emissions from Two Naturally Ventilated Dairy Cattle Buildings and the Influence of Climatic Factors on Ammonia Emission. *Manuscript submitted to Atmospheric Environment*.

Wu, W., Kai, P., Zhang, 2012b. An assessment of a partial pit ventilation system to reduce emission under slatted floor-Part 1: Scale Model Study. *Computers and Electronics in Agriculture* 83, 127-133.

Zhang, J.S., Christianson, L.L., Wu, G.J., Riskowski, G.L., 1992. Detailed measurements of room air distribution for evaluating numerical simulation models. ASHRAE Transactions 98, 58 – 65.

Zhang, G., Strom, J. S., Li, B., Rom, H.B., Morsing, S., Dahl, P., Wang, C., 2005. Emission of Ammonia and other Contaminant Gases from Naturally Ventilated Dairy Cattle Buildings. *Biosystems Engineering* 92 (3), 355-364..

Chapter 4

Evaluation of methods for determining air exchange rate in a naturally ventilated dairy cattle building with large openings using computational fluid dynamics (CFD)

Paper III:

Wu, W., Zhai, J., Zhang, G., Nielsen, P.V., 2012. Evaluation of methods for determining air exchange rate in a naturally ventilated dairy cattle building with large openings using computational fluid dynamics (CFD)**.** (Submitted to a peer review journal).

Abstract

Naturally ventilated dairy cattle buildings are a major source of ammonia and greenhouse gas emissions. Accurate estimation in gas emissions constitutes the first step towards reducing the negative impact of emissions on the local environment. The greatest uncertainty in the emission estimation is the calculation of the air exchange rate (AER). Computational fluid dynamics (CFD) was used to quantify the AER in a naturally ventilated dairy cattle building. The objective of this study was to assess the performance of three techniques for estimating ventilation rates: (1) integration of volume flow rates (VFR) through openings; (2) tracer gas decay (TGD) and (3) constant tracer gas injection (CTG). In the developed CFD model, the animal occupied zone (AOZ) was treated as porous media and the resistance coefficient of porous zone was derived by pressure drops across AOZ using a sub-CFD model. The results showed that AERs predicted by VFR and TGD were in good agreement with each other within a large range of wind speeds. The large difference in AER estimation using CTG and VFR indicates that the mean CO_2 concentration of the entire room may not represent the concentration at the air exit. It may not be suitable to calculate AER using mean concentration of internal sampling positions. When wind became stronger, the accuracy of CTG decreased. The gas sampling positions should be located adjacent to the openings or even in the openings. To reduce the uncertain introduced by wind direction, all the openings, especially of different azimuths, should possess sampling tubes. The maximum gas concentrations could be the optimum value to represent the concentration in the exit air.

***Key words*:** *porous media; ventilation; tracer gas; emission; sampling position*

4.1. Introduction

Naturally ventilated dairy cattle buildings are a major source of ammonia and greenhouse gas emissions to the atmosphere (Pereira et al., 2010; Ngwabie et al., 2011; Schrade et al., 2012). Reduction of emissions from dairy cow buildings will contribute to mitigate environmental pollution. However, it still lacks of reliable measurement and quantification methods of gas emissions from naturally ventilated livestock buildings. The greatest uncertainty in the emission estimation is the calculation of natural ventilation rates. Unlike the mechanically ventilated livestock buildings, it is more difficult to determine the naturally ventilation rates (Demmers et al., 1998; Demmers et al., 2000; Demmers et al., 2001; Teye and Hautala, 2007). Bruce (1978) applied Bernoulli's theorem to derive the air exchange rate through a simple livestock house under rather simple conditions. However, the airflow in a real cattle building is usually irregular and multidirectional. The large opening may act as an inlet during one period and as an outlet during another period due to the wind conditions (Zhang et al, 2005). These facts make it difficult to directly apply the theory in a real dairy cattle building. To date, numerous methods have been attempted to estimate natural ventilation rates from livestock buildings. Demmers et al. (2001) measured the pressure differences at the openings and converted them to air velocities using Bernoulli's equation; the airflow rates can be calculated from the air velocities and the opening areas. This method is equivalent to summing the volume flow rates (VFR) through openings. But the method failed to balance the mass flow rates through all the openings. The method of tracer gas decay (TGD) has been successfully used in determining the ventilation rates in livestock buildings (Demmers et al., 2001; Zhang et al, 2005). The accuracy of TGD method relies on complete mixing of air, which is unlikely in livestock buildings. CO_2 production model has also been demonstrated a suitable approach by assuming that the animals are the only source of CO_2 (CIGR, 2002; Zhang et al., 2005). The total CO_2 production was estimated by cow weight and milk yield (CIGR, 2002; Zhang et al., 2005). Prior to calculating ventilation rate, the only parameter to be ascertained in CO_2 production model is the background and outlet CO_2 concentration. The continuous CO_2 sample in measurement may take place at a few positions due to the limitation and the capability of the experimental instrument. The average concentration of all the sampling positions is generally used to represent the outlet CO_2 concentration. This concentration is named as representative CO_2 concentration in the exit air. CO_2 production model is equivalent to injecting constant tracer gas and thus is abbreviated to CTG.

In order to accurately quantify the natural ventilation rate, the capability of the three methods (VFR, TGD and CTG) should be investigated and documented. While the investigation required detailed information on the internal flow field, an on-farm measurement may not provide enough velocity and concentration data to compare the above methods. Given that the detailed airflow inside naturally ventilated livestock buildings can also be described by Computational Fluid Dynamics (CFD) (Norton et al., 2010a; Norton et al., 2010b). CFD was applied to determine the air exchange rate (AER) in this paper.

The objectives of this study are to:

(1) develop and validate a CFD model to calculate the AER in a naturally ventilated dairy cattle building; the CFD model included a sub-model, which was used to derive the resistance coefficients of the cows to the airflow;
(2) evaluate the performance of TGD and CTG against VFR for quantifying the AER;
(3) determine optimum positions to sample CO_2 to obtain the representative outlet CO_2 concentration.

4.2. Materials and methods

The performance of the three methods namely VFR, TGD and CTG to estimate AER was evaluated by a CFD model of a naturally ventilated dairy cattle building. Since it was too comprehensive to include the cows in the CFD model, the animal occupied zone (AOZ) was treated as a porous volume in order to consider the resistance introduced by cows. The resistance coefficients of AOZ were obtained by a sub-model. To ensure the accuracy of the CFD model, thermal boundary conditions for walls and roofs were documented in this work. The CFD model must be validated by experiments before it was used for quantifying AER. This section starts with the introduction of a field measurement, which is used for validating CFD models. The CFD model including the sub-model, mesh and thermal boundary conditions is given after the description of the measurement. This section ends with a discussion on how to quantify AER using the three methods in CFD.

4.2.1. The field measurement for model validation

The experimental study of Wu et al. (2012a) was used to validate CFD prediction of natural ventilation. One of the two naturally ventilated dairy cattle buildings in Wu et al. (2012a) was employed to establish the CFD model. The dimensions of the full-scale cattle building are given in Fig. 4.1a. The building had a length of 111.4 m, a width of 36.0 m, an eave height of 4.30 m and a ridge height of 11.7 m. The height of the side wall was 1.20 m. Two sidewall openings can be controlled by automatically regulating curtains according to indoor thermal condition and outdoor climate. In the simulated case, the curtain height was 0.82 m that left a sidewall opening height of 1.08 m. The width of the ridge opening was 0.60 m.

Air velocities and CO_2 concentrations inside and outside the building were measured. Air velocities were measured by ultrasonic anemometers – WindMaster (Gill instruments Ltd, Hampshire, UK). Detail on WindMaster can be found in the work of Wu et al. (2012b). All the anemometers were connected to a multi-port adapter, which supplies electricity power to anemometers and transfers the data to a computer. The three-dimensional air velocities were measured in a frequency of 20 Hz. An ultrasonic anemometer was placed 10 m above the ground to monitor the external wind velocities. Air velocities inside the buildings were

recorded at 6 positions (Fig. 4.1b): two were near one sidewall openings; two were placed in the centre of the buildings near ridge openings; two were near another sidewall openings. The CO_2 concentrations were measured using a Photo-acoustic Multi-gas Monitor, model 1312 and a multiplexer, model 1303 (Innova air Tech Instruments A/S, Denmark). The internal concentrations were sampled by three 20 m long tubes (Fig. 4.1b) with 20 uniformly distributed holes. The three tubes were near the three groups of velocity sensors, respectively. Gases at two outside positions about 2 m from a side wall were also sampled as background reference. Data measured in October 26th, 2010 was used for validation of CFD simulation.

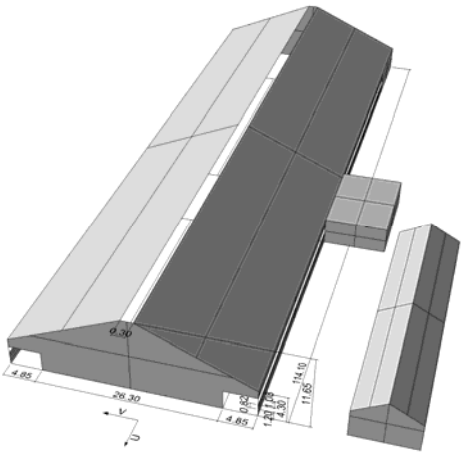

(a) Geometry

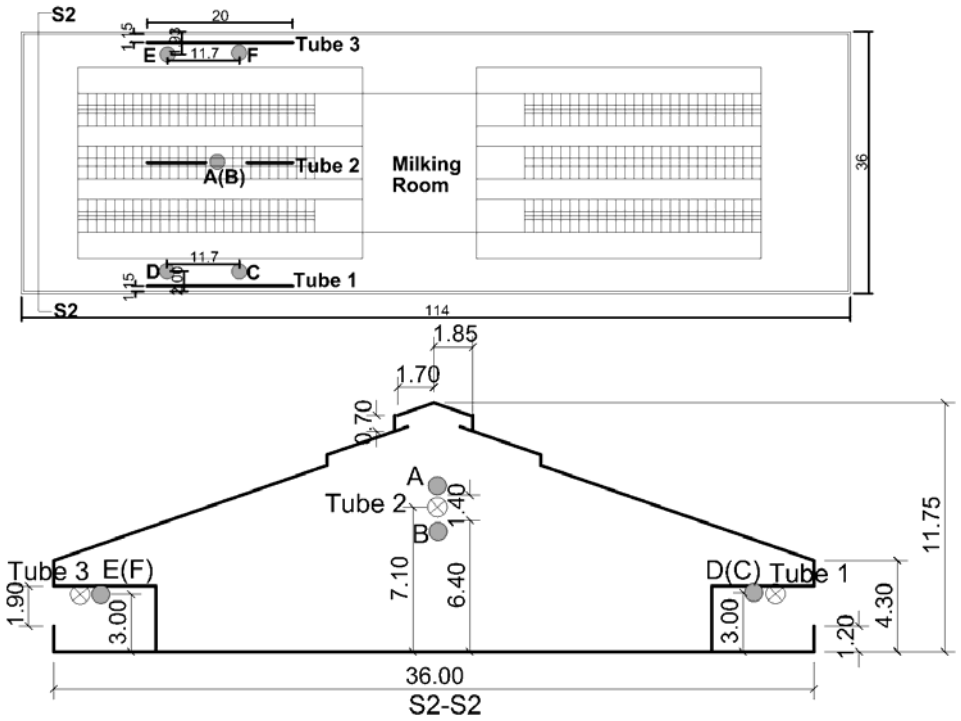

(b) the sensor positions: Solid circles marked with A, B, C, D, E, F denote positions for velocity measurements; Thick lines and circles with cross denote the sampling locations for gas measurements.

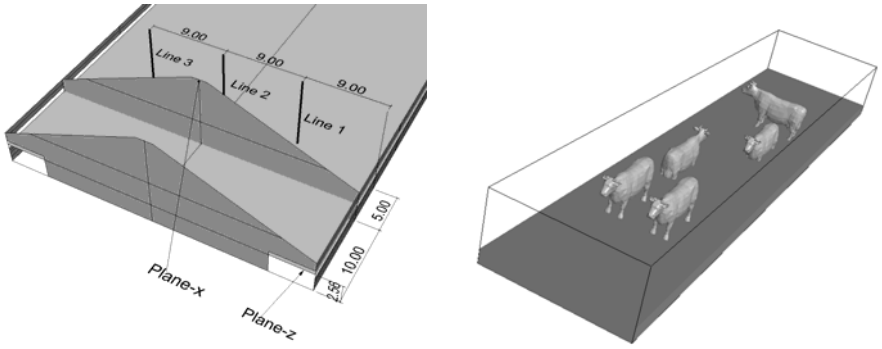

(c) Positions for data analysis (d) The sub-model for AOZ

Fig. 4.1 Geometry of the cattle building, the measurement setup and the sub-model for AOZ

4.2.2. CFD Model details

4.2.2.1. The CFD model and the sub-model for AOZ

The CFD model is depicted in Fig. 4.1a. The CFD model was constructed according to the real dimensions of the full-scale building. Two surrounding buildings were also established in the model. Since a detailed simulation of animals, slatted floor and partitions within AOZ will require massive meshes and long time to iterate the calculations, and will cause the problem of iteration convergence, Sun et al. (2004) and Bjerg et al. (2008) presumed the AOZ as porous media with a resistance to airflow in order to consider the effect of the animals on the air motion. The resistance coefficients of porous media needed to be set up in the simulation but there was not enough data to derive the coefficients by measurement. Bjerg et al. (2008) assumed a uniform distribution of animals and extracted part of AOZ to calculate the pressure drop using CFD. The coefficients were obtained by a linear regression from the pressure drops and the associated inlet velocities. In order to gain the resistance introduced by the existing of animals, the first step was to develop a sub-model for AOZ to characterize the animal's blocking effects on horizontal airflow. The representative geometry of the sub-model is shown in Fig. 4.1d. The length of the sub-model domain is 17 m; the width is 4 m; the height is 1.6 m. Similar to a whole AOZ in a building, the sub-model was divided into a walking area, a feeding area and a laying area. The density of the animals on the different areas was assumed uniform. Based on the total cow number and the total floor area, the density of cows in the sub-model was as follow: two cows stood in the feeding area, one cow lay down in each of the two laying sections, and one cow stood in the walking alley.

The second step was to fit the pressure drops and the associated inlet velocities into the following relation

$$\frac{\Delta p}{l} = (\mu D + \frac{1}{2} F \rho \mid u \mid) u \qquad (4.1)$$

where, $\frac{\Delta p}{l}$ is pressure drop per unit length, Pa m^{-1}; D is viscous resistance, m^{-2}; F is inertial resistance, m^{-1}; μ is air viscosity, N s m^{-2}; ρ is air density, kg m^{-3}.

4.2.2.2. Numerical method and mesh

The standard $k-\varepsilon$ turbulence (Launder and Spalding, 1974) model was used for all the simulations. SIMPLE scheme was employed to couple pressure and velocity. Second order upwind method was used to discretize convection term. Residuals, velocity at one point and mass balance for inlet and outlet are monitored to achieve iteration convergence.

Mesh is the most important factor for an accurate modelling of environmental flow around and inside buildings. The optimum mesh distribution (Fig. 4.2) and cells number were determined by conducting a mesh convergence study. Four different grid systems were constructed for finding a proper mesh. The cells number for each grid system is given in Table 4.1.

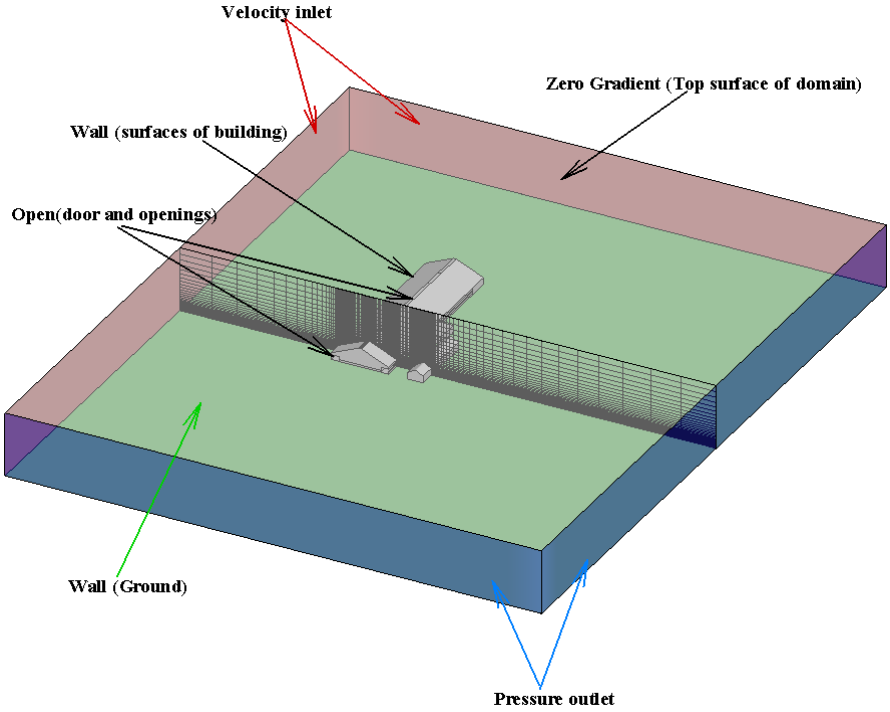

Fig. 4.2 The mesh and boundary conditions

Mesh convergence can be assessed by the level of agreement between velocities computed using meshes of different resolutions and that using the finest mesh. This agreement level can be evaluated by root mean square deviation (RMSD):

$$RMSD = \bar{x}_f^{-1}\sqrt{\frac{\sum_{i=1}^{n}(x_{c,i}-x_{f,i})^2}{n}} \qquad (4.2)$$

where, $x_{c,i}$ is the velocity from coarse mesh at one position, $x_{f,i}$ is the velocity from the finest mesh at the same position with $x_{c,i}$. $\bar{x}_f$ is the mean value of $x_{f,i}$.

The small RMSD value (0.15) (Table 4.1) between grid 3 and grid 4 also indicated that grid 3 with 1,091,540 cells was optimum in this study.

Table 4.1 Cells number and mesh convergence

Mesh	grid4	grid3	grid2	grid1
Cells No.	1,997,932	1,091,540	534,802	257,760
Ratio [a]	1.83	2.04	2.07	-
RMSD [b]	-	0.15	0.34	0.52

[a] ratio between grid i+1 and grid i (i=1, 2, 3)

[b] RMSD-Root mean squared deviation between finest mesh grid4 and coarse mesh grid 3, gird 2, grid 1

4.2.2.3. Wind profile

The power law function was proposed to represent the vertical inlet profile of the computation domain,

$$u_z = U_{ref}(z/10)^{\alpha} \tag{4.3}$$

$$k_z = \frac{u^{*2}}{\sqrt{C_\mu}} \tag{4.4}$$

$$\varepsilon_z = \frac{u^{*3}}{\kappa(z + z_0)} \tag{4.5}$$

$$u^* = \frac{\kappa U_{ref}}{\ln((10 + z_0)/z_0)} \tag{4.6}$$

where, u_z is the vertical mean velocity, m s^{-1}; U_{ref} is the reference velocity at 10 m height, m s^{-1}; u^* is the friction velocity, m s^{-1}; κ is the von Karman Constant, 0.40-0.42; z is vertical coordinate of the computational domain, m; z_0 is terrain roughness length; k_z is the kinetic energy, m^2 s^{-2}; C_μ is a model constant for the $k-\varepsilon$ model, 0.09; ε_z is the turbulence energy dissipation rate, m^2 s^{-3}.

As the simulated building located in an open farm land with few trees and buildings, z_0 was approximately 0.03 and α was 0.14 (Wieringa, 1992). Riddle et al (2004) observed significant profile changes along an empty domain when $k-\varepsilon$ model was employed without roughness modification. In a CFD simulation, the flow profiles of the mean speed and turbulence quantities those were applied at the inlet plane of the computational domain should be representative of the roughness characteristics of the upstream domain (Blocken et al, 2007). In CFD software,Fluent, the roughness is expressed in terms of the roughness height k_s and roughness constant C_s (0.5). k_s in Fluent is obtained by (Norton et al, 2010a)

$$k_s = \frac{9.793 z_0}{C_s} \tag{4.7}$$

k_s is about 0.59 m. Ansys Ltd. (2011) mentioned that y_p (the distance from centre point P of the wall-adjacent cell to the wall) should be larger than k_s. Accordingly, the size of the wall-adjacent cell should be larger than1.18 m, which is too coarse for the CFD simulation. Therefore, $k_s = z_0$ proposed by Blocken et al (2007) was used in this simulation.

The simulation for validation was carried out under an external wind speed of 3.00 m s^{-1} for U-component and 1.53 m s^{-1} for V-component at 10 m height above the ground. Direction U and V are shown in Fig. 4.1a.

4.2.2.4. Thermal boundary conditions

Natural ventilation is driven by wind and thermal buoyancy. To consider the contribution of thermal buoyancy to ventilation rate, the thermal boundary conditions of the building envelops and the heat released from animals should be included in the CFD simulation. Norton et al (2010a) applied the following heat balance equation to estimate the wall temperature,

$$Q_{sol} - (Q_{co} + Q_{ci} + Q_{ro} + Q_{ri}) = 0 \tag{4.8}$$

where, Q_{sol} is solar irradiation, W m^{-2}; Q_{co}, Q_{ci} is convective heat flux with outside and inside air, W m^{-2}; Q_{ro}, Q_{ri} is radiant heat flux, W m^{-2}. The net exchange of radiation between different surfaces were assumed zero. The inner surface and outer surface temperatures were assumed equal for walls and roofs. The following equation can be used to calculate roof temperature (Norton et al, 2010b)

$$T_{rf} = \frac{\alpha_s I + h_{co} T_o + h_{ci} T_i + h_{r,sky} T_{sky}}{h_{co} + h_{ci} + h_{r,sky}} \tag{4.9}$$

where, α_s is the fraction of absorbed solar radiation, 0.2 (Kreith and Kreider, 1978); I solar irradiation, 498.04 W m^{-3} in this simulation; h is the convective heat transfer coefficient, W m^{-2} K^{-1}; T indicates temperature, K; subscript co, ci, sky means convective heat transfer with outside, inside air and sky. The outside and inside air temperature is obtained from the measurements, T_o =279.2 K, T_i =282.2 K. Sky temperature can be derived using (Chen et al, 1995)

$$T_{sky} = (S/\sigma)^{1/4} \tag{4.10}$$

where, S is global thermal radiance, 227.375 W m^{-2}; σ is Stefan-Boltzman constant, 5.6697x10^{-8}.

Convective heat transfer coefficient can be expressed by (Roy et al, 2002)

$$h_c = \frac{KNu}{L} \tag{4.11}$$

where, K is the thermal conductivity for roof, 0.0242 W m^{-1} K^{-1}; L is characteristic length, which is perceived as roof width, 17 m; for turbulent flow, Nusselt number Nu can be given by (Roy et al, 2002)

$$Nu = 0.036\,\mathrm{Re}^{4/5}\,\mathrm{Pr}^{1/3} \tag{4.12}$$

When equation (4.8) was applied to the side walls, the surface temperature will be

$$T_{so} = \frac{h_{co}T_o + h_{ci}T_i + \alpha_s I_{ver} + h_{r,sky}T_{sky}}{U_w} \tag{4.13}$$

$U_w = h_{ci} + h_{co} + h_{sky}$; I_{ver} is the solar irradiation on the vertical wall, 498 W m^{-2} in this simulation.

The thermal boundary conditions are given in table 4.2.

Table 4.2 Thermal boundary conditions

	Inlet air	Ground	floor	roof	side wall
type	Temperature, K	Temperature, K	heat flux	Temperature, K	Temperature, K
value	279.2	279.7	0	275.94	276.18

4.2.2.5. Quantifying AER using the three methods – VFR, TGD and CTG in CFD

VFR method is quite straightforward. The function of the openings can be distinguished by examination of the flow direction across the associated opening. Then the ventilation rate is the summation of the volume flow rates across all the inlet or outlet openings. In order to use TGD, all the computational cells inside the building must be filled with a scalar of initial fraction – unity. The fraction of the scalar in the computational cells surround the building must be zero in the initial stage. The CFD simulation is then run to determine the decay rate of the scalar (Norton et al., 2010a), which is converted to ventilation rate. In CTG method, CO_2 produced by dairy cows was used as tracer gas source. The CO_2 production rate was determined based on the model (CIGR, 2002) by the body weight, milk yield and pregnancy of the cows and it was released uniformly inside the AOZ. The mean of the CO_2 concentration in the entire room was taken as the representative concentration. The

ventilation rate was the multiplication of the CO_2 production rate and the reciprocal of the representative CO_2 concentration.

4.3. Results and discussion

In order to display the airflow patterns and profile of velocity, temperature and concentration, two planes (plane-x and plane-z) and three lines (line 1, line 2 and line 3) are positioned in Fig. 4.1 c and were taken as the reference positions for data analysis.

4.3.1. Model validation

Pressure distributions in the sub-model (Fig. 4.1 d) with an inlet velocity 0.1 m s^{-1} are shown in Fig. 4.3 a. The resistance coefficient by regression (Fig. 4.3 b) was 7.71 m^{-2} for viscous force and 0.06 m^{-1} for inertial force. Bjerg et al (2008) calculated resistance coefficients for AOZ in a pig production unit; the viscous and inertial resistance coefficient was around 400-1500 m^{-2} and 0.4-1.3 m^{-1}, respectively. The lower resistance for the cow AOZ should be caused by the lower density of cows (12 m^2 cow^{-1}) compared with the higher density of pigs (2.36 m^2 cow^{-1}).

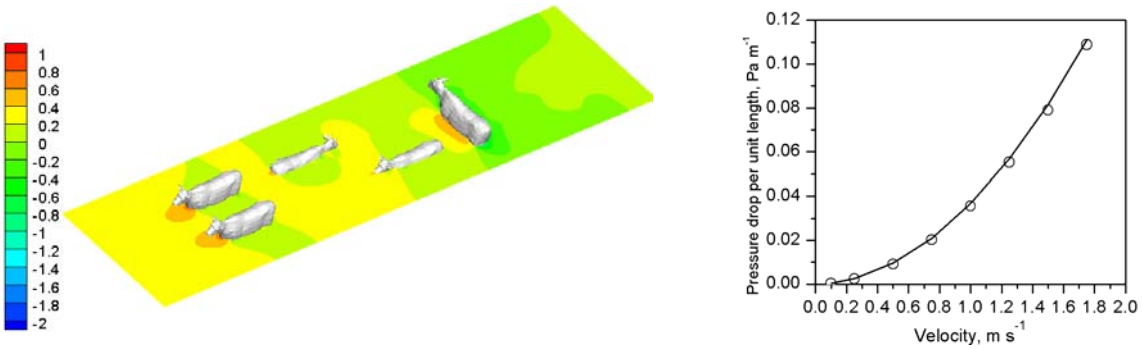

(a) (b)

Fig. 4.3 Results from the sub-model: (a) Pressure drop (Pa) with an inlet velocity 0.1 m s^{-1}; (b) the relationship between pressure drop and inlet air velocity. Circle denotes the simulated values from the sub-model; line denotes the values from the equation 1.

4.3.1.1. Airflow patterns and validating air velocities

Horizontal and vertical airflow patterns at plane-z are shown in Fig. 4.4. The downwind side opening was divided into left and right section by a wall (the purple line).Two big vortices were formed and maintained in the right section. The upwind opening acted as air inlet; the ridge and downwind openings mainly acted as air outlet in this case.

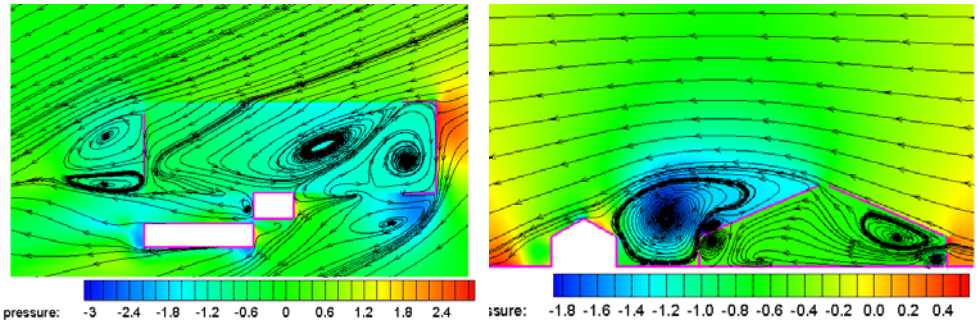

Fig. 4.4 Horizontal and vertical airflow patterns (Purple lines mark the side walls)

Table 4.3 shows the measured and simulated air velocities at different positions. Overall, good agreement was generally found between the simulated and measured air velocities. The simulated velocities in the middle section of the room were within the variation of the measured fluctuated data. For example, at the position near ridge opening, the simulated velocity was 0.22 m s^{-1}, the measured velocity ranged from 0.10 to 0.30 m s^{-1} considering the mean velocity 0.20 m s^{-1} and its fluctuation 0.10 m s^{-1}. A relatively larger discrepancy existed at the position about 10 m away from the downwind side wall, where the simulated and measured velocity magnitude was 0.52 and 0.29±0.08 m s^{-1}, respectively. Near this position, the direction of the outward flow through the opening was altered by the separated flow that began at the leading edge of the neighbour building (Fig. 4.4). In such a region the standard $k-\varepsilon$ model may have challenge. It was reported that standard $k-\varepsilon$ model has difficulty to predict the flow separation (Castro and Apsley, 1997; Norton et al, 2010b). More uncertainties would be enrolled in the calculation of velocities near a separation region.

Table 4.3 Velocity magnitude of measurement and simulation

Coordinate in domain			Position	Measurement	Simulation
X	Y	Z		(m s^{-1})	(m s^{-1})
19.5	1.75	2.85	Near side opening	0.25±0.09	0.43
31.2	1.75	2.85	Near side opening	0.29±0.08	0.57
27.3	18	7.8	In the middle	0.16±0.09	0.18
27.3	18	9.2	Near ridge opening	0.20±0.10	0.22

4.3.1.2. Temperature distribution

The mean temperature (Fig. 4.5) from CFD simulation was around 281 K in the room. High temperature 284.7 K was found in the downwind side of the AOZ. The right section of the room for calves had a uniform temperature around 280.6 K. The vertical temperature distribution showed that heat was brought up from the AOZ to the roof and the ridge opening functioned to discharge the heat.

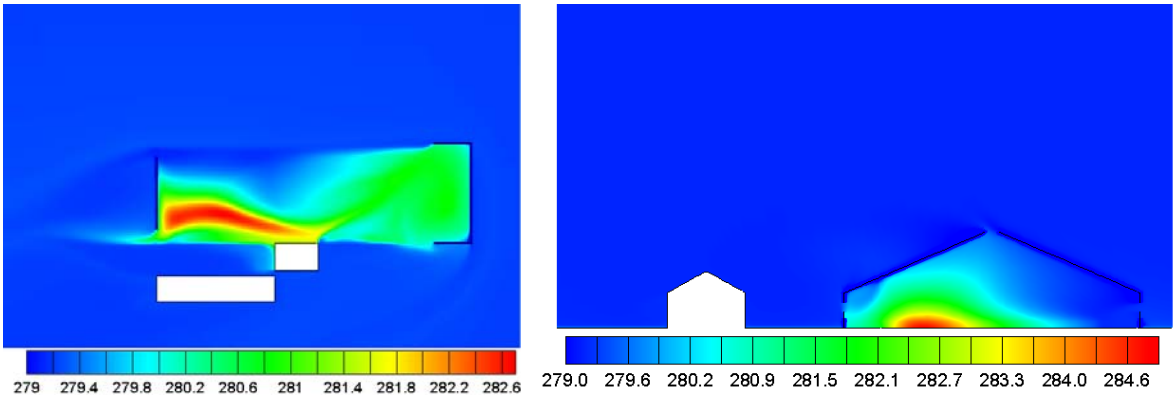

Fig. 4.5 Horizontal and vertical temperature distribution (K)

Cooper et al. (1998) developed a thermal balance model to estimate the mean internal temperature of livestock buildings. A mean temperature 282.2 K for inside room was estimated using this model. As described early, the solar radiation and global thermal radiance were not simulated directly but were transformed into thermal conditions of roofs and sidewalls using equation (4.8). The heat production from animals was estimated using a heat production model (CIGR 2002). The mean room temperature 281 K calculated by CFD agreed with the mean room temperature 282.2 K predicted by the thermal balance model of Cooper et al (1998).

4.3.1.3. Validating CO_2 concentration and AER

The horizontal distribution (Fig. 4.6) showed that high CO_2 concentration was found near the flow vortex. From the vertical field, most CO_2 was confined inside the AOZ and a part of it was transported to upwind side below the roof due to the air recirculation in the upwind side (Fig. 4.4).

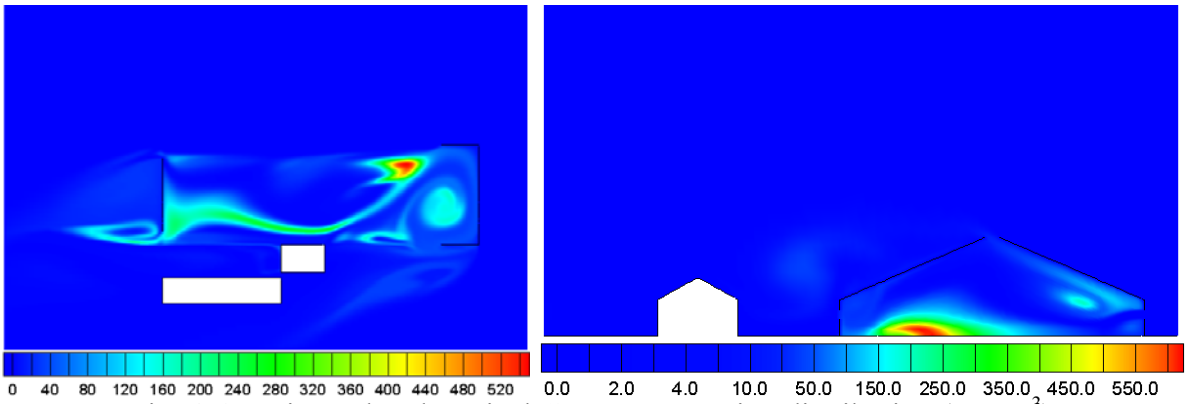

Fig. 4.6 Horizontal and vertical CO_2 concentration distribution (mg m^{-3})

Both simulated and measured CO_2 concentrations are presented in table 4.4. Very good agreements were found. The mean concentration of three positions was 175.9 mg m^{-3} for measurement and 167.5 mg m^{-3} for simulation. The relative difference was smaller than 5%.

Table 4.4 CO2 concentrations and AER from measurement and simulation

Position	CO2 (mg m^{-3})		AER (h^{-1})	
	Simulation	Measurement	Simulation	Measurement
Near the upwind side opening	18.5	23.2	103.6	82.6
In middle of the room	162.3	149.5	11.8	12.8
Near the downwind side opening	321.7	355.0	6.0	5.4
Mean of three positions	167.5	175.9	11.4	10.9

Table 4.4 also shows the AER calculated using simulated and measured CO_2 concentration and the variability of AER with respect to CO_2 sampling positions. The representative CO_2 concentration was the mean of those at the three sampling positions. The measured AER 10.9 h^{-1} was consistent with simulated AER 11.4 h^{-1}. The relative difference between them was 4.6%.

Through a thoughtful validation of velocity, temperature and concentration, the CFD model was proved to be accurate and can be used for further systematic investigation and analysis.

4.3.2. Assessing the capability of VFR, TGD and CTG to calculate AER

To study the performances of the three techniques– VFR, TGD and CTG, AER was calculated at different wind speeds ranging from 2.83 to 12.73 m s^{-1} with the same wind direction of 315°. The predicted AERs are showed in Fig. 4.7. AER predicted by TGD and VFR had a small deviation. The AERs calculated by CTG using the mean concentration of the entire room were consistently higher than those by VFR and TGD methods for all the cases. For example, the simulated AER calculated by VFR and TGD was 69.9 and 68.5 h^{-1} while the AER calculated by CTG was 106.3 h^{-1}, when the external wind speed was 12.73 m s^{-1}. The relative difference between the results from CTG and VFR was 50%, which was very large. The discrepancies can be explained by the requirements of using CTG. The accuracy of CTG highly depended on the selection of the representative CO_2 concentration at the air exit. The average concentration of the entire room used for calculation of AER may not represent the outlet gas concentration. In this case, the average concentration of the entire room was smaller than the truly representative concentration. Fiedler and Müller (2011) indicated that more sampling positions were required so that the mean concentration of all sampling positions can be closer to the representative value. However, this study implies that even the mean concentration of the entire room may not be an appropriately representative concentration at the air exit. Therefore, using mean concentration of internal sampling positions would add more uncertainties to the estimation of ventilation. Demmers et al. (2000) also reported large error in ventilation rate estimate using internal sampling points;

they also indicated that no obvious zones or locations, which offered a representative concentration, could be identified within the building section.

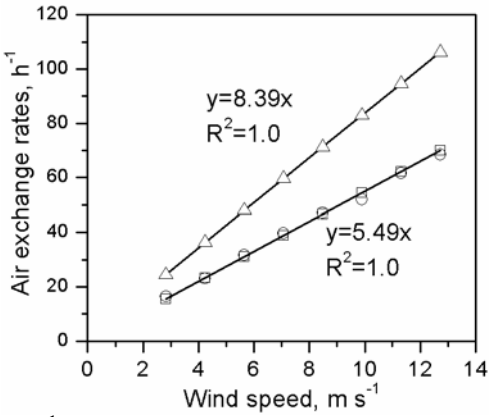

Fig. 4.7 Air exchange rate (h^{-1}) calculated by three techniques using CFD. Square – VFR; Circle – TGD; Triangle – CTG. The upper line – fitted using CTG data; the lower line – fitted using VFR data.

Among the three techniques used in CFD, VFR was the direct way to obtain ventilation rates and was thus set as the reference method in this study. Compared with VFR, TGD also highlighted an accurate measure of ventilation rates. The result was consistent with the work of Norton et al. (2010a). However, TGD is time consuming in CFD simulations. It requires the calculation in a transient mode, and data at different time steps need to be saved and handled individually. Although CTG can be easily implemented in CFD simulations, its accuracy (Fig. 4.7) is questionable due to the fact that a representative concentration cannot be easily identified if the sampling positions are located inside the livestock building.

Fig. 4.7 shows a strong correlation (R^2=1) between wind speed and AER based on the methods – VFR and CTG. High wind speed causes high ventilation rates. When wind speed varied from 2.83 to 12.73 m s^{-1}, AER increased from 15.5 to 69.8 h^{-1} predicted by VFR and from 24.5 to 106.3 h^{-1} predicted by CTG. The same correlation between AER and wind speed was also found in the work of Wu et al. (2012a). The deviation of AER obtained by CTG and VFR increased from 8.9 to 36.4 h^{-1}. The reason is that stronger wind leads to poorer mixing of indoor air (Norton et al., 2010b; Teye and Hautala, 2007). The poorer air mixing makes the concentration of the entire room farther away from the truly representative concentration at the air exit. Hence, the accuracy of such a CTG method decreases when the wind becomes stronger.

4.3.3. The representative CO_2 concentration at the exit air

The mean gas concentration of the entire room failed to represent that in the exit air for calculating AER using CO_2 production model. In order to find the optimum representative concentration, AERs were calculated based on CTG using the gas concentrations at different positions (Tube 1, Tube 2, Tube 3, see Fig. 1b). For the convenience of further analysis, the

CTG method using the mean concentration of the entire room, the mean concentration of the three tubes, the mean concentration of the tube (Tube 2) near ridge opening and the downwind sampling tube (Tube 1), the mean concentration of the downwind sampling tube (Tube 1) was abbreviated to CTG, CTG1, CTG2, CTG3, respectively, without further claim.

Fig. 4.8 a shows the AERs determined with different representative CO_2 concentrations under different wind speeds, when the wind blew to the building with an angle of 315°.

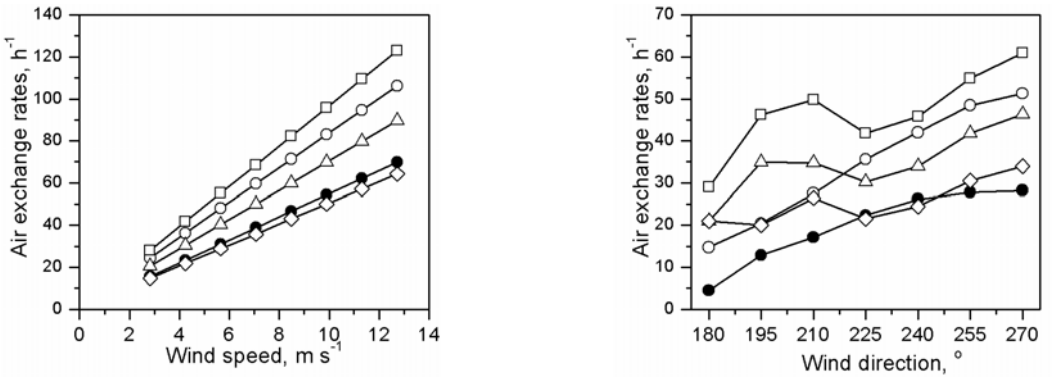

(a) (b)

Fig. 4.8 AERs calculated with CTG method using different representative CO_2 concentrations in the exit air: circle – using mean concentration of the entire room; square – using mean concentration of the three sampling positions (Fig.1 b); triangle- using mean concentration of the middle and downwind sampling positions; diamond – using mean concentration of the downwind position. ACRs calculated with VFR (solid circle) were also plotted as reference. (a) shows AERs with respect to different wind speeds; (b) shows AERs with respect to different wind directions.

A large difference was found in AERs predicted using the mean concentration at different sampling positions. It reveals the high sensitivity of CTG method according to the sampling locations. AERs predicted by CTG3 and VFR were consistent within a large range of wind speeds (2.83 - 12.73 m s^{-1}). For example, the AER was 14.7 h^{-1} based on CTG3, which had a relative difference of 5.2% with 15.5 h^{-1} calculated by VFR, when the wind speed was 2.83 m s^{-1}. While the wind speed varied to 12.73 m s^{-1}, the relative difference between 64.2 h^{-1} based on CTG3 and 69.9 h^{-1} based on VFR was 8.2%. AERs were overestimated by CTG1 compared to those by VFR and the overestimation became larger when the wind speed increased. AER calculated by CTG1 ranged from 28.2 to 123.1 h^{-1} when the wind speed varied from 2.83 - 12.73 m s^{-1}. The largest relative difference with that estimated by VFR was 76%. Tube 3 in the simulations was located near the upwind opening. The concentration sampled by this tube was close to that in the background. The mean concentration of the three tubes may underestimate the representative gas concentration by taking the mean concentration of the upwind tube into the average. Consequently, the AERs were overestimated by CTG1. CTG2 showed a better performance to estimate AER

compared with CTG and CTG1. However, CTG2 also overestimated AERs significantly during different wind speeds. Demmers et al. (1998) estimated ventilation rates in a dairy cattle building based on CTG using two sampling systems; the tracer concentration was measured at nine positions in openings around the perimeter of the building (CTG3) as well as around a ring sampling line in the building (CTG); they reported that during windy weather (>5 m s^{-1}) the ventilation was overestimated by the ring line (CTG) compared to the perimeter samples (CTG3). The results in this work were consistent with that of Demmers et al. (1998).

Fig. 4.8b shows the AERs determined by different representative CO_2 concentrations under different wind directions with the same wind speed of 4 m s^{-1}. The wind direction was of outstanding effect on estimation of AER using different representative CO_2 concentrations. When wind direction was smaller than 225°, all the methods based on constant tracer gas (CTG, CTG1, CTG2 and CTG3) failed to predict AERs at the same level with VFR. The reason is that the CO_2 concentration used in the three methods cannot represent the outlet concentration for these cases according to the external wind direction. The estimation on AER ranged from 4.5 to 14.8 h^{-1} by VFR and from 28.2 to 51.3 h^{-1} by CTG. The overestimation by CTG was intolerable. AERs were more overestimated by CTG1, CTG2 and CTG3 compared to those by CTG. When the wind direction became larger than 225°, CTG3 started to show a better capability to estimate AERs compared with VFR. Therefore, the mean concentration of Tube 3 can represent the concentration in the exit air but subject to the wind directions. It can be explained by the function as inlet and outlet of the openings through examining the airflow patterns at different wind directions. Fig. 4.9 shows the airflow patterns coloured with CO_2 concentration distribution on plane-x. When the wind blew parallel to the openings (180°), most parts of the long opening on the upper part of the graph (Fig. 4.9a) and the right opening on the lower part of the graph (Fig. 4.9a) acted as air inlet; the left opening on the lower part of the graph (Fig. 4.9a) acted as air outlet; that can explain why the CTG3 did not show a better performance compared with CTG. When the wind direction varied to 195°, most parts of the three sidewall openings acted as air inlet (Fig. 4.9b); the mean CO_2 concentration near sidewall openings thus cannot represent the concentration in the exit air. When the wind direction became larger than 225°, the long opening on the upper part of the graph (Fig. 4.9c) acted as air inlet and the two openings on the lower part of the graph (Fig. 4.9c) started to act as air outlet; consequently, the mean concentration of the Tube 3, which was near downwind openings, can well represent the concentration in the exit air; therefore, under this circumstance, CTG3 estimated more accurate AERs compared with VFR method.

Through the above discussions, it can be concluded that the gas sampling positions should be close to the openings or even in the openings; the maximum gas concentrations in the different openings could be the optimum value to represent the concentration in the exit

air. The sampling positions located inside the room may introduce more errors in estimation of AER.

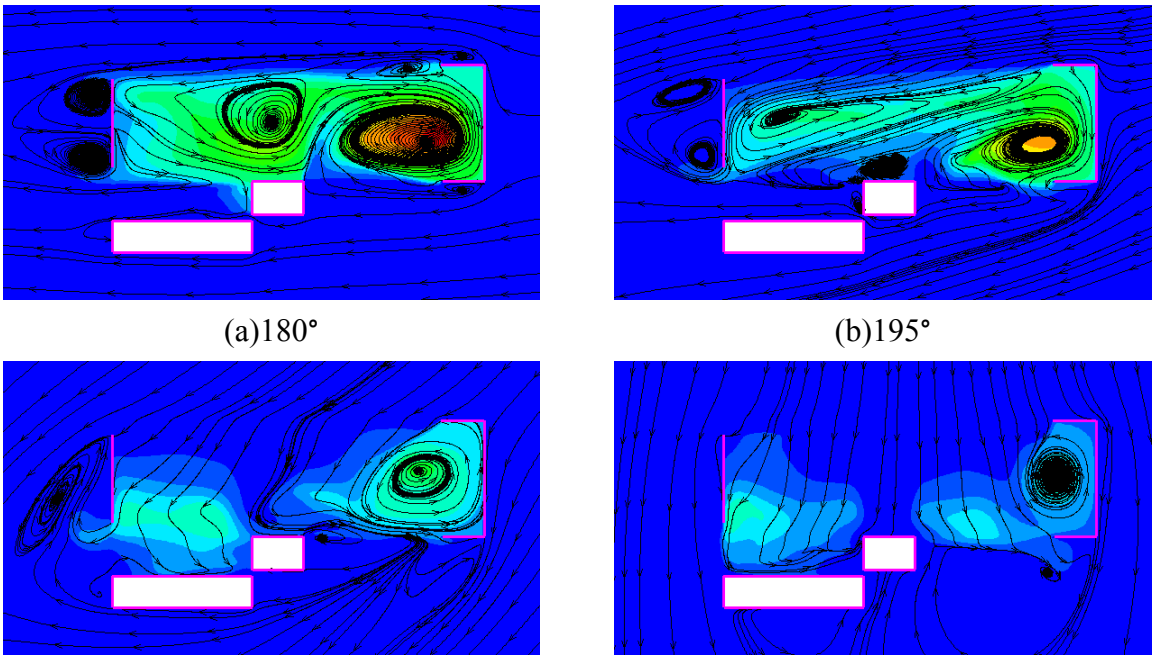

(a)180° (b)195°

(c) 225° (d)270°

Fig. 4.9 Airflow patterns coloured with CO_2 concentration distribution at different wind directions

4.3.4. Further discussion

Based on the requirement of the international conventions, there is a pressing need for inventory of NH_3, CH_4, CO_2 and N_2O emissions from naturally ventilated livestock buildings (Wu et al., 2012a). The remained and greatest uncertainty in the estimation of the above gas emissions was the calculation of the ventilation rates. The main purpose of this article was to evaluate the performance of the different and existing methods to determine ventilation rates. The above-mentioned performance of the three techniques does not match their applicability while they are used in field measurements. Naturally ventilated livestock buildings generally possess large openings which make the velocity measurement in the openings rather difficult. Therefore, VFR seems impossible to be implemented in reality. Demmers et al. (1998) indirectly used VFR via measuring the pressure difference across the openings. But the method failed to balance the mass flow rates in and out through the buildings. When TGD is applied to an on-site building, the building must be fully covered initially in order to distribute the tracer gas uniformly across the entire building. This is perhaps not suitable when the animals are inside the building. Since ventilation rates depend on the external wind conditions, it will be very difficult to measure the ventilation rates continuously by TGD method. These are why the CTG method is very popular in the field measurement. CTG is

usually employed in form of an equivalent approach – CO_2 production model (Zhang et al., 2005; Feidler and Müller, 2011).

When the CO_2 production model is applied to estimate natural ventilation rates, the key problem is to ascertain the outlet CO_2 concentration since the total CO_2 production and background CO_2 concentration can be easily determined or measured. It can be concluded from this study that the gas sampling positions should be located adjacent to the openings or even in the openings. To reduce the uncertain introduced by wind direction, all the openings especially of different azimuths should possess sampling tubes. The maximum gas concentrations in the different openings could be the optimum value to represent the concentration in the exit air.

This work can be helpful to design the field measurements of gas emissions from naturally ventilated livestock buildings; especially can guide engineers to determine the gas sampling positions when CO_2 production model is applied to estimate natural ventilation rates and emission rates.

The AOZ was treated as porous media in this paper. The uncertainty was not presented due to the lack of data on air velocities and gas concentrations in the AOZ. The advantages of using porous media were: (1) simplifying the geometry, consequently, reducing the grid cells and simplifying the boundary conditions; (2) generally, the cows were randomly distributed and randomly moved in AOZ; thus, a prescribed uniform CO_2 release in porous media was also reasonable. The limitation of using porous media was that the derivation of airflow resistance coefficients was not validated against experimental data. In addition, the difference of using porous media and simulating the cows directly was unknown. Such a difference can be future work.

4.4. Conclusion

The performances of three techniques – integrating volume flow rates (VFR), tracer gas decay (TGD) and constant tracer gas (CTG) were assessed by CFD to quantify ventilation rates from a naturally ventilated livestock building. The following conclusions can be drawn:

(1) The developed CFD model documented with detailed thermal boundary conditions was validated by air velocities and CO_2 concentration data; the resistance coefficients of AOZ were derived by a sub-model; the coefficient was 7.71 m^{-2} for viscous force and 0.06 m^{-1} for inertial force.

(2) AERs predicted by VFR and TGD were in good agreement with each other within a large range of wind speeds.

(3) Large difference in AER estimation using CTG and VFR indicates that the mean CO_2 concentration of the entire room may not represent the outlet concentration.

(4) When wind became stronger, the accuracy of CTG decreased.

The gas sampling positions should be located adjacent to the openings or even in the openings. To reduce the uncertain introduced by wind direction, all the openings especially of

different azimuths should possess sampling tubes. The maximum gas concentrations in the different openings could be the optimum value to represent the concentration in the exit air.

References

Anonymous, 2009. Fluent help Release 12.0. Ansys Inc., Southpointe, 275 Technology Drive, Canonsburg, PA 15317, USA.

Bjerg B., Zhang, G., Kai, P., 2008. Porous media as boundary condition for air inlet, slatted floor and animal occupied zone in numerical simulation of airflow in a pig unit. AgEng2008 International Conference on Agricultural Engineering, Hersonissos, Crete-Greece.

Blocken, B., Stathopoulos, T., Carmeliet, J., 2007.CFD simulation of the atmospheric boundary layer: wall function problems. Atmospheric environment 41, 238-252.

Castro, I.P., Apsley, D.D., 1997. Flow and dispersion over topology: a comparison between numerical and laboratory data for two dimensional flows. Atmospheric Environment 31, 839-850.

Chen, B., Clark, D., Mei, W., Kasher, J., 1995. Measurement of Night Sky Emissivity in Determining Radiant Cooling from Cool Storage Roofs and Roof Ponds. *Proceedings of the American Solar Energy Society* Annual Meeting, Minneapolis, MN.

CIGR, 2002. Report of Working Group on Climatization of Animal Houses – Heat and Moisture Production at Animal and House Levels. *CIGR Section II, Commission International Du Genie Rural (International Commission of Agricultural Engineering)*.

Cooper, K., Parsons, D.J., Demmers, T., 1998. A thermal balance model for livestock buildings for use in climate change studies. J. Agric. Eng. Res. 69, 43-52.

Demmers, T.G.M., Burgess, L.R., Short, J.L., Phillips, V.R., Clark, J.A., Wathes., C.M., 1998. First experiences with methods to measure ammonia emissions from naturally ventilated cattle buildings in the U.K. *Atmospheric Environment* 32,285-293.

Demmers, T.G.M., Burgess, L.R., Phillips, V.R., Clark, J.A., Wathes., C.M., 2000. Assessment of Techniques for Measuring the Ventilation Rate, using an Experimental Building Section. *Journal of Agricultural Engineering Research* 76, 71-81.

Demmers, T.G.M., Phillips, V.R., Short, J.L., Burgess, L.R., Hoxey, R.P., Wathes., C.M., 2001.Validation of Ventilation Rate Measurement Methods and the Ammonia Emission from Naturally Ventilated Dairy and Beef Buildings in the United Kingdom. *Journal of Agricultural Engineering Research* 79 (1), 107-116.

Feidler, A.M., Müller, H.J., 2011. Emissions of ammonia and methane from a livestock building natural cross ventilation. *Meteorologische Zeitschrift* 20 (1), 059-065.

Kreith, F., Kreider, J.F., Principles of Solar Energy, Hemisphere Publishing, New York, 1978.

Launder, B.E., Spalding, D.B., 1974. The numerical computational of turbulent flows. Computer Methods in Applied Mechanics and Engineering 3, 269-289.

Ngwabie, N.M., Jeppsson, K.H., C., Gustafsson, G., Nimmermark, S., Swensson, 2009. Effects of Animal Activity and Air Temperature on Methane and Ammonia Emissions from a Naturally Ventilated Building for Dairy Cows. *Atmospheric Environment* 45, 6760-6768.

Norton, T., Grant, J., Fallon, R., Sun, D.W., 2010a. Assessing the ventilation effectiveness of naturally ventilated livestock buildings under wind dominated conditions using computational fluid dynamics. Biosystems engineering 103 (1), 78-99.

Norton, T., Grant, J., Fallon, R., Sun, D.W., 2010b. A computational fluid dynamics study of air mixing in a naturally ventilated livestock building with different porous eave opening conditions. Biosystems engineering 106 (2), 125-137.

Norris, S.E., Richards, P.J., 2010. Appropriate Boundary Conditions for Computational Wind Engineering Models Revisited. The fifth international Symposium on computational wind engineering (CWE2010), Chapel Hill, North California, USA.

Pereira, J., Misselbrook, T., Chadwick, D.R., Coutinho, J., Trindade, H., 2010. Ammonia Emissions from Naturally Ventilated Dairy Cattle Buildings and Outdoor Concrete Yards in Portugal. *Atmospheric Environment* 44, 3413-3421.

Riddle, A., Carruthers, D., Sharpe, A., McHugh, C., Stocher, J., 2004. Comparisons between FLUENT and ADMSfor Atmospheric Dispersion Modelling. Atmospheric Environment 38 (7), 1029-1038.

Roy, J.C., Boulard, T., Kittas, C., Wang, S., 2002. Convective and Ventilation Transfers in Greenhouses, Part 1: the Greenhouse considered as a Perfectly Stirred Tank. Biosystems engineering 83 (1), 1-20.

Schrade, S., Zeyer, K., Gygax, L., Emmenegger, L., Hartung, E., Keck, M., 2012. Ammonia Emissions and Emission Factors of Naturally Ventilated Dairy Housing with Solid Floors and an Outdoor Exercise Area in Switzerland. *Atmospheric Environment* 47, 183-194.

Sherman, M.H., 1990. Tracer-gas Techniques for Measuring Ventilation in a Single Zone. *Building and Environment* 25 (4), 365-374.

Snell, H.G.J., Seipelt, F., Van Den Weghe, H.F.A., 2003. Ventilation Rates and Gaseous Emissions from Naturally Ventilated Dairy Houses. *Biosystems Engineering* 86 (1), 67-73.

Sun, H.W., Keener, H.M., Deng, W., Michel, F., 2004. Development and Validation of 3-D Models to Simulate Airflow and Ammonia Distribution in a High-rise Hog Building during Summer and Winter Conditions. *Agricultural Engineering International CIGR Journal* 6, Manuscript BC 04 044.

Teye, F.K., Hautala, M., 2007. Measuring Ventilation Rates in Dairy Buildings. *International Journal of Ventilation* 6 (3), 1473-3315.

Wieringa, J., 1992. Updating the Davenport roughness classification. Journal of wind engineering and industrial aerodynamics 41-44, 357-358.

Wu, W., Zhang, G., Kai, P., 2012a. Ammonia and Methane Emissions from Two Naturally Ventilated Dairy Cattle Buildings and the Influence of Climatic Factors on Ammonia Emissions. *Manuscript submitted to Atmospheric Environment*.

Wu, W., Kai, P., Zhang, 2012b. An assessment of a partial pit ventilation system to reduce emission under slatted floor-Part 1: Scale Model Study. *Computers and Electronics in Agriculture* 83, 127-133.

Wu, W., Zhang, G., Bjerg, B., Nielsen, P.V., 2012c. An assessment of a partial pit ventilation system to reduce emission under slatted floor-Part 2: Feasibility of CFD prediction using RANS turbulence models. *Computers and Electronics in Agriculture* 83, 134-142.

Zhang, G., Strom, J. S., Li, B., Rom, H.B., Morsing, S., Dahl, P., Wang, C., 2005. Emission of Ammonia and other Contaminant Gases from Naturally Ventilated Dairy Cattle Buildings. *Biosystems Engineering* 92 (3), 355-364.

Chapter 5

An assessment of a partial pit ventilation system to reduce emission under slatted floor-Part 1: Scale Model Study

Paper IV:

Wu, W., Kai, P., Zhang, 2012. **An assessment of a partial pit ventilation system to reduce emission under slatted floor-Part 1: Scale Model Study**. *Computers and Electronics in Agriculture* 83, 127-133.

Abstract

Emissions of ammonia and greenhouse gases from naturally ventilated livestock houses cause contamination of the surrounding atmospheric environment. Requests to reduce ammonia emissions from livestock farms are growing in Denmark. It is assumed that using an additional mechanical pit exhaust unit with a minimised ventilation rate can remove the most polluted part of the air from the slurry pit and treat it with an air purification unit. This system can result in reduction of ammonia emissions from naturally ventilated livestock production units. To study the efficiency of a partial pit ventilation to reduce emissions, a 1:2 scale model of manure pit section of a dairy cattle house was built with slatted floor and a mechanical pit exhaust at side-walls. Investigations were performed under varied airflow velocities above the floor, two slatted floor opening ratios (The ratio of the opening area to the whole floor area), two pit ventilation rates and two exhaust directions. CO_2 was used as tracer gas and was added to the mixing chamber of the pit model with a constant flux. The removal ratio was defined as the percentage of the gases removed by the pit exhaust. The results showed that a partial pit exhaust system could abate gas emissions from the slurry pit. The performance of the system was influenced by the following factors: airflow velocities above the floor, the slatted floor opening ratio, the pit ventilation rates and the pit exhaust position. For downwind exhaust, the removal ratios were decreased from about 80% to 50% when the air velocity above the floor was increased from 0.78 to 1.94 m s^{-1}. The mean of the removal ratios was 83.1% for all upwind exhaust cases and some downwind exhaust cases. There was no clear velocity dependency. Lower floor opening ratio could reduce more emission than the higher opening ratio for most of the cases. Higher pit ventilation rates resulted in higher removal ratios for most cases of downwind exhaust but did not always give higher removing efficiency for upwind exhaust. Overall, the upwind exhaust can discharge 8% more CO_2 than the downwind exhaust. Removal capability was better correlated to the four factors (airflow velocities above the floor, the slatted floor opening ratio, the pit ventilation rates and the pit exhaust position) combined when compared to the correlation to each individual factor.

The results from the scale model measurements need to be validated by full-scale experiments.

Key words: *Ammonia Pit ventilation; slatted floor; scale model; wind tunnel; livestock; tracer gas*

Nomenclature

B	width of the scale model (m)	Rr	removal ratio (%)
C_{back}	background CO_2concentration (mg m^{-3})	TIV	the integrated variable
C_{exh}	CO_2 concentration in the pit exhaust duct (mg m^{-3})	U_H	air velocity at 0.15 m height above wind table (m s^{-1})
C_i	the concentration at different positions (mg m^{-3})	ΔP	pressure difference of upstream and downstream of the orifice (Pa)
$\overline{C}$	concentration difference (mg m^{-3})	Subscripts	
G	CO_2 generation rate (mg h^{-1})	$back$	background
H	height of headspace of pit (m)	exh	pit exhaust duct
PEP	pit exhaust position (-1~upwind, 1~downwind)	i	different positions
Q_{exh}	pit ventilation rate (m^3 h^{-1})	fo	floor opening ratio
R_{fo}	slatted floor opening ratio	H	height

5.1. Introduction

Emissions of ammonia and greenhouse gases from naturally ventilated livestock houses cause the problem of atmospheric pollution. Ammonia is also known to damage ecosystems via eutrophication (Monteny and Erisman, 1998.). In Denmark the requests for reduction of ammonia emission from livestock farms is growing (Saha et al, 2010.). In order to reduce the negative impact of the emission on the environment, the polluted air should be purified before released into the atmosphere.

In a naturally ventilated livestock building, it is difficult to collect the exhausted air for further air cleaning. However, partial pit ventilation may be adapted into the system, i.e., remove a part of the most polluted air under slatted floor and connect the exhaust channel to an air purification unit. Saha et al. (2010) investigated the effects of a partial pit ventilation system on ammonia emission from a fattening pig room with a diffuse ceiling inlet, a ceiling-roof-top air exhaust and a pit exhaust. The pit exhaust operated with only 10% of the total ventilation capacity and the ceiling-roof-top exhaust operated as the major ventilation unit regulated according to the thermal conditions in the room. Saha et al. (2010) concluded that a partial pit exhaust with purification system could reduce total ammonia emission significantly even though air exhausted through the pit constituted a relatively small share of the total ventilation capacity.

Challenges of applying partial pit ventilation system to naturally ventilated dairy cattle buildings are the wider slatted floor area above the slurry channel and also the more complex airflow characteristics above the slatted floor due to natural wind effects. It brings up the issues on how to design a suitable system for such an application.

The hypothesis is that using an additional mechanical pit exhaust unit with a minimised ventilation rate can remove polluted air and treat them with an air purification unit, which can reduce ammonia emission from naturally ventilated livestock production systems. The objectives of this study are:

(1) to validate this hypothesis in a laboratory condition using a scale model and to investigate the ability of a partial pit ventilation system to reduce gas emissions.

(2) to investigate the effects of the opening ratios of the slatted floor, the pit ventilation rates and the pit ventilation positions on the capacity of partial pit ventilation to reduce gas emissions.

5.2. Materials and Methods

Experimental investigations were carried out in Air Physics Lab, Engineering Centre Bygholm, Aarhus University, Denmark.

5.2.1. Experimental facility

5.2.1.1. Scale model for slurry pit

A one-half scale model of manure pit section was built of wood materials and was composed

of slatted floor and slurry pit beneath (Fig. 5.1-(a)). The size of the scale model was 1.5m×1.25m×0.5m. The height of the head space was 0.4 m and at the bottom of the pit, there was a tracer gas mixing chamber of 0.1 m in height (Fig. 5.1-(a)). The detailed dimensions of the scale model are shown in Fig. 5.1-(c). The mixing chamber had a loft plate with 63 evenly distributed holes (Fig. 5.1-(c)) and covered with porous membrane (Fig. 5.1-(a) (c)). The plate and membrane were used to release gases. The diameter of each hole was 0.006 m and the distance between each hole was 0.142 m. Two exhaust openings (Fig. 5.1-(a) (c)) were placed at the each end of the model. The centres of the openings were in the middle height of the pit headspace. The diameter of each opening was 0.10m. On the top of the headspace was a slatted floor (Fig. 5.1-(b)). The dimensions of the slats are shown in Fig. 5.1-(c). The width of each slot on the floor was 0.02m.

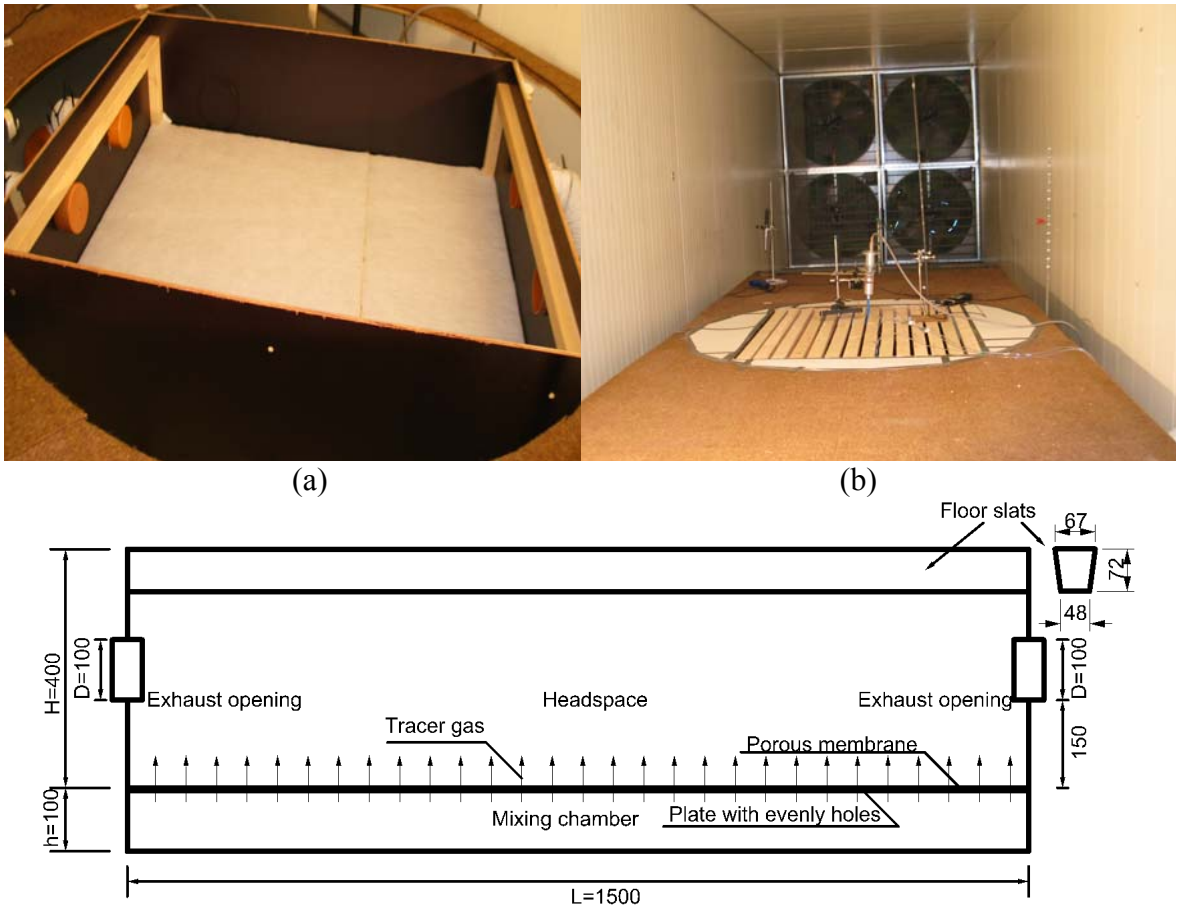

Fig. 5.1- The experimental facility. (a) The photograph of the scale model; (b)The photograph of the wind tunnel system; (c)The dimensions of the scale model and the slats. All the units are in mm.

5.2.1.2. Wind tunnel

The size of the wind tunnel is 11m×2.8m×2.8m. Initial measurement showed a minor difference in air velocity above two side edges (along the length of the wind tunnel) of a wind table when air velocity is smaller than 0.4m/s.

A wind table was placed in the wind tunnel to simulate solid floors in naturally ventilated cattle houses (Fig. 5.1-(b)). The size of the wind table is 6m×2m.The pit model was placed in the centre of the table and the top of the slatted floor was at the same level with the top of the table. The slats (Fig. 5.1-(b)) of the pit model were orientated parallel to the airflow direction in the wind tunnel to simulate a case of cross ventilation in a dairy cattle buildings.

5.2.1.3. Pit exhaust system

Part of the released gas from the mixing chamber was removed by the pit exhaust system (Fig. 5.2) and the rest escaped the headspace through the slatted floor slots. Two exhaust positions were used at the two ends of the model to simulate the exhaust at two sides of slurry pit channel in a practical dairy cattle building. The normal directions of the exhaust opening were parallel to the slats on the floor. When the pit exhaust duct was connected to the openings at the side of upstream of the wind, it was specified as upwind exhaust; otherwise, it was specified as downwind exhaust (Fig. 5.2).

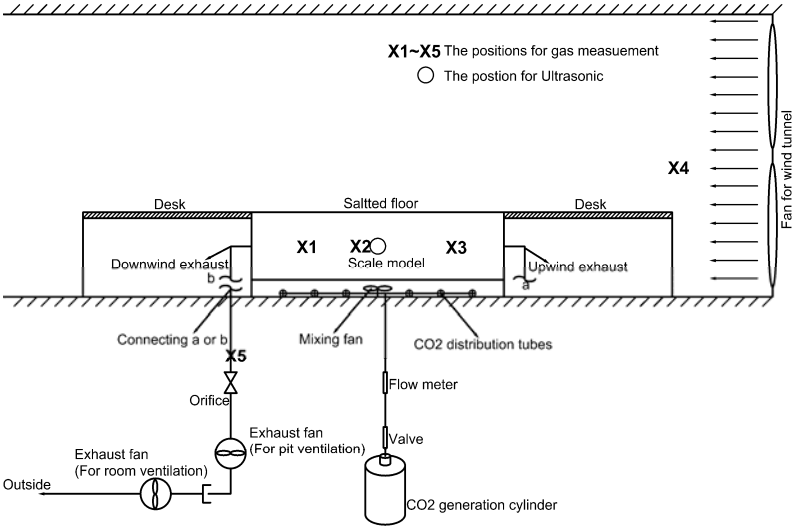

Fig. 5.2 - The experimental system

5.2.1.4. Tracer gas generation

To simulate emission of ammonia and greenhouse gas from the manure surface in the pit, carbon dioxide (CO_2) was supplied to the mixing chamber via a set of distributed tubes and the release openings of the tubes were evenly placed in the bottom of the chamber (Fig. 5.2). A mixing fan was used in the chamber to make sure that CO_2 was mixed homogeneously (Fig. 5.2). The plate with uniformly spaced holes and the covered porous membrane created a uniform distribution surface for CO_2 released from the mixing chamber to the headspace of the pit.

CO_2 was supplied from a pressurized gas cylinder and controlled via an adjustable valve and a flow meter (Fig. 5.2). A constant flux was kept for all experimental treatments.

5.2.2. Experimental set-up and measurements

5.2.2.1. Experimental set-up

Investigations were performed at five airflow velocities above the floor, at two pit ventilation rates and at two slatted floor opening ratios (The ratio of the opening area to the whole floor area) in a wind tunnel. The varied air velocities above the slatted floor were reached by adjusting the operation frequency of the wind tunnel fan motor. The velocities at 0.15 m height above the wind table in front of the slatted floor are listed in Table 5.1. The used pit ventilation rates were 120 and 60 m^3 h^{-1}. Two floor opening ratios (21% and 9.7%) and two pit exhaust positions (downwind and upwind exhaust) were used.

Table 5.1. The velocities at 0.15 m height from the wind table

Frequency (Hz)	Velocity (m/s)	Accuracy (±, m/s)
2	0.19	0.01
5	0.49	0.01
9	0.78	0.01
14	1.46	0.01
20	2.06	0.02

* Frequency is the frequency of wind fan motor

5.2.2.2. Measurement of the velocities and the pit ventilation rates

Air velocity at 0.15 m height above the floor level and at upwind of the pit model was monitored by Testo 400 (Testo AG, Lenzkirch, Germany) velocity sensor. The monitor position was at the symmetrical plane (aligned with length of wind tunnel) of the wind tunnel table. The sensor has a measurement range of 0-20 m s^{-1} and an accuracy of ±0.01 m s^{-1} (0-1.99 m s^{-1}), ±0.02 m s^{-1} (2-4.9 m s^{-1}) and ±0.04 m s^{-1} (5-20 m s^{-1}).

Air velocity inside the headspace was measured by an ultrasonic anemometer – WindMaster (Gill instruments Ltd, Hampshire, UK). It has a velocity range of 0-45 m s^{-1} and a resolution of 0.01 m s^{-1}. The direction range is 0-359.9° and the resolution is 1°. The sample rate can be 20 Hz and 32 Hz. 20 Hz with an output rate of 1 Hz was used in this measurement. Velocity at each measurement point was recorded for 5 min. The unit is designed not to require re-calibration within lifetime (Anonymous, 2009). According to standard calibration, it has accuracy at 12 m s^{-1} of 1.5% RMS for wind speed and 2° for wind direction. The head of ultrasonic is 233.5 mm high which is nearly half of the height of headspace. Thus only velocities at the height of 0.2 m above bottom surface of the headspace were measured. The ultrasonic sensor can be moved along central slot of the slatted floor to record velocities at different sites.

A flow meter, type FMU/FMDRU 100-80 (Lindab Ventilation, Båstad, Sweden) was used to measure pit ventilation rates. The accuracy is 5%.The ventilated flow in the pit exhaust duct is determined using the equation

$$Q_{exh} = 15.84\sqrt{\Delta P} \qquad (5.1)$$

where, Q_{exh} is the pit ventilation rate, $m^3 h^{-1}$; 15.84 is a constant from manufactory; ΔP is pressure difference between upstream and downstream side of the orifice, Pa. The pressure differences were measured by a pressure sensor (Model 694, Huba Control, Würenlos, Switzerland) with a range of 0 – 300 Pa, an accuracy of ±0.7% and a resolution of 0.1% of full dimension. The data was collected through a data logger (CR1000 Campbell Scientific, Utah, USA). The sampling frequency was 0.1 Hz and the data was recorded as averages of each one minute.

5.2.2.3. The measurement of CO_2 concentration

A constant CO_2 flux of 5.76×10^4 mg h^{-1} was injected into the mixing chamber and monitored by a flow meter (FM-487 variable area rotameter, Porter Instrument, Hatfield, PA, USA). The total injection rate was determined by the following method. Pit ventilation was started to discharge the total generated CO_2. The top of the slatted floor was tightly covered but a very narrow slot was left open at the opposite side of the pit exhaust openings. The narrow slot was used to introduce fresh air. The total CO_2 injection rate can be decided by the following equation:

$$G = Q_{exh}(C_{exh} - C_{back}) \quad (5.2)$$

where, G is CO_2 generation rate, mg h^{-1}; Q_{exh} is pit exhaust ventilation rate, $m^3 h^{-1}$; C_{exh} is CO_2 concentration in the pit exhaust duct, mg m^{-3}; C_{back} is background CO_2 concentration, mg m^{-3}.

CO_2 concentration was measured with a 1312 Photoacoustic Multi-gas Monitor and a multiplexer 1303 (Innova air Tech Instruments A/S, Denmark). A reference measurement point was placed in the centre of the mixing chamber to monitor the gas balance of each experiment setup. When CO_2 concentration at this point became constant, the system was perceived to be at equilibrium. The background concentration of the airflow above the slatted floor was measured in the upwind side of the wind tunnel, about 2 m away from the pit side wall. The concentrations were also measured in the exhaust duct and in three positions X 1, X 2, X 3 (Fig.1-d) at the half height of the headspace. All the three positions were located in the symmetric plane of the pit model and parallel to the slots of the floor. After about 2 h when the system achieved a steady-state condition, the data was sampled for 20 min. The sampling period for each measurement was 20 s, followed by 20 s cleaning time to replace the air in the measuring chamber of the gas monitor before a new measurement channel started to sample.

5.2.3. Estimation of air exchange rate using removal ratio

Removal ratio, defined as the ratio of CO_2 flux exhausted by the pit ventilation and the

injected CO_2 flux, was used to evaluate the performance of the pit ventilation system under the different external conditions. It can be expressed as

$$Rr = \frac{Q_{exh}(C_{exh} - C_{back})}{G} \times 100 \quad (5.3)$$

where, Rr is removal ratio, %. The larger the Rr, the more CO_2 is exhausted through the pit ventilation, thus the more efficient the pit ventilation is.

5.2.4. The integrate variable to evaluate the effect of all factors on the performance of pit ventilation

There are four factors: air velocity above the wind table (U_H), opening ratio of slatted floor (R_{fo}), pit ventilation rate (Q_{exh}) and pit exhaust position, which influenced the removal ratio of the system. The four factors may have a synergistic effect on the performance of the pit ventilation and there is no consistent relationship between removal ratio and each individual factor. Based on this hypothesis, a new index normalized by all the four factors was proposed as follow and named as the integrated variable (IV).

$$IV = (U_H BH / Q_{exh}) \cdot R_{fo} \cdot PEP \quad (5.4)$$

where, B is width of the scale model; H is the height of headspace of the scale model; R_{fo} is slatted floor opening ratio; *PEP* was used to quantify the pit exhaust position. It could be described as

$$PEP = \begin{cases} -1 & upwind \quad pit \quad ventilation \\ +1 & downwind \quad pit \quad ventilation \end{cases} \quad (5.5)$$

5.2.5. CO_2 concentration difference

CO_2 concentration difference between pit head space and background was calculated from

$$\overline{C} = C_i - C_{background} \quad (5.6)$$

Where $\overline{C}$ is concentration difference, mg m^{-3}; C_i is the concentration at different positions X1, X2 or X3 (Fig.2), mg m^{-3}; i represents position X1, X2 or X3.

5.3. Results

5.3.1. CO_2 concentration inside the pit headspace

$\overline{C}$ and the standard error are given in Table 5.2. The average $\overline{C}$ at the three positions was 2419±371 mg m^{-3} for the case without exhaust and this concentration difference was reduced to 1782±278 and 1567±285 mg m^{-3} when the downwind pit ventilation rate was 60 and 120 $m^3 h^{-1}$, respectively. In the cases of upwind exhaust, $\overline{C}$ was largely reduced to 243±78 and 62±19 mg m^{-3} for pit ventilation rate 60 and 120 $m^3 h^{-1}$.

Table 5.2. CO_2 concentration difference between pit headspace and background (mg m^{-3})

Position	Without exhaust		Downwind exhaust Ventilation rate (m^3 h^{-1})				Upwind exhaust Ventilation rate (m^3 h^{-1})			
			60		120		60		120	
	Mean	SE[a]	Mean	SE	Mean	SE	Mean	SE	Mean	SE
X1[b]	1034.40	27.79	665.06	28.50	585.78	27.59	60.02	4.20	10.46	1.12
X2	2249.68	392.68	1745.56	446.23	1041.22	60.84	103.80	10.80	10.20	4.34
X3	3973.24	447.30	2937.80	163.90	3075.30	183.92	567.18	158.46	166.84	2.79
Mean[c]	2419.11	371.02	1782.81	278.57	1567.43	285.48	243.66	78.52	62.50	19.79

CO_2 concentration was measured when the air velocity above the floor was 0.78 m s^{-1} and the slatted floor opening was 21%.

[a]SE standard error

[b]see Fig.1- (d) for different positions

[c]Averages of the concentration difference at three positions

It should be pointed out that $\overline{C}$ and the related standard errors were higher in the upwind side (X3). In the case without exhaust, $\overline{C}$ was 1034±62 mg m^{-3} in the downwind side (X1) and it was 3.84 times higher in the upwind side (X3).

5.3.2. The effect of the air velocity

Fig. 5.3 shows that the removal ratios were affected by the pit ventilation rates and positions, slatted floor opening ratio and the air velocities above the floor. When U_H was increased from 0.78 to 1.94 m s^{-1} for the cases of downwind exhaust, the removal ratios decreased from about 80% to 50%. The mean of the removal ratios was 83.1% for all the cases of upwind exhaust and some cases of downwind exhaust when U_H was smaller than 0.78 m s^{-1}. The removal ratios varied from about 70% to 98% but there was no clear velocity dependency.

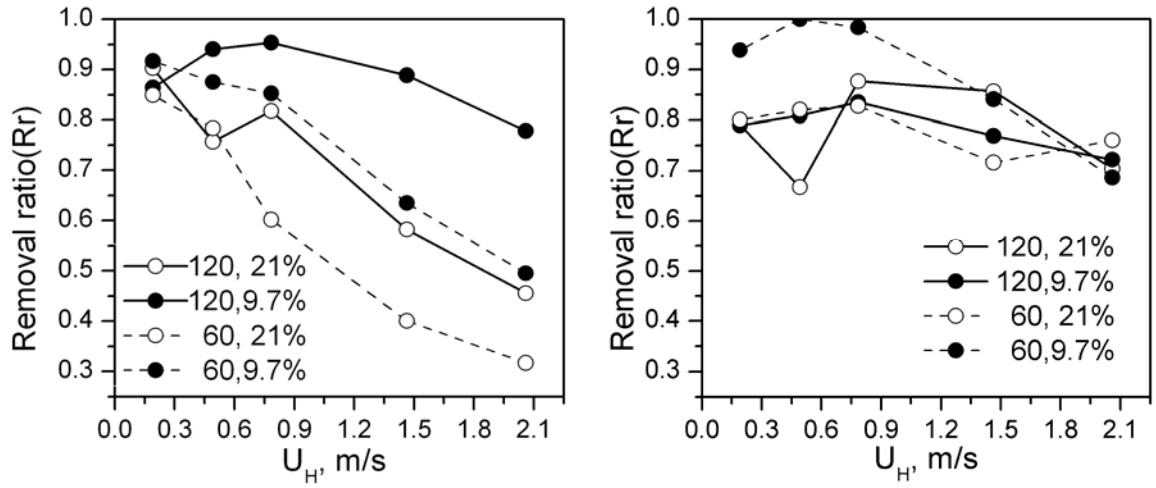

Fig. 5.3 – The change of removal ratio with airflow velocities at 0.15 m above the wind table: (a) downwind exhaust and (b) upwind exhaust. 120 and 60 represent the two ventilation rates in m^3 h^{-1}; and 21% and 9.7% represent the two floor opening ratios.

5.3.3. The effect of the slatted floor

In all cases of downwind exhaust, the lower floor opening ratio (9.7%) resulted in of 20% or

more gas removing in average than the higher opening ratio (21.0%) (Fig. 5.3-a).
For the upwind exhaust, the lower floor opening ratio (9.7%) resulted in of 10% or more gas removing than the higher opening ratio (21%) for most cases of Q_{exh}=60 m^3 h^{-1}. When the pit ventilation rate was 120 m^3 h^{-1}, the lower opening ratio (9.7%) did not result in higher removal ratios (Fig.3 - b); in this situation, lower and higher opening ratio exhausted 77.9% and 78.5% emission averagely by pit ventilation system, respectively.

5.3.4. The effect of the pit ventilation configurations (Ventilation rate and position)
Higher ventilation rates caused higher removal ratios for most cases of downwind exhaust (Fig. 5.3a). Generally, using the higher pit ventilation rates (120 m^3 h^{-1}) removed on average about 79% CO_2 and using the lower ventilation rates (60 m^3 h^{-1}) removed on average about 67% CO_2.

For the upwind pit exhaust, there was not such a trend as in downwind side. When floor opening ratio was 21%, higher ventilation rates (120 m^3 h^{-1}) did not remove more emission, compared with lower ventilation rates (120 m^3 h^{-1}). Both ventilation rates exhausted about 78% CO_2. When floor opening ratio was 9.7%, lower ventilation rates (60 m^3 h^{-1}) removed on average79% CO_2; higher ventilation rates (120 m^3 h^{-1}) removed on average 89% CO_2.

Pit ventilation position had a significant influence on the removal capability (Fig. 5.3). Overall, upwind exhaust discharged 8% more CO_2 through the pit ventilation system. When the air velocity was lower than 0.49 m s^{-1}, removal ratios did not change much with exhaust positions. When the air velocity was higher than 0.49 m s^{-1}, about 15% more CO_2 could be exhausted by changing downwind to upwind pit ventilation. The minimum removal ratios were 31.7% and 66.7% for downwind and upwind exhaust, respectively. Ventilation position on upwind side can abate emission more significantly, when compared to that on the downwind side.

5.3.5. The overall effect of the four factors
Fig. 5.4 shows the relationship between the removal ratio and the integrated variable *IV*. When *IV* was higher than 1.91, the higher *IV* resulted in lower removal ratios (Fig. 5.4). The removal ratio decreased with the increase of the velocity, with the decrease of the pit ventilation rate and with the decrease of the slatted floor opening areas. When *IV* was lower than 1.91 and higher than -12, the removal ratios did not change according to the variation of *IV*.

5.4. Discussion

5.4.1. CO_2 concentration inside the pit headspace
Higher CO_2 concentration inside the pit headspace could lead to higher emission into the room space due to convection and diffusion. The highest CO_2 concentration under the slatted floor occurred in the case without pit ventilation system and the concentration was

significantly reduced with the application of pit exhaust. The results showed the ability of the partial pit ventilation to reduce the gases under the slatted floor.

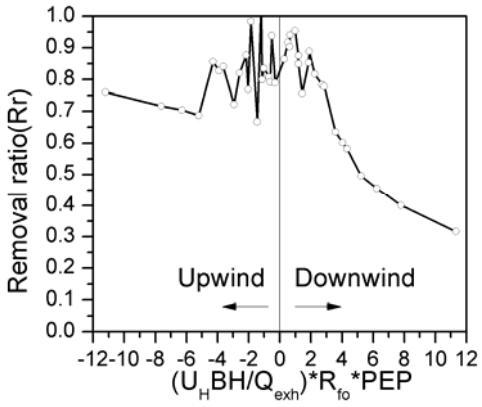

Fig. 5.4 – Removal ratios from measurement under the influence of different pit ventilation rates, airflow velocities above the wind table and two slatted floor opening ratios.

The concentration on upwind side was higher than that on downwind side (Table 2) by a factor of 2~3 when the air was exhausted on the downwind side, comparable to the findings of Liu and Barth (2001). The reason might be that the airflow above the slatted floor entered the pit mainly from the downwind side; part of it was exhausted directly by pit ventilation system; part of it attached to the downwind side wall and re-circulated to the upwind side. CO_2 was thus accumulated in the upwind side and caused high concentration. Johnson and Hunter (1998) reported a similar airflow type in a study of flow over street canyon, which was similar to the flow over a pit.

The standard errors of concentration were very large, compared with corresponding mean values. This showed high fluctuations of CO_2 concentration. The unsteady behavior of pollutant distribution was also reported in the work of Sagrado et al, (1998).

5.4.2. The effect of air velocity

The air velocity above the floor affected the air exchange rates in the headspace of the slurry pit. Higher air velocity (2 m s^{-1}) can mix the entrained fresh air and the injected CO_2 better. Consequently, more pollutants could be brought out by advection and diffusion.

Liu and Barth (2001) found that pollutant in a cavity was transported to free stream mainly by turbulence. When the air velocity above the floor was increased, the Reynolds number in the floor opening was increased; consequently, the airflow inside pit became more turbulent. More CO_2 was transported into the wind tunnel space from upwind side. This could explain that the removal ratios were decreased by the increase of the air velocity (U_H >0.78 m s^{-1}) above the floor for downwind exhaust. When air velocity was lower than 0.78 m s^{-1}, the Reynolds number in the floor opening was very small and the flow regime could be between laminar and turbulence. The transient flow could cause the instability of the airflow

patterns. This could explain that the removal ratios varied around 83.1% when air velocity was smaller than 0.78 m $s^{-1}$for both downwind and upwind exhaust.

5.4.3. The effect of the slatted floor

Fig. 5.3 shows that smaller slatted floor opening ratio resulted in lower emissions in most of the cases. The results were similar to those reported by Zhang et al. (2008). It was straightforward that smaller floor opening area could confine more CO_2 under the slats than larger floor opening area. In some upwind exhaust cases (Q_{exh}=120 m^3 h^{-1} and U_H=0.78~1.49 m s^{-1}), the mean values of removal ratios with lower floor opening ratio (9.7%) were smaller than that with higher floor opening ratio (21%); however, the removal ratios for the two floor openings were not significantly different ($p>0.15$) during this condition.

5.4.4. The effect of pit exhaust configurations

The fact that CO_2 concentrations in the pit headspace using the upwind exhaust were much lower than that using the downwind exhaust (Table 5.2) proved that the most polluted air in the vicinity of the upwind side was discharged directly to outside by using the upwind exhaust. Upwind exhaust avoided the recirculation of CO_2 inside the pit thus reducing the chance of being emitted to the free stream. This means that upwind exhaust can remove more emission from the pit headspace than downwind exhaust.

As expected, higher pit ventilation rates removed more CO_2 from the pit. However, in some cases of upwind exhaust, more gas was removed by lower pit ventilation rates (60 m^3 h^{-1}). It could be explained as follow. For upwind exhaust, pressure of upwind side of the pit became negative. The negative pressure produced a drag force. As a result, the part of the airflow above the floor did not have enough energy to travel to downwind side wall of the pit. It entrained the headspace from somewhere near upwind side and was discharged through exhaust system. Therefore, a vortex was formed close to upwind side. Meanwhile, a second vortex was formed in the downwind side. A similar airflow pattern containing two vortices in a cavity can be found in the work of Chang and Meroney (2003). Under this airflow distribution, the presence of the second vortex would give pollutant more chance to be transported to the free stream. When the pit ventilation rate was increased, the negative pressure difference was increased and thus the position of the airflow entering the pit would be closer to the upwind side wall of the pit. The second vortex would become larger. More pollutant would be involved in the second vortex; consequently, less pollutant would be removed by the pit exhaust. Therefore, increased pit ventilation rates could probably not remove more contaminant in such a case.

5.4.5. The overall effect of all the factors

Fig. 5.4 shows that the removal ratios in downwind exhaust conditions ($IV \leqq 1.90$) and in all upwind exhaust conditions varied around the mean value of 83.1% (with a standard deviation 8.8%). According to statistical analysis, the removal ratios were normally distributed. Therefore, $Rr = 83.1\%$ could be used to predict the removal ratios in the previous conditions. In most of the cases, the removal ratios were close to each other when the values of corresponding *IV* were close. It can be concluded that the removal ratios were more linked to *IV* rather than each individual factor.

The concept of *IV* can help engineers to design partial pit ventilation system. Fig.4 shows that when the air velocity above the floor was small (U_H <0.78 m s^{-1}) or the directions of the pit exhaust and airflow above the floor were opposite, the overall removal capacity of the system was nearly constant. The worst removal capacity occurred when the direction of the airflow was the same with that of pit exhaust. The determination of the pit ventilation rate could be based on the possibly worst removal capability.

In a naturally ventilated livestock house, the airflow condition near the slatted floor will be much more complicated than that in the wind tunnel. Airflow patterns above and under the slatted floor were also affected by the thermal conditions (Zhang et al., 1996.). Furthermore, differences in scale may affect emissions because of different turbulence scales and concentration boundary layers near the floor (Saha et al., 2011.). Therefore, the performance of the partial pit ventilation to reduce emission needs to be investigated and validated by full-scale experiments.

5.5. Conclusions

Partial pit ventilation is able to remove a large portion of polluted gases under the slatted floor.

When the air velocity was increased from 0.78 to 1.94 m s^{-1} for the cases of downwind exhaust, the removal ratios were decreased from about 80% to 50%. The mean of the removal ratios was 83.1% for all the cases of upwind exhaust and some cases of downwind exhaust and there was no clear velocity dependency.

In most cases, the lower floor opening ratio (9.7%) could reduce more gas than the higher opening ratio (21.0%).

Higher ventilation rates caused higher removal ratios for most cases of downwind exhaust.

For the upwind side, higher ventilation rates (120 m^3 h^{-1}) did not always remove more emission.

Pit ventilation position had a significant influence on the removal capability. Overall, upwind exhaust can discharge 8% more CO_2 by pit ventilation system than downwind exhaust.

Removal ratios were more linked to the integrated effect of all the factors rather than each individual one.

The work could help to design pit ventilation system and decide rational ventilation rates. The results from the scale model measurements need to be validated by full-scale experiments.

References

Anonymous, 2009. User Manual: WindMaster & WindMaster Pro Ultrasonic Anemometer. Doc No. 1561-PS Issue 04. Gill Instruments Limited, Saltmarsh Park, 67 Gosport Street, Lymington, Hampshire SO41 9EG, UK.

Chang, C.H., Meroney, R.N., 2003. Concentration and flow distributions in urban street canyons: wind tunnel and computational data. Journal of wind engineering and industrial aerodynamics 91, 1141-1154.

Monteny, G. J., Erisman, J. W., 1998. Ammonia Emission from Dairy Cow Buildings: A review of measurement techniques, influencing factors and possibilities for reduction. Netherlands Journal of Agricultural Science 46, 225-247.

Johnson, G.T., Hunter, L.J., 1998. Urban wind flows: wind tunnel and numerical simulations —a preliminary comparison. Environmental Modelling and Software 13, 279–286.

Liu, C.H., Barth, M.C., 2001. Large-Eddy Simulation of Flow and Scalar Transport in a Modeled Street Canyon. Journal of Applied Meteorology 41, 660-673.

Sagrado, A.P.G., Beeck, J.V., Rambaud, P., Olivari D., 2002. Numerical and experimental modelling of pollutant dispersion in a street canyon. Journal of Wind Engineering and Industrial Aerodynamics 90, 321-339.

Saha, C.K., Zhang, G., Kai, P., Bjerg B., 2010. Effects of a partial pit ventilation system on indoor air quality an ammonia emission from a fattening pig room. Biosystems Engineering 105 (3), 279-287.

Saha, C.K., Wu, W., Zhang, G., Bjerg B., 2011.Assessing effect of wind tunnel sizes on air velocity and concentration boundary layers and on ammonia emission estimation using computational fluid dynamics. Computers and Electronics in Agriculture 78, 49-60.

Zhang, G., Morsing, S., Strom, J. S., 1996.Modeling jet drop distances for control of a non-isothermal, flap adjusted ventilation jet. Transactions of the ASAE 39 (4), 1421-1431.

Zhang, G., Strom, J. S., Li, B., Rom, H.B., Morsing, S., Dahl, P., Wang, C., 2005. Emission of Ammonia and other Contaminant Gases from Naturally Ventilated Dairy Cattle Buildings. Biosystems Engineering 92 (3), 355-364.

Zhang, G., Bjerg, B., Strøm, J.S., Morsing, S., Kai, P., Tong, G., Ravn, P., 2008. Emission effects of three different ventilation control strategies - a scale model study. Biosystems Engineering 100 (1), 96-104.

Chapter 6

An assessment of a partial pit ventilation system to reduce emission under slatted floor-Part 2: Feasibility of CFD prediction using RANS turbulence models

Paper V:

Wu, W., Zhang, G., Bjerg, B., Nielsen, P.V., 2012. **An assessment of a partial pit ventilation system to reduce emission under slatted floor-Part 2: Feasibility of CFD prediction using RANS turbulence models**. *Computers and Electronics in Agriculture* 83, 134-142.

Abstract

CFD simulations were carried out to assess the feasibility of using RANS (Reynolds - averaged Navier – Stokes) turbulence models to evaluate the performance of a partial pit ventilation system to reduce gas emission under slatted floor. The entire system included a pit model with slatted floor and pit exhaust system, a wind table to simulate ground and a wind tunnel to simulate room space of a naturally ventilated livestock house. CFD simulations started with the selection of a proper domain. Two domains were chosen to evaluate the effect of domain simplification. The results showed that the effect was significant. The assessment of different turbulence models including the standard, RNG, realizable $k-\varepsilon$ *models; transition SST* $k-\omega$ *model; Reynolds Stress Models were conducted. Results of RSM were found out to agree best with measured results. In order to understand the transportation mechanism of pollutant through slatted floor, vertical mean and turbulent flux were defined and calculated. It was found that turbulence diffusion dominates the transportation of pollutant from the pit headspace into the free stream. Although discrepancies existed for some conditions, good agreements of measured and calculated removal ratios were found for most of cases. It was feasible to use RSM to predict the removal capability.*

The future research should focus on depicting the airflow patterns inside the pit by using scale model under well controlled laboratory conditions and generating benchmark data to validate and improve CFD methods. Unsteady CFD simulation using large eddy simulation could be conducted to make more precise predictions of removal capability of the partial pit ventilation system by considering the unsteady phenomena of gas emission.

Key words: *CFD; RANS; pit ventilation; slatted floor; turbulence diffusion*

Nomenclature

b	power of the power-law function, 0.22
C	average concentration of CO_2, (g s^{-1} m^{-3})
c'	the deviation from the mean concentration (mg m^{-3})
C_μ	constant, 0.09
F_m	vertical flux of CO_2 by mean flow (g m^{-2} s^{-1})
F_t	vertical flux of CO_2 by turbulent flow (g m^{-2} s^{-1})
K_c	coefficient of scalar transport
Q_{exh}	pit ventilation rate (m^3 h^{-1})
R_{fo}	slatted floor opening ratio
Rr	removal ratio (%)
Sc_t	turbulent Schimidt number, 0.9
TIV	the integrated variable
U_H	air velocity at 0.15 m height above the slatted floor (m s^{-1})
U	the velocity (m s^{-1})
W	average vertical velocity (m s^{-1})
X	X coordinate, aligned with the length of the wind tunnel (m)
Y	Y coordinate, aligned with the width of the wind tunnel (m)
Z	Z coordinate, from wind tunnel ground to its top wall (m)
Z_H	the reference height, 0.15 m
z	the height from wind table, m
w'	the deviation from the mean vertical velocity (m s^{-1})
k	turbulent kinetic energy
ε	the dissipation rate

Subscripts

fo	floor opening ratio
H	height

6.1. Introduction

A one-half scale model of manure pit section was built and placed in a wind tunnel to simulate the emission conditions from the slurry pit of a naturally ventilated dairy cattle house. The scale model contained a headspace and a mixing chamber, which were separated by a plate with uniformly spaced holes and a porous membrane. CO_2 was supplied to the mixing chamber beneath the pit headspace. The scale model was equipped with a slatted floor and a mechanical pit exhaust system. The objective of this system is to study the ability of a partial pit ventilation system to reduce gas emission under slatted floor. A complete description of the experimental set-up and results can be found in the work of Wu et al. (2012).

Although the pit model can be placed in a wind tunnel to investigate the performances of a pit exhaust under controlled laboratory conditions, it is still difficult to observe and visualise the airflow patterns in the pit headspace. Therefore, the mechanism of gas transportation through the slatted floor cannot be well understood. Additionally, the influence of the air velocity above floor, the floor opening ratios and pit ventilation configurations on the performance of the pit ventilation system was investigated under limited scenarios. It was due to the fact that the wind tunnel measurements were relatively expensive and time consuming. The possibility of using Computational Fluid Dynamics (CFD) was studied in this work and CFD was intended to supplement the limitations of scale model.

CFD has become a useful and popular tool to predict airflow characteristics and assess gas emissions across wide research areas: airflow distribution in greenhouses (Bartzanas et al, 2002); ammonia emission from pig houses (Rong et al, 2010); dynamic flux chamber methodology (Saha et al, 2011). CFD simulation has also been performed to evaluate the efficiency of a partial pit ventilation system to reduce ammonia emission in pig units with animals and slatted floor (Bjerg et al, 2008a) and in a naturally ventilated cattle building (Bjerg and Andersen, 2010).

In the work of Bjerg et al (2008a), the slatted floor was handled in a form of porous media. However, the effect of the slatted floor on the mechanism of emission transportation should be critical and the slatted floor should be modelled in geometrical details. For the application of pit ventilation in a naturally ventilated building (Bjerg and Andersen, 2010), a two dimensional model was adopted and the results were not validated with measurements. Research related to the application of CFD on partial ventilation system is still necessary in order to consider the three dimensional effects, validation with measurements and the detailed simulation of the slatted floor. No report on this kind of simulation has been found in literature.

So far, most CFD models have been successfully used for airflow around bluff structures (Castro and Apsley, 1997) and airflow inside confined spaces (Zhai, 2007). But it

is not sure if the current turbulence models and numerical methods can be applied to the case that involves airflow through cavities (the pit headspace) and interacting with the free stream through narrow slots. Studies on airflow over cavities can be found in the field of urban wind flows (Li et al, 2006), where research was focused on the pollutant dispersion in urban street canyons.

Different turbulence models were evaluated to study urban wind flows. A two-dimensional numerical investigation by Huang et al. (2000) showed a good agreement between the calculated and observed concentrations, which made it possible to use the standard $k-\varepsilon$ turbulence model (Launder and Spalding, 1974) to analyze the pollutant distributions emitted from vehicles within urban street canyons. Sagrado et al., 2002 showed that the realizable $k-\varepsilon$ model (Shih et al., 1995) with a two-layer zonal approach to a wall had been found to be the most accurate one in $k-\varepsilon$ models; the conclusion was achieved by comparing the results with direct numerical simulation on separated flows and flows with complex secondary flow features in street canyons. A three-dimensional simulation with the RNG $k-\varepsilon$ turbulence scheme (Choudhury, 1993) by Kim et al.(2004) indicated that the main features of mean flow were simulated well although the velocities were underestimated in some parts of the street canyons. A work presented by Sahm et al. (2002) pointed out that the velocity discrepancies among results of different $k-\varepsilon$ turbulence models and measurements were not negligible at individual locations, even though the case was relatively simple.

According to the review of the research on the CFD simulation of urban wind flow, different turbulence models were found to be suitable for different cases and discrepancy between simulation and experiment was also found to be negligible. The flow in this study should be more complex because of the involvement of pit exhaust system and the slatted floor. The slatted floor makes the boundary layer above and under the floor rather difficult to model. Turbulence models will be crucial for an accurate simulation of the flow in slots and headspace.

The objective of this study is to assess the feasibility of using RANS (Reynolds - averaged Navier - Stokes) turbulence models to evaluate the performance of a partial pit ventilation system to reduce gas emission under slatted floor. The accuracy of the three $k-\varepsilon$ turbulence models (standard, RNG, realizable) (Davidson, 1997), the transition SST $k-\omega$ turbulence model (Menter, 1994) and RSM (Reynolds Stress Models) (Hanjalic, 1999) were tested to predict the removal ratio, which was defined as the percentage of contaminant removed by pit exhaust.

6.2. Materials and Methods

A 1:2 scale model of slurry pit section with slatted floor and CFD simulation were used as tools to study the efficiency of a partial pit ventilation system to reduce emission under

slatted floor. A detailed description of scale model study can be found in the work of Wu et al. (2012). Set-up of CFD is given in the following sections.

6.2.1. Basic concept of CFD and software

The basic concept of CFD is to solve a set of partial differential equations. The governing equations are the Navier-Stokes and continuity equations (Launder and Spalding, 1974). CO_2 was used as tracer gas in previous experiments (Wu et al, 2010). It was treated as scalar in this CFD simulation. The transport equation for CO_2 is written as (Baik and Kim, 1998):

$$\frac{\partial C}{\partial t}+U\frac{\partial C}{\partial x}+V\frac{\partial C}{\partial y}+W\frac{\partial C}{\partial z}=\frac{\partial}{\partial x}(K_c\frac{\partial C}{\partial x})+\frac{\partial}{\partial y}(K_c\frac{\partial C}{\partial y})+\frac{\partial}{\partial z}(K_c\frac{\partial C}{\partial z})+S_c \qquad (6.1)$$

where, C is the mean concentration of a passive pollutant, t is the time, U , V and W are the mean velocities in the X , Y and Z coordinate direction, respectively. K_c is the turbulent diffusivity for the scalar variable and S_c denotes the source or sink term of the pollutants.

$$K_c=\frac{C_\mu k^2}{Sc_t\varepsilon} \qquad (6.2)$$

where, C_μ is a constant and equal to 0.09; k is the turbulent kinetic energy; ε is the dissipation rate; Sc_t is the turbulent Schmidt number and specified as 0.9 (Sini et al., 1996).

Commercial software Fluent 12.0 was used to solve the equations on the basis of finite volume method. Standard $k-\varepsilon$, $k-\varepsilon$ RNG, $k-\varepsilon$ Realizable, transition SST $k-\omega$ and RSM turbulence models were tested in this work. All the velocity and turbulence terms for convection were approximated using second order upwind scheme. Diffusion terms were discretised using central difference scheme. SIMPLE method was employed for the pressure-velocity correction.

6.2.2. Computational domain

CFD simulation starts from the specification of the computational domain. The experimental facility is usually geometrically simplified in order to make the calculation feasible and easy. To assure the quality of the simulated results, the computational domain should be as close to the original geometry as possible. Two computational domains were included in this work.

The whole wind tunnel containing the wind table and the scale model was built as the first computational domain, defined as domain 1 (Fig. 6.1a). The set-up of the first domain was exactly the same as that in the experiment. The difficulty of using this domain was to define the boundary condition of the wind tunnel fan. Data of the fan was not available.

Since the measured velocity profiles above the wind table were available, an alternative was to cut off the spaces under wind table and extend the wind table to the whole wind tunnel. In this way, only the space above the wind table and the headspace of the scale model was treated as a domain, defined as domain 2 (Fig. 6.1b). The length, width and height of

domain 2 were the same with domain 1. The measured velocity profiles can be easily used as the inlet boundary condition.

For both domains, X, Y, Z coordinate was aligned with the length, width and height of the wind tunnel, respectively.

The simulation results of using the two domains were evaluated in this work.

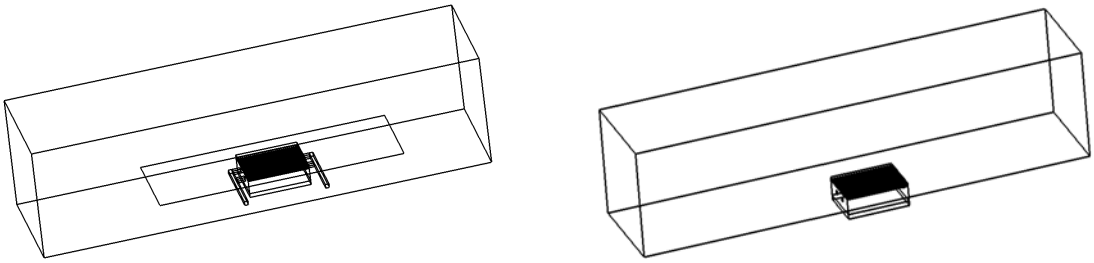

(a) (b)

Fig. 6.1 – Schematic of the two domains: (a), domain 1; (b), domain 2.

6.2.3. Boundary conditions

For domain 1, the upstream end of the wind tunnel was defined as velocity inlet with fixed velocity magnitudes. Since only the air velocities above the wind table were known, the corresponding velocities for the fan were determined by the following procedure. An initial speed was assigned to the fan for a preliminary calculation. A velocity profile above the wind table was obtained from the calculation. The initial speed was calibrated by the ratio of the calculated velocities to those from the measurements. By iterations of calculation and calibration, a proper air velocity generated by the fan was finally decided. The final velocity profiles from simulations and measurements are given in Fig. 6.2.

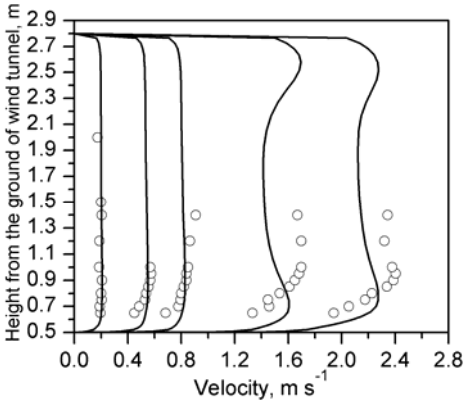

Fig. 6.2 – Velocity profiles of measurements (open circles) and simulations (solid lines) in the upwind side of the wind tunnel and above the wind table. The simulated velocity profiles were obtained by using domain 1.

For domain 2, the inflow surface was defined as velocity inlet and assumed to follow a power-law profile (Tsai and Chen, 2004). The power-law function was given by

$$U = U_H (z / Z_H)^b \tag{6.3}$$

where, U is the velocity, m s^{-1}; z is the height from the wind table, m. b is 0.22 according to the linear regression of the measured velocities; U_H (m s^{-1}) is the air velocity at 0.15 m height above the wind table and can be found in Table 1 of Wu et al. (2011); Z_H is the reference height, 0.15 m.

The outlet of the wind tunnel was defined as pressure outlet for both domains. The measured pit ventilation rates were converted to velocities that were used as the input values of the boundary condition of the exhaust openings. The bottom surface of the headspace of the pit was specified as wall and appointed as emission surface. The tracer gas was treated as a scalar quantity in the simulation and 1 kg s^{-1} m^{-2} was set as the scalar generation rate of the emission surface. No scalar distribution was assumed to the whole domain as initial condition. Other surfaces of both domains were considered as walls.

6.2.4. Mesh

More grids were allocated around the slatted floor and inside the slatted slot. The width of the slot was 0.02 m. Thus the smallest grid distance was required to be smaller than 0.02 m. The mesh size of other edges was increased proportionally based on that of the shortest edge. Hence the coarse grid number was relatively large, which was 1308854 and 739020 for domain 1 and domain 2, respectively. The medium and fine grid number were 1888437, 2726686 for domain 1 and 1042018, 1490086 for domain 2. The optimum grid distribution for each domain was achieved by comparing the results of three meshes. Velocity profiles in the pit headspace from three different meshes for the domain are compared in Fig. 6.3. The velocities calculated from medium mesh were very close to that from the fine mesh. It proved that medium mesh was good enough for achieving mesh convergence. In the same manner, medium mesh for domain 2 was chosen.

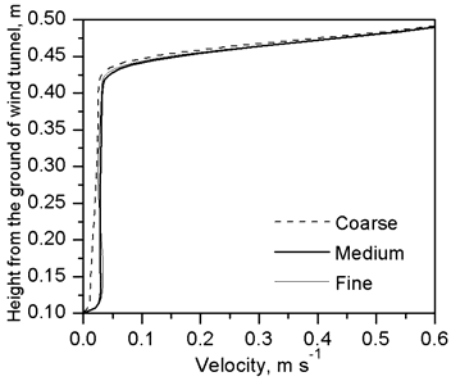

Fig. 6.3 – Investigation of mesh convergence: velocity profiles in the pit headspace (from Z =0.10 m to Z =0.50 m) in the middle of the pit model

6.2.5. Calculation of vertical mean and turbulence flux

An instantaneous velocity u can be decomposed into a mean flow component U and with a fluctuation value u' superimposed on it. Considering a steady case without source, gas is transported by mean flow (U) and its fluctuation (u'). The part of gas transported by mean flow is called mean flux (F_m); whereas the rest of gas transported by its fluctuation is named as turbulent flux (F_t). The investigation of the relationship between mean flux and turbulent flux would benefit finding the transportation mechanism.

The vertical flux of the scalar by mean and turbulent flow was calculated using (Baik and Kim, 2002)

$$F_m = CW \tag{6.4}$$

$$F_t = c'w' = -K_c \frac{\partial C}{\partial z} \tag{6.5}$$

where, C is the mean concentration of the scalar, W is the vertical mean velocity; c' is the deviation from the mean concentration and w' is the deviation from the mean vertical velocity. K_c is the turbulent diffusivity defined in equation (6.2).

6.3. Results

6.3.1. The effect of simplification of computational domains

Domain 2 was aimed to simplify the geometry and to use measured velocity profiles as inlet boundary condition. Removal ratios for all the cases were higher than 90% by using domain 2. The large discrepancy between simulation and measurement made domian2 unacceptable. Removal ratios using domain 1 were comparable with those from measurement. Therefore, domain 1 was selected to conduct all the following simulations.

6.3.2. The effect of different RANS turbulence models

Table 6.1 shows the air velocities in the pit headspace and the removal ratios calculated using different RANS turbulence models and those obtained from measurements. The simulations were conducted under the same condition (U_H =0.78 m s^{-1}, R_{fo} =21.0%, Q_{exh} =120 m^3 h^{-1} and downwind exhaust) for all the turbulence models. X =4.550 to 5.450 m was upwind side to downwind side of the pit headspace. The velocities predicted by CFD agreed with the measurement values very well at upwind side and discrepancy became larger and larger when the position was approaching downwind side. Generally, the velocities from RSM agreed better with the measured velocities. An underestimation of Rr was noticed for all the turbulence models. The transition SST $k-\omega$ turbulence model underestimated Rr more than

8.1%. The three $k-\varepsilon$ models predicted similar removal ratios (around 75%). The deviations from the measured values were larger than 5%. The best agreement between CFD simulation and measurement was achieved by RSM turbulence model. The deviation was less than 2%. Therefore, RSM was chosen for further calculations of Rr under different conditions.

Table 6.1 Comparison of measured velocity magnitudes and removal ratios with that calculated from different turbulence models

Turbulence models and measurement	Velocity (m s-1)					Rr
	At position (m): Y=1.426, Z=0.3					
	X=5.450	X=5.150	X=5.000	X=4.850	X=4.550	
$k-\varepsilon$ Standard	0.133	0.097	0.082	0.065	0.028	76.8%
$k-\varepsilon$ RNG	0.115	0.09	0.072	0.062	0.036	75.9%
$k-\varepsilon$ Realizable	0.128	0.09	0.077	0.07	0.039	74.2%
SST $k-\omega$	0.158	0.073	0.073	0.05	0.04	73.1%
RSM	0.112	0.103	0.074	0.062	0.044	79.7%
Experiment	0.103 (±0.027)	0.062 (±0.029)	0.051 (±0.027)	0.058 (±0.026)	0.047 (±0.021)	81.8%

* Simulations were carried out in the condition of U_H=0.78 m s^{-1}, R_{fo}=21.0%, Q_{exh}=120 m^3 h^{-1} and downwind exhaust.

6.3.3. Distribution of velocities and concentrations

Two planes in the domain were used to demonstrate the velocity, concentration fields and airflow patterns. Plane 1 (Fig. 6.4) was aligned with Y coordinate and perpendicular with the direction of the slats. Plane 2 (Fig. 6.4) was aligned with X coordinate and parallel to the direction of the slats.

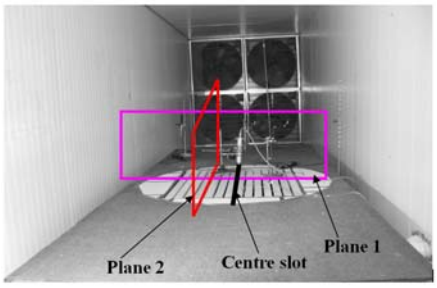

Fig. 6.4 – Schematic of the position Plane 1 and Plane 2

Examples of velocity and concentration distribution are shown in Fig. 6.5 for U_H=0.78 m s^{-1}, R_{fo}=21.0%, Q_{exh}=120 m^3 h^{-1} at the downwind exhaust. For both planes, the velocity magnitude was about 0.80 m s^{-1} in the space above the wind table; the scalar concentration was below 0.01 kg m^{-3}. Little scalar was transported to the space above the floor. The velocities on Plane 1 were below 0.1 m s^{-1} for most parts of the pit headspace (Fig. 6.5a). Both velocity and concentration fields showed symmetry along the Y middle plane aligned with the width of the wind tunnel (Fig. 6.5a, c). It can be seen from Plane 2 that the fresh air

travelled from the upwind side edge of the pit to the downwind side edge of the pit; part of that was exhausted by the pit ventilation system; the rest of the air circulated to the upwind direction and its return distance was 1/3 of the length of the pit (Fig. 6.5b). The concentration was high on upwind side of the pit headspace (Fig. 6.5d).

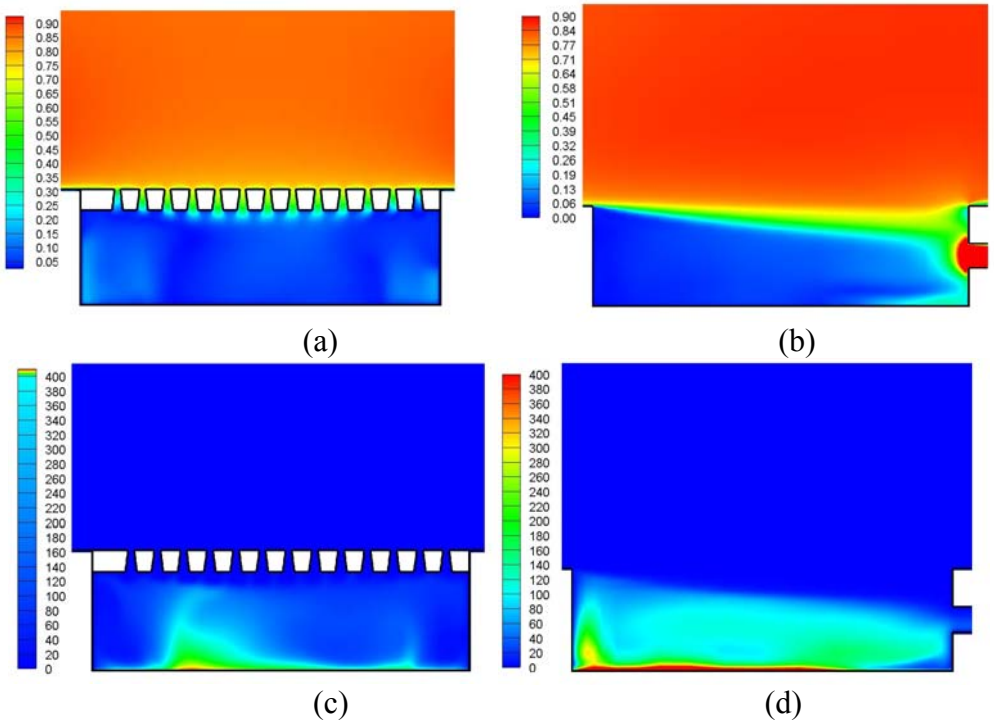

Fig. 6.5 – Velocity field of: (a) Plane 1; (b) Plane 2 and Scalar distribution of: (c) Plane 1; (d) Plane 2 in the case of U_H =0.78 m s^{-1}, R_{fo} =21.0%, Q_{exh} =120 m^3 h^{-1} and downwind exhaust

6.3.4. Airflow patterns

Fig. 6.6 shows that airflow patterns on Plane 1 with varied velocity (U_H) for R_{fo} =21.0%, Q_{exh} =120 m^3 h^{-1} at the downwind exhaust. When U_H was 0.19 m s^{-1}, fresh air entered the pit headspace through all the slots (Fig. 6.6a). When U_H was increased to 2.06 m s^{-1}, air entrained the middle slots but some air exit to the space above the floor from the slots near the two edges (parallel to the slot opening) of the pit model (Fig. 6.6b). General simulation results in all cases showed that airflow patterns on Plane 1 were affected by the air velocity above the slatted floor U_H. No similar effect on airflow pattern in plane 1 was found by changing R_{fo}, Q_{exh} and the exhaust position.

Fig. 6.7 shows that the airflow patterns on Plane 2 varied with exhaust positions for R_{fo} =21.0%, Q_{exh} =120 m^3 h-1 and U_H = 2.06 m s^{-1}. Both conditions show a similar airflow pattern: air travelled from the upwind edge to the downwind edge of the pit wall, and attached to the downwind side wall; part of the flow returned to the upwind direction along the bottom surface of the pit. The significant difference was the travel distance of the return

flow. Return flow can travel more close to upwind side by using upwind exhaust (Fig. 6.7b). The overall simulation results in all cases showed that airflow patterns in Plane 2 were mainly affected by exhaust positions rather than R_{fo}, Q_{exh} and U_H.

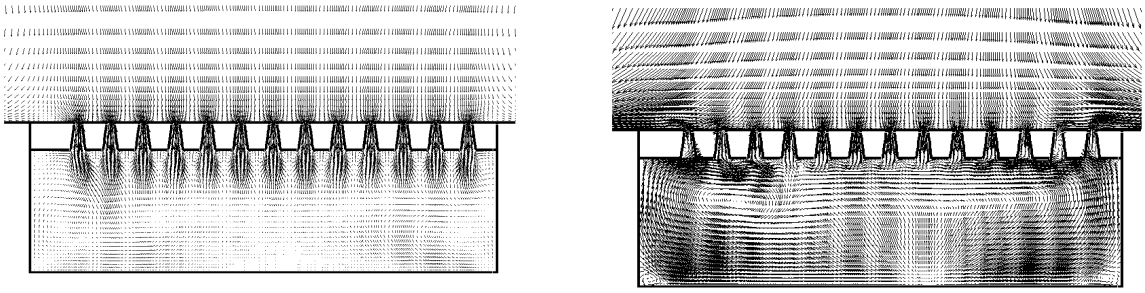

(a) (b)

Fig. 6.6 – Airflow patterns in Plane 1: (a) U_H =0.19 m s^{-1}; (b) U_H = 2.06 m s^{-1} when R_{fo} =21.0%, Q_{exh} =120 m^3 h^{-1} and the pit ventilation position is at downwind side

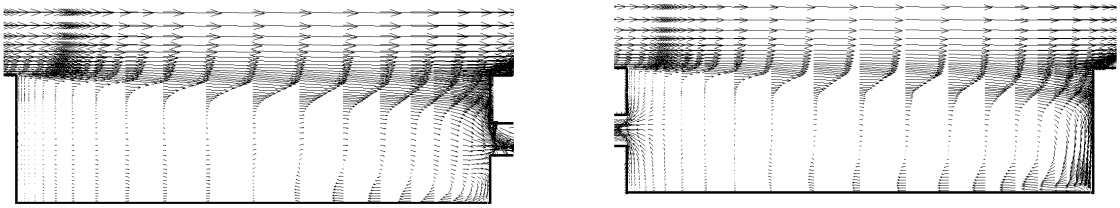

(a) (b)

Fig. 6.7 – Airflow patterns in plane 2: (a) downwind exhaust; (b) upwind exhaust when U_H = 2.06 m s^{-1}, R_{fo} =21.0% and Q_{exh} =120 m^3 h^{-1}

6.3.5. Removal ratios predicted by CFD

Removal ratios based on CFD simulations under different cases are presented in Fig. 6.8.

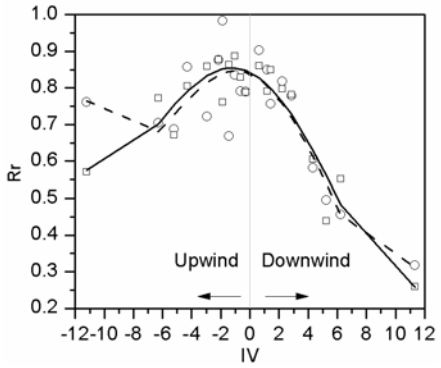

Fig. 6.8 – Removal ratios under the influence of different pit ventilation rates, airflow velocities at the slatted floor level and two-slatted floor opening ratios. Open circle-experimental values; open square-simulated values; dash line-fourth order polynomial fitted values using measured data (R^2=0.805); solid line-fourth order polynomial fitted values using simulated data (R^2=0.895)

In order to display the overall trend of Rr varying with IV, defined by Wu et al. (2012), the measured and simulated Rr values were fitted using 4th-order polynomial function. The predicted Rr follow the trend of measured Rr in most of the cases. A large discrepancy was found when IV was about -11.6, and the Rr predicted by CFD was 20% lower than the measured values. The discrepancy made the trends of measurement and simulation different for IV <-7. The simulation results showed a decrease of Rr with the increase of absolute values of IV. But the decrease for downwind exhaust was fast than that for upwind exhaust.

Good agreement was found between measured and predicted Rr values. When U_H =0.49 and 2.06 m s^{-1}, the discrepancy between simulated and measured removal ratios was about 10%~20%.

6.3.6. The vertical CO_2 flux through the slatted floor openings

Fig. 6.9 shows the horizontal distributions of the calculated vertical mean and turbulent flux of CO_2 through the top surface of the centre slot (see Fig. 6.4). The calculation was based on U_H =0.78 m s^{-1}, R_{fo} =21.0%, Q_{exh} =120 m^3 h^{-1} at the downwind exhaust. X=4.25 was at the upwind side edge of the pit, and X=5.75 was at the downwind side edge of the pit. For the downwind side, both mean and turbulent flux approached 0 g s^{-1} m^{-2}. For upwind side, the vertical mean flux was negative and moved downward into the pit. The average mean flux was -11.09 g s^{-1} m^{-2}. The vertical turbulent flux was positive and moved upward to wind tunnel space. The average turbulent flux was 30.25 g s^{-1} m^{-2}. Fig. 6.9 indicated that the total vertical flux was positive by integrating F_m and F_t along X-axis.

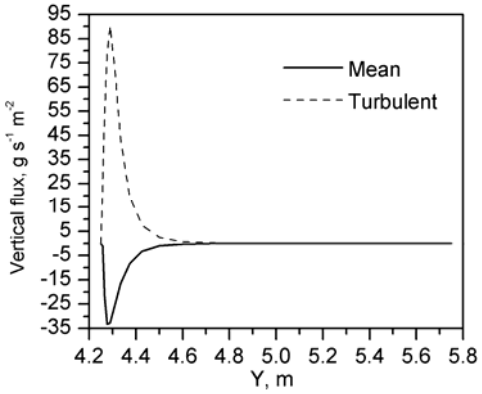

Fig. 6.9 – Horizontal distributions of the vertical mean and turbulent flux of CO_2 through the top surface of the centre slot (see Fig.4). The simulation was performed under the condition of U_H =0.78 m s^{-1}, R_{fo} =21.0%, Q_{exh} =120 m^3 h^{-1} and downwind exhaust

6.4. Discussion

6.4.1. The simplification of computational domains

Simplifications of detailed geometries are needed to simulate reality. The purpose of simplification could be: (1) the difficulty in including some parts in simulations, for example,

it is hard to use detailed locations and shapes of animals in a livestock house; (2) to reduce number of cells, for example, the narrow openings of slatted floor cause a large number of cells, which would be reduced by treating slatted floor as porous media (Bjerg et al, 2008a); (3) to simplify boundary conditions, for example, the domain 1 in this work was intended to avoid modelling the fans of the wind tunnel directly. But the accuracy of simplification of CFD domain was usually not evaluated in literature. By comparison of two computational domains, a significant effect of domain was found. Domain 2 failed to predict removal ratios. The reason could be as follow. In domain 2, the wind table was extended to whole wind tunnel. Hence, the airflow above the wind table was parallel to slats and the vertical velocity magnitude was nearly zero everywhere. The free stream in the wind tunnel confined the airflow inside the pit. Therefore, more than 90% gases were exhausted by the pit ventilation system in all cases. However, in domain 1, there was space between side-edge of wind table and sidewall of wind tunnel. Vertical air circulation was observed above wind table. The vertical vortex can bring more contaminant into the space of wind tunnel. Thus domain 1 predicted removal ratios more precise than domain 2.

6.4.2. Velocity fields and effects of different RANS turbulence models

The discrepancy between the simulated and measured velocities can be due to the measuring instrument. An ultrasonic anemometer was used to measure the air velocities. The sensor head/measurement volume was comparatively large to the headspace of the slurry pit. It covered a volume larger than 0.1m×0.1m×0.1m. The measured velocity was actually the averaged value in the air space covered. The velocity gradient (Fig. 6.5b) was much steeper on the downwind side according to the simulation. The averaged value by the ultrasonic anemometer in some regions of the downwind side is very different from the exact point value achieved by CFD. This can be the reason that the discrepancy of velocities at downwind side was larger than that on upwind side.

Another reason of the discrepancy between CFD and measurement results could be the defined air velocity boundary condition generated by the fan. Since detailed information of the wind tunnel fan was not available, an assumption of a fixed velocity at wind tunnel inlet based on the calibrations by the measured velocity profile above wind table was applied (Fig. 6.2). The fixed velocity might not well describe the boundary condition generated by the fans.

The third reason might be the inability to apply $k-\varepsilon$ and other RANS turbulence models on the cavity flow. In this study, the cavity flow was featured with strong streamline curvatures and separation. Isaev et al. (2006) reported that the $k-\varepsilon$ turbulence models sharply overestimated the eddy viscosity in the primary vortex zone and underestimated the separated flow intensity. A correction for the curvature of streamlines in the expression of the

turbulent viscosity definition was not proposed in the $k-\varepsilon$ turbulence models. The three $k-\varepsilon$ turbulence models underestimated velocities near upwind wall and overestimated velocities near downwind wall of pit. Transition SST $k-w$ highly overestimated velocities near exhaust openings and resulted in a largest prediction discrepancy on removal ratio compared with other RANS models. Transition SST $k-w$ was used to consider low-Re effect inside the pit but it did not improve the simulated results. Results from RSM agreed best with the measurements. Although it took much more iterations for a converged solution, RSM was most promising according to this study.

6.4.3. Removal ratios predicted by CFD

Removal ratios (Rr) based on CFD simulations were very close to measured values in most cases. It was feasible to use RSM to assess the ability of a partial pit ventilation system to reduce emission under slatted floor.

The same conclusions can be drawn from both measurements and simulations: (1) the changes of *Rr* following the variation of air velocity above the floor was similar to simulations and measurements for U_H <0.78 m s^{-1} at the downwind exhaust or all upwind exhaust cases; (2) smaller slatted floor opening can lead to higher removal capacity/efficiency; (3) upwind exhaust was more efficient than downwind exhaust.

Differences between measured and simulated results were also found. In the measurements, the mean Rr was 83.1% for all cases upwind exhaust cases and some downwind exhaust cases. There was no clear velocity dependency (Wu et al., 2012). However, when U_H increased from 0.78 to 1.94 m s^{-1}, the simulated Rr decreased from 87.7% to 77.2% for the upwind exhaust and showed the same velocity dependency in the cases of downwind exhaust. For the upwind exhaust in the measurements, higher ventilation rates (120 m^3 h^{-1}) did not always remove more emission. The reason for this case can be that the airflow patterns were different for ventilation rates 120 and 60 m^3 h^{-1} (Wu et al., 2012). But in the simulations, higher ventilation rates (120 m^3 h^{-1}) always resulted in higher removal ratio. The airflow patterns (Fig. 6.7b) at the two ventilation rates were similar to each other from the simulations.

The differences between measured and simulated values could arise for several reasons. The first reason can be the difference of turbulence diffusion in the measurement and in the simulation. Both the mean flow field and the turbulence transportation controlled the gas dispersion through the slatted floor. Fig. 6.9 shows that the CO_2 transportation to free stream above the slatted floor was dominated by the turbulent diffusion, which was consistent with the studies on scalar transport in street canyons (Lee and Park, 1994; Baik and Kim, 1999). The RSM turbulence models probably had difficulty to estimate turbulence diffusion accurately in the slatted slots.

Unsteady mass transport phenomena can be another reason. Wu et al. (2012) reported that the standard deviation of CO_2 concentration was very large compared with its mean value. It indicates that the transportation of CO_2 was rather unsteady. It was also consistent with the experiment and computational studies of Chang and Meroney (2003), which revealed that the dispersion of gaseous pollutants within the cavity of street canyons was essentially unsteady. Johnson and Hunter (1998) also pointed out that transient flow was a very important factor for modelling passive pollutant concentration fields from the wind tunnel measurements. The nature of RANS models is a steady state methodology. Therefore, it was limited to take transient turbulent transportation of CO_2 into account.

In order to validate the explanations, further measurements should be conducted to depict the airflow patterns inside the pit, which may require advanced measurement setups and instrumentations. An unsteady CFD methodology such as large eddy simulation could be used to assess the effect of unsteady transportation of scalar.

6.5. Conclusion

RSM (Reynolds Stress Models) was found to be the best of the used RANS turbulence models.

RSM can be used to predict the removal capability of a partial pit ventilation system to reduce emission under slatted floor.

Turbulence diffusion dominated the mass transfer from pit headspace into free stream above the floor.

Future research should focus on depicting the airflow patterns inside the pit by using scale model under well controlled laboratory conditions, and generating benchmark data to validate and improve CFD methods. Unsteady CFD simulation using large eddy simulation could be conducted to make more precise predictions of removal capability of the partial pit ventilation system by considering the unsteady phenomena of gas emission.

References

Baik, J.J., Kim, J.J., 1998. A numerical study of flow and pollutant dispersion characteristics in urban street canyons. Journal of applied meteorology 38, 1576-1589.

Baik, J.J., Kim, J.J., 2002. On the escape of pollutants from urban street canyons. Atmospheric Environment 36, 527-536.

Bartzanas, T., Boulard T., Kittas, C., 2002. Numerical simulation of the airflow and temperature distribution in a tunnel greenhouse equipped with insect-proof screen in the openings. Computers and Electronics in Agriculture 34, 207-221.

Bjerg B., Andersen M., 2010. Numerical simulation of a pit exhausts system for reduction of ammonia emission from a naturally ventilated cattle building. XVIIth world congress of

the international commission of agricultural and biosystems engineering (CIGR). Quebec City, Canada.

Bjerg B., Zhang, G., Kai, P., 2008a. CFD investigations of a partly pit ventilation system as method to reduce ammonia emission from pig production units. The Eighth ASABE International Livestock Environment Symposium (ILES Ⅷ)

Bjerg B., Zhang, G., Kai, P., 2008b. Porous media as boundary condition for air inlet, slatted floor and animal occupied zone in numerical simulation of airflow in a pig unit. AgEng2008 International Conference on Agricultural Engineering, Hersonissos, Crete-Greece.

Castro, I.P., Apsley, D.D., 1997. Flow and dispersion over topology: a comparison between numerical and laboratory data for two dimensional flows. Atmospheric Environment 31, 839-850.

Chang, C.H., Meroney, R.N., 2003. Concentration and flow distributions in urban street canyons: wind tunnel and computational data. Journal of wind engineering and industrial aerodynamics 91, 1141-1154.

Choudhury, D., 1993. Introduction to the Renormalization Group Method and Turbulence Modeling. Fluent Inc. Technical Memorandum TM-107.

Davidson, L. 1997. An Introduction to Turbulence models. Dept. of Thermo and Fluid Dynamics, Chalmers University of Technology, Gothenburg, Rept. 97/2.

Hanjalic, K. 1999. Second-Moment Turbulence Closures for CFD: Needs and Prospects. Int. J. Heat and Fluid Flow 12, 667-697.

Huang, H., Akutsu, Y., Arai, M., Tamura, M., 2000. A two-dimensional air quality model in an urban street canyon: evaluation and sensitivity analysis. Atmospheric Environment 34, 689-698.

Isaev, S.A., Baranov, P.A., Kudryavtsev, N.A., Lysenko, D.A. and Sachov, A.E. U., 2005. Complex analysis of turbulence models, algorithms, and grid structures at the computation of recirculating flow in a cavity by means of VP2/3 and Fluent packages. Part 2. estimation of models adequacy, Thermophysics and Aeromechanics 13 (4), 55-65.

Johnson, G.T., Hunter, L.J., 1998. Urban wind flows: wind tunnel and numerical simulations —a preliminary comparison. Environmental Modelling and Software 13, 279–286.

Kim, J.J., Baik, J.J., 2004. Effects of inflow turbulence intensity on flow and pollutant dispersion in an urban street canyon. Journal of Wind Engineering and Industrial Aerodynamics 91, 309-329.

Launder, B.E., Spalding, D.B., 1974. Numerical computation of turbulent flows. Computers and Mathematics in Applied Mechanics and Engineering 3, 269-289.

Lee, I.Y., and Park, H.M., 1994. Parameterization of the pollutant transport and dispersion in urban street canyons. Atmospheric Enviroment 28, 2343-2349.

Li, X.X., Liu, C.H., Leung, D. Y.C., Lam, K.M., 2006. Recent progress in CFD modelling of wind field and pollutant transport in street canyons. Atmospheric Environment 40, 5640-5658.

Menter, F.R. 1994. Two-equation Eddy-viscosity Turbulence Models for Engineering Applications. AIAA J. 32, 1598-1605

Rong L., Nielson, P. V., Zhang, G., 2010. Experimental and numerical study on effects of airflow and aqueous ammonium solution temperature on ammonia mass transfer coefficient. J.Air & Waste Manage. Assoc. 60, 419-428.

Sagrado, A. P. G., Beeck, J., Rambaud, P., Olivari, D., 2002. Numerical and experimental modelling of pollutant dispersion in a street canyon. Journal of Wind Engineering and Industrial Aerodynamics 90, 321-339.

Saha CK; Wu W; Zhang G; Bjerg B (2011). Assessing effect of wind tunnel sizes on air velocity and concentration boundary layers and on ammonia emission estimation using computational fluid dynamics (CFD). Computers and Electronics in Agriculture, 78(1): 49-60

Sahm, P., Louka, P., Ketzel, M., Guilloteau, E., Sini, J. F., 2002. Intercomparison of numerical urban dispersion models – part1: street canyon and single building configurations. Water, Air, and Soil Pollution: Focus 2, 587-601.

Shih, T.-H., Liou, W. W., Shabbir, A., Yang, Z., Zhu, J. 1995. A New $k-\varepsilon$ Eddy-Viscosity Model for High Reynolds Number Turbulent Flows - Model Development and Validation. Computers Fluids 24(3), 227-238.

Sini, J. F., Anquetin, S., Mestayer, P. G., 1996. Pollutant despersion and thermal effects in urban street canyons. Atmospheric Environment 95, 1352-2310.

Tsai, M.Y., Chen, K.S., 2004. Measurements and three dimensional modelling of air pollutant dispersion in an urban street canyon. Atmospheric Environment 38, 5911-5924.

Wu, W., Kai, P., Zhang, G., Bjerg, B., Nielsen, P. V., 2011. Assessment of a partial pit ventilation system to reduce emission under slatted floor – part1: Scale model study. Manuscript submitted to Computers and Electronics in Agriculture.

Zhai, Z., Zhang, Z., Zhang, W., Chen. Q., 2007. Evaluation of various turbulence models in predicting airflow and turbulence in enclosed environments by CFD: Part-1: summary of prevent turbulence models. HVAC & R research 13(6), 1-21.

Chapter 7

Large eddy simulation of airflow and pollutant transport under slatted floor of a slurry pit model

Paper VI:

Wu, W., Zong, C., Zhang, G., 2012. **Large eddy simulation of airflow and pollutant transport under slatted floor of a slurry pit model**. (Submitted to a peer review journal)

Abstract

For dairy cattle buildings with slatted floor systems, about 40% of the ammonia emission originates from the slurry pit. In order to find a solution to abate this part of emission, a better understanding of the ammonia transportation from the pit to the room space is crucial. Large eddy simulation (LES) was adopted to investigate the transportation of airflow and ammonia under slatted floor. To tackle the involvement of the slatted floor, two approaches were proposed: modelling slatted floors directly with geometrical details (LESD) and treating them as porous media (LESP). The main purpose of this work was to study the potential of using porous media to model the slatted floor. The LES results were validated by the air velocities measured using a LDA (Laser Doppler anemometer) in a 1:8 scale pit model placed in a wind tunnel. The results showed that LESP was able to estimate the mean air velocities and turbulence kinetic energy in the core of the pit headspace; but it cannot satisfactorily predict the mean air velocities and turbulence kinetic energy in the space next to the upwind wall. Apparent vertical air motion in the top surface of the slot was observed for LESD results. There was not such trend found for LESP results. Both the air velocity and NH_3 mass fraction fluctuated weaker for LESP results. By spectral analysis, LESP was able to capture the entire power spectrum compared with LESD. A dominant Strouhal number 0.23 was found for LESD results but no dominant strouhal number was found for LESP results. The emission rate and total mass of NH_3 in the pit headspace calculated by LESD was double of those calculated by LESP. Pollutants were confined in the headspace for longer time by means of using LESP than using LESD. For both LESD and LESP, turbulence transportation was the dominant removal mechanism to transport pollutants from the headspace to the free stream.

Key words: *CFD; LES; porous media; wind tunnel; Strouhal number*

7.1. Introduction

Dairy cow buildings constitute one of the largest sources of ammonia emissions among various animal husbandry operations in Denmark (Pederson, 2006). Solutions to curtail the dairy cow emissions include changes in housing and floor design. Slatted floor with scrapers on the floor surface as well as channel scraper show the potential to keep ammonia emissions at a low level (Zhang et al., 2005; Wu et al., 2012a). For a cattle building with slatted floors, about 60% of the total ammonia emission originates from floor surface, whereas 40% is released from the slurry pit (Braam et al., 1997). In order to find a solution to abate the portion of emission coming from the slurry pit and improve the design of the floor system, a better understanding of the ammonia transportation mechanism from the pit to the room space is necessary. So far, some studies regarding airflow patterns and pollutant dispersion in dairy cow buildings have been limited to the space above the slatted floor (Norton et al., 2010a; Norton et al., 2010b; Wu et al., 2012b). However, the knowledge of the characteristics of the airflow and mass transport under the slatted floor is still missing, although it is crucial to estimate the ammonia emission from the slurry pit correctly. Wu et al. (2012c) applied CFD to study the airflow characteristics under slatted floor in a 1:2 scale pit model, in which the slatted floor was simulated in geometrical detail. However, the measured air velocities were limited due to the spatial resolution of the sensors and the experimental facilities (Wu et al., 2012d). Considering that obtaining the characteristics of the air motion under slatted floor in a full scale livestock building is the final research goal, modelling of slatted floor in reality becomes the main concern. The slot width in a real cattle building is about 0.02 m, while the shortest building dimension is generally longer than several metres. The small ratio of slot width and building dimension prevents a direct modelling of the geometrical details. Therefore, slatted floor is usually handled as porous media (Sun et al., 2004; Bjerg et al., 2008a; Bjerg et al., 2008b). However, up to date, the information on the difference that might exist between simulations using geometrical details and porous media cannot be found in literature. The uncertainty of using porous media to replace the slatted floor above the slurry pit in simulations should be investigated.

The crucial prerequisite of an investigation on the difference between modelling slatted floors with geometrical details and treating them as porous media is to accurately simulate the flow passing by the pit headspace - a cubic cavity. The phenomenon is known to be difficult to model due to the flow separation. The research of similar cavity flow can be found in the area of modelling airflow in street canyons (Vardoulakis et al., 2003). Reynolds-averaged Navier-Stokes (RANS) models are the most commonly adopted turbulence models in calculating street canyon wind flow. The RANS models ever employed in street canyon field are the standard $k-\varepsilon$ model (Johnson and Hunter, 1998; Baik and Kim, 1999; Baik and Kim, 2002; Kim and Baik, 2003; Neofytou et al., 2006) and its variants, RNG $k-\varepsilon$ model (Tsai and Chen, 2004) as well as realizable $k-\varepsilon$ model

(Sagrado et al., 2002). Despite of the widely utilization of $k-\varepsilon$ models, the main deficiency pointed out by Solazzo et al. (2009) is the underestimation of the turbulence kinetic energy and air velocities within some parts of the cavity. The experimental and computational studies of Chang and Meroney (2003) revealed that the dispersion of gaseous pollutants within the street cavity was essentially unsteady. Johnson and Hunter (1998) also reported that the transient flow was a very important factor in quantifying the gas dispersion from street canyon. Hence, the precise prediction of gas dispersion from a cavity may not be reached by assuming a steady state process. Due to the weakness of RANS models, large eddy simulation (LES) was used to examine the flow features in street canyons by Liu et al. (2005) and the LES results agreed reasonably well with wind tunnel measurements. Walton and Chen (2002) compared the accuracy of $k-\varepsilon$ and LES turbulence closure schemes against experimental results and found that the LES results exhibited the best agreement with measured results.

The cavity flow in this study is much more complicated than the above mentioned studies on street canyon due to the involvement of a porous layer (the slatted floor). The main purpose of this work is to use Large Eddy Simulation (LES) to investigate the difference of airflow and pollutant transportation in the pit headspace between modelling slatted floor directly (LESD) and modelling slatted floor as porous media (LESP).

7.2. Materials and methods

This section will start with an introduction to the wind tunnel measurements used to validate the large eddy simulation. It follows with a description of the development of the CFD model and theories of LES. At the end of this section, the methods to analyze the simulation results will be presented.

7.2.1. Measurements for model validation

7.2.1.1. Experimental apparatus

The experiment was carried out in a wind tunnel at the air physics lab, Aarhus University, Denmark. The wind tunnel (Fig. 7.1 a) was 3.67 m long with cross section area of $W \times H$ = 0.35 m×0.35 m. At working section of the wind tunnel there was a 0.80 m long transparent glass window for velocity measurement using a Laser Doppler anemometer (LDA). Smoke was injected at the wind tunnel inlet to provide the seeding for LDA to measure air velocity. A ventilator (Type CK 200 B CBU, Lindab A/S, Denmark) was installed at the tunnel outlet to drive the air motion through the tunnel.

A 1:8 scale pit model (Fig. 7.1b) with $L_p \times W_p \times H_p$ = 0.35 m×0.35 m×0.09 m was constructed at the working section. The top of the pit model was covered with 17 slats, which were orientated

parallel to the flow direction. The dimension of the slats is shown in Fig. 7.1b. The top of the slatted floor was at the same level with the surface of the tunnel floor.

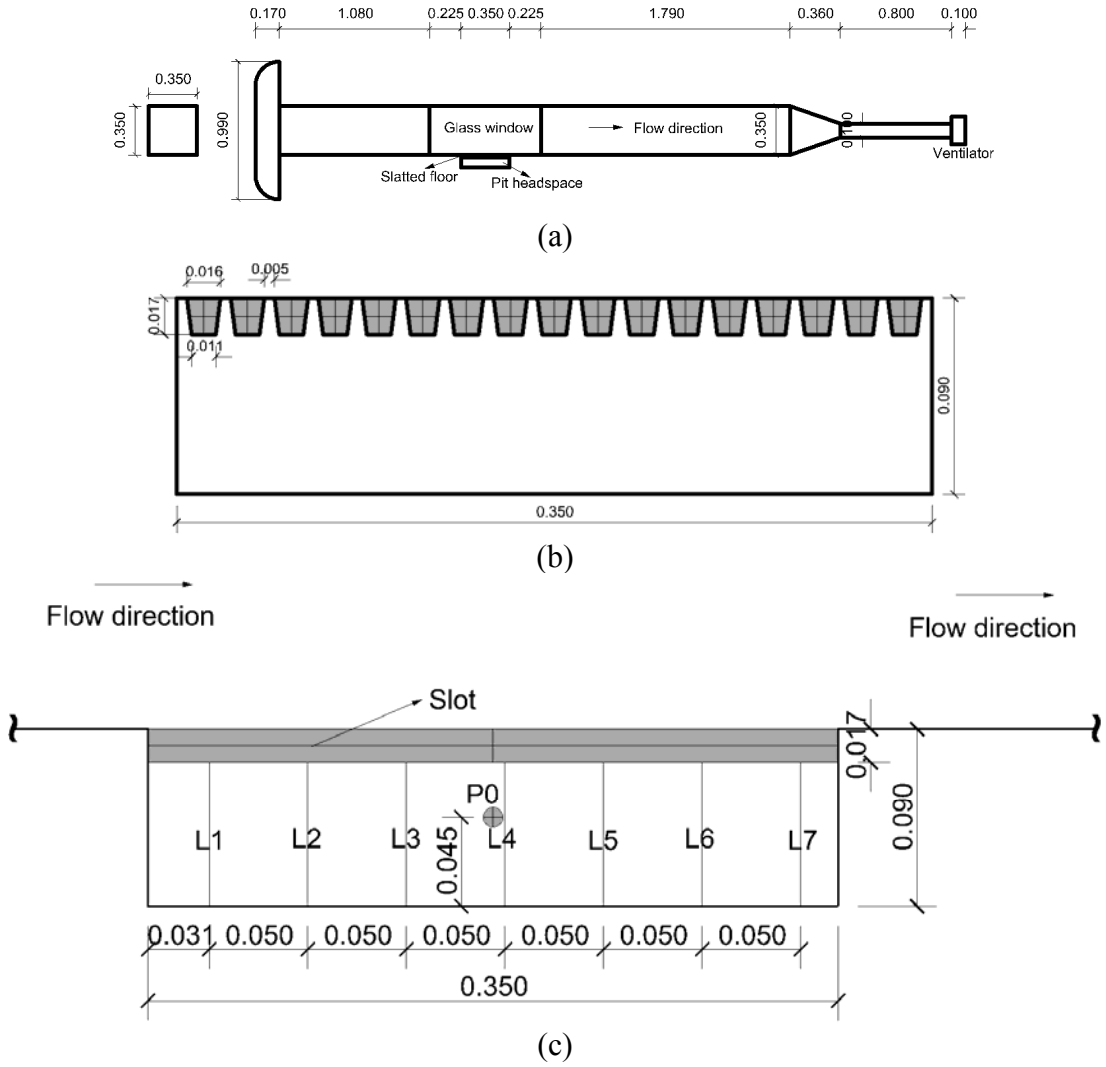

Fig. 7.1 Schematic of (a) the wind tunnel; (b) the pit model and the slats; (c) the velocity measurement locations (L1-L7). All dimensions are in m.

7.2.1.2. Air velocity and turbulence measurement

Air velocity and turbulence were recorded at 7 vertical heights (0.022, 0.027, 0.032, 0.037, 0.042, 0.047 and 0.057 m) from the bottom surface of the pit and at 7 locations L1-L7 (Fig. 7.1c) along the longitudinal direction of the pit. These 7 locations were under a slot in the middle plane of the wind tunnel and the distance between each other was 0.05 m. The first location was 0.031 m away from the windward wall of the pit.

A 2-D LDA (Type 58N40-FVA enhanced, DANTEC Dynamics, Skovlunde, Denmark) was used to measure the air velocities and turbulence quantities. The work principle of LDA was clarified by Saha et al. (2010). The recording time for each position was 2.5 min.

7.2.2. CFD modelling

7.2.2.1. Numerical representation of the pit model with slatted floor

Fig. 7.2a shows that a slot bounded with two half slats forms a rectilinear geometry in the cross direction of the flow. The periodical occurrence of slats distribution enables a slot with two adjacent half-slats to represent the entire slatted floor system. It was observed in the experiment that the velocity gradient was zero at 0.5*H* height of the wind tunnel. Therefore, the half height of the wind tunnel space was used in the CFD model. Fig. 7.2b illustrates the simplified geometry for the CFD model.

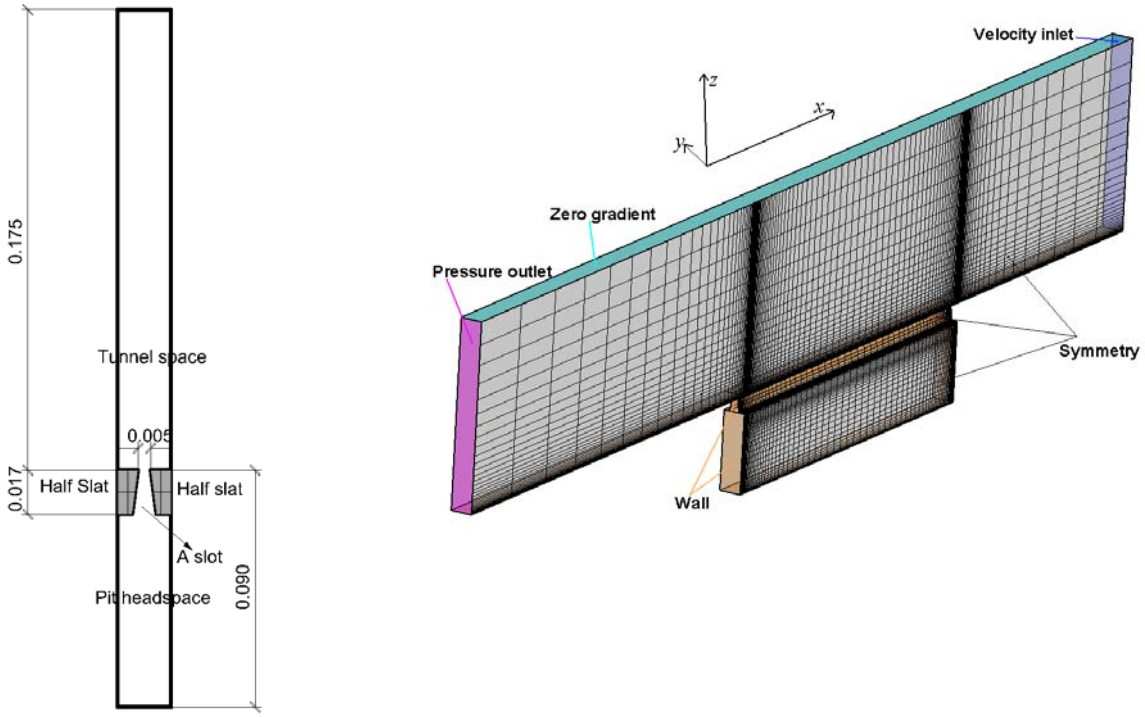

(a) (b)

Fig. 7.2 (a) The CFD representation of the pit model geometry with slatted floor; (b) CFD domain, mesh and boundary conditions

7.2.2.2. Boundary conditions and mesh

The computational domain with mesh and boundary conditions is shown in Fig. 7.2b. The height of the domain was 0.5*H*. The free surface layer extended $3H_p$ and $5H_p$ in upstream and downstream directions, respectively. The top surface of the free stream was defined as zero gradient boundary condition. The ventilator created an air speed 1.41±0.11 m s^{-1} at 0.5*H* height, which was used as the inlet air velocity (*U*). The associated Reynolds number was 8.69×10^3 based on the inlet velocity *U*

and the height of the pit H_p. Pressure outlet was prescribed as the outlet boundary condition. Symmetry planes were imposed on the two domain sides along the streamline direction, which allowed a slot and two half slats to translate themselves periodically towards the direction perpendicular to the free streamlines. No-slip wall was imposed on the solid surfaces. As above mentioned objectives, the slatted floor was modelled directly in one case and was handled as porous media in another case. In the case of simulating slatted floor directly, the volume occupied by slats was defined as solid material. Otherwise, the volume was defined as air, the identical material with the whole fluid domain. A resistance was added to the cell zones representing the space of the two half slats and the slot. The resistance thus generated the pressure drop when air went though the cell zones. A concrete description of modelling flow through porous media can be found in the work of Wu et al. (2012c). The resistance coefficient of the porous zone was taken as 10000 m^{-2} for viscous resistance and 50 m^{-1} for inertial resistance. The estimation of the resistance coefficients was based on the methodology proposed by Bjerg et al. (2008a).

Three mesh systems with 148876, 253140 and 454458 cells were constructed to test grid independence. Fig. 7.3 shows the horizontal air velocities with respect to heights at location L5. The medium mesh predicted very similar air velocities with fine mesh. Therefore, the medium mesh with 253140 cells was used for further calculations.

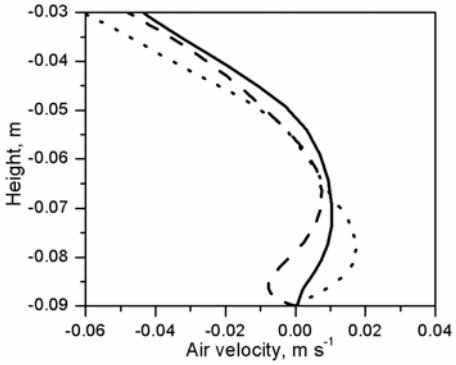

Fig. 7.3 Mesh convergence study of the velocities at L5: dotted line – coarse mesh; solid line – medium mesh; dashed line – fine mesh.

Since the simulations were activated in a transient mode, the time step should be defined according to Courant-Friedrichs-Lewy condition,

$$\frac{u_x \Delta t}{\Delta x} + \frac{u_y \Delta t}{\Delta y} + \frac{u_z \Delta t}{\Delta z} \leq Cons\tan t \qquad (7.1)$$

where, x, y, z are coordinates; u_x, u_y, u_z are velocity scales; Δx , Δy , Δz are grid spaces in three coordinates, respectively; Δt is time step. The smallest grid was 2×10^{-4} m for all the three coordinates and the free stream velocity U were set as the reference velocity scale for the three dimensions. The time step was 1×10^{-4} s. The height of the pit headspace H_p was taken as the length

scale. The time scale T was calculated as H_p/U, which was 0.064 s. The simulations were run 50 T for the turbulent flow to achieve quasi-steady state. Another 50T was computed for data sampling.

7.2.2.3. Turbulence modelling

LES approach computes the larger eddies for each problem with a time dependent solution. The universal behaviours of small eddies are captured with a compact model. Instead of time averaging, LES uses a spatial filtering operation to separate the larger and smaller eddies. The method starts with the selection of a filtering function and a certain cut-off width. Box filter used in the finite volume implementations can be written as follow

$$G(x,x',\Delta)=\begin{cases}1/\Delta^3 & |x-x'|\le\Delta/2\\ 0 & |x-x'|>\Delta/2\end{cases} \tag{7.2}$$

where, $G(x,x',\Delta)$ is a filter function; Δ is filter cut-off width. In the next step spatial filtering operation is performed on the time dependent flow equations. The spatial filtering operation is defined as

$$\overline{\phi}(x,t)\equiv\int_{-\infty-\infty-\infty}^{+\infty+\infty+\infty}\int\int G(x,x',\Delta)\phi(x',t)dx_1'dx_2'dx_3' \tag{7.3}$$

where, $\overline{\phi}(x,t)$ is filtered function; $\phi(x',t)$ is original function. Applying the filter operation (3) to the unsteady and incompressible continuity and Navier-Stokes equations yields the LES equations,

$$\frac{\partial\rho\overline{u}_i}{\partial x_i}=0 \tag{7.4}$$

$$\frac{\partial\rho\overline{u}_i}{\partial t}+\frac{\partial}{\partial x_j}\rho\overline{u}_i\overline{u}_j=\frac{\partial\overline{p}}{\partial x_i}-\frac{\partial\tau_{ij}}{\partial x_j}+\mu\frac{\partial^2\overline{u}_i}{\partial x_j\partial x_j} \tag{7.5}$$

where, $\overline{u}_i,\overline{u}_j$ are the larger scale velocities in the i,j direction; $\overline{p}$ is larger scale pressure. μ is dynamic viscosity. After spatial filtering operation, information related to the smaller eddies which is filtered out is described by means of sub-grid-scale stresses (SGS), denoted as τ_{ij} in equation (5).

$$\tau_{ij}=\rho\overline{u_iu_j}-\rho\overline{u}_i\overline{u}_j \tag{7.6}$$

The SGS stresses is computed by employing Boussinesq hypothesis,

$$\tau_{ij} - \frac{1}{3}\tau_{ii}\delta_{ij} = -2\mu_t \bar{S}_{ij} \tag{7.7}$$

in which δ_{ij} is Kronecker's delta; μ_t is the SGS turbulent viscosity; the rate of strain tensor $\bar{S}_{ij}$ is defined by

$$\bar{S}_{ij} = \frac{1}{2}\left(\frac{\partial \bar{u}_i}{\partial x_j} + \frac{\partial \bar{u}_j}{\partial x_i}\right) \tag{7.8}$$

In this study, μ_t is provided by Smagorinsky-Lilly model,

$$\mu_t = \rho L_s^2 \left|\bar{S}\right| \tag{7.9}$$

where, L_s is the mixing length for SGS. It is determined by

$$L_s = \min(\kappa d, C_s \Delta) \tag{7.10}$$

where, κ is the von Karman constant, d is the distance to the closest wall, C_s is the Smagorinsky constant (0.1 is used in this work).

7.2.2.4. Modelling pollutant transportation

Ammonia is considered as the pollutant in this study. Applying the filter operation (7.3) to the species transportation equation gives the mass equation for LES,

$$\frac{\partial \rho \bar{c}}{\partial t} + \frac{\partial}{\partial x_i}\rho \bar{u}_i \bar{c} = -\frac{\partial \tau_{i,c}}{\partial x_i} + D\frac{\partial^2 \bar{c}}{\partial x_i \partial x_i} \tag{7.11}$$

where, $\bar{c}$ is the filtered ammonia fraction; $\tau_{i,c}$ is SGS flux term

$$\tau_{i,c} = \rho\overline{u_i c} - \rho \bar{u}_i \bar{c} \tag{7.12}$$

which is modelled using the same methodology for SGS stresses. D is the mass diffusivity and can be estimated by (Sommer et al., 2006)

$$D = \frac{10^{-7} T^{1.75} * (1/M_{NH3} - 1/M_{air})^{1/2}}{p(20.1^{1/3} + 14.9^{1/3})^2} \tag{7.13}$$

where, M is the molecular weight; p is the atmospheric pressure, atm; T is the air temperature, K; the meaning of all the constants is explained by Sommer et al. (2006).

7.2.3. Strouhal number

The difference of simulating slatted floor directly and indirectly (as porous media) may be illustrated by the vortex oscillation in the headspace of the pit. The oscillating flow under the slatted floor can be described by Strouhal number (*St*),

$$St = \frac{fH_p}{U} \tag{7.14}$$

where, f is the frequency of the vortex vibration in the headspace of the pit model. For large St (order of 1), viscosity dominates the flow; for low St, the quasi steady state portion of the fluid movement dominates the oscillation.

7.2.4. Retention time

Liu et al. (2005) defined a time scale of pollutant residing in a street canyon as the pollutant retention time. The concept of retention time is adopted in this study. The aim is to identify the consistency of the time scale of pollutant residing under slatted floor while the slatted floor is simulated directly and indirectly (as porous media). The retention time (Γ) is determined by

$$\Gamma = \frac{\Theta}{Q} \tag{7.15}$$

where, Q is the pollutant emission rate, which can be obtained by integrating the pollutant in the outlet of the free stream; Θ signifies the total mass of the pollutant confined under the slatted floor, which can be calculated using

$$\Theta = \iiint_{\Omega} \rho \bar{c} d\Omega \tag{7.16}$$

where, Ω is the volume of the headspace of the pit.

7.2.5. Vertical mass flux induced by turbulent diffusion and mean flow

Baik and Kim (2002) proposed two formulas CW and $c'w'$ to calculate vertical mass flux induced by mean flow and turbulence, respectively. c' and w' are the deviations from the mean NH_3 mass fraction C and mean vertical velocity W, respectively at the slatted floor level. Wu et al. (2012c) employed CW and $c'w'$ to study the transportation mechanism of pollutant through the slatted floor. $c'w'$ may help to find the difference of transportation mechanism through a real slot (simulating slatted floor directly) and through a porous zone (simulating slatted floor as porous media).

7.3. Results and discussion

7.3.1. Model validation

7.3.1.1. Comparison of air velocity profiles

Fig. 7.4 shows the vertical profiles of mean air velocity in the pit headspace. At L1 and L2 near the upwind wall, LESD results achieved very good agreements with measured results both on the shape of the velocity profile and on each velocity component (U_x, U_z), while LESP cannot predict correct mean air velocities at these

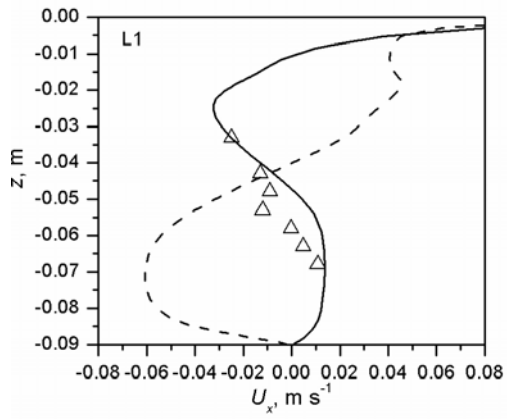
L1
z, m
U_x, m s^{-1}

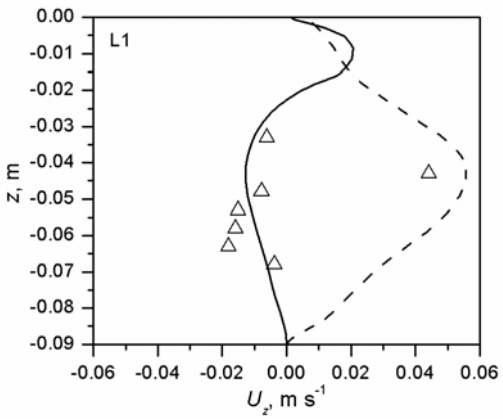
L1
z, m
U_z, m s^{-1}

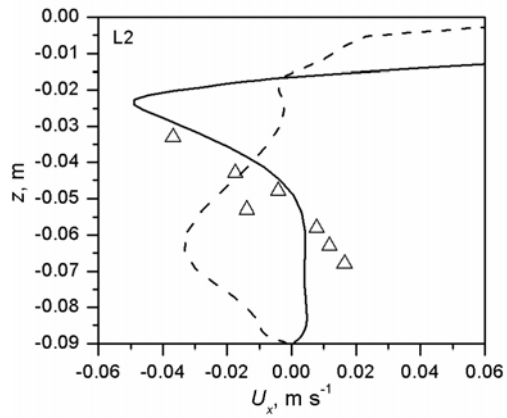
L2
z, m
U_x, m s^{-1}

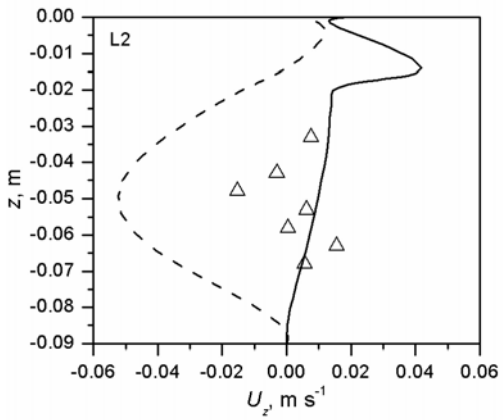
L2
z, m
U_z, m s^{-1}

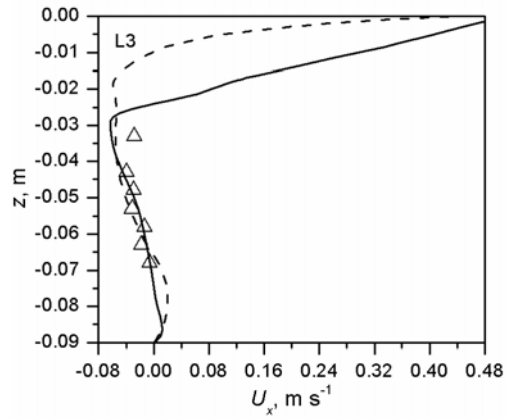
L3
z, m
U_x, m s^{-1}

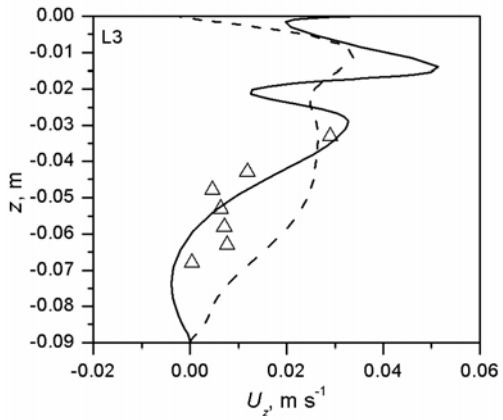
L3
z, m
U_z, m s^{-1}

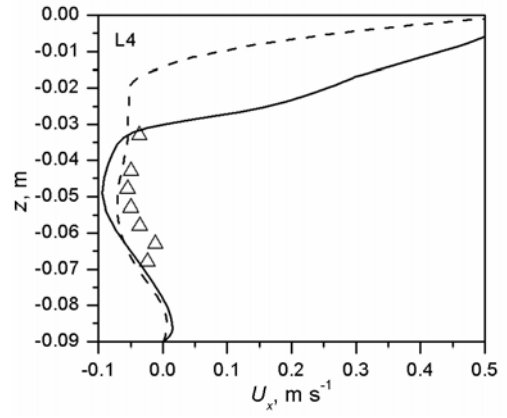
L4
z, m
U_x, m s^{-1}

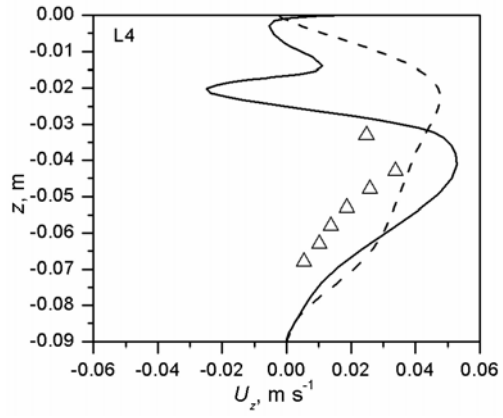
L4
z, m
U_z, m s^{-1}

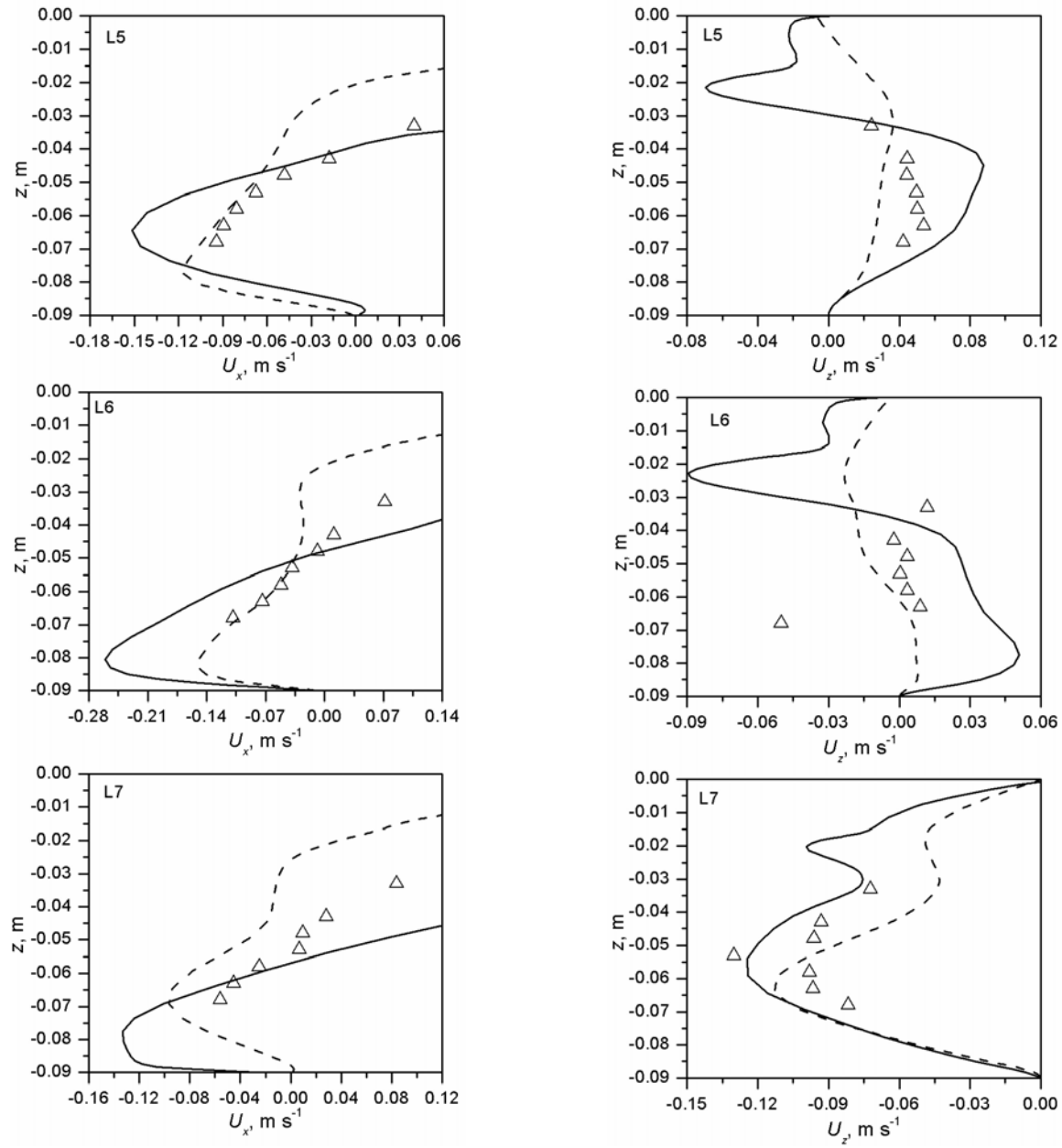

Fig. 7.4 Vertical profiles of mean air velocity in the pit headspace: triangle – measured values; solid line – simulated values by modeling SF directly; dashed line – simulated values by treating SF as porous media. (a) U_x – horizontal velocity; (b)U_z – vertical velocity.

two locations. When the flow reached the core of the headspace (L3-L5), both the simulations were able to predict mean air velocities in line with the measured values and LESP results showed a little better agreement with measurement results compared with LESD results. For the vertical air velocity (U_z), the profiles obtained by LESD had four peaks at -0.0025, -0.01, -0.02, -0.03 m, but the profiles calculated by LESP were more constant. Next to the downwind wall (L6 to L7), the

simulated U_x, U_z using LESD and LESP fitted well with the measured values. But the profile shapes were quite different. Generally, the LESD showed better performance than the LESP.

7.3.1.2. Turbulence modelling

Fig. 7.5 shows the vertical profiles of turbulence kinetic energy in the pit headspace. A large discrepancy was found between the turbulence kinetic energy predicted by LES and measured values at L1. At L2 to L7, both the LES results can agree well with the measured results. The profile pattern from LESD and LESP was similar except that the kinetic energy calculated by LESD was almost 4 times of that calculated by LESP in the slot (around -0.01 m).

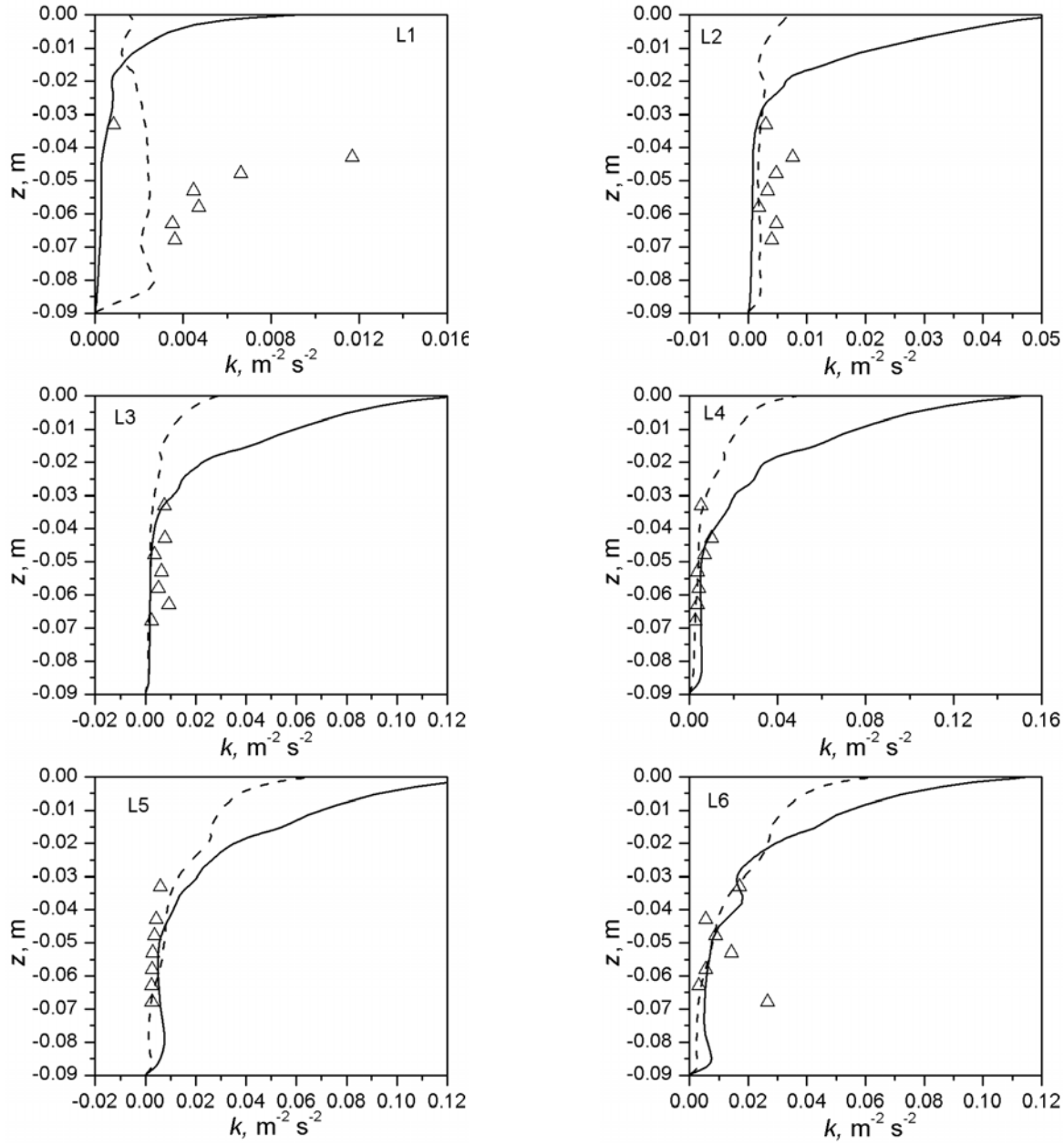

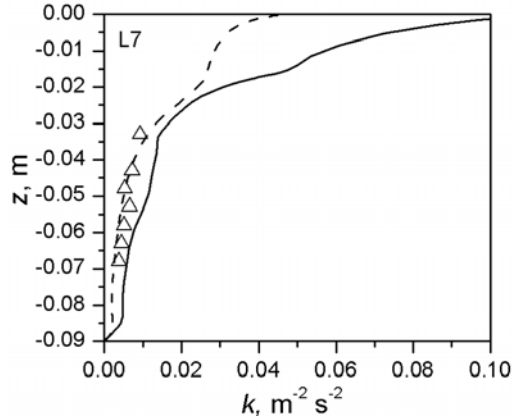

Fig.5 Vertical profiles of turbulent kinetic energy in the pit headspace: triangle – measured values; solid line – simulated values by modeling SF directly; dashed line – simulated values by treating SF as porous media.

7.3.2. Flow field and NH_3 distribution in the headspace

Fig. 7.6 shows the time-averaged airflow patterns, velocity magnitude and NH_3 mass fraction in the pit headspace obtained by LESD and LESP. Both modelling methods predicted 3 vortices in the headspace. Via treating the slatted floor as porous media, the 3 vortices shifted slightly to the upwind direction. For LESD results, a big circulation started to be formed by the reflection of the downwind wall and was extended to the upwind wall. For LESP results, a similar eddy started to circulate from the downwind wall but did not reach the downwind wall and was ended in the middle section of x coordinate. Air velocity in the slot was about 0.5 to 1 m s^{-1}, while it was smaller than 0.2 m s^{-1} in the porous zone. The higher air velocity in the slot enabled the air to attach the bottom surface of the pit at a higher speed 0.3 m s^{-1} and had more energy to travel long distance to the upwind side. LESP results showed that the process of the attachment to bottom surface of pit was weaker compared with LESD results. This may explain the difference of the big circulation obtained by the two different methods. Another difference of the airflow patterns between the two simulation methods should be noticed. For LESD results, the air on the top surface of slot had significant vertical movement and can flow out of the cavity. However, for LESP results, there was no significant vertical air movement on the interface of the porous layer and the tunnel space.

High concentration of NH_3 was found in the upwind side of the pit headspace. The NH_3 mass fraction obtained by LESD was higher than that calculated by LESP.

7.3.3. Velocity and NH_3 fluctuation in the headspace

Fig. 7.7 shows the time history of air velocity and NH_3 fraction at P0. The air velocities obtained by LESD were more fluctuated and had a higher mean value of 0.28 m s^{-1} while the LESP results were less oscillated and had a lower mean air velocity of 0.12m s^{-1}. The NH_3 fraction displayed same fluctuation feature with the air velocities at P0 for two the simulation methods. But the oscillation

of mass transfer was slower than the oscillation of flow. During 50*T*, flow finished about 12 periods while the mass transfer underwent only about 3 circles.

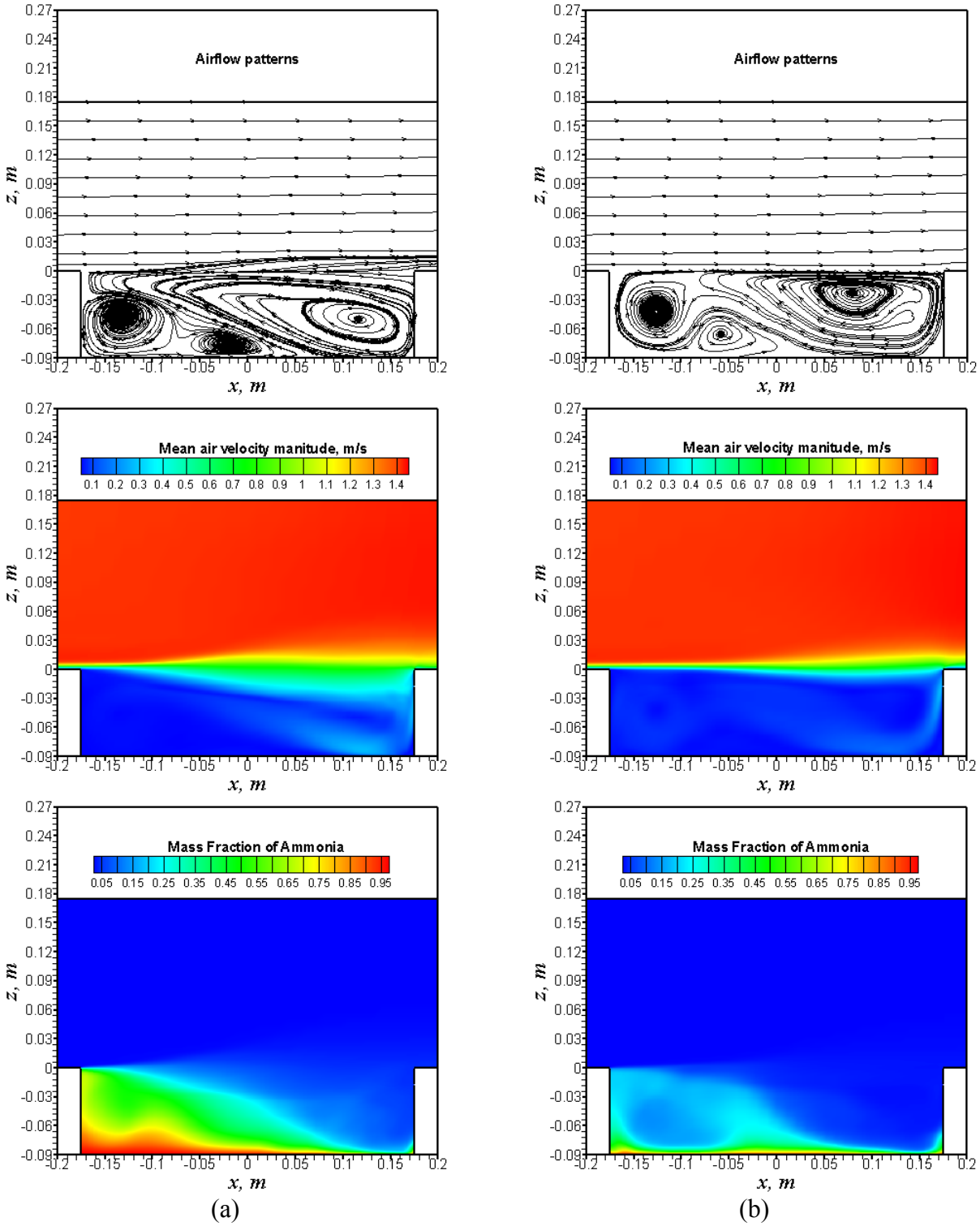

Fig. 7.6 Airflow patterns, velocity magnitude, ammonia mass fraction in the pit headspace: (a) modeling SF directly; (b) treating SF as porous media.

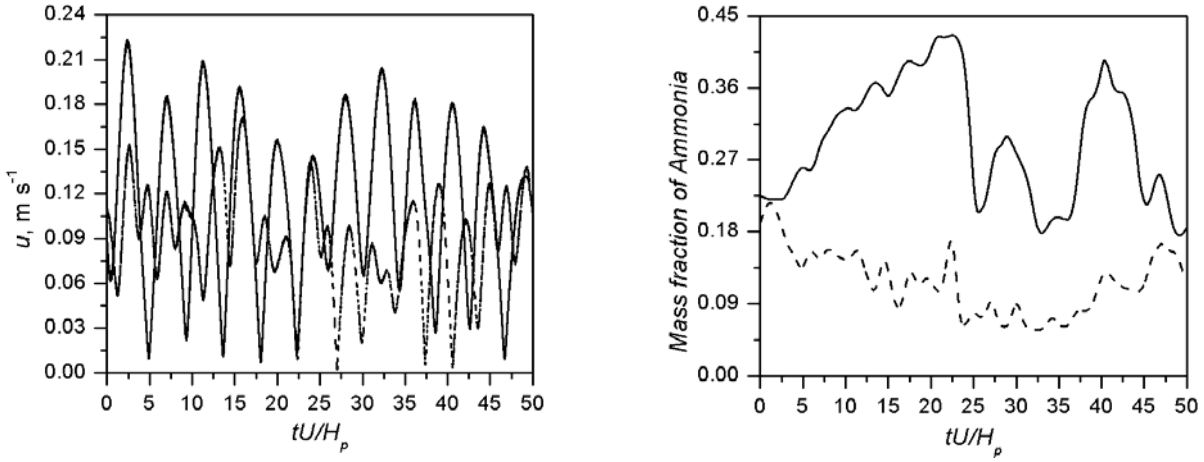

(a) (b)

Fig. 7.7 Time history of ensemble-averaged variables at point P0: (a) air velocity magnitude and (b) mass faction of ammonia in the pit headspace. Solid and dashed lines denote results from modeling SF directly and treating SF as porous media, respectively.

Fig. 7.8 (a) shows the power spectral density of air velocity with respect to frequency at P0. The overlap of the two spectrums suggested that LESP method can capture the entire power spectrum of vortex oscillation in the pit headspace. Fig. 7.8 (b) shows the power spectral density against the Strouhal number. A dominant *St* existed for the LESD results and was approximated 0.23. However, the dominant *St* did not occur for the LESP results.

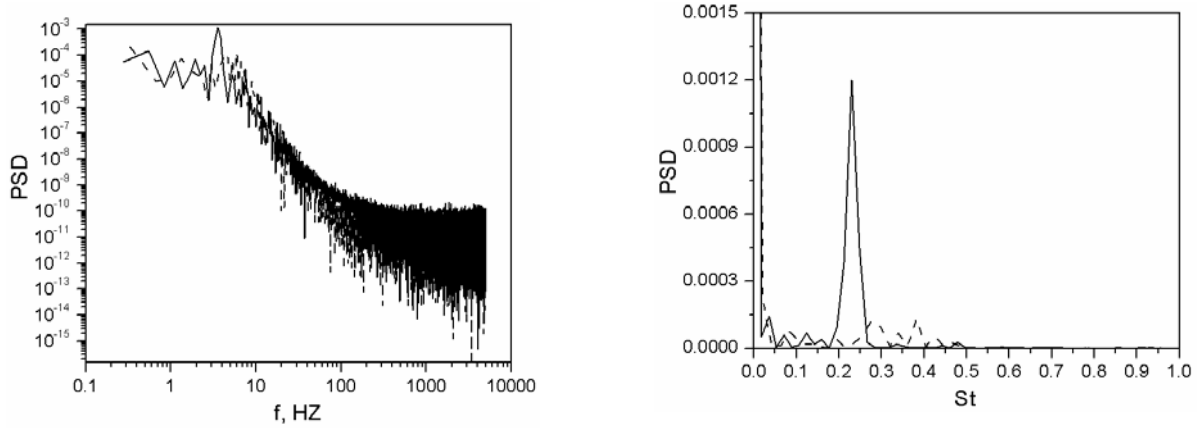

(a) (b)

Fig.7.8 Spectral analysis of time history of air velocity magnitude on point P0: (a) power spectral density with respect to frequency; (b) power spectral density with respect to Strouhal number. Solid and dashed lines denote results from modeling SF directly and treating SF as porous media, respectively.

The higher fluctuation in LESD may be explained as follow. The presence of slats in the simulation introduced turbulence kinetic energy production inside the slot. This can be proved by the higher kinetic energy in the slot at L1to L7 calculated by LESD compared to that calculated by

LESP (Fig. 7.5). After the slatted floor was handled as porous media, the turbulence kinetic energy generated by slats cannot be recovered in the zone of slatted floor. Therefore, the turbulence kinetic energy generated by slats caused flow in the pit headspace more unstable and fluctuated. The turbulence kinetic energy generated by slats and the flow separation of the shear layer in the vicinity of slats might be attributed to the instabilities and vortex oscillation at P0 in the LESD simulation.

7.3.4. Retention time

Retention time defined by equation (7.15) was used to investigate the time scale of the NH_3 transport in the pit headspace in order to study the difference of the two simulation methods. The NH_3 emission rate, total NH_3 emission confined in the pit headspace and retention time are given in Table 7.1. The emission rate and total mass confined in the headspace of NH_3 calculated by LESD was double of those from LESP. The vertical air motion (Fig. 7.6) may cause more pollutants to escape from the headspace by means of LESD simulation. However, the difference of the retention time for the two simulation methods was 0.29 s. Given that the reference time scale was 0.064 s, the dimensionless difference of retention time was 4.5*T*. The NH_3 was confined in the cavity for 4.5T longer by using LESP than by using LESD.

Table 7.1 Emission rate, Total mass in the pit headspace and retention time of NH_3

Modelling method	Emission rate (mg s^{-1})	Total mass in the pit headspace (mg)	Retention time (s)
LESD	34.3	215	6.27
LESP	16.8	110	6.56

7.3.5. The pollutant removal mechanism for the two simulation methods

Fig. 7.9 shows the vertical NH_3 flux transported by mean flow U_z and turbulence u'_z in LESD and LESP. For both of the simulation results, more than 87% of the pollutants were removed by turbulence transportation (87.9% in LESD, 87.4% in LESP). In the downwind side, the mean flow even transported the pollutants back to the cavity. The negative flux was -0.65 and -1.88 mg s^{-1} for LESD and LESP results, respectively. The maximum removal of pollutants happed at position x=-0.05 m (0.05 m away from the cavity centre and in the upwind side) for both simulation methods. The maximum transportation (84.3 mg s^{-1} for LESD and 59.1 mg s^{-1} for LESP) was driven by turbulence. This agrees well with other research reports and further confirms that the pollutant removal from a cubical cavity was mainly due to turbulence diffusion (Lee and Park, 1994; Baik and Kim, 1998; Wu et al., 2012d).

7.3.6. Further discussion and future work

Through the examination of the performance of two numerical methods to model the airflow and pollutant transportation under slatted floor, LESP seemed able to estimate the mean air velocities and turbulence kinetic energy in the core of the pit headspace. However, differences between results of LESD and LESP also existed. The major difference could be due to the inability of LESP to

include the turbulent kinetic energy generated by the presence of slats. This part of kinetic energy affected the vertex oscillation and the pollutant removal through the slots. Due to the strong oscillation led by slats, more pollutant had the chance to escape the cavity (Fig.9). To make the utilization of porous media more efficient to represent slatted floor, not only a pressure drop was added to the Navier-Stoke (N-S) equation but also a correction to the extra energy production in the slots should be well considered.

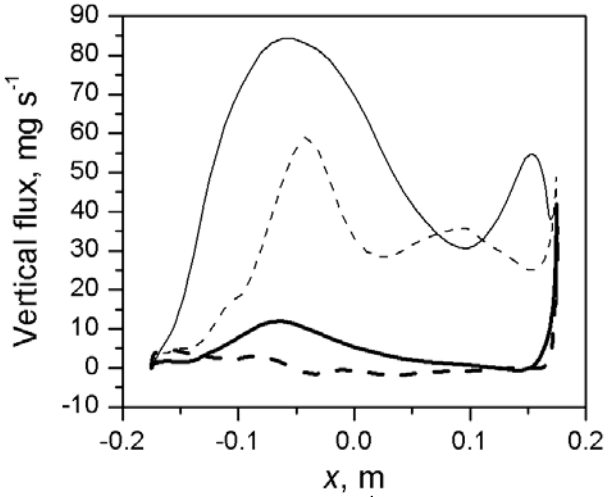

Fig.7.9 Vertical ammonia flux transported by U_z and u'_z: Solid and dashed lines denote results from modeling SF directly and treating SF as porous media, respectively; Thick and thin lines mark ammonia transportation by U_z and u', respectively

The time scale for pollutants to reside in the cavity was found inconsistent for LESD and LESP. One reason might be due to the change of the length scale when porous media was used instead of modelling slatted floor directly. The narrow slot may decompose the large eddy from the free stream to small eddies. The process can cause turbulent kinetic energy cascade and dissipation. When the flow went through the slots, the length scale was changed again. However, in the current LES, the variation of the length scale was not considered in the N-S equation.

This work only considers the case when the slats were oriented parallel to the flow direction. To reduce uncertainties of using porous median, different orientations of slats such as perpendicular to the flow direction should be investigated in the future. Correction of turbulence kinetic energy production in the porous zone will also be the perspective work.

7.4. Conclusions

The main objective of this work was to evaluate the performance of using porous media to simulate slatted floor. Two numerical methods, modelling slatted floors directly with geometrical details (LESD) and treating them as porous media (LESP), were proposed. Main conclusions can be drawn from the results:

(1) LESP was able to estimate the mean air velocities and turbulence kinetic energy in the core of the pit headspace. LESP cannot well predict the mean air velocities and turbulence kinetic energy in the space next to upwind wall.
(2) The airflow patterns obtained by LESD and LESP were different. Clear vertical air motion in the top surface of the slot was observed for LESD results. There was not such trend found for LESP results.
(3) Both the air velocity and NH_3 fraction fluctuated weaker for LESP results.
(4) By spectral analysis, LESP was able to capture the entire power spectrum compared with LESD. A dominant Strouhal number 0.23 was found for LESD results but no dominant Strouhal number was found for LESP results.
(5) The emission rate and total mass in the pit headspace of NH_3 calculated by LESD was double of those calculated by LESP. Pollutants were confined in the headspace for longer time by means of using LESP than using LESD.
(6) For both LESD and LESP, turbulence transportation was the dominant removal mechanism to transport pollutants from the headspace to the free stream.

References

Baik, J.J., Kim, J.J., 1998. A numerical study of flow and pollutant dispersion characteristics in urban street canyons. *Journal of applied meteorology* 38, 1576-1589.

Baik, J.J., Kim, J.J., 2002. On the Escape of Pollutants from Urban Street Canyons. *Atmospheric Environment* 36, 527-536.

Blocken, B., Stathopoulos, T., Carmeliet, J., 2007.CFD simulation of the atmospheric boundary layer: wall function problems. *Atmospheric environment* 41, 238-252.

Bjerg B., Zhang, G., Kai, P., 2008a. Porous media as boundary condition for air inlet, slatted floor and animal occupied zone in numerical simulation of airflow in a pig unit. *AgEng2008 International Conference on Agricultural Engineering, Hersonissos, Crete-Greece*.

Bjerg B., Zhang, G., Kai, P., 2008b. CFD investigations of a partly pit ventilation system as method to reduce ammonia emission from pig production units. *The Eighth ASABE International Livestock Environment Symposium (ILES Ⅷ)*.

Braam, C. R., Smits, M.C.J., Gunnink, H., Swierstra, D., 1997a. Ammonia Emission from a Double-sloped Solid Floor in a Cubic House for Dairy Cows. *Journal of Agricultural Engineering Research* 68(4), 375-386.

Johnson, G.T., Hunter, L.J., 1998. Urban wind flows: wind tunnel and numerical simulations—a preliminary comparison. *Environmental Modelling and Software* 13, 279–286.

Kim, J.J., Baik, J.J., 2003. Effects of inflow turbulence intensity on flow and pollutant dispersion in an urban street canyon. *Journal of Wind Engineering and Industrial Aerodynamics* 91, 309-329.

Launder, B.E., Spalding, D.B., 1974. Numerical computation of turbulent flows. *Computers and Mathematics in Applied Mechanics and Engineering* 3, 269-289.

Lee, I.Y., and Park, H.M., 1994. Parameterization of the pollutant transport and dispersion in urban street canyons. *Atmospheric Enviroment* 28, 2343-2349.

Liu, C., Leung, D., Barth., M.C., 2005. On the Prediction of Air and Pollutant Exchange Rates in the Street Canyons of Different Aspect Ratios using Large-eddy Simulation. *Atmospheric Environment* 39, 1567-1574.

Morsing, S., Strøm, J.S., Zhang, G., Kai, P., 2008. Scale Model Experiments to Determine the Effects of Internal Airflow and Floor Design on Gaseous Emissions from Animal Houses. *Biosystems Engineering* 99, 99-104.

Neofytou, p., Venetsanos, A.G., Rafailidis, S., Bartzis, J.G., 2006. Numerical investigation of the pollutant dispersion in an urban street canyon. *Environmental Modelling and Software* 21, 525 – 531.

Norton, T., Grant, J., Fallon, R., Sun, D.W., 2010a. Assessing the ventilation effectiveness of naturally ventilated livestock buildings under wind dominated conditions using computational fluid dynamics. *Biosystems engineering* 103 (1), 78-99.

Norton, T., Grant, J., Fallon, R., Sun, D.W., 2010b. A computational fluid dynamics study of air mixing in a naturally ventilated livestock building with different porous eave opening conditions. *Biosystems engineering* 106 (2), 125-137.

Pedersen, S., 2006. Agricultural Best Management Practices in Denmark. In: *Proc. Agricultural Air Quality: State of the Science*, 56-67.

Sagrado, A.P.G., van Beeck, J., Rambaud, p., Olivari, D., 2002. Numerical and experimental modelling of pollutant dispersion in a street Canyon. *Journal of Wind Engineering and Industrial Aerodynamics* 90, 321-339.

Saha, C.K., Zhang, G., Ni, J., 2010. Airflow and Concentration Characterization and Ammonia Mass Transfer Modelling in Wind Tunnel Studies. *Biosystems Engineering* 107 (4), 328-340.

Solazzo, E., Cai, X., Vardulakis, S., 2009. Improved parameterisation for the numerical modelling of air pollution within an urban street canyon. *Environmental Modelling and Software* 24, 381 – 388.

Sommer, S.G., Zhang, G., Bannink, A., Chadwick, D., Hutchings, N.J., Misselbrook, T., Menzi, H., Ni, J.-Q., Oenema, O., Webb, J., Monteny, G.-J.,2006. Algorithms Determining Ammonia Emission from Livestock Houses and Manure Stores. *Advances in Agronomy* 89 (6), 261–335.

Sun, H.W., Keener, H.M., Deng, W., Michel, F., 2004. Development and Validation of 3-D Models to Simulate Airflow and Ammonia Distribution in a High-rise Hog Building during Summer and Winter Conditions. *Agricultural Engineering International CIGR Journal* 6, Manuscript BC 04 044.

Tsai, M.Y., Chen, K.S., 2004. Measurements and three dimensional modelling of air pollutant dispersion in an urban street canyon. *Atmospheric Environment* 38, 5911-5924.

Vardoulakis, S., Fisher, B.E.A., Pericleous, k., Flesca, N.G., 2003. Modelling air quality in street canyons: a review. *Atmospheric Environment* 37: 155-182.

Walton, A., Chen, A.Y.S., Yeung, W.C., 2002. Large eddy simulation of pollution dispersion in an urban street canyon – part II: idealized canyon simulation. *Atmospheric Environment* 36: 3615-3627.

Wu, W., Zhang, G., Kai, P., 2012a. Emissions of Ammonia and Greenhouse Gases from Two Naturally Ventilated Dairy Cattle Buildings to Atmosphere – Quantifying the Emissions and Investigating the Influencing Factors. *Manuscript submitted to Atmospheric Environment*.

Wu, W., Zhai, J., Zhang, G., Nielsen, P.V., 2012b. Evaluation of methods for determining air exchange rate in a naturally ventilated dairy cattle building with large openings using computational fluid dynamics (CFD). *Manuscript submitted to Atmospheric Environment*.

Wu, W., Zhang, G., Bjerg, B., Nielsen, P.V., 2012d. An assessment of a partial pit ventilation system to reduce emission under slatted floor-Part 2: Feasibility of CFD prediction using RANS turbulence models. *Computers and Electronics in Agriculture* 83, 134-142.

Wu, W., Kai, P., Zhang, 2012d. An assessment of a partial pit ventilation system to reduce emission under slatted floor-Part 1: Scale Model Study. *Computers and Electronics in Agriculture* 83, 127-133.

Zhang, G., Strom, J. S., Li, B., Rom, H.B., Morsing, S., Dahl, P., Wang, C., 2005. Emission of Ammonia and other Contaminant Gases from Naturally Ventilated Dairy Cattle Buildings. *Biosystems Engineering* 92 (3), 355-364.

Chapter 8

Numerical Study on the potential of a partial pit ventilation system to reduce ammonia emissions from a naturally ventilated cattle building

Abstract

The hypothesis of this work is to apply a partial pit ventilation system with an air purification unit to reduce the ammonia emissions from naturally ventilated cattle buildings. Computational fluid dynamics (CFD) was used to investigate such a potential. The results showed that a pit exhaust with a capacity of 37.3 $m^3 h^{-1} HPU^{-1}$ can reduce ammonia emission only by 3.16% compared with the case without pit ventilation when the external wind was 4.2 m s^{-1}. When the external wind was decreased to 1.4 m s^{-1} and the sidewall opening area were reduced to half, such a pit ventilation capacity can reduce ammonia emission by 85.2%. The utilization of pit ventilation system must be integrated with the control of the natural ventilation rates of the building.

Key words: *CFD; pit ventilation; ammonia emission; livestock building*

8.1. Introduction

A partial pit ventilation system with an air purification unit has been known as an efficient approach to reduce ammonia and odour emissions from pig production units (Bjerg et al., 2008a; Saha et al., 2010). Bjerg et al. (2008a) investigated a partly pit ventilation system to reduce ammonia emission from mechanically ventilated pig production units by using computational fluid dynamics (CFD); they showed that evacuating and cleaning of 10% of the total ventilation capacity from the pit may reduce the ammonia emission of the system by 73%, and the ammonia concentration in the room was significantly reduced. Saha et al. (2010) studied the effects of a partial pit ventilation system on ammonia emission from a fattening pig room with a diffuse ceiling inlet, a ceiling-roof-top air exhaust and a pit exhaust; the pit exhaust operated with only 10% of the total ventilation capacity and the ceiling-roof-top exhaust operated as the major ventilation unit regulated according to the thermal conditions in the room; they concluded that reductions in the ammonia emission of 37-53% might be achieved by using an additional air cleaning system.

The potential of a partial pit ventilation system to reduce ammonia emissions is seldom tested in a naturally ventilated cattle building. Bjerg and Andersen (2010) developed a CFD model to investigate the potentials of a pit ventilation system to abate ammonia emission from a naturally ventilated cattle building; the results indicated that a pit ventilation system with a capacity of 80 m^3 h^{-1} HPU^{-1} had the potential to reduce ammonia emission of at least 30%. However, the CFD model was 2-D and not validated with measurement. Wu et al. (2012a) used a 1:2 scale model of manure pit section to study the efficiency of a partial pit ventilation to reduce gas emissions; the experiment was carried out in a wind tunnel. More than 50% of the tracer gas can be removed by the pit ventilation system. However, the airflow in the wind tunnel cannot represent the wind condition in a naturally ventilated livestock building.

The objective of this work was to apply CFD methods to investigate the potential of a partial pit system to reduce ammonia emissions from a full scale and naturally ventilated dairy cattle building.

8.2. Material and methods

8.2.1. Geometry and mesh

The cubical dairy cow building had a length of 114.0 m, a width of 36.0 m and a height of 11.75 m (Fig. 8.1a). The detailed description of the naturally ventilated building can be found in the work of Wu et al. (2012b), in which the building was numbered 2. An office room was adjacent to the building. Another two neighbour buildings were also included in the simulation. A milking parlour (Fig. 8.1b) was located in the middle section of the room. The building included four 42.9 m long slatted floor aisles (Fig. 8.1b). Under the slatted floors were the slurry pits and the pit exhaust systems were installed to pit headspaces.

Hexahedral mesh was constructed to the entire computational domain (Fig. 8.1c). After a test of mesh convergence, 1887447 cells were proved to be the optimum grid number for simulations.

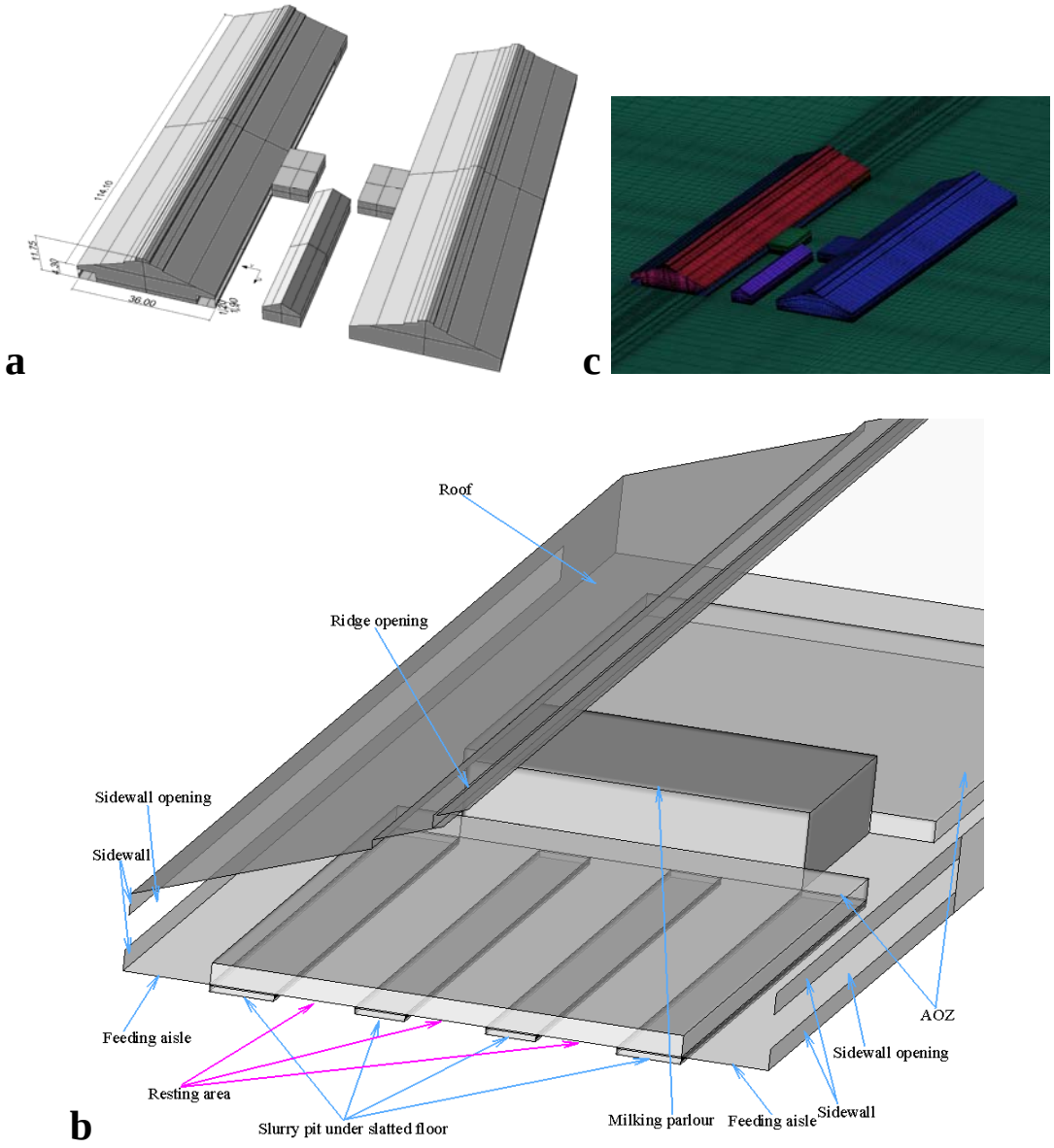

Fig. 8.1 The CFD model and mesh

8.2.2. Boundary conditions

The prescribed boundary conditions are given in Fig. 8.2.

8.2.2.1. Climatic data

The investigation was based on a summer period during Jun 20th and Jul 14th, 2011. The average wind speed at 10 m height was 4.2 m s^{-1} and the frequent wind direction was 225° (see Fig. 8.1). But to study the influence of the external wind speeds, some simulations were carried out at 1.4 to 9.8 m s^{-1} which covers most levels of the wind speeds during the investigation time. Table 1

provides the reference wind speeds at 10 m height for different simulations cases. The above wind speeds with a power law function (Norton et al., 2012a) was applied to the velocity inlet (Fig. 8.2) of the computational domain. The average temperature during the period was 17 °C. The estimation of thermal conditions for walls in Fig.2 was based on the work of Norton et al. (2012b).

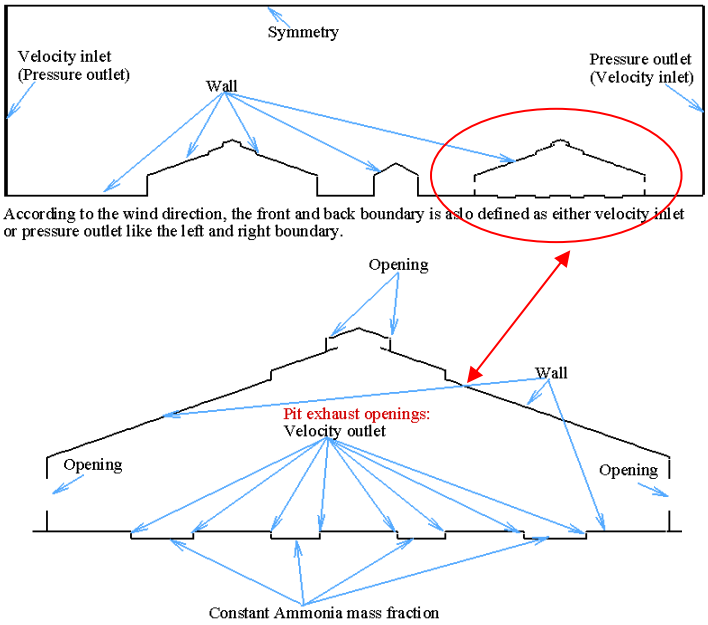

Fig. 8.2 Boundary conditions for the CFD model

8.2.2.2. Pit ventilation capacity

During the investigation time, the house held 128 (Holstein Frisian) dairy cows with an average weight of 625 kg on average. According to the survey of Seedorf et al. (1998), the mean natural ventilation rates were 0.77 $m^3 h^{-1} kg^{-1}$ for dairy cows in cubical houses in Denmark during summer time. The ventilation rate was equivalent to 373 $m^3 h^{-1} HPU^{-1}$. 10%, 20% and 30% of the mean natural ventilation rates were taken as the tested pit ventilation rates, which were about 37.3, 74.5 and 112 $m^3 h^{-1} HPU^{-1}$. The three associated air velocities 0.06, 0.12 and 0.18 $m s^{-1}$ for pit exhaust openings were specified to the velocity outlet in Fig. 8.2 and the airflow direction was normal to the outlet.

8.2.2.3. Animal Occupied Zone (AOZ) and slatted floor

Heat release from animals was estimated using the method proposed in CIGR (2002). The sensible heat production was 1291 W cow^{-1}. The resistance introduced by cows was considered as pressure drop. AOZ was treated as porous media (Bjerg et al., 2008b). The resistance coefficients were 7.71 m^{-2} for viscous force and 0.06 m^{-1} for inertial force calculated by Wu et al. (2012c).

Slatted floor was also tackled as porous media. The assumed opening areas were 15%. The resistance coefficients for 15% opening area were 10000 m^{-2} for viscous force and 50 m^{-1} for

inertial force (Bjerg et al., 2008b). Another two slatted floor opening ratios 30% and 7.5% were also used in this study to investigate the effect of floor openings ratios.

8.2.2.4. Ammonia release

The total ammonia emission rate was generally an unknown parameter. Hence, constant ammonia mass fraction was specified to the emission surface. Braam et al. (1997) reported about 60% of the total ammonia emission originates from slatted floor surface, whereas 40% was released from the slurry pit. The CFD model should consider the both release sources. However, the slatted floor was treated as porous media and it was impossible to prescribe a constant mass fraction to the slat surfaces. Therefore, the ammonia was assumed to originate only from slurry pit and the emission surfaces were marked in Fig. 8.2.

8.2.3. Turbulence models and numerical methods

Wu et al. (2012d) reported that it was feasible to use RSM turbulence models to predict the removal capability of a partial pit ventilation system. Hence, the widely RSM was adopted in this work. Commercial software Fluent 12.0 was used to solve the equations on the basis of finite volume method. All the velocity and turbulence terms for convection were approximated using second order upwind scheme. Diffusion terms were discretised using central difference scheme. SIMPLE method was employed for the pressure-velocity correction.

8.2.4. Validation of the CFD model

The measured air velocities by Wu et al. (2012a) were used to validate the CFD model. Air velocities were measured by 7 ultrasonic anemometers – WindMaster (Gill instruments Ltd, Hampshire, UK). An ultrasonic anemometer was placed 10 m above the ground to monitor the external wind speeds. Air velocities inside the buildings were recorded at 6 positions: two were near one sidewall openings; two were placed in the centre of the buildings and near ridge openings; two were near another sidewall openings. Meanwhile, velocity profiles were measured in the animal occupied zones (AOZ) and above feeding aisle. The measured positions and details were not repeated here and can be found in the work of Wu et al. (2012b).

8.3. Results

8.3.1. Model validation

Fig. 8.3 compares the numerical and experimental air velocity magnitudes at different positions (Wu et al., 2012a) in the building. The RMSD between simulated and measured mean air velocities was 0.32. Good agreements were found at the six positions. Fig. 8.4 compares the numerical and measured air velocity profiles under position D and A (Wu et al., 2012a). Big deviation existed between the simulated and measured velocity profile. The simulated air velocities were lower than the minimum values of measurement below 2 m above the ground.

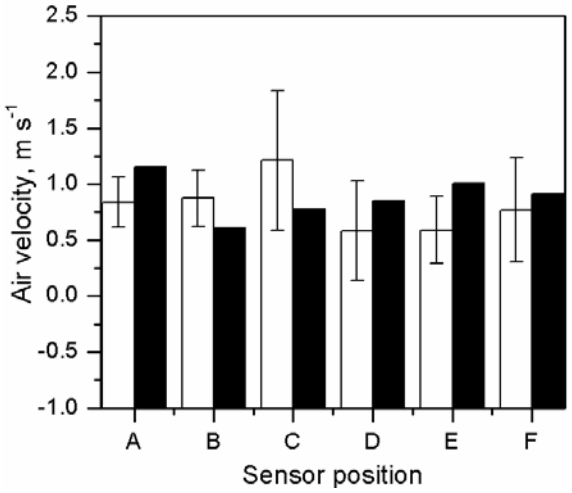

Fig. 8.3 Comparison of numerical (filled bar) and experimental (empty bar) air velocity magnitudes at different positions (Wu et al., 2012a) in the building

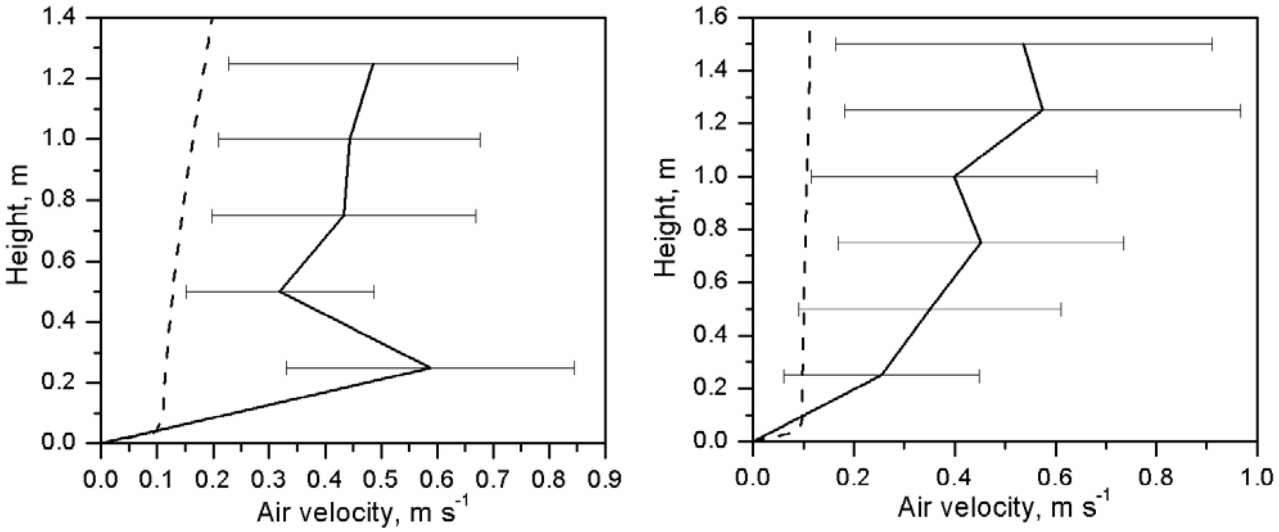

Fig. 8.4 Comparison of numerical (dashed line) and experimental (solid line) air velocity profiles under the position (Wu et al., 2012a): (a) D and (b) A

8.3.2. Potential of pit ventilation system to reduce ammonia

Table 8.1 shows the reduction of ammonia emission. Case 0 in a situation without pit ventilation, with fully open door and sidewall openings was taken as the reference case. The ammonia reduction was based on case 0. Discharge of 37.3 $m^3 h^{-1} HPU^{-1}$ polluted air through the pit exhaust system can only lead to ammonia emission reduction by 3.16%. By tripling the pit ventilation rate, only 6.07% more emission was abated. While the sidewall openings were constrained to 50% of the fully open, a reduction of ammonia by 43.1% can be achieved compared with Case 0. Pit ventilation with a capacity of 37.3 $m^3 h^{-1} HPU^{-1}$ combined with reducing half opening area of the sidewall openings

was able to reduce ammonia emission by 46.0% compared with Case 0. However, compared with Case 5, pit ventilation abated ammonia emission by 2.9%. The major reduction was indeed achieved by closing the sidewall openings. When the pit ventilation rate was tripled to 112 $m^3 h^{-1}$ HPU^{-1}, 5.6% more ammonia emission was reduced compared with pit ventilation rate 37.3 $m^3 h^{-1}$ HPU^{-1}. Increasing (Case 10) or decreasing (Case 9) slatted floor opening ratio did not lead to ammonia reduction in current simulations.

Table 8.1. Reduction of ammonia emission compared with the reference case 0 at the external wind speed 4.2 m s^{-1} and wind direction 225°.

Cases	pit ventilation rate (m3 h-1 HPU-1)	Door (% of fully open)	sidewall openings (% of fully open)	Slatted floor opening ratio (%)	Reduction of ammonia emission (%)
0	0	100	100	15	0
1	37.3	100	100	15	3.16
2	74.5	100	100	15	6.21
3	112	100	100	15	9.23
4	0	0	100	15	7.57
5	0	100	50	15	43.1
6	37.3	0	50	15	46
7	74.5	0	50	15	48.9
8	112	0	50	15	51.6
9	0	100	100	7.5	0
10	0	100	100	30	0

Fig. 8.5 shows the estimated reduction of ammonia emission as function of external wind speeds at pit ventilation rate 37.3 $m^3 h^{-1}$ HPU^{-1} and 50% of the fully open of the sidewall openings. The pit ventilation system was very efficient at low wind speeds (1.4 m s^{-1}). Compared with Case 0, ammonia reduction by 85.2% was achieved. Compared with Case 5, pit ventilation system had ability to reduce 42.2% ammonia emission at low wind speeds.

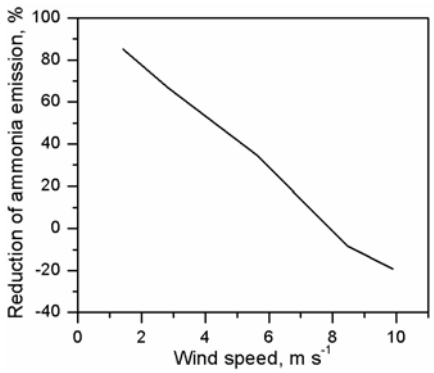

Fig. 8.5 Estimated reduction of ammonia emission as function of the external wind speeds, at a pit ventilation rate of 74.5 $m^3 h^{-1}$ HPU^{-1} and sidewall openings of 50%

8.4. Discussion

8.4.1. Model validation

CFD underestimated the air velocities below 2 m above the floor. The air velocities within this height were influenced by the AOZ including the existence of partitions, the distribution and movement of animals. But the influence cannot be fully considered due to the complexity of the geometrical details. Therefore, AOZ was treated as porous media. The use of porous media may lead to a difference between simulated and measured air velocities below 2 m. Moreover, the external wind was unsteady during the measurement. However, the simulation was based on the mean air velocity and was carried on in a steady situation. The fluctuation of the external wind might also be responsible for the difference of the numerical and experimental velocity profiles.

The AOZ and the slatted floor were treated as porous media for the purpose of geometry simplification. Therefore, the effect of slatted floor opening ratio on the ammonia emission was considered by changing the resistance of porous media. Case 9 and Case 10 did not show a reduction or an increase in ammonia emission compared with Case 0 by decreasing or increasing the resistance of porous media. Wu et al. (2012a, d) reported that decreasing the slatted floor opening ratio can lead to a significant reduction in gas emission. The discrepancy between the current results and the former research could originate from treating the slatted floor as porous media. Wu et al. (2012e) reported the difference between simulating slatted floor directly and treating it as porous media. However, it was difficult to simulate the slatted floor directly in this simulation. The uncertain of treating slatted floor as porous media cannot be analyzed. In future work, the uncertain of using porous media should be investigated and the solutions to improve the accuracy of treating slatted floor as porous media should also be proposed.

8.4.2. Potential of pit ventilation system to reduce ammonia

When the external wind speed was 4.2 m s^{-1} and the sidewall openings were fully open, the three designed pit ventilation rates seemed to remove limited ammonia emission (below 10%). The ventilation rate calculated by CFD simulation in Case 0 was 4485 $m^3 h^{-1} HPU^{-1}$. The designed pit ventilation rates were only 0.83%, 1.66% and 2.49% of the estimated natural ventilation rates by CFD. When the external wind speed was 1.4 m s^{-1} and the sidewall openings were 50% of the fully open, the calculated ventilation rate for the building was 663 $m^3 h^{-1} HPU^{-1}$. The pit ventilation system with a capacity of 37.3 $m^3 h^{-1} HPU^{-1}$ (5.6% of the calculated ventilation rate) can reduce ammonia emission by 85.2% compared with Case 0 and by 42.2% compared with Case 5. This indicates that utilization of pit ventilation system must be integrated with the control of the natural ventilation rates of the building. When the building was over-ventilated (Case 0 in this study), the pit ventilation system might not take good effect. But when the sidewall opening area was reduced according to external wind and the natural ventilation was kept in a level lower than 663 $m^3 h^{-1}$

HPU^{-1}, ammonia emission from the building can be significantly reduced by the pit ventilation system.

8.5. Conclusion

Computational fluid dynamics (CFD) was used to investigate the potential of a partial pit ventilation system with an air purification unit to reduce ammonia emission from naturally ventilated cattle buildings. Following conclusions can be drawn. A pit exhaust with a capacity of 37.3 $m^3 h^{-1} HPU^{-1}$ can reduce ammonia emission only by 3.16% compared with the case without pit ventilation when the external wind was 4.2 $m s^{-1}$. When the external wind was decreased to 1.4 $m s^{-1}$ and the sidewall opening area were reduced to half, such a pit ventilation capacity can reduce ammonia emission by 85.2%. The utilization of pit ventilation system must be integrated with the control of the natural ventilation rates of the building.

References

Bjerg B., Andersen M., 2010. Numerical simulation of a pit exhausts system for reduction of ammonia emission from a naturally ventilated cattle building. XVIIth world congress of the international commission of agricultural and biosystems engineering (CIGR). Quebec City, Canada.

Bjerg B., Zhang, G., Kai, P., 2008a. CFD investigations of a partly pit ventilation system as method to reduce ammonia emission from pig production units. The Eighth ASABE International Livestock Environment Symposium (ILES Ⅷ)

Bjerg B., Zhang, G., Kai, P., 2008b. Porous media as boundary condition for air inlet, slatted floor and animal occupied zone in numerical simulation of airflow in a pig unit. AgEng2008 International Conference on Agricultural Engineering, Hersonissos, Crete-Greece.

Braam, C. R., Smits, M.C.J., Gunnink, H., Swierstra, D., 1997a. Ammonia Emission from a Double-sloped Solid Floor in a Cubic House for Dairy Cows. *Journal of Agricultural Engineering Research* 68(4), 375-386.

CIGR, 2002. Report of Working Group on Climatization of Animal Houses – Heat and Moisture Production at Animal and House Levels. *CIGR Section II, Commission International Du Genie Rural (International Commission of Agricultural Engineering)*.

Launder, B.E., Spalding, D.B., 1974. The numerical computational of turbulent flows. Computer Methods in Applied Mechanics and Engineering 3, 269-289.

Norton, T., Grant, J., Fallon, R., Sun, D.W., 2010a. Assessing the ventilation effectiveness of naturally ventilated livestock buildings under wind dominated conditions using computational fluid dynamics. Biosystems engineering 103 (1), 78-99.

Norton, T., Grant, J., Fallon, R., Sun, D.W., 2010b. A computational fluid dynamics study of air mixing in a naturally ventilated livestock building with different porous eave opening conditions. Biosystems engineering 106 (2), 125-137.

Saha, C.K., Zhang, G., Kai, P., Bjerg B., 2010. Effects of a partial pit ventilation system on indoor air quality an ammonia emission from a fattening pig room. Biosystems Engineering 105 (3), 279-287.

Seedorf, J., Hartung, J., Schroder, M., Linkert, K.H., Pedersen, S., Takai, H., Johnsen, J.O., Metz, J.H.M., Groot Koerkamp, P.W.G., Uenk, G.H., Phillips, V.R., Holden, M.R., Sneath, R.W., Short, J.L.L., White, R.P., Wathes, C.M., 1998. A Survey of Ventilation Rates in Livestock Buildings in Northern Europe. *Journal of Agricultural Engineering Research* 70, 39-47.

Wu, W., Kai, P., Zhang, 2012a. An assessment of a partial pit ventilation system to reduce emission under slatted floor-Part 1: Scale Model Study. *Computers and Electronics in Agriculture* 83, 127-133.

Wu, W., Zhang, G., Kai, P., 2012b. Ammonia and Methane Emissions from Two Naturally Ventilated Dairy Cattle Buildings and the Influence of climatic Factors on Ammonia Emissions. *Accepted by Atmospheric Environment.*

Wu, W., Zhai, J., Zhang, G., Nielsen, P.V., 2012c. Evaluation of methods for determining air exchange rate in a naturally ventilated dairy cattle building with large openings using computational fluid dynamics (CFD). *Submitted to a peer review journal.*

Wu, W., Zhang, G., Bjerg, B., Nielsen, P.V., 2012d. An assessment of a partial pit ventilation system to reduce emission under slatted floor-Part 2: Feasibility of CFD prediction using RANS turbulence models. *Computers and Electronics in Agriculture* 83, 134-142.

Wu, W., Zong, C., Zhang, G., 2012e. Large eddy simulation of airflow and pollutant transport under slatted floor of a slurry pit model. *Submitted to a peer review journal.*

Chapter 9

General discussion and conclusions

9.1. Introduction

According to the objectives, this thesis is subsequently divided into two sections: predicting emissions from naturally ventilated dairy cattle buildings and establishing a systematic approach to reduce the emissions.

The first section includes **Chapter 2**, **3**, and **4**. **Chapter 2** is aimed at predicting gas emissions from naturally ventilated cattle buildings. Therefore, gas concentrations and their influencing parameters like air velocity and temperature were measured in two farm buildings. The emission rates of ammonia and methane as well as ventilation rates can thus be calculated by CO_2 production model (CIGR, 2002; Zhang et al., 2005; Feidler and Müller, 2011). The influence of air velocity and temperature on ammonia emissions was analyzed by multiple linear regressions. Both the ventilation rate and the gas concentration distribution were not only affected by air velocities but also by turbulence. The turbulence characteristics were discussed in an individual chapter – **Chapter 3**. The air velocity time series for turbulence calculation were measured by ultrasonic and the setup of the measurement in the two farm buildings was presented in Chapter 2. A discussion of the uncertainty of CO_2 production model was barely found in literature. Hence, it was investigated in **Chapter 4** using computational fluid dynamics (CFD) by comparisons with other methods. Moreover, one remained challenge of using CO_2 production model was the determination of the sampling positions for the outlet gas concentration, which was termed as representative gas concentration in this thesis. The representative positions to sample outlet gas were thus proposed.

In the second section including **Chapter 5**, **6**, **7** and **8**, efforts were put on developing a partial pit ventilation system to mitigate the emissions. Scale model of slurry pit was constructed and wind tunnel tests were conducted to study the contaminant removal efficiency of such a system under varied air speeds above floor, and ventilation configurations. The laboratory experiment and research results were presented in **Chapter 5**. The laboratory tests need to be verified by full scale investigations. Partial pit ventilation systems have not been applied to naturally ventilated dairy cattle buildings. Therefore, the full scale investigations had to be carried out by CFD simulations. Prior to full scale simulations, **Chapter 6** stated the possibility of using RANS turbulence models to perform investigations on pollutant transportation from slurry pit configured with mechanical pit exhaust systems. The simulations were calibrated by the laboratory measurements described in **Chapter 5**. The geometrical details of slatted floor generally cannot be modelled directly in a full scale simulation (Bjerg et al., 2008). Bjerg et al. (2008) dealt with the slatted floor as porous media. However, the uncertainty of treating slatted floor as porous media and modeling them directly was not analyzed in literature. The uncertainty was vital even if the porous media had to be used. The difference of pollutant transportation by treating slatted floor as porous media and modeling them directly was studied by CFD in **Chapter 7**. Simulations were validated by air velocities measured by Laser Doppler anemometer in a wind tunnel. After finishing the preparation work in Chapter 6

and 7, the full scale simulation was eventually performed in **Chapter 8**. Pit ventilation systems were tested in different conditions.

9.2. Determination of ventilation and gas emission rates

To predict ammonia and methane emissions, gas concentrations were measured inside and outside two naturally ventilated buildings (**Chapter 2**). The emission rates of ammonia and methane as well as ventilation rates can thus be calculated by CO_2 production model (CIGR, 2002; Zhang et al., 2005; Feidler and Müller, 2011). As the CO_2 was assumed to come from animals, and the production was known based on the cow weight and milk yield. The inputs for CO_2 production model to calculate ventilation rates were background and outlet CO_2 concentrations. The background concentration was sampled outside the buildings. The outlet concentration was sampled near the side wall and ridge openings inside the buildings. The gas concentration near the openings was assumed to be able to represent the outlet concentration, which was termed as representative gas concentration in this thesis. The setup of the measurements was supported by the research of Demmers et al. (1998), which showed that the mean tracer gas concentration measured in the openings was better to represent the outlet gas concentration than that measured in the building. The predicted ventilation rates as well as background and outlet concentrations of associated gas were used to calculate emission rates were the. Therefore, the accuracy of the quantification of the gas emission rates using CO_2 production model was highly depended on the performance of the CO_2 production model and the sampling positions of outlet gas concentrations.

In order to evaluate the performance of the CO_2 production model to predict ventilation rates or emission rates, the method should be validated against or compared to other methods. Natural ventilation rates can be decided using three existing methods – integrating volume flow rates (VFR) across all the openings, tracer gas decay (TGD) and constant tracer gas (CTG). CO_2 production model can be grouped into CTG. Demmers et al. (1998) showed that VFR was impossible to implement in reality due to the large openings and small pressure difference across each opening. TGD method cannot discover the ventilation variability during the decay process. Moreover, the external wind conditions could vary rapidly from one hour to next hour. Hence, it is hard to associate the ventilation rates estimated by TGD to the values estimated by CTG subjecting to the same external wind conditions. Due to the above limitations, computational fluid dynamics (CFD) has become a surge to assess the performance of CO_2 production model against VFR and CTG. All the three methods can be easily implemented in CFD. To find the sampling positions of outlet gas concentrations via experiment, more instruments and measurement systems are needed. It will also be very expensive, time consuming and laborious. But the same things can be easily performed in CFD simulations. In addition, CFD modelling can exploit insights into the airflow patterns, temperature and concentration distribution governing the gas emissions. Hence, CFD is used as a tool to assess the uncertainty in quantifying gas emission rates using CO_2 production model.

The CFD simulation results were validated by air velocity and CO_2 concentration data (**Chapter 4**). While the VFR was set as reference method, TGD demonstrated its good agreements with VFR. CO_2 production model using the mean concentration of the position near downwind sidewall opening also agreed with VFR over a wide range of external wind speeds and directions. CO_2 production model using the mean concentration of the entire room failed to predict consistent ventilation rates with VFR and TGD. Therefore, the sampling positions are vital to the accuracy of the CO_2 production model.

In order to find the optimum gas sampling positions four gas concentrations were compared which were (1) the mean gas concentration of the entire room calculated by CFD; (2) the mean gas concentration of three positions respectively near upwind sidewall opening, ridge opening and downwind sidewall opening; (3) the mean gas concentration of two positions respectively near ridge opening and downwind sidewall opening; (4) the mean gas concentration of the position near downwind sidewall opening. The mean gas concentration of the entire room failed to represent that in the exit air. The result agreed with the work of Demmers et al. (2000), which also reported large error in ventilation rate estimate using internal sampling points; they also indicated that no obvious zones or locations, which offered a representative concentration, could be identified within the building section. The mean gas concentration of the position near downwind sidewall opening was proved to best represent the outlet gas concentration. If CO_2 production model was used to calculate ventilate rates or emission rates from naturally ventilated livestock buildings, the gas sampling positions should be adjacent to or even located in the openings. The maximum gas concentration at different positions will be the representative gas concentration.

9.3. Climatic factors on gas emissions

Emission issues including odour, gas and particle from a naturally ventilated livestock building were controlled by the climatic factors such as wind speed, direction, temperature and turbulence as well as building components such as ventilation opening areas, positions and slatted floor. This information is also essential to model naturally ventilated cattle buildings using CFD.

9.3.1. Air velocity and temperature

The climatic data was collected synchronously with the concentration data as presented in **Chapter 2**. The correlation between climatic factors and ammonia emissions was analyzed by multiple linear regressions. Wind speeds and air temperature showed significant and positive correlation with ammonia emission. The similar conclusions were confirmed by literature (Snell et al., 2003; Zhang et al., 2008; Schrade et al., 2012). The wind speeds and directions can be monitored by ultrasonic placed outside and inside the buildings. The external wind speeds and directions can then be transformed to velocity profiles prescribed as the boundary conditions of the CFD model. Since the temperature was identified as an import factor influencing emissions, the temperature of external air

and wall surfaces of building should be defined. No measured wall temperature was available. The associated values were derived by heat balance equation, which was described in **Chapter 4**.

9.3.2. Air turbulence characteristics

The turbulence characteristics in two naturally ventilated cattle buildings were analyzed in detail in terms of autocorrelation, kinetic energy, turbulence energy dissipation rate, integral time and length scale as well as Kolmogorov microscale of length. Spectral analysis was also applied to the time series of external and internal air velocities in order to investigate the coherency of turbulence structures. An outstanding outcome of the air turbulence analysis was the irregular distribution of all the statistical descriptors except that the kinetic energy. When the external wind speed was increased, the internal kinetic energy at all the measured internal positions was increased accordingly. The purpose of the analysis of air turbulence in the buildings was to find the correlation between gas emission process and turbulence. Although no simple trend or correlation was found among the different statistical descriptors, the calculation of turbulence parameters can be useful in the following manners:

(1) CFD is a major tool in this research. The calculation of turbulence length scale, kinetic energy and dissipation rate can provide appropriate boundary conditions for the CFD model.

(2) Spectral analysis might be used to build mathematical models to predict natural ventilation rates (Lay and Bragg, 1998); Velocity time series might be transformed to frequency domain; a mathematical model to ventilation rate based on velocity data could be established in frequency domain.

9.4. Potential of partial pit ventilation systems to reduce emission

9.4.1. Laboratory measurements

In a mechanically ventilated livestock building, an air purification unit can be mounted to the exhaust duct and reduce the gas emissions. Unlike the mechanically ventilated buildings, it is difficult to collect the exhausted air for further air cleaning in a naturally ventilated livestock building. However, a concept of partial pit ventilation may be adapted into the housing system. A mechanical ventilation system can be connected to the headspace of the slurry pit and removed a part of the most polluted air under the slatted floor. The exhausted air was then purified by filtering apparatus. The hypothesis was firstly validated in a laboratory condition using a scale model. The detailed setup was described in **Chapter 5**. Partial pit ventilation was approved to be able to remove a large portion of polluted gases under the slatted floor in the scale model measurement. More than 50% of the contaminants can be removed by the pit ventilation system. The laboratory test may exaggerate the function of the pit ventilation system compared with the practical situation. Braam et al. (1997) reported about 60% of the total ammonia emission originated from slatted floor surface,

whereas 40% was released from the slurry pit in a naturally ventilated cow building. However, the scale model measurement in this study did not consider the emission from the surface of the slatted floor. Another deficiency of the scale model measurement was that the airflow distribution above the slatted floor in the wind tunnel may not represent that in a practical building.

9.4.2. Using CFD to investigate the performance of pit ventilation system

Different RANS turbulence models were tested and an underestimation of removal ratio was noticed for all the turbulence models. The transition SST $k-\omega$ turbulence model underestimated the removal ratio more than 8.1%. The three $k-\varepsilon$ models predicted similar removal ratios. The deviations from the measured values were larger than 5%. The best agreement between CFD simulation and measurement was achieved by RSM turbulence model. The deviation was less than 2%. Successful modelling of the flow over the pit headspace depended on the ability of the associated turbulence models to simulate the separation of fluid. The eddy-viscosity turbulence models like $k-\varepsilon$ models can sometimes over-predict the turbulence kinetic energy and were not sensitive to the interaction between streamline curvature and turbulence anisotropy. RSM, on the other hand, accounted for several turbulence features like streamline curvature. This may explain why the RSM showed a better performance.

Removal ratios based on CFD simulations were very close to measured values in most cases. It was feasible to use RANS turbulence models to assess the ability of a partial pit ventilation system to reduce emission under slatted floor. However, the study also showed that the gas transportation from the slurry pit to the free stream was dominated by the turbulence diffusion. Johnson and Hunter (1998) suggested that transient flow was an important factor to model flow and pollutant transportation dominated by turbulence diffusion.

9.4.3. Modeling of slatted floor

Slatted floors were the major component of the housing system with slatted floors. Except that slatted floors were the emission source, they were also the interfaces of the polluted air in the pit headspace and the air in the room. The boundary layer around the slatted floors governed the pollutant transportation from the pit headspace to the room space. Therefore, the accuracy of modeling of slatted floor decided the accuracy of simulating gas emissions from naturally ventilated cattle buildings. In practical buildings, hundreds of slats were used and a detailed simulation of the geometry using CFD was not realistic. They were generally treated as porous media. However, the uncertainty analysis of using porous media cannot be found in current literature. Although it was hard to avoid using porous media to simulate full scale buildings with slatted floor, an investigation of modeling slatted floor directly and treating them as porous media was particularly useful. To validate the CFD model, a 1:8 scale pit model was constructed in a wind tunnel. To consider the transient effect of turbulence diffusion, large eddy simulation was adopted to study the ammonia

transportation. To tackle the involvement of the slatted floor, two CFD models were established: modelling slatted floors directly with geometrical details (LESD) and treating them as porous media (LESP). LESP and LESD estimated similar mean air velocities and turbulence kinetic energy in the core of the pit headspace. Large discrepancy existed next to the upwind wall between both methods. Some other major differences between the LESP and LESD were:

(1) A dominant Strouhal number 0.23 was found for LESD results but no dominant strouhal number was found for LESP results.
(2) The emission rate and total mass of NH_3 in the pit headspace calculated by LESD was double of those calculated by LESP. Pollutants were confined in the headspace for longer time by means of using LESP than using LESD.
(3) The airflow patterns were different between LESP and LESD. Clear vertical air motion in the top surface of the slot was observed for LESD results but not for LESP.

The current simulation only considered the case when the slats were oriented parallel to the flow direction. However, the difference of LESP and LESD may be related to the orientation of the slats. For instance, if the slats were perpendicular to the flow direction, the difference might be more significant. From the point view of emission rates and the flow patterns, porous media may be not sufficient to represent the slatted floor. New methods may be needed to simplify and simulate the slatted floors.

9.4.4. Full scale simulation

CFD has been proved to be a feasible approach to study the ventilated flow in livestock buildings (Norton et al., 2010). The full scale investigation of the potential of partial pit ventilation systems to reduce emissions was completed by CFD. Although treating slatted floor as porous media might introduce uncertainties to the results, using porous media cannot be avoided due to the complicity of the building geometry and the computational capacity. If the livestock building was over-ventilated, pit ventilation with 10% capacity of the designed room ventilation rates may not be able reduce emissions efficiently. In this study, pit ventilation systems can be efficient only if the curtains of sidewall openings were regulated according to the external wind conditions. In practice, the sidewall openings are usually fully open during summer in naturally ventilated cattle buildings in order to remove the heat and the humidity. Under this circumstance, the buildings in windy zones (Denmark) are generally over-ventilated. During winter, the sidewall openings might be closed to provide warmer indoor climate for cows and ventilation might be dominated by stack effect. In this situation, pit ventilation systems can be very efficient to reduce the gas emissions.

9.5. Perspectives

The first part of the thesis solved the uncertainties concerning quantification of ventilation and emission rates using CO_2 production model. As a result, a major outcome was to find the optimum

gas sampling positions to represent the outlet concentration. The optimum gas sampling positions were determined by CFD. In future, different sampling systems and positions should be setup in the field measurement. Therefore, the optimum positions determined by measurement can be compared with those found by CFD. Further study may also be focused on proposing new methodology to determine natural ventilation rate instead of using CO_2 production model. The new methodology to determine natural ventilation rates may be complemented by Fourier transform of data in time domain into frequency domain. A mathematical model on ventilation rates might be developed in frequency domain by necessary parameters. In addition, the emission inventories in this study were campaigned in two naturally ventilated dairy cattle buildings. More measurement of gas concentration data were needed to add to the database for national emission inventories.

The second part of the thesis was devoted to applying pit ventilation systems to reduce emissions. It was first tested in a scale model, and then the full scale investigation was done by CFD simulations. There existed many uncertainties introduced by simplification building components and animals. Animals were treated as porous media in this study according to Bjerg et al. (2008). To compare the effect of animals, different simplification methods like treating them as blocks can be the potential work. In chapter 7, slatted floor was modeled directly and as porous media. Simulations on different orientations of slats relative to the flow direction were necessary to study the uncertainty of using porous media. Moreover, new numerical methods to tackle slatted floor may be proposed to model this essential zone. The current simulations were conducted in steady conditions. As it was pointed out in literature, transient flow was an important feature of pollutant transportation. Unsteady simulations of natural ventilation across livestock buildings can be very helpful to study the potential of partial pit ventilation systems to reduce emissions.

9.6. General conclusions

The following general conclusions were drawn from this thesis:

- The NH_3 emission rates varied from 32-77 g HPU^{-1} d^{-1} in building 1 and varied from 18-30 g HPU^{-1} d^{-1} in building 2. The average emission of CH_4 was 290 and 230 g HPU^{-1} d^{-1} from building 1 and 2, respectively. Diurnal pattern was found for NH_3 and CH_4 emission rates.
- From multiple linear regression models, there was a significant linear relationship between NH_3 emission rates and climatic factors including the external wind speed as well as the air temperature (P<0.001), but not with the external wind directions (P>0.05).
- The distribution of turbulence time and length integral scale was very irregular. The internal kinetic energy had a positive correlation with the external wind speed. Larger turbulence energy dissipation rate (0.49 m^2 s^{-3}) was found near side openings, where the integral length scale was smaller. Kolmogorov microscales were quite isotropy for the natural airflow in this study. Air velocities near downwind side openings possessed higher power spectra at both

low and high frequency, compared with those in the middle section or near upwind side openings.

- Air exchange rates (AER) predicted by integrating volume flow rate (VFR) and tracer gas decay (TGD) were in good agreement with each other within a large range of wind speeds. Large difference in AER estimation using constant tracer gas method (CTG) and VFR indicates that the mean CO_2 concentration of the entire room may not represent the outlet concentration.
- The gas sampling positions should be located adjacent to the openings or even in the openings. To reduce the uncertain introduced by wind direction, all the openings especially of different azimuths should possess sampling tubes. The maximum gas concentrations in the different openings could be the optimum value to represent the concentration in the exit air.
- Scale model experiment showed that partial pit ventilation was able to remove a large portion of polluted gases under the slatted floor.
- RANS turbulence models especially RSM can be used to predict the removal capability of a partial pit ventilation system to reduce emission under slatted floor.
- Two CFD approaches were used to tackle the involvement of the slatted floor: modelling slatted floors directly with geometrical details (LESD) and treating them as porous media (LESP). LESP and LESD estimated similar mean air velocities and turbulence kinetic energy in the core of the pit headspace. Large discrepancy existed next to the upwind wall between both methods. The emission rate and total mass of NH_3 in the pit headspace calculated by LESD was double of those calculated by LESP. Pollutants were confined in the headspace for longer time by means of using LESP than using LESD. The airflow patterns were different between LESP and LESD. Clear vertical air motion in the top surface of the slot was observed for LESD results but not for LESP.
- A pit exhaust with a capacity of 37.3 $m^3\ h^{-1}\ HPU^{-1}$ can reduce ammonia emission only by 3.16% compared with the case without pit ventilation when the external wind was 4.2 m s^{-1}. When the external wind was decreased to 1.4 m s^{-1} and the sidewall opening area were reduced to half, such a pit ventilation capacity can reduce ammonia emission by 85.2%. The utilization of pit ventilation system must be integrated with the control of the natural ventilation rates of the building.

References

Bjerg B., Zhang, G., Kai, P., 2008b. Porous media as boundary condition for air inlet, slatted floor and animal occupied zone in numerical simulation of airflow in a pig unit. AgEng2008 International Conference on Agricultural Engineering, Hersonissos, Crete-Greece.

Braam, C. R., Smits, M.C.J., Gunnink, H., Swierstra, D., 1997a. Ammonia Emission from a Double-sloped Solid Floor in a Cubic House for Dairy Cows. *Journal of Agricultural Engineering Research* 68(4), 375-386.

CIGR, 2002. Report of Working Group on Climatization of Animal Houses – Heat and Moisture Production at Animal and House Levels. *CIGR Section II, Commission International Du Genie Rural (International Commission of Agricultural Engineering)*.

Demmers, T.G.M., Burgess, L.R., Short, J.L., Phillips, V.R., Clark, J.A., Wathes., C.M., 1998. First experiences with methods to measure ammonia emissions from naturally ventilated cattle buildings in the U.K. *Atmospheric Environment* 32,285-293.

Demmers, T.G.M., Burgess, L.R., Phillips, V.R., Clark, J.A., Wathes., C.M., 2000. Assessment of Techniques for Measuring the Ventilation Rate, using an Experimental Building Section. *Journal of Agricultural Engineering Research* 76,71-81.

Feidler, A.M., Müller, H.J., 2011. Emissions of ammonia and methane from a livestock building natural cross ventilation. *Meteorologische Zeitschrift* 20 (1), 059-065.

Johnson, G.T., Hunter, L.J., 1998. Urban wind flows: wind tunnel and numerical simulations—a preliminary comparison. Environmental Modelling and Software 13, 279 – 286.

Lay, R. M., Bragg, G. M., 1998. Distribution of Ventilation air – Measurement and Spectral Analysis by Microcomputer. *Building and Environment*, 23 (3), 203-213.

Norton, T., Grant, J., Fallon, R., Sun, D.W., 2010a. Assessing the ventilation effectiveness of naturally ventilated livestock buildings under wind dominated conditions using computational fluid dynamics. Biosystems engineering 103 (1), 78-99.

Schrade, S., Zeyer, K., Gygax, L., Emmenegger, L., Hartung, E., Keck, M., 2012. Ammonia Emissions and Emission Factors of Naturally Ventilated Dairy Housing with Solid Floors and an Outdoor Exercise Area in Switzerland. *Atmospheric Environment* 47, 183-194.

Snell, H.G.J., Seipelt, F., Van Den Weghe, H.F.A., 2003. Ventilation Rates and Gaseous Emissions from Naturally Ventilated Dairy Houses. *Biosystems Engineering* 86 (1), 67-73.

Zhang G; Bjerg B; Strøm JS; Morsing S; Kai P; Tong G; Ravn P, 2008. Emission Effects of Three different Ventilation Control Strategies - A Scale Model Study. Biosystems Engineering 100(1), 96-104.

Wentao Wu, Modelling and reducing gas emissions from naturally ventilated livestock buildings, 2012

Department of Engineering
Aarhus University
Edison, Finlandsgade 22
8200 Aarhus N
Denmark

Tel.: +45 4189 3000